

**Titre:** Control of the wet end of a pilot scale paper machine  
Title:

**Auteur:** Nancy Harnois  
Author:

**Date:** 2001

**Type:** Mémoire ou thèse / Dissertation or Thesis

**Référence:** Harnois, N. (2001). Control of the wet end of a pilot scale paper machine  
Citation: [Mémoire de maîtrise, École Polytechnique de Montréal]. PolyPublie.  
<https://publications.polymtl.ca/27343/>

 **Document en libre accès dans PolyPublie**  
Open Access document in PolyPublie

**URL de PolyPublie:** <https://publications.polymtl.ca/27343/>  
PolyPublie URL:

**Directeurs de  
recherche:** Michel Perrier  
Advisors:

**Programme:** Non spécifié  
Program:

UNIVERSITÉ DE MONTRÉAL

CONTROL OF THE WET END OF A PILOT SCALE PAPER MACHINE

NANCY HARNOIS  
DÉPARTEMENT DE GÉNIE CHIMIQUE  
ÉCOLE POLYTECHNIQUE DE MONTRÉAL

MÉMOIRE PRÉSENTÉ EN VUE DE L'OBTENTION  
DU DIPLÔME DE MAÎTRISE ÈS SCIENCES APPLIQUÉES (M.Sc.A.)  
(GÉNIE CHIMIQUE)  
MAI 2001

© Nancy Harnois, 2001.

UNIVERSITÉ DE MONTRÉAL

ÉCOLE POLYTECHNIQUE DE MONTRÉAL

Ce mémoire intitulé:

CONTROL OF THE WET END OF A PILOT SCALE PAPER MACHINE

présenté par: HARNOIS Nancy

en vue de l'obtention du diplôme de: Maîtrise ès science appliquées

a été dûment accepté par le jury d'examen constitué de:

M. LAFLEUR Pierre, Ph.D., président

M. PERRIER Michel, Ph.D., membre et directeur de recherche

M. ORCCOTOMA Jose Antonio, Ph.D., membre et codirecteur de recherche

M. VALIQUETTE Jean, M.Sc.A, membre

Nothing in life is to be feared.  
It is only to be understood.

Marie Curie

# Acknowledgements

Pour réaliser un projet de cette envergure, le support d'une équipe est essentiel. Dans l'année et demie nécessaire pour réaliser ce mémoire, plusieurs groupes m'ont aidée et j'aimerais prendre quelques lignes pour les remercier.

Il y a eu bien sûr le groupe de l'Unité de recherche en contrôle de procédé (URCPC). Tout au long de mon passage à Polytechnique, j'ai été fière d'être membre de ce groupe, d'apprendre à travers de discussions enlevantes avec les anciens (Stéphane, Jean-François, Antoine et David) et les nouveaux (Michal, Ilich, Jennifer, et Lyne). Autour du pot du vendredi, les discussions étaient moins sérieuses et permettaient à tous d'apprécier le temps passé ensemble. J'espère pouvoir retrouver une équipe de ce genre dans le futur. Je dois un merci bien spécial à Michel Perrier pour m'avoir acceptée dans ce groupe et m'avoir donné des responsabilités qui m'ont permis d'apprendre beaucoup. Je pense particulièrement aux charges de travaux dirigés et à la supervision des projets de fin d'études (PFE) de Nicolas, Brice et Raj.

Ce projet n'aurait pu se réaliser sans la collaboration des équipes de Paprican et du Centre Spécialisé en pâtes et papier. Grâce à eux, j'ai eu la possibilité d'avoir des données et de mieux comprendre le procédé papetier. Je tiens à souligner tout particulièrement la patience de Charles Gabriel. Ses réponses à mes questions ont toujours été bien appréciées tant celles sur le DCS que celles sur le chocolat.

The realisation of this project would have been impossible without the collabo-

ration of Byoung-Uk Cho. I would like to thank him for its time, answers, advices, and corrections of the first draft of this master thesis.

Je dois un merci bien spécial à Julie, Alex, Nicole et Marianne qui ont pris de leur temps pour relire une première version de ce manuscrit. Leurs commentaires ont été bien appréciés.

Enfin, j'aimerais remercier ma famille et mes amis qui ont su me supporter et me distraire. Je tiens à remercier tout particulièrement Jeffrey, qui a si bien su m'encourager.

# Résumé

Les opérations de la machine à papier et le papier produit sont grandement influencées par les interactions de la partie humide. L'optimisation de la partie humide est donc un moyen peu coûteux pour améliorer les opérations de la machine. Dans un premier temps, la fermeture de la boucle de l'eau blanche a montré l'amélioration qu'on pouvait apporter aux performances de la machine à papier. Pour continuer d'augmenter la productivité de la machine, il a été proposé d'intégrer les boucles de contrôle de la partie humide avec celles de la partie sèche.

Ce travail se propose d'étudier une stratégie de commande intégrée. Pour ce faire, une représentation du procédé est nécessaire. Des modèles de type entrée/sortie ont été bâtis à partir d'un algorithme de régression linéaire modifié. De ces modèles, la matrice de gain relatif (RGA) et le nombre de conditionnement ont été calculés. Ces indices indiquent l'importance des interactions dans le système multivariable. La stratégie de commande résultante est testée avec des simulations. Pour représenter la réalité, deux modèles sont utilisés. Un modèle linéaire est utilisé pour paramétrer les contrôleurs et un modèle nonlinéaire est utilisé pour simuler le procédé. Les variables de la partie humide qui sont considérées dans ce travail sont: la consistance totale et la consistance en cendre de la caisse d'arrivée, la consistance totale et la consistance en cendre de l'eau blanche, le débit de pâte épaisse, le débit de charge, le débit de bentonite, et le débit de (poly)acrylamide cationique. Les variables de la partie sèche qui sont étudiées sont le taux de cendre dans la feuille et le grammage.

D'après les indices de contrôle, la stratégie intégrée trois-par-trois commande la consistance totale de l'eau blanche, le contenu en cendre et le grammage. Les variables manipulées utilisées sont le débit de polymère, le débit de charge, et le débit de pâte épaisse. Des contrôleurs de type PID et MPC sont utilisés pour contrôler le système. La performance du MPC par rapport à celle du PID dépend de la qualité du modèle utilisé. Lorsque le modèle reproduit fidèlement le procédé, la performance du MPC est supérieure à celle du PID. Lorsque le modèle ne reproduit pas le procédé, la performance du MPC est similaire ou inférieure à celle du PID. Des études préliminaires ont également été faites pour augmenter le nombre de variables contrôlées. Le but est d'inclure la consistance totale à la caisse d'arrivée dans le contrôleur. De cette façon, le grammage peut être contrôlé même si une casse survient sur la machine. Des essais ont été faits sur une machine à papier pilote pour mesurer la performance de la boucle de commande de la consistance à la caisse d'arrivée. Un contrôleur PI a été en mesure de maintenir le point de consigne et les échantillons pris montrent un grammage contrôlé.



# Abstract

Wet-end operations greatly influence paper machine operations and the resulting produced paper. Their optimisation provides an inexpensive way of increasing paper machine productivity. White water consistency control has shown the potential benefits of improving wet-end operations. To further increase the productivity, it was proposed to integrate wet-end control loops with dry-end control loops.

This work proposes to investigate an integrated strategy. To perform an analysis, a representation of the process is needed. Input/output models are developed from a modified linear regression algorithm. Relative gain array (RGA), condition number and simulations are used to assess the amount of interactions in the multivariable system. To test the resulting control strategy, simulations are done. To obtain a more realistic setting, the control strategy tuning is done using linear models and tested on a nonlinear model. Wet-end variables studied are the headbox ash and total consistencies, white water ash and total consistency, thick stock flowrate, filler flowrate, bentonite flowrate, and Cationic (Poly)AcrylAmide (CPAM) flowrate. The dry-end variables studied are sheet ash content and basis weight.

Based on the control indices, the three-by-three integrated system controls white water total consistency, ash content and basis weight by manipulating CPAM flowrate, filler flowrate and thick stock flowrate. PID controllers and model-based controllers (MPC) are used to control the system. MPC controller performance is strongly dependant on its model quality. When the models reproduce well the

plant, the MPC regulating performance is superior to the PID performance. When the models do not reproduce well the plant, the MPC performances are similar to or worst than the PID performance. A preliminary study has been done to augment the three-by-three system with headbox consistency. This would allow to keep the control in the event of a sheet break. The tests consist in closing the headbox consistency control on a pilot paper machine. Results show that a PI controller maintains the headbox consistency setpoint. Measured samples show a basis weight under control.

## Condensé

Le papier a progressivement pris une importance prépondérante dans la vie de tous les jours. En 1998, la consommation mondiale de papier et de ses dérivées était de 28.4 million de tonnes desquelles 20 % ont été produites au Canada (CPPA 2000). L'organisation de la nourriture et de l'agriculture des Nations Unies estime qu'en 2010, la consommation mondiale de papier sera un tiers plus élevée. Malheureusement, le coût de production de l'industrie canadienne est élevé. Chaque année, la compétition mondiale entre producteurs de papier réduit la marge de profit des entreprises canadiennes. Pour prévenir la fermeture d'usine, il est primordiale d'augmenter la productivité des usines. L'optimisation des procédés est une discipline qui analyse les procédés pour déterminer les conditions d'opération optimales. Ces conditions sont maintenues par la commande de procédés. Ensemble, l'optimisation et la commande de procédés donnent une solution qui a un coût d'investissement peu élevé et qui peut aider l'industrie canadienne des pâtes et papier à trouver un avantage compétitif.

La production de papier est une suite de procédés complexes. La complexité est accrue par la variabilité de la matière première. Des différentes étapes de la production du papier, ce projet se concentre sur la partie humide de la machine à papier. Il y a plusieurs raisons qui incitent à étudier la partie humide. L'expérience des producteurs et des études en laboratoire ont démontré que plusieurs propriétés du papier sont directement influencées par les conditions opératoires de la partie

humide. Il est généralement plus facile de corriger un problème potentiel au bout humide qu'au bout sec de la machine. De plus, les tendances au niveau de l'opération de la machine comme: l'utilisation de pâtes mécaniques; l'augmentation de la fermeture des circuits d'eau blanche; l'augmentation du pourcentage de charge dans la feuille; l'utilisation de pâte recyclée qui contienne une proportion élevée de fines et de contaminants; et, bien sûr, l'obligation de réduire les coûts de production ont augmenté la pression sur la performance de la partie humide en réduisant son aire d'opération. Son optimisation devient une nécessité. De plus, la partie humide a un effet direct sur le grammage, une spécification importante lors de la vente du papier. Présentement, le grammage est contrôlé au bout sec de la machine. Il y a donc un long délai entre la lecture et l'action du contrôleur. La réduction de ce délai et de la variabilité du grammage serait un résultat important de l'optimisation de la partie humide de la machine à papier.

## **Revue de la littérature**

La théorie sur la chimie de la partie humide (Swerin & Odberg 1997) est assez avancée pour définir qualitativement la situation nécessaire pour des conditions d'opération optimale. Mais, elle ne peut donner des recommandations qui sont applicable à l'optimisation. Donc, pour optimiser la partie humide, on doit trouver les variables qui reflètent la variabilité du procédé. Les variables de la partie humide peuvent être divisée en deux groupes: variables d'entrée et de sortie. Les variables d'entrée, qui expliquent la variabilité de la partie humide, peuvent être sous-divisées en deux autres groupes:

1. Variables manipulées (paramètres que le producteur contrôle);
2. Perturbations (paramètres que le producteur ne peut contrôler).

Le groupe des variables de sortie peut aussi être re-divisé en deux:

1. Conséquences sur le procédés (facteurs qui affectent le procédé: rétention, drainage, productivité, etc.);
2. Conséquences sur le produit (facteurs qui affectent le produit: formation, sizing, uniformité, etc.).

Le groupe des variables d'entrée affectent le groupe des variables de sortie par l'intermédiaire des interactions moléculaires et colloïdales, i.e., la chimie de la partie humide. Une approche possible pour l'optimisation est de réduire le plus possible la variabilité du groupe d'entrée, ce qui réduira la variabilité de la chimie de la partie humide. Une première étape dans cette approche est de réduire la variabilité d'un sous-système qui explique une bonne partie de l'ensemble de la variabilité. Il y a plusieurs variables qui peuvent être choisie comme sous-système: le taux de drainage, la rétention de première passe, la conductivité, le pH, la température, la formation, etc. Par contre, toutes ces variables ne peuvent être mesurées ou contrôlées. Lorsque l'optimisation de la partie humide est devenu un sujet de recherche important, au début des années 1990, la plupart des machines à papier contrôlait la température et le pH. Il n'y avait pas de capteurs fiables pour mesurer le drainage ou la formation. Donc, la rétention de première passe (FPR), définie par l'équation 1.2, a été proposée comme premier sous-système à stabiliser parceque (Nazir & Carnegie-Jones 1991):

1. C'est une mesure de l'efficacité de la section de formation
  2. C'est une mesure de l'efficacité des additifs de rétention
  3. C'est un indicateur de la rétention d'autres additifs
  4. C'est une mesure des phénomènes microscopiques et macroscopique présents.
- Le FPR est sensible aux changements de la chimie du système et au niveau de cisaillement.

5. C'est une mesure de la propreté du système
6. C'est mesurable: grâce aux capteurs de consistance, on peut calculer le FPR.

Plusieurs articles ont expliqué l'effet du contrôle de la rétention, par le contrôle de la consistance de l'eau blanche, sur des machines pilotes et sur des machines industrielles (voir le tableau 1.5). Tous ces auteurs ont rapporté que le contrôle de la rétention aide la productivité et la stabilité de la machine à papier. Certains auteurs ont remarqué une diminution dans la variabilité du grammage et de l'épaisseur de la feuille dans le sens machine (Nokelainen, Piirainen & Ramsey 1993, Nokelainen & Piirainen 1995, Yeager 1997, Olsson & Renaud 2000). Plusieurs auteurs avancent que le contrôle de la rétention réduit la quantité de cassure sur la machine (Nokelainen et al. 1993, Nokelainen & Piirainen 1995, Rantala, Tarhonen & Koivo 1994*b*, Proulx, Morissette & Ruel 1999). D'autres ont rapportée une augmentation de la vitesse de la machine à papier (Olsson & Renaud 2000, Lang, Nokelainen, Rantala, Huhtelin, Tian & Kuusisto 1999). De plus, une réduction dans le coût du papier est rapporté due à une réduction de la quantité de vapeur utilisée, une augmentation de la quantité de cendres dans la feuille, et à une optimisation de la quantité de polymères utilisés (Yeager 1997). Le coût du traitement de l'eau blanche diminue grâce à une plus petite concentration de fines dans les rejets (Kortelainen 1991). Plusieurs auteurs ont rapporté un effet domino qui réduit la variabilité d'autres variables du bout humide (consistance à la caisse d'arrivée, la concentration en cendre, le grammage) lorsque la consistance de l'eau blanche est contrôlée. (Nokelainen et al. 1993, Proulx et al. 1999, Sopenlehto 1995, Proulx & Renaud 2000).

## Intégration de la commande des parties humide et sèche

L'étape suivante, la plus logique, consiste à stabiliser plus d'un sous-système de la partie humide, i.e., avoir plus d'une boucle de contrôle. Le but est de réduire les variations du bout humide pour obtenir un papier qui rencontre le mieux possible les besoins du consommateur. Une des premières exigences du consommateur est un grammage constant. La présente boucle de contrôle, où le capteur de la partie sèche modifie l'ouverture de la vanne du cuvier machine, peut seulement réduire les longues variations. Un contrôle basé dans la partie humide n'aurait pas ce long délai. La stratégie est, donc, d'intégrer les boucles de contrôle du bout sec à celles du bout humide. Une stratégie intégrée a été proposée par (Rantala, Nokelainen & Artama 1999). Cependant, cette stratégie n'a pas été installée au complet sur une machine à papier. Ils ont identifié la consistance, les cendres, la conductivité, le pH, la charge et la température comme des variables importantes qui expliquent les variations de la partie humide. L'hypothèse de leur stratégie est que si les sous-systèmes importants sont contrôlés, les plus importantes perturbations vont être éliminées (voir figure 1.6).

## Objectifs

Avant d'utiliser une stratégie de commande, il est important de quantifier les interactions entre les différentes variables. Plusieurs articles récents ont présenté des stratégies de commande intégrant plusieurs boucles (Rantala et al. 1999, Lang et al. 1999). Les interactions entre les variables sont au mieux qualitativement définies. Par exemple, dans la seule application MPC, les auteurs n'ont pas trouvé une amélioration de la performance lorsqu'ils ont inclus la consistance de l'eau blanche dans le contrôleur. Un contrôleur PI donnait d'aussi bons résultats. Une analyse des interactions entre les variables permettrait de mieux comparer les stratégies de commande

existantes, et pourrait en proposer de nouvelles si cela s'avérait nécessaire. De plus, une analyse des interactions entre les variables devrait aider à déterminer le type de contrôleur le plus approprié pour mieux contrôler le procédé.

Les objectifs de ce projet sont:

- quantifier les interactions entre les variables manipulées et les variables contrôlées.

Les variables analysées seront: la consistance en cendre et totale de la caisse d'arrivée, la consistance en cendre et totale de l'eau blanche, le contenu en cendre de la feuille et le grammage.

- définir et tester une stratégie de commande intégrant la partie humide et sèche d'une machine à papier.

Les performances de différent types de contrôleur (PID et MPC) seront également étudiées.

## Méthodologie

Pour rencontrer les objectifs, il est nécessaire de développer des modèles. Deux méthodes sont généralement utilisées pour bâtir des modèles: les bilans de matière et les équations entrée/sortie. Dans ce travail, les deux types de modèles sont utilisés mais seulement les modèles de type entrée/sortie sont développés. Les modèles de type entrée/sortie sont des équations qui représentent les effets de la variable d'entrée sur la variable de sortie. Plusieurs équations peuvent représenter le même groupe de données. Dans ce travail, des équations linéaires (voir 2.8) sont obtenus à partir d'un algorithme de régression linéaire modifié (voir annexe B). Les modèles sont calculés sur un groupe de données et validés sur un deuxième groupe de données. Le modèle représentant le mieux les données est conservé comme le meilleur



modèle. De ces modèles, la matrice de gain relatif (RGA) et le nombre de conditionnement sont calculés. Ces indices indiquent l'importance des interactions dans le système multivariable. La stratégie de commande résultante est testée avec des simulations. Lorsque des essais avec contrôleurs sur la machine étaient impossibles, deux modèles sont utilisés pour représenter la réalité. Un modèle linéaire est utilisé pour paramétrer les contrôleurs et un modèle nonlinéaire est utilisé pour simuler le procédé.

Des données sont nécessaires pour obtenir les modèles de type entrée/sortie. Les données ont été obtenues de deux machines à papier pilote différentes. Des essais ont été effectués sur la machine à papier pilote de Paprican pour améliorer la commande de la consistance à la caisse d'arrivée. De ces données, quatre modèles sont construits et analysés. Les variables manipulées sont la vanne du cuvier machine et la vitesse de rotation de la pompe de mélange. Les variables contrôlées sont la consistance à la caisse d'arrivée et le débit à la caisse d'arrivée. D'autres essais ont été effectués sur la machine à papier pilote du Centre Spécialisé en Pâte et Papier du Cégep de Trois-Rivières. Ces essais avaient pour but l'étude des interactions entre les variables de la partie humide et de la partie sèche de la machine à papier. De ces données, vingt-quatre modèles sont construits et analysés. Les variables étudiées sont: la consistance en cendre et totale de la caisse d'arrivée, la consistance totale et en cendre de l'eau blanche, le grammage, le contenu en cendre, le débit de pâte épaisse, le débit de charge, le débit de (poly)acrylamide cationique, le débit de bentonite et le ratio des additifs de rétention.

## Résultats et conclusions

Pour répondre aux objectifs de ce projet, les modèles entre les variables manipulées et les variables contrôlées sont cruciaux. Conséquemment, beaucoup de temps et

d'effort ont été mis dans le développement des modèles de type entrée/sortie. La qualité des modèles obtenus est dépendante de la qualité des données sur lesquelles les modèles sont bâtis. Les données qui contiennent assez d'information sur la dynamique du procédé permettent de d'obtenir de bons modèles. Pour ce faire, le temps d'échantillonnage des données doit être assez rapide, plusieurs échelons doivent être faits sur le procédé et le bruit ne doit pas empêcher de voir la réaction du procédé.

Lorsque les modèles ont été développés, il est possible d'analyser les interactions entre les différentes variables. D'après les indices de contrôle, la stratégie intégrée trois-par-trois commande la consistance totale de l'eau blanche, le contenu en cendre et le grammage. Les variables manipulés utilisées sont le débit de polymère, le débit de charge, et le débit de pâte épaisse.

Des contrôleurs de type PID et MPC sont utilisés pour contrôler le système. Le système est représenté par un modèle non-linéaire basée sur des bilan de matières. La performance du MPC par rapport à celle du PID dépend de la qualité du modèle utilisé. Lorsque le modèle reproduit fidèlement le procédé, la performance du MPC est supérieure à celle du PID. Lorsque le modèle ne reproduit pas le procédé, la performance du MPC est similaire ou inférieure à celle du PID.

Des études préliminaires ont également été faite pour augmenter le nombre de variables contrôlées. Le but est d'inclure la consistance en cendre et totale à la caisse d'arrivée dans le contrôleur. Ces variables sont les équivalents dans la partie humide de la teneur en cendre et du grammage, les variables de la partie sèche. De cette façon, le grammage peut être contrôlé même si une casse survient sur la machine. Pour ce faire, un prédicteur basée sur les variables de la partie humide est nécessaire. Le prédicteur donnerait une plage de valeurs acceptables pour les consistance en cendre et totale. En mode d'opération normale, si les consistances de

la caisse d'arrivée sont à l'intérieur de la plage prescrite, le contrôleur optimiserait les variables de la partie sèche. Par contre, si les consistances sont à l'extérieur de la plage d'opération, le contrôleur ramènerait ces variables en priorité dans leur plage de contrôle. Lors d'une casse, le contrôleur utiliserait seulement les variables de la partie humide pour garder la machine sous contrôle. Naturellement, des simulations sont nécessaires pour confirmer le tout. Mais, avant d'étudier cette stratégie intégrée, il faut s'assurer que le grammage peut être contrôlé avec la consistance totale à la caisse d'arrivée.

Des essais ont donc été faits sur une machine à papier pilote de Paprican pour mesurer la performance de la boucle de commande de la consistance à la caisse d'arrivée. Le contrôleur PI a été en mesure de maintenir le point de consigne et les échantillons pris montrent un grammage contrôlé.

# Contents

<b>Acknowledgements</b>	<b>v</b>
<b>Résumé</b>	<b>vii</b>
<b>Abstract</b>	<b>ix</b>
<b>Condensé</b>	<b>xi</b>
<b>List of Tables</b>	<b>xxiii</b>
<b>List of Figures</b>	<b>xxvi</b>
<b>Glossary</b>	<b>xxxix</b>
<b>1 Problem Definition</b>	<b>1</b>
1.1 Process Description . . . . .	2
1.2 Literature Review . . . . .	2
1.2.1 Understanding wet-end chemistry . . . . .	3
1.2.2 Optimising wet-end chemistry . . . . .	14
1.3 Research Objectives . . . . .	26
<b>2 Model Identification</b>	<b>28</b>
2.1 Input-Output Models . . . . .	29
2.1.1 Linear transfer functions family models . . . . .	29
2.1.2 Model comparison and validation . . . . .	32
2.1.3 Cooked example . . . . .	35
2.2 First-Principle Model: Paper Machine . . . . .	37
2.2.1 Mass balances . . . . .	38
2.2.2 Case study: CSPP paper machine . . . . .	40

<b>3</b>	<b>Case Study of Headbox Consistency Control</b>	<b>43</b>
3.1	Experimental . . . . .	44
3.1.1	Pilot paper machine . . . . .	44
3.1.2	Open loop tests . . . . .	47
3.1.3	Models . . . . .	49
3.1.4	Controller synthesis . . . . .	54
3.1.5	Simulation . . . . .	55
3.2	Results . . . . .	60
3.2.1	Setpoint changes . . . . .	62
3.2.2	Provoked disturbances . . . . .	62
3.2.3	Periodicity propagation . . . . .	63
3.2.4	Basis weight . . . . .	67
3.3	Conclusion . . . . .	68
<b>4</b>	<b>Control Strategies</b>	<b>70</b>
4.1	Models . . . . .	70
4.2	Interactions Analysis . . . . .	76
4.2.1	Scaling . . . . .	76
4.2.2	Variables selection . . . . .	78
4.3	Controller Types and Tuning . . . . .	84
4.3.1	Standard controllers . . . . .	84
4.3.2	MPC controller . . . . .	87
4.4	Controller Comparison . . . . .	94
<b>5</b>	<b>Conclusions</b>	<b>100</b>
	<b>References</b>	<b>105</b>
<b>A</b>	<b>Schematics of different wet-end control strategies reported in the literature</b>	<b>111</b>
<b>B</b>	<b>Linear Regression Algorithm</b>	<b>116</b>
<b>C</b>	<b>Identification Data and Models of Paprican Pilot Paper Machine</b>	<b>121</b>
C.1	Headbox consistency models ( $y_1$ ) . . . . .	121
C.1.1	Machine chest valve ( $u_1$ ) . . . . .	122
C.1.2	Fanpump rpm ( $u_2$ ) . . . . .	124
C.1.3	Machine chest flowrate ( $u_3$ ) . . . . .	127
C.2	Headbox flowrate models ( $y_2$ ) . . . . .	130
C.2.1	Machine chest valve ( $u_1$ ) . . . . .	130

C.2.2	Fanpump rpm ( $u_2$ )	133
C.2.3	Machine chest flowrate ( $u_3$ )	137
C.3	Machine chest flowrate models ( $u_3$ )	139
C.3.1	Machine chest valve ( $u_1$ )	140
C.3.2	Small machine chest valve ( $u_4$ )	143
<b>D</b>	<b>Identification Data and Models of CSPP Pilot Paper Machine</b>	<b>147</b>
D.1	Headbox consistency models ( $y_1$ )	148
D.1.1	Machine chest flowrate ( $u_3$ )	148
D.1.2	Fresh filler flowrate ( $u_8$ )	150
D.2	Headbox ash consistency models ( $y_3$ )	154
D.2.1	Machine chest flowrate ( $u_3$ )	155
D.2.2	Fresh filler flowrate ( $u_8$ )	157
D.3	White water consistency models ( $y_4$ )	160
D.3.1	Machine chest flowrate ( $u_3$ )	160
D.3.2	Bentonite flowrate ( $u_5$ )	163
D.3.3	C-PAM flowrate ( $u_6$ )	166
D.3.4	Ratio of bentonite to C-PAM ( $u_7$ )	167
D.3.5	Fresh filler flowrate ( $u_8$ )	171
D.4	White water ash consistency models ( $y_5$ )	174
D.4.1	Machine chest flowrate ( $u_3$ )	174
D.4.2	Bentonite flowrate ( $u_5$ )	176
D.4.3	C-PAM flowrate ( $u_6$ )	180
D.4.4	Ratio of bentonite to C-PAM ( $u_7$ )	182
D.4.5	Fresh filler flowrate ( $u_8$ )	185
D.5	Ash Content models ( $y_8$ )	188
D.5.1	Machine chest flowrate ( $u_3$ )	189
D.5.2	Bentonite flowrate ( $u_5$ )	191
D.5.3	C-PAM flowrate ( $u_6$ )	193
D.5.4	Ratio of bentonite to C-PAM ( $u_7$ )	196
D.5.5	Fresh filler flowrate ( $u_8$ )	198
D.6	Basis weight models ( $y_9$ )	201
D.6.1	Machine chest flowrate ( $u_3$ )	201
D.6.2	Bentonite flowrate ( $u_5$ )	204
D.6.3	C-PAM flowrate ( $u_6$ )	206
D.6.4	Ratio of bentonite to C-PAM ( $u_7$ )	209
D.6.5	Fresh filler flowrate ( $u_8$ )	211

# List of Tables

1.1	Main paper furnish components . . . . .	4
1.2	Smallest dimensions of main paper furnish components . . . . .	5
1.3	Ability of different control methods to dampen the effect of 20% dilution in retention chemical strength . . . . .	18
1.4	Typical paper machine dynamics under feedback control . . . . .	20
1.5	Summary of papers reporting retention control . . . . .	23
2.1	Common parametric models . . . . .	32
2.2	Models retained from the preliminary analysis . . . . .	37
3.1	Sensors values archived for the headbox consistency analysis . . . . .	46
3.2	Definition of models built for analyzing headbox consistency interactions . . . . .	48
3.3	Matrix of Output-Error(1,1) models for the Paprican Paper Machine . . . . .	50
3.4	Matrix of elaborate models for the Paprican Paper Machine . . . . .	52
3.5	Matrix of disturbance models for the Paprican Paper Machine . . . . .	53
3.6	Models between $u_3$ and small valve $u_4$ . . . . .	55
3.7	Estimated period of different signals of the approach system . . . . .	66
4.1	Models for the CSPP paper machine . . . . .	73
4.2	Traditional controller types obtained by direct synthesis method . . . . .	87
4.3	Hard constraints imposed on the manipulated variables . . . . .	93
4.4	MPC tuning parameter values . . . . .	93
4.5	MPC tuning parameter values for MPC 1 implementation . . . . .	95
4.6	Performance of different type of controllers to different perturbations . . . . .	96
C.1	Preliminary models between $y_1$ and $u_1$ . . . . .	124
C.2	Characteristics of the chosen models between $y_1$ and $u_1$ . . . . .	124
C.3	Preliminary models between $y_1$ and $u_2$ . . . . .	127
C.4	Characteristics of the chosen models between $y_1$ and $u_2$ . . . . .	127

C.5	Preliminary models between $y_1$ and $u_3$ . . . . .	130
C.6	Characteristics of the chosen models between $y_1$ and $u_3$ . . . . .	130
C.7	Preliminary models between $y_2$ and $u_1$ . . . . .	133
C.8	Characteristics of the chosen models between $y_2$ and $u_1$ . . . . .	133
C.9	Preliminary models between $y_2$ and $u_2$ . . . . .	136
C.10	Characteristics of the chosen models between $y_2$ and $u_2$ . . . . .	137
C.11	Preliminary models between $y_2$ and $u_3$ . . . . .	139
C.12	Characteristics of the chosen models between $y_2$ and $u_3$ . . . . .	139
C.13	Preliminary models between $u_3$ and $u_1$ . . . . .	142
C.14	Characteristics of the chosen models between $u_3$ and $u_1$ . . . . .	143
C.15	Preliminary models between $u_3$ and $u_4$ . . . . .	145
C.16	Characteristics of the chosen models between $u_3$ and $u_4$ . . . . .	146
D.1	Preliminary models between $y_1$ and $u_3$ . . . . .	150
D.2	Characteristics of the chosen model between $y_1$ and $u_3$ . . . . .	150
D.3	Preliminary models between $y_1$ and $u_8$ for the step up . . . . .	153
D.4	Preliminary models between $y_1$ and $u_8$ for the step down . . . . .	153
D.5	Characteristics of the chosen models between $y_1$ and $u_8$ . . . . .	154
D.6	Preliminary models between $y_3$ and $u_3$ . . . . .	156
D.7	Characteristics of the chosen model between $y_3$ and $u_3$ . . . . .	157
D.8	Preliminary models between $y_3$ and $u_8$ for the step up . . . . .	159
D.9	Preliminary models between $y_3$ and $u_8$ for the step down . . . . .	160
D.10	Characteristics of the chosen models between $y_3$ and $u_8$ . . . . .	162
D.11	Preliminary models between $y_4$ and $u_3$ . . . . .	162
D.12	Characteristics of the chosen model between $y_4$ and $u_3$ . . . . .	163
D.13	Characteristics of the chosen model between $y_4$ and $u_5$ . . . . .	165
D.14	Preliminary models between $y_4$ and $u_6$ . . . . .	169
D.15	Characteristics of the chosen model between $y_4$ and $u_6$ . . . . .	169
D.16	Preliminary models between $y_4$ and $u_7$ for the low range . . . . .	170
D.17	Preliminary models between $y_4$ and $u_7$ for the high range . . . . .	171
D.18	Characteristics of the chosen models between $y_4$ and $u_7$ . . . . .	171
D.19	Preliminary models between $y_4$ and $u_8$ . . . . .	173
D.20	Characteristics of the chosen model between $y_4$ and $u_8$ . . . . .	174
D.21	Preliminary models between $y_5$ and $u_3$ . . . . .	176
D.22	Characteristics of the chosen model between $y_5$ and $u_3$ . . . . .	177
D.23	Preliminary models between $y_5$ and $u_5$ . . . . .	179
D.24	Characteristics of the chosen model between $y_5$ and $u_5$ . . . . .	180
D.25	Preliminary models between $y_5$ and $u_6$ . . . . .	181
D.26	Characteristics of the chosen model between $y_5$ and $u_6$ . . . . .	182



D.27 Preliminary models between $y_5$ and $u_7$ for the low range . . . . .	184
D.28 Preliminary models between $y_5$ and $u_7$ for the high range . . . . .	185
D.29 Characteristics of the chosen models between $y_5$ and $u_7$ . . . . .	185
D.30 Preliminary models between $y_5$ and $u_8$ . . . . .	187
D.31 Characteristics of the chosen models between $y_5$ and $u_3$ . . . . .	188
D.32 Preliminary models between $y_8$ and $u_3$ . . . . .	190
D.33 Characteristics of the chosen model between $y_8$ and $u_3$ . . . . .	191
D.34 Preliminary models between $y_8$ and $u_5$ . . . . .	193
D.35 Characteristics of the chosen model between $y_8$ and $u_5$ . . . . .	193
D.36 Preliminary models between $y_8$ and $u_6$ . . . . .	196
D.37 Characteristics of the chosen model between $y_8$ and $u_6$ . . . . .	196
D.38 Characteristics of the chosen model between $y_8$ and $u_7$ . . . . .	198
D.39 Characteristics of the chosen model between $y_8$ and $u_8$ . . . . .	200
D.40 Preliminary models between $y_9$ and $u_3$ . . . . .	203
D.41 Characteristics of the chosen model between $y_9$ and $u_3$ . . . . .	203
D.42 Preliminary models between $y_9$ and $u_5$ . . . . .	206
D.43 Characteristics of the chosen model between $y_9$ and $u_5$ . . . . .	206
D.44 Preliminary models between $y_9$ and $u_6$ . . . . .	208
D.45 Characteristics of the chosen model between $y_9$ and $u_6$ . . . . .	209
D.46 Preliminary models between $y_9$ and $u_7$ . . . . .	211
D.47 Characteristics of the chosen model between $y_9$ and $u_7$ . . . . .	211
D.48 Preliminary models between $y_9$ and $u_8$ . . . . .	214
D.49 Characteristics of the chosen model between $y_9$ and $u_8$ . . . . .	214

## List of Figures

1.1	Proposed retention mechanisms . . . . .	8
1.2	Adhesion of polymer to filler and fibre . . . . .	10
1.3	Microparticle system floc formation . . . . .	12
1.4	Microparticle system interaction mechanisms . . . . .	13
1.5	Relation between microscopic interactions and macroscopic variables .	15
1.6	An integrated wet-end control strategy . . . . .	25
2.1	Identification data for the cooked example . . . . .	35
2.2	Candidate model . . . . .	36
2.3	Simulated model against the Validation Data . . . . .	38
2.4	Block diagram of the modelled wet-end . . . . .	40
2.5	Pilot Paper machine at the CSPP . . . . .	41
2.6	Effect of CPAM dosage on sheet ash content . . . . .	42
2.7	Effect of filler initial concentration on sheet ash content . . . . .	42
3.1	Schematic of the approach system of Paprican's pilot plant. . . . .	45
3.2	Different control strategies implemented on the pilot paper machine .	56
3.3	Comparison of the response to a setpoint change in headbox consistency of the different control strategies . . . . .	60
3.4	Comparison of the response to a setpoint change in headbox flowrate of the different control strategies . . . . .	61
3.5	Headbox consistency without and with control . . . . .	61
3.6	Headbox consistency setpoint changes . . . . .	62
3.7	Effect of known disturbances on the headbox consistency control loop	63
3.8	Autocorrelogram of the press broke pulper consistency . . . . .	65
3.9	Basis weight of samples . . . . .	68
4.1	Identification data for the model between headbox consistency and CPAM . . . . .	72
4.2	RGA over the frequency range . . . . .	85

4.3	Singular values over the frequency range . . . . .	86
4.4	Calculation flowsheet of MPC algorithm . . . . .	90
4.5	Responses of the different models to step changes in machine chest flowrate . . . . .	92
4.6	Response of controlled and manipulated variables to a step change in filler concentration . . . . .	94
A.1	Retention control . . . . .	111
A.2	Retention and headbox ash control . . . . .	111
A.3	Headbox consistency control . . . . .	112
A.4	White water consistency control . . . . .	112
A.5	White water consistency ratio control . . . . .	112
A.6	White water ash and total consistencies control . . . . .	112
A.7	Ash cascade control . . . . .	112
A.8	Breaktime ash control . . . . .	113
A.9	Feedforward control of thick stock consistency . . . . .	113
A.10	Feedforward control of thick stock ash consistency . . . . .	114
A.11	Cationic demand and white water control . . . . .	114
A.12	Integrated strategy: cascade control for ash and basis weight, and white water consistency control . . . . .	114
A.13	Integrated strategy: white water consistency, basis weight and ash control . . . . .	115
C.1	Identification data for the model between $y_1$ and $u_1$ . . . . .	122
C.2	Candidate models between $y_1$ and $u_1$ . . . . .	123
C.3	Simulation of chosen models between $y_1$ and $u_1$ against the validation data . . . . .	125
C.4	Identification data for the model between $y_1$ and $u_2$ . . . . .	125
C.5	Candidate models between $y_1$ and $u_2$ . . . . .	126
C.6	Simulation of chosen models between $y_1$ and $u_2$ against the validation data . . . . .	128
C.7	Identification data for the model between $y_1$ and $u_3$ . . . . .	128
C.8	Candidate models between $y_1$ and $u_3$ . . . . .	129
C.9	Simulation of chosen models between $y_1$ and $u_3$ against the validation data . . . . .	131
C.10	Identification Data for the Model between $y_2$ and $u_1$ . . . . .	132
C.11	Candidate Models between $y_2$ and $u_1$ . . . . .	132
C.12	Simulation of chosen models between $y_2$ and $u_1$ against the validation data . . . . .	134
C.13	Identification Data for the Model between $y_2$ and $u_2$ . . . . .	134

C.14 Candidate Models between $y_2$ and $u_2$ . . . . .	135
C.15 Simulation of chosen models between $y_2$ and $u_2$ against the validation data . . . . .	136
C.16 Identification data for the model between $y_2$ and $u_3$ . . . . .	137
C.17 Candidate models between $y_2$ and $u_3$ . . . . .	138
C.18 Simulation of chosen models between $y_2$ and $u_3$ against the validation data . . . . .	140
C.19 Identification data for the model between $u_3$ and $u_1$ . . . . .	141
C.20 Candidate models between $u_3$ and $u_1$ . . . . .	141
C.21 Simulation of chosen models between $u_3$ and $u_1$ against the validation data . . . . .	143
C.22 Identification Data for the Model between $u_3$ and $u_4$ . . . . .	144
C.23 Candidate Models between $u_3$ and $u_4$ . . . . .	144
C.24 Simulation of chosen models between $u_3$ and $u_4$ against the validation data . . . . .	146
D.1 Identification data for the model between $y_1$ and $u_3$ . . . . .	149
D.2 Candidate models between $y_1$ and $u_3$ . . . . .	149
D.3 Simulation of chosen model between $y_1$ and $u_3$ against the validation data . . . . .	151
D.4 Identification data for the model between $y_1$ and $u_8$ . . . . .	152
D.5 Candidate models between $y_1$ and $u_8$ . . . . .	152
D.6 Simulation of chosen models between $y_1$ and $u_8$ against the validation data . . . . .	154
D.7 Identification data for the model between $y_3$ and $u_3$ . . . . .	155
D.8 Candidate models between $y_3$ and $u_3$ . . . . .	156
D.9 Simulation of chosen model between $y_3$ and $u_3$ against the validation data . . . . .	157
D.10 Identification data for the model between $y_3$ and $u_8$ . . . . .	158
D.11 Candidate models between $y_3$ and $u_8$ . . . . .	158
D.12 Simulation of chosen models between $y_3$ and $u_8$ against the validation data . . . . .	160
D.13 Identification data for the model between $y_4$ and $u_3$ . . . . .	161
D.14 Candidate models between $y_4$ and $u_3$ . . . . .	161
D.15 Simulation of chosen model between $y_4$ and $u_3$ against the validation data . . . . .	163
D.16 Identification data for the model between $y_4$ and $u_5$ . . . . .	164
D.17 Candidate models between $y_4$ and $u_5$ . . . . .	164

D.18 Simulation of chosen model between $y_4$ and $u_5$ against the validation data . . . . .	165
D.19 Identification data for the model between $y_4$ and $u_6$ . . . . .	166
D.20 Candidate models between $y_4$ and $u_6$ . . . . .	167
D.21 Simulation of chosen model between $y_4$ and $u_6$ against the validation data . . . . .	168
D.22 Identification data for the models between $y_4$ and $u_7$ . . . . .	168
D.23 Candidate models between $y_4$ and $u_7$ . . . . .	170
D.24 Simulation of chosen models between $y_4$ and $u_7$ against the validation data . . . . .	172
D.25 Identification data for the model between $y_4$ and $u_8$ . . . . .	172
D.26 Candidate models between $y_4$ and $u_8$ . . . . .	173
D.27 Simulation of chosen model between $y_4$ and $u_8$ against the validation data . . . . .	174
D.28 Identification data for the model between $y_5$ and $u_3$ . . . . .	175
D.29 Candidate models between $y_5$ and $u_3$ . . . . .	175
D.30 Simulation of chosen model between $y_5$ and $u_3$ against the validation data . . . . .	177
D.31 Identification data for the model between $y_5$ and $u_5$ . . . . .	178
D.32 Candidate models between $y_5$ and $u_5$ . . . . .	178
D.33 Simulation of chosen model between $y_5$ and $u_5$ against the validation data . . . . .	179
D.34 Identification data for the model between $y_5$ and $u_6$ . . . . .	180
D.35 Candidate models between $y_5$ and $u_6$ . . . . .	181
D.36 Simulation of chosen model between $y_5$ and $u_6$ against the validation data . . . . .	182
D.37 Identification data for the models between $y_5$ and $u_7$ . . . . .	183
D.38 Candidate models between $y_5$ and $u_7$ . . . . .	183
D.39 Simulation of chosen models between $y_5$ and $u_7$ against the validation data . . . . .	186
D.40 Identification data for the model between $y_5$ and $u_8$ . . . . .	186
D.41 Candidate models between $y_5$ and $u_8$ . . . . .	187
D.42 Simulation of chosen model between $y_5$ and $u_8$ against the validation data . . . . .	188
D.43 Identification data for the model between $y_8$ and $u_3$ . . . . .	189
D.44 Candidate models between $y_8$ and $u_3$ . . . . .	190
D.45 Simulation of chosen model between $y_8$ and $u_3$ against the validation data . . . . .	191
D.46 Identification data for the model between $y_8$ and $u_5$ . . . . .	192

D.47 Candidate models between $y_8$ and $u_5$ . . . . .	192
D.48 Simulation of chosen model between $y_8$ and $u_5$ against the validation data . . . . .	194
D.49 Identification data for the model between $y_8$ and $u_6$ . . . . .	194
D.50 Candidate models between $y_8$ and $u_6$ . . . . .	195
D.51 Simulation of chosen model between $y_8$ and $u_6$ against the validation data . . . . .	197
D.52 Identification data for the model between $y_8$ and $u_7$ . . . . .	197
D.53 Candidate models between $y_8$ and $u_7$ . . . . .	198
D.54 Simulation of chosen model between $y_8$ and $u_7$ against the validation data . . . . .	199
D.55 Identification data for the model between $y_8$ and $u_8$ . . . . .	199
D.56 Candidate models between $y_8$ and $u_8$ . . . . .	200
D.57 Simulation of chosen model between $y_8$ and $u_8$ against the validation data . . . . .	201
D.58 Identification data for the model between $y_9$ and $u_3$ . . . . .	202
D.59 Candidate models between $y_9$ and $u_3$ . . . . .	202
D.60 Simulation of chosen model between $y_9$ and $u_3$ against the validation data . . . . .	204
D.61 Identification data for the model between $y_9$ and $u_5$ . . . . .	205
D.62 Candidate models between $y_9$ and $u_5$ . . . . .	205
D.63 Simulation of chosen model between $y_9$ and $u_5$ against the validation data . . . . .	207
D.64 Identification data for the model between $y_9$ and $u_6$ . . . . .	207
D.65 Candidate models between $y_9$ and $u_6$ . . . . .	208
D.66 Simulation of chosen model between $y_9$ and $u_6$ against the validation data . . . . .	209
D.67 Identification data for the model between $y_9$ and $u_7$ . . . . .	210
D.68 Candidate models between $y_9$ and $u_7$ . . . . .	210
D.69 Simulation of chosen model between $y_9$ and $u_7$ against the validation data . . . . .	212
D.70 Identification data for the model between $y_9$ and $u_8$ . . . . .	213
D.71 Candidate models between $y_9$ and $u_8$ . . . . .	213
D.72 Simulation of chosen model between $y_9$ and $u_8$ against the validation data . . . . .	214

# Glossary

## Control abbreviations

C : Controller

CV : Control valve

$e$  : controlled error ( $y - r$ )

FF : Feedforward controller

$\gamma$  : matrix condition number

$\lambda$  : closed loop time constant

MPC : Model Predictive Control

PI : Proportional Integral controller

PID : Proportional Integral Derivative controller

$r$  : reference trajectory

RGA ( $\Lambda$ ) : Relative Gain Array

SP : Setpoint

$\sigma$  : matrix singular value

$u$  : manipulated variable

$y$  : controlled variable

## Process abbreviations

AK : Ash consistency  
BW : Basis weight  
C : Concentration (mass / volume)  
CD : Cationic demand  
CPAM : Cationic (Poly)AcrylAmide  
D.E. : Dry-End  
F : Flowrate  
R : First-pass retention  
HB : Headbox  
K : Consistency (%)  
MC : Machine chest  
N/A : Not available  
P : Pressure  
PA : Paper ash  
PBP : Press Broke Pulper  
PCC : Precipitated Calcium Carbonate (filler)  
rpm : revolutions per minute  
V : Volume  
WW : White water



## Model abbreviations

- $A, B, C, D, F$  : model polynomials
- ARX : Auto-Regressive with eXogenous input model
- ARMAX : Auto-Regressive Moving Average  
: with eXogenous input model
- ARARX : Auto-Regressive Auto-Regressive  
: with eXogenous input model
- ARARMAX : Auto-Regressive Auto-Regressive  
: Moving Average with eXogenous input model
- BJ : Box-Jenkins model
- $e$  : noise
- FOPDT : First Order Plus Dead Time model
- FPE : Final prediction error
- $g$  : transfer function model
- $\mathbf{G}$  : matrix of transfer function models
- $k$  :  $k_{th}$  sample time
- $K$  : process gain
- MISO : Multiple Inputs Single Output model
- $N$  : length of data set
- $na, nb, nc, nd, nf$  : order of the model polynomials
- $nk$  : model time delay in samples
- :

OE : Output-Error model  
 $R^2$  : model fit on data  
 $T_s$  : sampling period  
 $\tau$  : process time constant  
 $\theta$  : process time delay  
 $q^{-1}$  : backward shift operator  $q^{-1}y_k = y_{k-1}$   
 $u$  : input variable  
 $u_1$  : machine chest control valve  
 $u_2$  : fanpump speed  
 $u_3$  : machine chest flowrate  
 $u_4$  : small machine chest control valve  
 $u_5$  : bentonite flowrate  
 $u_6$  : CPAM flowrate  
 $u_7$  : ratio of bentonite to CPAM  
 $u_8$  : filler flowrate  
 $y$  : output variable  
 $y_1$  : headbox total consistency  
 $y_2$  : headbox flowrate  
 $y_3$  : headbox ash consistency  
 $y_4$  : white water total consistency  
 $y_5$  : white water ash consistency  
 $y_8$  : sheet ash content  
 $y_9$  : basis weight

# Chapter 1

## Problem Definition

The importance of paper and paper products in everyday life does not need to be emphasised. In 1998, the global consumption of paper and paper products was 28.4 million tons, 20 % of which had been produced in Canada (CPPA 2000). The United Nations Food and Agriculture Organisation has forecasted that by 2010, the world will use a thirty-three percent more paper and paperboard. As the competition amongst the world papermakers becomes more fierce from year to year, Canada must find ways to reduce its production costs. Only then will it be able to profit significantly from this forecasted increase in global paper consumption. It is, therefore, essential to increase the productivity of every mill in order to prevent their forced shutdown. Increased productivity is achieved through process optimisation. Process optimisation is the discipline of driving processes to their peak efficiency operating conditions. Through process optimisation, specific process control objectives are developed. Together, process optimisation and control yield a solution with relatively low capital investment thus helping the Canadian paper industry to gain a much needed competitive edge.

## 1.1 Process Description

Papermaking involves a series of complex processes. This project focuses on the wet-end of paper machines. There are many incentives to study the wet-end and to improve our comprehension of it. Experience has shown that many paper properties are directly influenced by the wet-end operations. Furthermore, it is usually easier to correct a potential problem in the wet-end rather than in the dry-end of the paper machine. Also, papermaking trends such as: the use of mechanical pulps; the increased white water closure; the increased percentage of fillers in paper; the use of recycled pulp with a high content of fines and contaminants; and, of course, cost management have increased the performance requirement of the wet-end and reduced its operating area. Its optimisation becomes a necessity. Furthermore, the wet-end has a direct effect on the basis weight and paper ash content, which are significant properties of paper. Presently, basis weight and ash content are controlled in the dry-end of the paper machine causing a long delay in the feedback loop. Reducing this delay and tightening the variability of the controlled variables would be a major benefit of wet-end optimisation.

To develop optimisation and control strategies for the wet-end of the paper machine, an understanding of the chemical reactions and the interactions between the different papermaking components is necessary. A review of wet-end chemistry and of wet-end control strategies is presented in the following pages. Thereafter, the specific objectives of this project are stated.

## 1.2 Literature Review

Paper machine operations are usually divided into two parts: the dry-end and the wet-end. In the dry-end, the sheet of paper is dried and rolled. In the wet-end, the

web is formed and pressed. To form the paper web, an aqueous cellulose wood fibre suspension is sprayed over the moving wire of the paper machine. Although the two principal components of the paper furnish are fibres and water, there are numerous other components that interact with them. Wet-end chemistry involves studying these interactions.

### 1.2.1 Understanding wet-end chemistry

Table 1.1 presents the main paper furnish components. On a paper machine, water usually constitutes 99 % percent of the slurry. Fillers are added to the paper furnish to reduce cost and/or enhance certain properties (i.e., brightness, opacity, smoothness, gloss, printability, etc.). Often, fillers affect more than one paper property. Electrolytes and surfactants are usually added to maintain the runnability of the machine (i.e., defoamer, retention aids, etc.). These components also affect the paper properties. The electrolyte and polyelectrolyte groups also include detrimental substances. These are commonly defined as being dissolved or colloidal, anionic or non-ionic materials, which adversely affect productivity and paper quality. It is important to remove detrimental substances from the paper machine system because they can: accumulate in the white water system and eventually form deposit on the machine; interfere with papermaking additives; and, increase the cost of the effluent treatment. An effective way of removing detrimental substances from the paper machine system is to retain them on the paper web.

Fines are defined as the portion of the papermaking stock that will pass through a 200-mesh screen (76  $\mu\text{m}$  diameter) excluding soluble and colloidal materials. Fines can be divided in two groups: fibre fines and filler fines. Determining the surface area of the fines allows their interactions on the paper machine to be predicted. It also explains their disproportionate importance in the final paper properties. Fibre

Table 1.1: Main paper furnish components

---

water
fibres
fines
fillers
dissolved electrolytes
surfactants
dissolved polyelectrolytes

---

*Source* : Scott (1991)

fines exhibit two kinds of behaviour. The flexible fibre fines tend to become negatively charged as do fibres, but swell more and absorb more water than fibres. The rigid fibre fines act as fillers in the sheet. According to Scott (1986), the main effects of fines on paper properties can be divided into two groups: direct, and selective adsorption effects. In the direct effects group, fines: reduce sheet strength, reduce drainage rate, reduce system cleanliness, decrease runnability, and improve sheet optical properties. In the selective adsorption effects group, fines accumulate disproportionate amounts of additives, especially cationic additives. This accumulation affects paper properties because: fines retention dictates the additives effectiveness; and, the distribution of fines through the z-direction of the web determines the two-sidedness of the paper. Therefore, the key to maximise the positive effects of fines and to reduce their negative effects is to retain them on the paper web. A measure of this is called the first-pass retention. First-pass retention (R) is defined as the ratio of material that forms the paper web with respect to the total amount of material that was fed to the headbox (see 1.1 and 1.2). (1.2) is usually used in the literature, although (1.1), being derived from a mass balance around the headbox, is more accurate. Using the hypothesis that the flowrate going to the headbox is approximately equal to the one entering the white water pit ( $F_{HB} \approx F_{WW}$ ), (1.2) is obtained. To optimise retention, it is necessary to understand, at least partially, the

interactions between paper furnish components which lead to enhanced retention.

$$R = \frac{F_{HB}K_{HB} - F_{WW}K_{WW}}{F_{HB}K_{HB}} \quad (1.1)$$

$$R = \frac{K_{HB} - K_{WW}}{K_{HB}} \quad (1.2)$$

$$K = \frac{\text{dry solid mass}}{\text{slurry mass}} \times 100 \quad (1.3)$$

where

R First-pass retention

F Flowrate

K Consistency

*HB* Headbox

*WW* White water

## Retention mechanisms

Table 1.2 presents the smallest dimensions of the main paper components. Paper components are colloidal as they are very small particles with large surface areas. The interactions between them will therefore be governed by the colloidal chemistry.

Table 1.2: Smallest dimensions of main paper furnish components

Component	Smallest dimension
Fibre	10-20 $\mu\text{m}$
Fine	1-2 $\mu\text{m}$
Filler	0.1-10 $\mu\text{m}$

*Source* : Scott (1991)

According to colloidal chemistry, particle interactions are governed by the electrostatic charges that accumulate at the surface. Fibres and fines become anionic

in water. They will therefore attract positively charged particles. The strength of the particle interactions will depend on the charge density at the surface of each particle. There is no direct way of measuring this charge. The measuring method currently available utilises the zeta potential. Zeta potential is the electrical potential at the point where the two electrical layers surrounding the particle are touching each other. In the first layer (Stern layer), the electrical field is strong and decreases with increasing distance from the particle. In the second layer (Gouy-Chapman layer), the electrical field is weaker and decreases to zero with increasing distance but at a much slower rate. The zeta potential is, therefore, related to the surface charge and to the strength of interactions between particles.

In papermaking, the different paper constituents must agglomerate to form a paper web. The capacity of the furnish to flocculate will depend on the electrical balance between attractive and repulsive forces and the collision frequency between the different particles. Three different mechanisms are believed to influence the formation of flocs. They are: charge neutralisation, patch, and bridge models.

The charge neutralisation model works by reducing the electrical layers surrounding the particle. To achieve this, cationic particles are added to the solution, thereby reducing the repulsive forces between the particles. Figure 1.1(a) illustrates this mechanism. The patch model works by creating positively charged patches on the anionic surface of the particle. Low molecular weight cationic polymers are added to the solution and adsorbed onto the anionic surface. This positive patch can then form an electrostatic bond with another particle. Figure 1.1(b) illustrates this mechanism. The bridge model works by creating bridges which are large enough to overcome the electrical repulsive layers between particles. To achieve this, high molecular weight cationic polymers are added to the solution. Polymers adsorb onto the anionic surface. Since they are long polymers, they have a tail in the solution

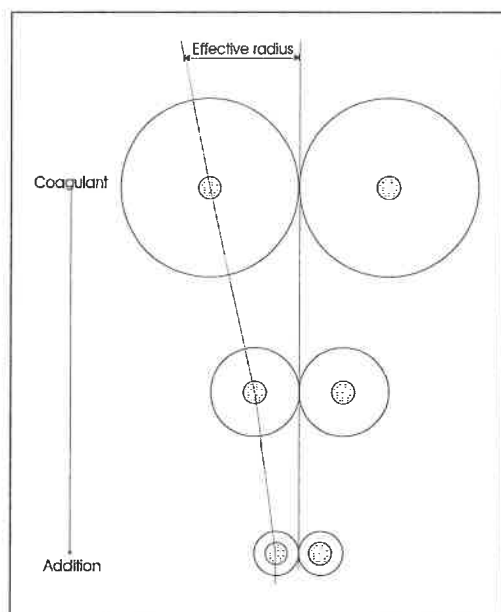


that can adsorb onto another particle, thereby joining the two particles. Figure 1.1(c) illustrates this mechanism.

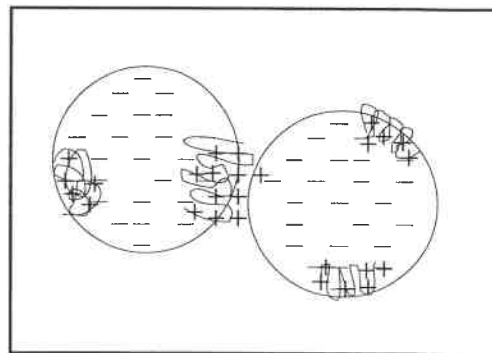
To attain an acceptable retention level on the paper machine, cationic additives are essential. This is easy to deduce from the mechanisms of interactions between particles. These mechanisms are derived from colloidal chemistry theory, and apply to every colloidal system. Little attention has been given to the fact that this solution is the pulp furnish of a paper machine. The main point to consider is that the slurry will be submitted to shear forces. The following paragraphs explain the interactions between the fines, the fibres and the high molecular weight polymeric additives, the most popular retention aid, on the paper machine.

The kinetics of adsorption between polymers and fibres will be governed by the collision frequency of the particles. Shear or diffusion can induce collisions. On a paper machine, shear is the dominant process leading to collisions between polymers and fibres. After a collision, adsorption occurs in a fraction of a second. Polymers also adsorb onto fillers, but at a much slower rate. An important point to consider in the adsorption of the polymer on the fibre surface is the stability of the link. The link is affected by the redistribution of polymers and the polymer reformation.

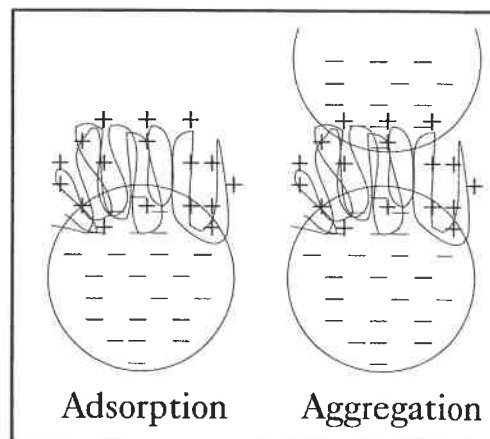
The redistribution of polymers is a mechanism where an adsorbed polyelectrolyte desorbs and diffuses into the solution to be adsorbed onto another particle. This mechanism is diffusion-limited and is very slow on the paper machine. The redistribution of polymers can also be induced by shear. This is commonly referred to as *polymer transfer*. In that case, a filler or a fine has already deposited itself onto a surface of a fibre with adsorbed polymer and a floc has formed. When shear is applied to the suspension, the floc is destroyed. The adsorbed polymer is generally cut in half. Part of the polymer stays on the fibre and the other part on the filler. The final distribution of the polymer in the solution is governed by the charges available



(a) Neutralisation model



(b) Patch model



(c) Bridge model

Figure 1.1: Proposed retention mechanisms

Source a : Chung, Cantrell & Lefevre (1993)

Source b and c : Scott (1992)

on the respective particles which can be roughly approximated by the surface areas of the particles. This explained the importance of fines and fillers since their surface areas are many times that of fibres. It is generally said that the fine surface area is 5 to 10 times that of the fibre.

Polymer conformation is a mechanism that explains the well-known fact that if a retention aid is added much before of the headbox, its efficiency is significantly reduced. This is due to fact that the polymer on the adsorbed surface flattens out from a rather large extension in the solution to a small one. The extended form is more efficient for flocculation. On a typical paper machine, 50 % of the adsorbed polymer molecules will have reformed in approximately 10 seconds. The flocculation capacity of the system will be affected by both the redistribution and the reformation of the polymer.

Flocculation occurs when a filler collides with a fibre-polymer complex. The filler is then adsorbed onto the polymer and a floc is formed. The collisions between fillers and fibres are more numerous than the filler/filler collisions on the paper machine but, nonetheless, there is some filler/filler flocculation happening. The flocculation of fibre and filler is preferred since heterocoagulation gives better sheet formation than homocoagulation (Boardman 1993). On the paper machine, polymer adsorption and filler/fibre collisions are parallel processes.

It is believed that once flocs are formed, the retention aids increase the adhesion of the filler particles to the fibre surfaces. The mechanism proposed to explain this behaviour is shown schematically in Figure 1.2. The polymer chain is folded between the filler and the fibre. Under shear, the polymer chain can act as an elastic. A shorter strand can break the bond (link A on Figure 1.2) between one of its surfaces (either the filler or the fibre). As long as the polymer is not stressed to the point where all of its attachment points have been severed, it will bond the two particles

together. It is believed that retention aids could give sufficient adhesion to withstand most of the shear levels on a paper machine (Swerin & Odberg 1997).

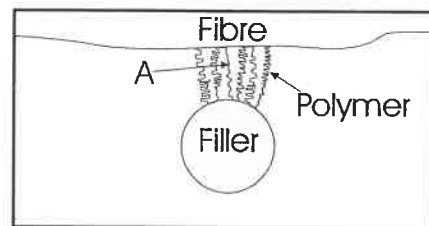


Figure 1.2: Schematic representation of adhesion of polymer to filler and fibre. A: first link to break under paper machine shear.

*Source* : Swerin & Odberg (1997)

It is a well-known fact that the efficiency of cationic polymers as flocculants is low in systems containing high amounts of dissolved anionic polymers (detrimental substances). The reactions between cationic retention aids and anionic polymers can seriously interfere with the flocculation of fillers to fibres since both processes take place on approximately the same time scale.

### **Microparticle retention aid systems**

The retention mechanisms described above involve only one additive: either a charge neutraliser, a low molecular weight cationic polymer, or a high molecular weight cationic polymer. Another widely used retention aid system is the dual microparticle system. Some examples of microparticle retention aid systems are:

- cationic starch and anionic colloidal silica;
- polyacrylamide and anionic montmorillonite;
- polyacrylamide and colloidal silica.

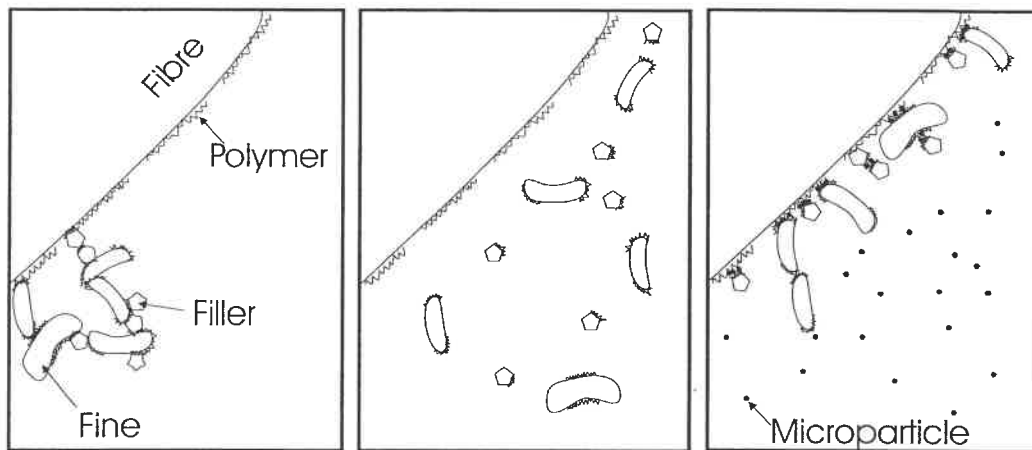
The main differences between microparticle retention aids and traditional one-component retention aid are that:

- microparticle systems are reversible or at least partially reversible retention/dewatering systems;
- microparticle systems often have a positive effect on both retention and drainage in the wire section and on the dewatering in the press section of the paper machine.

The microparticle system is said to be partly reversible because there is significant reflocculation that takes place after the dispersion of a flocculated suspension. This is explained by the flocculation mechanism in microparticle systems. The mechanism is believed to be as follows:

- polymers are adsorbed onto the fibres and fillers; coarse flocs are formed by the bridging mechanism (see Figure 1.3(a));
- the flocs are destroyed under the paper machine shear (see Figure 1.3(b));
- microparticles are added; physical bridges (electrostatic interactions) are formed between microparticle and adsorbed polymers (see Figure 1.3(c)).

This flocculation mechanism is therefore governed by both electrostatic interactions (Figure 1.4, link A) and interparticle bridging (Figure 1.4, link B). Swerin & Odberg (1997) suggested that initial polymeric floc breakage at the high shear level creates a larger number of sites available for interaction with the microparticles. To account for the increase in drainage experienced when microparticle systems are used, they claimed that the stock reflocculates to smaller and denser flocs.



(a) Floc formation by bridging mechanism

(b) Floc destruction under shear

(c) Microparticle floc formation

Figure 1.3: Microparticle system floc formation.

Source : adapted from Swerin & Odberg (1997)

Cho, Garnier, Paradis & Perrier (2001*b*) developed a model to predict filler retention based on the collision efficiency and the surface coverage of the fibres and fines. The model uses a dual-type retention system (cationic CPAM and bentonite). The state of the polymer layer ( original adsorption or transferred) is also included in the model.

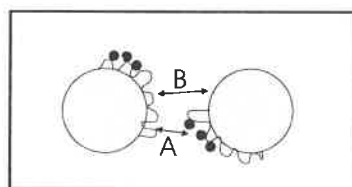


Figure 1.4: Microparticle system interaction mechanisms. A: electrostatic interactions, B: polymer bridging mechanism

*Source* : Swerin & Odberg (1997)

## Retention and formation

Formation is a measure of the quality of the produced sheet of paper. It is therefore very important to assess the effect of increasing the first-pass retention on the paper. It has been shown that it is more difficult to produce a paper with good sheet formation from a stock which exhibits a strong fibre flocculation. In other words, the formation exhibits a close relationship with the degree of flocculation. The fibre network strength is also an important parameter which influences the formation of the paper. The effect of chemical flocculant on fibre network strength is attributed to a combination of an increase in the number of active fibres constituting the network (i.e., to an increase in the average number of contact points per fibre), and an increase in the bonding strength in the fibre-fibre contact points. If the strength of the network is higher, the jet-to-wire ratio must also be higher to obtain good formation.

It is generally recognised among papermakers that a high retention level is often accompanied by an impaired formation. However, this is not necessarily true. One probable explanation is that at strong filler retention levels (above 65-70 %), the retention aid dosage induced a very strong fibre flocculation. One way to compensate for this (i.e. decrease the degree of fibre flocculation) would be to increase the shear during sheet forming. Possible ways to accomplish this are listed below:

- blade forming instead of roll forming (the retention aid system is not strong enough to withstand the high shear force of blade forming);
- increasing the jet-to-wire speed difference (discharge ratio) in twin-wire forming;
- increasing wire tension during blade forming (rearrange flocs and break fibre flocs without major detachment of filler particles).

### 1.2.2 Optimising wet-end chemistry

As we have seen, wet-end chemistry is quite advanced in terms of defining particle interactions. But as far as optimisation is concerned, its knowledge is not sufficient. Wet-end chemistry qualitatively defines the desirable situation: small flocs with a bonding strength that is not too high. There is no recommendation for the desirable size of the floc. Likewise, there is no recommendation for the value of the bonding strength. Therefore, research for the wet-end optimisation began with monitoring the variables that reflect its variability. The wet-end variables can be classified in two groups: input and output variables. The input variables, which account for all the wet-end variability, can be further divided into two groups:

1. Practical determinants (parameters that the papermaker controls);



- Disturbances (parameters that the papermaker cannot control).

The output group can also be divided into two groups:

- Process consequences (process factors: retention, drainage, runnability, etc.);
- Product consequences (product factors: formation, sizing, uniformity, etc.).

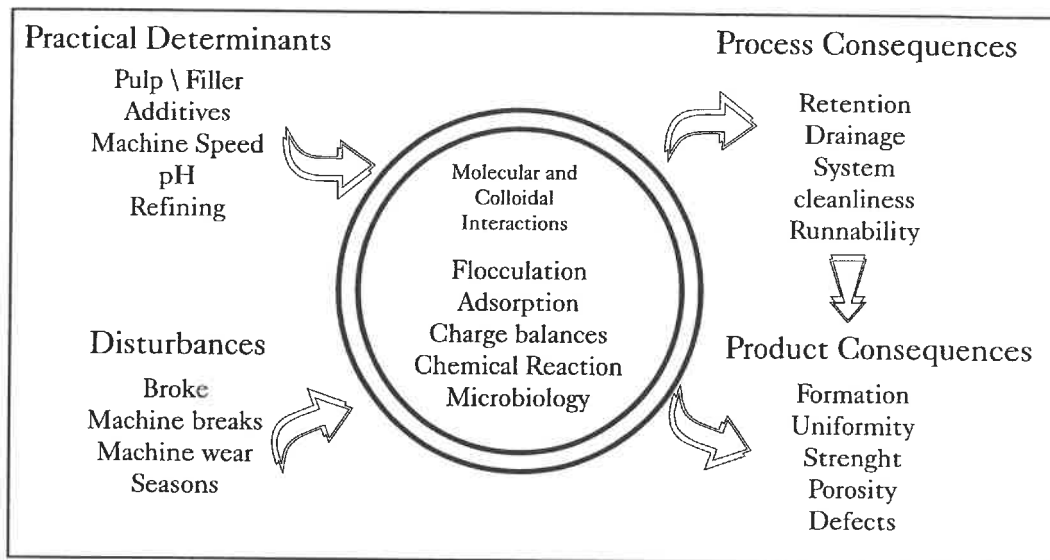


Figure 1.5: Relation between microscopic interactions and macroscopic variables  
*Source : Nazir & Carnegie-Jones (1991)*

Figure 1.5 presents this classification. It can be seen that the input group affects the output group through molecular and colloidal interactions, i.e, wet-end chemistry. A possible optimisation route is to reduce as much as possible the input variability which will in turn reduce wet-end chemistry variability. The first step in wet-end optimisation is to concentrate on one subsystem that will explain most of the wet-end variability and stabilise this key subsystem. There are many variables which could be monitored to reduce wet-end variability: drainage rate, first-pass retention, conductivity, pH, temperature, formation, etc. However, not all of these

variables can be monitored or even controlled. When wet-end optimisation began to be an active research area, most paper machines were already controlling the temperature and the pH. There were no reliable sensors for on-line drainage or formation. Therefore, Nazir & Carnegie-Jones (1991) proposed to monitor first-pass retention because:

1. It is a direct measure of the efficiency of the wire section to retain paper components.
2. It is a direct measure of the efficiency of the retention aid system.
3. It is an indicator of the retention of other additives.
4. It is a measure that connects the chemistry and the process variables. First-pass retention is sensitive to changes in system chemistry and in the level of hydrodynamic shear.
5. It is a measure of the system cleanliness.
6. It is measurable: consistency sensors make it possible to compute first-pass retention.

Since then, many papers have reported the effect of different variables on retention. Their results are based on the analysis of data collected through an on-line system after their mill installed a consistency sensor. Bernier & Begin (1994) concluded that polymer dosage is affected by the basis weight of the paper, the filler type, and the conductivity of the white water. They found that when basis weight increased, the polymer dosage decreased. When the filler surface area was greater, more polymer was needed. When the conductivity was low, less polymer and bentonite were needed. Kortelainen (1991) observed that the retention level is mainly

determined by the basis weight being produced and that the broke addition rate has an important effect on filler retention. This author also mentioned that filler retention is an indicator more sensitive to the wet-end operation than is total retention. Olsson & Renaud (2000) concluded that the dosage of retention aid affected the basis weight and the runnability of the machine. Furthermore, they showed that retention aid overdosing had a negative effect on the machine. Miyanishi, Imamura & Hata (1990) showed that the correlation of first-pass retention and sheet formation depended on the degree of microturbulence created on the paper machine wire. At low microturbulence, the first-pass retention could not be improved without deteriorating the sheet formation. At high microturbulence, it was possible to improve first-pass retention without impairing the formation up to 50%. The effect of zeta potential on the retention has been assessed by several authors (Chung et al. 1993, Brouwer 1991). They concluded that for best performances of the retention system, the zeta potential should be slightly negative. Stitt (1998) stated that care must be taken not to drive the system cationic as it causes: reduction in wet-strength development; excess foam due to free-floating excess wet-strength resin; inconsistent formation and retention; unrecoverable felt filling; and colour variation. Honig, Turnbull & Wheeler (1999) compared the effect of different retention system on the sheet properties. They concluded that sheet properties were mainly affected by the filler, retention, and drainage levels, but were essentially independent of the retention aids at comparable retention and drainage. Cho, Garnier, Paradis & Perrier (2001a) studied the dynamics of filler retention. They concluded that the main factor which affected sheet ash content was first-pass retention of solids and parameters related to the white water short circulation loop. Since the white water network is fixed for a given machine, the first-pass retention becomes an important tool for optimisation.

### White water consistency control

Once the effect of retention aids on retention is quantified, a control system can be put into action. In the beginning of the 1990s, a Finnish group began investigating retention control. From their pilot plant tests, they were able to identify a model and subsequently maintained retention at its nominal operating point. They also investigated the effect of the controlled variable. From their results presented in Table 1.3, they concluded that controlling the white water consistency gave better results than directly controlling the retention. This can easily be explained by (1.1) or (1.2). These equations show that the retention is a ratio of two quantities. It is possible that the two quantities vary simultaneously, thereby keeping the retention constant. But the consistency of each does vary. Thereafter, retention control aims at keeping the white water consistency constant by manipulating the retention aid flowrate.

Table 1.3: Ability of different control methods to dampen the effect of 20% dilution in retention chemical strength

Controlled Variable	Monitored Variables	
	Total Retention	Total Consistency in White Water
Total Retention	76 % response in 18 min	76 % response in 19 min
Ash Retention	83 % response in 13 min	85 % response in 18 min
White Water Total Consistency	94 % response in 10 min	89 % response in 8 min

*Source* : Nokelainen et al. (1993)

The literature has reported many pilot plant trials and subsequent mill implementations where white water consistency control is used to stabilise the wet-end. Many papers suggest an implementation procedure (Rantala et al. 1994*b*, Artama & Nokelainen 1997, Proulx et al. 1999). It could be summarised in four steps. First, retention aid chemical injection points are determined by chemical effectiveness and

can be located anywhere between the machine chest and the headbox. The injection points are very important as they will determine the retention and drainage behaviours. Second, a setpoint mechanism is devised and implemented. Third, the loop is tuned based on a 'bump test' performed under normal operating conditions. If the paper machine is producing many grades, a test must be performed for every grade. The white water consistency sensor must sample fast enough to be representative of the system dynamics. Fourth, limits and alarms are installed. Whenever there is a failure and it is possible, the control loop should switch to manual mode and hold the last retention aid chemical flowrate. There should be:

- a limit on minimum and maximum retention aid dosage;
- an alarm on the white water consistency sensor reading range;
- an alarm on the retention aid pump;
- an alarm on the retention control system to detect any system malfunction.

Renaud, Svensson & Tomicic (1998) and Proulx & Renaud (2000) are the only authors to offer some precision on the speed of sampling of the consistency sensor. They suggest a sampling rate of every minute or so. This sampling rate is considered suitable to control the retention chemical dosage. Table 1.4 shows the rationale behind this recommendation. It can be seen that white water consistency is a relatively slow process, and a sampling rate of one minute is acceptable.

The determination of the setpoint of the consistency has posed some problems. Most authors use the white water consistency that the machine used to have before the control loop was installed as setpoint. Laurikkala, Vuoti, Huhtelin & Koivo (1998) tried to install an automatic setpoint determination algorithm for grade change. Their results were inconclusive. Proulx & Renaud (2000) implemented

Table 1.4: Typical paper machine dynamics under feedback control

Typical dynamics	$\tau$	$\lambda \approx 3\tau$	$T_c \approx \pi\lambda$
Headbox total head	1 sec	3 sec	20 sec
Consistency	5 sec	15 sec	1.5 min
Basis weight	1 min	3 min	20 min
Moisture	2 min	6 min	40 min
White water	5 min	15 min	100 min
Legend:	$\tau$ : process time constant		
	$\lambda$ : closed loop time constant		
	$T_c$ : period at cut-off frequency		

*Source* : Proulx & Renaud (2000)

a percent-applied calculation to automatically adjust the ratio between retention aid dosage and production rate (the thick stock flowrate is used as production rate). In their opinion, this ensures that the system will be responsive to grade and speed changes. But, Kessler, Magee & VanPembrook (2000) disagree. In their implementation, the controller setpoint was initially calculated on production rate. This caused more upsets because the polymer flowrate was reduced when basis weight was lowered. As the lighter basis weight retained less fines, unnecessary oscillations were produced. In the end, the controller setpoint was manually entered by operators.

Today, most mills use a dual retention system offering different possibilities for the manipulated variable, and many authors have presented different solutions. One approach is to manipulate the ratio of the two polymers (Tomney, Pruszyński, Armstrong & Hurley 1998, Rantala et al. 1994b, Cho et al. 2001a). Bernier & Begin (1994) kept the flow of microparticles constant, using only the flow of flocculant as the manipulated variable. Olsson & Renaud (2000) used a strategy where the white water ash consistency controlled the amount of flocculant and the total white water consistency controlled the amount of microparticles. Proulx et al. (1999) proposed to use the flow of flocculant as a manipulated variable for the white water consistency, and the flow of coagulant as a manipulated variable for the dewatering

capability of the headbox furnish (this strategy uses a drainage sensor).

The controller used in most of these papers is a normal PI or PID. It was initially tuned with the 'bump test' model and then fine-tuned on-line. Only Rantala, Tarhonen & Koivo (1993) reported a more complicated model: a MISO-ARX model of the total and ash retention. The total retention was best-fitted with a recursive least-square algorithm to a first-order process. The ash retention was best-fitted to a second order process. The important inputs were: alum, retention polymers, fillers, refining grade, and furnish. This more complicated model has been used to tune a normal PID-controller and the fine tuning was done on-line. Rantala et al. (1994b) used an adaptative PID but they reported no benefit over a scalar PID. Lang et al. (1999) installed a model predictive controller (MPC) on a paper machine. The three-by-three MPC controlled the basis weight, paper ash and white water consistency by manipulating, respectively, thick stock valve, filler flowrate, and retention aid flowrate. They reported an improvement over the single loop strategy for the basis weight and paper ash, but the white water loop performed just as well with a normal PI.

All published papers claimed that retention control helps the runnability and the stability of the paper machine. Various authors have reported a decrease in machine direction basis weight and caliper variations (Nokelainen et al. 1993, Nokelainen & Piirainen 1995, Yeager 1997, Olsson & Renaud 2000). Many authors claimed that retention control reduces the number of web breaks on the paper machine (Nokelainen et al. 1993, Rantala et al. 1994b, Nokelainen & Piirainen 1995, Proulx et al. 1999). Others reported an increase in paper machine speed (Lang et al. 1999, Olsson & Renaud 2000). Also, Yeager (1997) reported reduction in paper cost due to a decrease in steam usage, an increase in ash content, and an optimisation of polymer usage. The white water treatment cost also decreased due to a lower concentra-

tion of fines in the effluent (Kortelainen 1991). Many authors reported a cascade effect reducing the variability of many other wet-end variables (headbox consistency, ash content, and basis weight) after having installed a white water consistency loop (Nokkelainen et al. 1993, Sopenlehto 1995, Proulx et al. 1999, Proulx & Renaud 2000). Recently, combinations of white water control with cationic demand control (stabilisation of the electrical charge of the furnish) have been implemented (Berger 2000, Nokkelainen 2000, Patton & Lee 1993). Berger (2000) did not find any direct relationship between anionic detrimental substance and retention level. However, charge control allows the retention chemicals to better perform. Similarly, Nokkelainen (2000) found that the loops cooperate and gave better results when used together. They also showed that using only charge control does not stabilise the paper machine as much as white water consistency control does.

Table 1.5 presents a summary of the different retention control strategies that have been reported in the literature. The first and second columns present the controlled and the manipulated variables. The superscript in the first column informs on the implementation conditions: a <sup>M</sup> stands for a mill implementation, and a <sup>P</sup> stands for a pilot plant implementation. The third column reports the improvement obtained on the controlled variable variability. For purpose of comparison, the numbers are reported as percentage<sup>1</sup>. When no data is reported, the paper did not present the situation without control. The fifth column gives the name of the authors. The sixth column refers to the figure in Appendix A, where the control strategy is illustrated. In the case when more than one number is reported, the authors used different strategies on different paper machines.

---

<sup>1</sup>Improvement is calculated based on:  $100 \left( 1 - \frac{\text{value with control}}{\text{value without control}} \right)$



Table 1.5: Summary of papers reporting retention control

Controlled	Monitored Variables Manipulated (flowrate)	Reduction in the controlled variable variations	Reference	Figure
Retention <sup>M</sup>	Retention aid		(Piiro & Koivo 1991a)	A.1
HB K <sup>P</sup>	Thick Stock			A.3
Retention <sup>P</sup>	Retention aid 1		(Rantala, Tarhonen & Koivo 1994a)	A.2
HB Ash K <sup>P</sup>	Retention aid 2 Filler	33% (r)		
WW K <sup>M</sup>	Retention aid		(Piiro & Koivo 1991b)	A.4
WW K <sup>M</sup>	Retention aid	81.4 % (s.d.)	(Nokelainen et al. 1993)	A.4
WW K <sup>M</sup>	Polymer	65% (c.o.v)	(Bernier & Begin 1994)	A.4
WW K <sup>M</sup>	Retention aid	80% (r)	(Nokelainen & Piirainen 1995)	A.4
WW K <sup>M</sup>	Cationic Polymer	50% (s.d.)	(Yeager 1997)	A.4
WW K <sup>M</sup>	Polymer	84 % (s.d.)	(Renaud et al. 1998)	A.4
WW K	Flocculant	50% (s.d.)	(Proulx et al. 1999)	A.4
WW K <sup>M</sup>	PAM	44 % (s.d.)	(Olsson & Renaud 2000)	A.4
WW Filler K <sup>M</sup>	PAM	70 % (s.d.)		A.6
WW K <sup>M</sup>	nanoparticle			
WW K <sup>M</sup>	Ratio of retention aids (Compozil)	66% (r)	(Rantala et al. 1994b)	A.5
WW K <sup>M</sup>	ratio of Flocculant and Coagulant	87% (r)	(Tomney et al. 1998)	A.5

Legend: WW : white water, HB : headbox, K : consistency  
<sup>M</sup> : results from a mill, <sup>P</sup> : results from a pilot plant  
(s.d.) : improvement based on standard deviation  
(r) : improvement based on range of variation  
(c.o.v): improvement based on coefficient of variation:  $100(\frac{s.d.}{\mu})$

Table 1.5: (continued)

Monitored Variables Controlled	Variables Manipulated (flowrate)	Reduction in the controlled variable Variations	Reference	Figure
WW K <sup>P</sup>	Polymer	50% (r)	(Rantala et al. 1993)	A.12
HB Ash K <sup>P</sup> HB K <sup>P</sup>	Filler Thick Stock	60% (r)		
Production Rate <sup>M</sup>	Thick Stock	0 %	(Laurikkala et al. 1998)	A.3
WW K <sup>M</sup>	Retention aid	83% (r)		A.4
HB Ash K <sup>M</sup>	Filler	33.3 % (s.d.)		A.7
Thick Stock K <sup>M</sup>	Thick Stock			A.9
Thick Stock K <sup>M</sup>	Thick Stock		(Rantala et al. 1999)	A.9
Thick Stock Ash <sup>M</sup>	Filler			A.10
HB Ash Cons <sup>M</sup>	Filler	56 % (r)		A.8
Cationic demand <sup>M</sup>	Coagulant	50 % (r)		A.11
WW K <sup>M</sup>	Retention aid	60 % (r)		
HB Ash K or			(Lang et al. 1999)	A.13
Paper Ash <sup>M</sup>	Filler	19 % (s.d.)		
WW K <sup>M</sup>	Retention aid	32 % (s.d.)		
Basis weight <sup>M</sup>	Thick Stock	12 % (s.d.)		
Legend:	WW : white water, HB : headbox, K : consistency <sup>M</sup> : results from a mill, <sup>P</sup> : results from a pilot plant (s.d.) : improvement based on standard deviation (r) : improvement based on range of variation (c.o.v): improvement based on coefficient of variation: $100(\frac{s.d.}{\mu})$			

### Integrated wet-end control

From Table 1.5, it can be seen that some strategies combined many control loops (see Figures A.2, A.6, A.11, A.12, and A.13). The obvious goal is to reduce as much as possible wet-end variations to obtain a paper product that meets the customer requirement. One of the first requirements is a constant basis weight. With the actual dry-end loop, where a basis weight sensor modified the thick stock valve

opening, only long variations can be dampened. Wet-end based control does not suffer from the long time delay of the dry-end based control. The strategy is then to integrate wet-end and dry-end control loops (as shown in figures A.12 and A.13).

A more complete strategy has been proposed by Rantala et al. (1999), although they did not implement it, as a whole, on a paper machine. They identified consistency, ash, conductivity, pH, charge and temperature as important variables that explain wet-end variations. The assumption of their strategy is that by keeping those important variables under control, most process upsets will be eliminated. Figure 1.6 shows this strategy, except for temperature control.

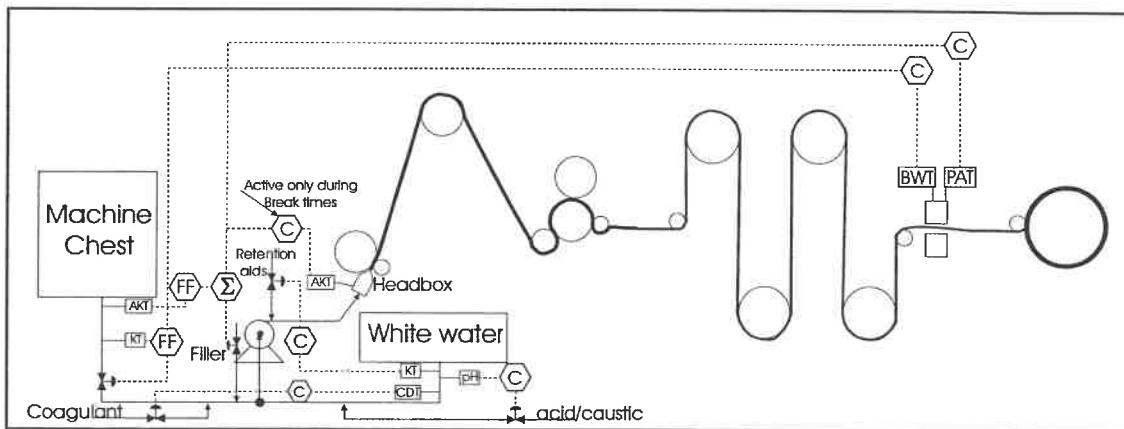


Figure 1.6: An integrated wet-end control strategy  
Source : Rantala et al. (1999)

A machine chest consistency value is given to a feed-forward controller that sets the flow of material going to the headbox according to the setpoint given by the basis weight controller. In this way, fast disturbances are prevented from reaching the headbox. White water consistency is controlled with the flow of a retention aid polymer. To avoid ash content variations during and after breaks, an alternate ash controller is set up to take over during a break; it keeps the headbox ash constant by adjusting the filler flow valve. During normal operation, the ash content is

measured at the dry end and the signal is sent to a summation block. To prevent high frequency disturbances, the machine chest ash content is also measured. This value is sent to a feedforward controller and added to the dry-end ash signal. The result adjusts the filler flow. The main pH control is done in the stock preparation. Adding a pH metre in the short circulation white water loop stabilises the pH value to its setpoint. The cationic demand of white water in the short circulation loop is measured to adjust the flowrate of the coagulant.

The ultimate goal of integrated strategies is to control the wet-end chemistry to such an extent that the paper machine is always operating at the peak level of efficiency. Current scientific knowledge is far from achieving this, but research continues in this field.

### 1.3 Research Objectives

In implementing a control strategy, it is important to assess the interactions among variables. Recent papers have presented advanced wet-end control strategies (Rantala et al. 1999, Lang et al. 1999). The interactions among the manipulated and the controlled variables are, at best, qualitatively defined. For example, in the only MPC application (Lang et al. 1999), the authors have found that white water control did not gain in term of performance over a traditional control. Interaction analysis will allow better comparison between the existing strategies, and will propose new ones, if necessary. Furthermore, it should help in determining which controller is best suited for a particular application.

The objectives for this project are:

- to quantify the interactions among the wet-end manipulated variables and the controlled variables.

The wet-end variables analyzed will be headbox ash and total consistencies,

white water ash and total consistencies. The dry-end variables analyzed will be sheet ash content and basis weight.

- to define and test an integrated control strategy.

The strategy must include variables from the wet-end and the dry-end. The choice between traditional control (PID) and newer control theory (MPC) will also be investigated. The advantages and the performances of each type of controller are going to be studied.

Process models are needed to fulfil the objectives. Chapter 2 will explain which models are going to be used and how they are going to be developed. With the models, it will be possible to test on a paper machine the headbox consistency control loop. This loop could be an inner loop of the basis weight control. Implementation tests are necessary as literature results are inconclusive (Laurikkala et al. 1998). Chapter 3 presents the results of these tests. In Chapter 4, an interaction analysis to discriminate between potential integrated strategies is carried out. Simulation results comparing different controllers are also shown. Finally, a discussion on the implication of the results on wet-end chemistry optimisation is presented.

## Chapter 2

# Model Identification

In order to analyze a process, we must first describe it. Most often, a process is described through the use of a mathematical model. The model will be a simplified version of the process, hopefully, capturing the behaviour under study. There are two main categories of models: first-principles and input-output. First-principles models are based on mass and energy balances around the boundary of the process. They are more general in nature and can efficiently describe category of processes, i.e. all paper machines. They usually incorporate few parameters that contain specific information about the process under study. Input-output models are based on collected data from a particular process. Mathematical functions are then derived from the data. They are relatively easy to construct, can faithfully represent the behaviour of the process; however they are process specific. It is also possible to derive input-output models from first-principles models. However, in this text, input-output models will always refer to mathematical functions derived strictly from data. For this thesis, the two types of models will be used, but only input-output models will be built in this project.

## 2.1 Input-Output Models

To be able to build input-output models, three items must be available:

1. A meaningful data set.
2. A set of candidate models.
3. A rule to select the *best* models.

The procedure is thoroughly explained by Ljung (1999). A summary relevant to this project is as follows. For more details and mathematical proofs, the reader is referred to Ljung's book. A meaningful data set simply means that the data is informative enough to provide a model that is close to the *true process*. It also encompasses the notion of uniqueness of model. To meet this criterion, the data was collected during specially designed experiments where each inputs were, in turn, excited. When such experiments were not available, the data was chosen in order to have an excited input. The next two points on the identification list are explained in more details in the following sections.

### 2.1.1 Linear transfer functions family models

A general representation of an input-output model is given in (2.1).  $y$  represents the output variable of interest and  $u$  represents input variables that affect  $y$ . This representation assumes that the  $y_k$  and  $u_k$  sequences are centred around their mean, and the  $e$  sequence represents white noise. The subscript  $k$  represents discrete points in time. Formally, one should write  $k_{\Delta t}$  with  $k = 1 : N$ . For simplicity, the  $\Delta t$  will be omitted and the length of the sequence will always be considered  $N$ .

$$y_k = G(q^{-1})u_k + H(q^{-1})e_k \quad (2.1)$$

where

$y_k$	output variable
$u_k$	input variable
$e_k$	noise, usually assumed white

The system identification task is to define the functions  $G(q^{-1})$  and  $H(q^{-1})$ . Two types of models can be used to approximate these functions: nonparametric and parametric. In this study, it was decided to concentrate on parametric models as imposing a model structure leads to fewer parameters. Furthermore, these models are better suited for controller synthesis. However, this leaves the difficult task of choosing a model structure. A very well-known approximation is to use a rational function as in (2.2). The parameters of the models can be solved by linear regression techniques (minimisation of the distance between the model and the data, see Appendix B for more details). With the linear regression techniques and statistical theory, the parameters can be shown to converge to the *true model* if the set is large enough (as  $N \rightarrow \infty$ ). The model's statistical properties are based on the input spectrum, and on the independence of the input and noise sequences. In most cases, it is very difficult to fulfill these requirements. But, as the *inventor* of this technique concluded:

In conclusion, the principle that the sum of the squares of the differences between the observed and the computed quantities must be minimum may, in the following manner, be considered independently of the calculus of probabilities. (Gauss 1809)

This family of models can also provide an error model. This can become useful if it is seen as a process disturbance model. Furthermore, this family is general enough to accurately describe many different types of linear processes. The processes under



study are non-linear. They will be approximated in their operating regions as linear models. At the validation stage, this assumption will be easily verified with the agreement between the data and model predictions.

$$A(q^{-1})y_k = \frac{B(q^{-1})}{F(q^{-1})}u_k + \frac{C(q^{-1})}{D(q^{-1})}e_k \quad (2.2)$$

where

$$A(q^{-1}) = 1 + a_1q^{-1} + a_2q^{-2} + a_3q^{-3} + \dots + a_{na}q^{-na} \quad (2.3)$$

$$B(q^{-1}) = b_1q^{-1} + b_2q^{-2} + b_3q^{-3} + \dots + b_{nb}q^{-nb} \quad (2.4)$$

$$C(q^{-1}) = 1 + c_1q^{-1} + c_2q^{-2} + c_3q^{-3} + \dots + c_{nc}q^{-nc} \quad (2.5)$$

$$D(q^{-1}) = 1 + d_1q^{-1} + d_2q^{-2} + d_3q^{-3} + \dots + d_{nd}q^{-nd} \quad (2.6)$$

$$F(q^{-1}) = 1 + f_1q^{-1} + f_2q^{-2} + f_3q^{-3} + \dots + f_{nf}q^{-nf} \quad (2.7)$$

Once the structure of the model has been chosen, the model builder must specify the number of parameters ( $na$ ,  $nb$ ,  $nc$ ,  $nd$ ,  $nf$ ) in each polynomial. Furthermore a delay of time  $nk$  can exist between the input and output. In this case, (2.2) can be rewritten as (2.8).

$$A(q^{-1})y_k = q^{-nk} \frac{B(q^{-1})}{F(q^{-1})}u_k + \frac{C(q^{-1})}{D(q^{-1})}e_k \quad (2.8)$$

Equation (2.8) is very general and seldom used in practice: testing all of the combinations for a given total number of parameters requires important computer power. Instead a parametric model derived from (2.8) is usually able to accurately represent the process. Table 2.1 lists such models. In the proceeding pages, when referring to different model, the abbreviation will be used. It will be followed, in parenthesis, by the number of parameters used for each polynomial, in alphabetical order.

Table 2.1: Common parametric models

Name of the model	Abbreviation	Polynomials of (2.8) used
Output-Error Model	OE( $nb, nf$ )	$B(q^{-1}), F(q^{-1})$
Autoregressive Model with Exogeneous Input	ARX( $na, nb$ )	$A(q^{-1}), B(q^{-1})$
Autoregressive Moving Average Model with Exogeneous Input	ARMAX( $na, nb, nc$ )	$A(q^{-1}), B(q^{-1}),$ $C(q^{-1})$
Autoregressive Autoregressive Model with Exogeneous Input	ARARX( $na, nb, nd$ )	$A(q^{-1}), B(q^{-1}),$ $D(q^{-1})$
Autoregressive Autoregressive Moving Average Model with Exogeneous Input	ARARMAX( $na, nb, nc, nd$ )	$A(q^{-1}), B(q^{-1}),$ $C(q^{-1}), D(q^{-1})$
Box-Jenkins Model	BJ( $nb, nc, nd, nf$ )	$B(q^{-1}), C(q^{-1}),$ $D(q^{-1}), F(q^{-1})$

### 2.1.2 Model comparison and validation

After having decided on a set of models, a method to choose the *best* one is necessary. In order to do so, a definition of *best model* is needed. To avoid long philosophical discussions, *best* will simply be defined as a model that fulfills its purpose. The objective of this project is to build models that can represent well enough the process such that a controller can be designed from them. The model needs not to be the *real* process description although it would be preferable. One way of selecting models could be to draw a graph and visually pick the *best* one. However, a more automatised way would be better. In the parameter estimation method, the prediction error is minimised. It could easily be used to compare different models estimated from the same data set and with the same total number of parameters ( $na + nb + nc + nd + nf$ ). To select between models with different number of parameters, the prediction error needs to be corrected. Each model computed will be

giving a Final Prediction Error (FPE) which is the prediction error corrected by the number of parameters. (2.9) presents the mathematical formulation (Ljung 1999, p.504).

$$\text{FPE} = \frac{1 + \frac{d_M}{N}}{1 - \frac{d_M}{N}} \frac{1}{N} \sum_{k=1}^N (y_k - \hat{y}_{k,\theta})^2 \quad (2.9)$$

where

$d_M$  total number of estimated parameters

$N$  length of data set

$\hat{y}_{k,\theta}$  estimated output value

The FPE is calculated with the data from which the model was built. To assess the quality of the model, it is important to see how the model can reproduce an entire new output sequence from its input sequence. Therefore, every data set will be separated into two parts: an identification sequence and a validation sequence. The models will be compared with this validation sequence in which the reproduction of the output data will be attempted. Again, visual agreement can be used to select the model. But, (2.10) is preferred (Ljung 1999, p.500). It yields a measure of the output variation that is explained by the model. However, using numerical procedures can lead to a rather complicated model that explains the noise instead of the process. Therefore, the *best* model will always be graphed to visually verify over-fitting of noise. An other useful way of verifying overfit is to ensure that the model's poles and zero do not cancel.

$$R^2(\%) = 100 \left( 1 - \frac{\frac{1}{N} \sum_{k=1}^N |y_k - \hat{y}_{k,\theta}|^2}{\frac{1}{N} \sum_{k=1}^N |y_k|^2} \right) \quad (2.10)$$

Both the FPE and fit ( $R^2$ ) do not rely on any statistical feature of the models. The above analysis is valid even if the linear regression did not give the *true* model.

The linear regression method guarantees that the model is the correct model if: the data set is large; the input sequence and the noise are independent; and, the noise is white. The verification of these assumptions is a good way of selecting between the models. White noise is defined as a sequence of uncorrelated identically distributed random variables with zero mean. Therefore for each model, the residuals sequence will be calculated (2.11). Then, the auto-correlation and the cross-correlation with the input sequence will be calculated. A model that better follows the linear regression assumptions will be favoured. When the linear regression assumptions are fulfilled, parameters standard deviation becomes available. These standard deviations could be used to compare models. I choose not to use this information as it was not always available. But, when available, the parameter statistical range was verified not to contain zero. If the range contains zero, the parameter can be eliminated. Therefore, a model with a parameter value equal to zero is not chosen. Lastly, the residuals are used to build another model. The model error model can give useful information about the dynamics that are not explained by the model. More importantly, it can assess if any dynamics were left out. The error model will be estimated as a Finite Impulse model (using polynomial  $B(q^{-1})$  with  $nb = 69$  of 2.8). The model quality will be assessed by looking at its fit ( $R^2$ ) on the residuals.

$$\varepsilon_{k,\theta} = y_k - \hat{y}_{k,\theta} \quad (2.11)$$

In case of equivalent models, the simplest model will always be kept. Higher order models are more troublesome to use in simulation and control design. It is important to remind oneself that the quality of the resulting model will be dependant on the input quality: did the input affect the output, did the input excite the system enough to force it to show its properties, and is the input informative enough to validate and invalidate the candidate models? Finally, it is important to stress that model selection is a subjective matter.

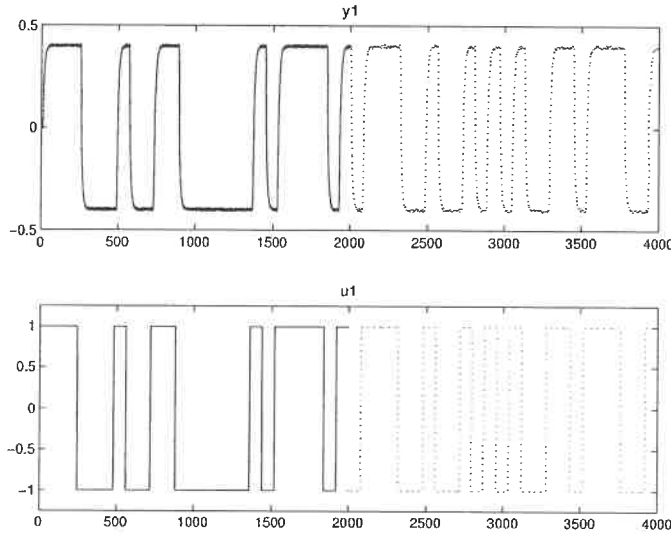


Figure 2.1: Identification data for the cooked example

### 2.1.3 Cooked example

In order to test the above method and assess its effectiveness, an example was computed. An arbitrary stable process with 3 poles and 1 zero was chosen (2.12). An output signal was generated by submitting the system to a pseudo-random binary sequence (PRBS) of 50 steps (-1 or 1), spread equally over 2000 seconds at a sampling rate of 0.5 second. Noise was added in the form of random number between -0.01 to 0.01. Figure 2.1 shows the identification data. The first part of the signal is used for identification and the second part for validation. In this example, the data is already centred around zero. When this is not the case, the mean is removed.

$$\frac{y}{u} = \frac{0.4(0.5s + 1)e^{-5s}}{3s^3 + 4s^2 + 5s + 1} \quad (2.12)$$

Due to a priori knowledge of the process and to reduce simulation time, the maximum number of parameters allowed for a model was 10. A total of 1002 different models were calculated corresponding to the different combinations of models presented in Table 2.1. Figure 2.2 presents the FPE (the bar plot) and the fit (the line

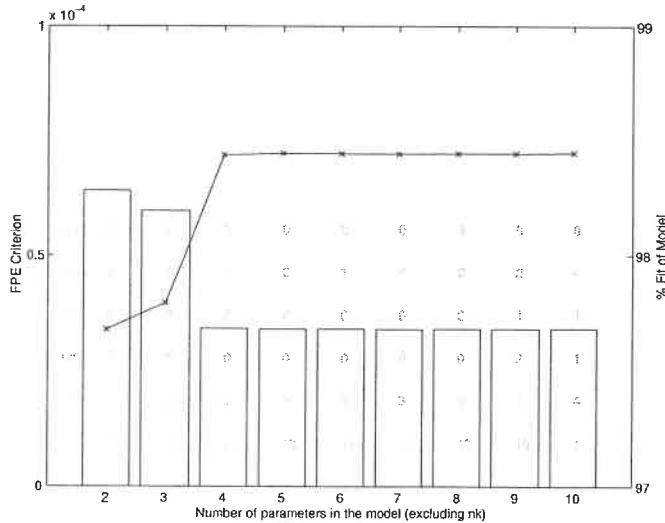


Figure 2.2: Candidate model

plot) of the *best* models for each different total number of parameters. The model retained for comparison is the *best* model amongst the ones with the same number of parameters (smallest FPE, greatest fit). Inside the bar, from top to bottom are the respective values of  $na$ ,  $nb$ ,  $nc$ ,  $nd$ ,  $nf$ ,  $nk$ .

From Figure 2.2, we can see that all the models represent quite well the data. However, there is not much improvement after adding the sixth parameter. Therefore, the following analysis will try to discriminate between the models with 4, 5 and 6 parameters. Table 2.2 presents the models and their parameter values.

The pole-zero map calculated by Matlab System Identification Toolbox is analyzed to make sure that no pole-zero cancellation occurred. In the present case, models OE(1,3) and OE(1,5) do not have zero. The remaining one does not have a pole-zero cancellation. The auto-correlation of the residuals and the cross-correlation between the residuals and the inputs are computed. For the three model structures, the correlations showed white noise within a 99 % confidence interval. An impulse error model was then computed. As expected, the error-model fit was very low (re-

Table 2.2: Models retained from the preliminary analysis

Model Name	Model
OE(1,3)	$y = \frac{0.01132q^{-11}}{1-2.249q^{-1}+1.823q^{-2}-0.5462q^{-3}}u + e$
OE(2,3)	$y = \frac{-0.001075q^{-10}+0.013q^{-11}}{1-2.228q^{-1}+1.797q^{-2}-0.5389q^{-3}}u + e$
OE(1,5)	$y = \frac{0.009345q^{-11}}{1-2.661q^{-1}+3.02q^{-2}-1.909q^{-3}+0.7166q^{-4}-0.1438q^{-5}}u + e$

spectively 2.7999, 2.4067, and 2.4458 %). Since these models are almost equivalent, the simplest one is chosen. Comparing this estimate with the real process, we can see that the delay and the pole were correctly estimated. The estimated model has 2 zeros compared with 1 for the real process. But, since the zero is in the left half plane, its influence is small and difficult to correctly pick by the identification procedure. Figure 2.3 presents the simulation of the chosen model against the validation data. Such a good agreement is expected as the model set contains the *true process*.

## 2.2 First-Principle Model: Paper Machine

To be able to build first-principle models, the following definitions must be available:

1. Model objectives.
2. System boundaries.
3. Knowledge of the inner-working of the process.

Usually, item 3 is never complete. The engineering practise is to impose some assumptions on the model. The resulting model is valid inside those assumptions. To

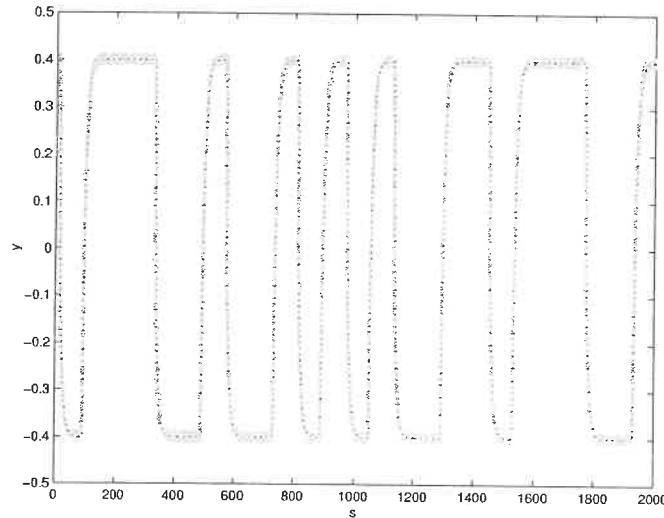


Figure 2.3: Simulated model (black line) against the Validation Data (grey line)

develop a model for the paper machine, its operations can be divided in three parts: formation section and press section (wet-end) and drying section (dry-end). Defining and testing control strategies between the wet-end and the dry-end is the purpose of this model. The control strategies must include wet-end chemistry knowledge to be representative of today's paper machine operations. Most wet-end chemistry interactions occur at the formation section. This section must be included in the model. The press and drying sections mainly remove water. To keep the generality of the desired model, only the very important features of the paper machine must be included. Furthermore, a simple model is preferred as it can always be expanded at a later time. Cho et al. (2001a) developed such a model which is presented below.

### 2.2.1 Mass balances

The model focuses on the section of the short circulation of white water. The selected system is the paper machine with a simplified flow sheet. The approach system (machine chest, screen, cleaners,...) is neglected. The recycling tanks (pulper, savealls,



couch pit, ...) are also neglected except for the white water wire pit. The press and drying sections are also neglected. In this model, the sheet leaves as wet web. Ash content and basis weight are then calculated. The resulting flowsheet is presented in Figure 2.4. Performing mass balances around each block determines the model. In the following equations, the exponent  $i$ , represents fibres, fines or fillers as each equation is written for each component. The headbox level is assumed constant. Then, the headbox operations are modelled with 2.13 and 2.14. The mass flowrate of bentonite and C-PAM are negligible compared to the other flowrates, and are not included in the model.

$$F_2 = F_8 + F_1 + F_5 \quad (2.13)$$

$$V_{HB} \frac{dC_2^i}{dt} = F_1 C_1^i + F_8 C_8^i + F_5 C_5^i - F_2 C_2^i \quad (2.14)$$

Since the wire exact operations are unknown, a model parameter is introduced to overcome this difficulty. The parameter chosen to model the wire is  $R^i$ , first-pass retention (2.15). This parameter also represents wet-end chemistry as it is affected by: the type and dosage of retention aids, pH, cationic demand, conductivity and refining degree (Cho et al. 2001a).

$$R^i = \frac{F_3 C_3^i}{F_2 C_2^i} = \frac{F_2 C_2^i - F_4 C_4^i}{F_2 C_2^i} \quad (2.15)$$

The wire pit operations are modelled using (2.16). Its volume  $V_{wp}$  is assumed constant and its concentration is assumed to be uniform.

$$\begin{aligned} V_{wp} \frac{dC_5^i}{dt} &= F_4 C_4^i - F_5^i C_5^i - F_6 C_5^i \\ V_{wp} \frac{dC_5^i}{dt} &= F_2 C_2^i (1 - R^i) - F_5 C_5^i - F_6 C_5^i \end{aligned} \quad (2.16)$$

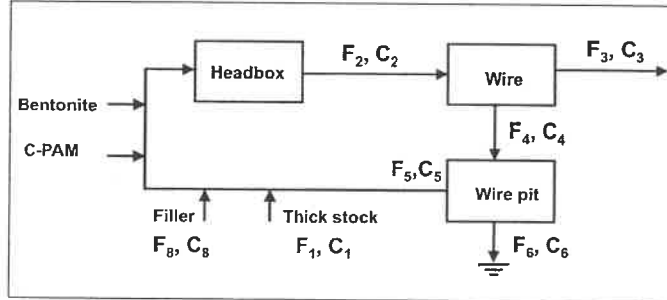


Figure 2.4: Block diagram of the modelled wet-end  
*Source : Cho et al. (2001a)*

To customise this model to a certain machine, it is necessary to have the volume of its wire pit and the values of  $R^i$ . In order to do so, the  $R$  parameters is fitted to 2.17 using the mass flowrates of variables affecting the retention. Therefore to compute it, the different mass flowrates must be available. Also, the consistencies (fiber, fine, fillers) of the white water must be known to evaluate  $R^i$ . Retention values are computed assuming  $F_2 \approx F_4$ , therefore, using (1.2).

$$R^i = \sum_{i=0}^n a_i (M_{HB}^{pulp})^i + \sum_{j=0}^m b_j (M_{HB}^{filler})^j + \sum_{k=0}^p a_k (M_{HB}^{polymer})^k + \sum_{l=0}^q a_l (M_{HB}^{filler})^l \quad (2.17)$$

### 2.2.2 Case study: CSPP paper machine

The model was tested on the pilot paper machine of the Centre Spécialisé en Pâtes et Papier (CSPP) of Cégep de Trois-Rivières (Figure 2.5). This is a fourdrinier-type machine, 76 cm wide, with an opened headbox. Its operating speed is 40 m/min. The pulp used consisted of hardwood bleached Kraft pulp (70 %) and softwood bleached Kraft pulp (30 %). The fines contents was 5.6 %. The filler type used was precipitated calcium carbonate (PCC). CPAM and bentonite were used as retention additives. Step changes were sequentially applied on CPAM dosage, bentonite dosage, filler initial concentration, and pulp flow.

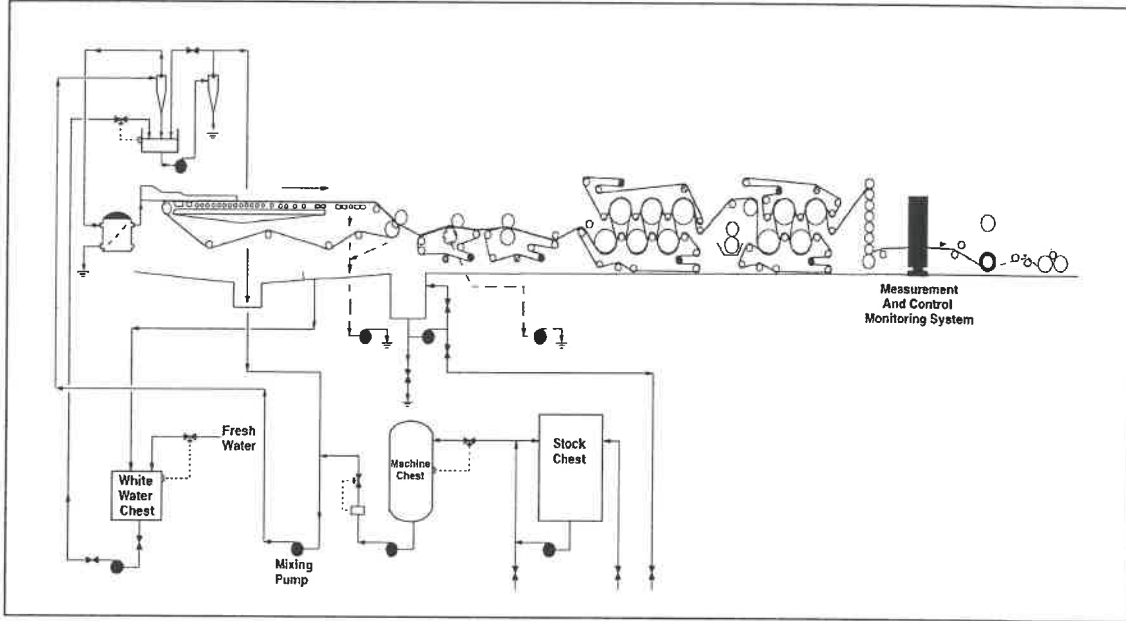


Figure 2.5: Pilot Paper machine at the CSPP

The model was built in Matlab Simulink. Figure 2.6 presents the model response to step change in CPAM dosage. This figure also compares the model response to the data. The model ash content is calculated with 2.18. The data ash content was measured on-line with an ACCURAY 1190-ABB sensor. We can see that the model is able to follow the dynamics quite well. Figure 2.7 presents the sensor and model ash content to change in initial filler concentration (PCC). Again, the model shows good agreement with the data. The model is particularly good in modelling the static non-linearities. In conclusion, this model can be used to discriminate between candidate control strategies.

$$\text{Ash Content (\%)} = 100 \frac{C_3^{filler}}{C_3^{fibre} + C_3^{fines} + C_3^{filler}} \quad (2.18)$$

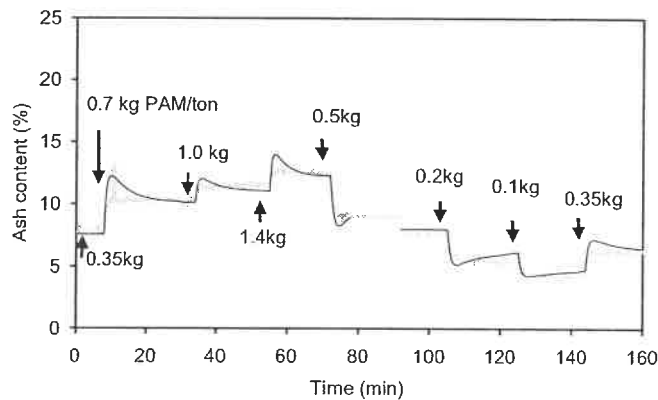


Figure 2.6: Effect of CPAM dosage on sheet ash content. The grey line represents the data and the black line, the model.

*Source : Cho et al. (2001a)*

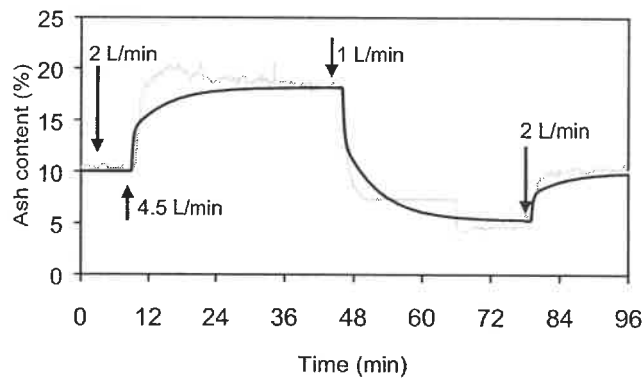


Figure 2.7: Effect on filler initial concentration on sheet ash content. The grey line represents the data and the black line, the model.

*Source : Cho et al. (2001a)*

## Chapter 3

# Case Study of Headbox Consistency Control

In the literature review (1.2.2), we have seen that most of the possible combinations between controlled variables and manipulated variables have been tested on paper machines, and have shown to give good results. It will be possible to compare simulation results with literature knowledge. But, in the only reported attempt to control headbox consistency (Laurikkala et al. 1998), the authors stated that no benefits are gained over traditional dry-end control. However, it is a well-known fact that paper machine basis weight control suffers from the long delay between the wet and dry ends of the machine. Rantala et al. (1999) have proposed to integrate wet-end and dry-end loops to improve basis weight control. Feedforward control of machine chest consistency combined with the basis weight setpoint fixed the opening of the machine chest valve (or flow). This combination prevents consistency disturbances to reach the headbox because the feedforward controller compensates for them. The machine used for this case study does not have a consistency sensor on the machine chest. Even if previous results are inconclusive, we propose to cascade the basis weight control loop with a headbox consistency loop. We will then be able to compare any combinations of input and output variables with paper

machine results. The objective is to use the basis weight measure as a set point for the consistency loop. The inner controller will keep the consistency stable by manipulating the thick stock flow valve. Before implementing this strategy, the inner loop performance must be determined.

This chapter addresses the problem of implementing a headbox consistency control on Paprican Pilot Paper Machine, Pointe-Claire, Canada. There is another incentive for closing this loop on the pilot paper machine: many trials do not need dry paper, and running only the wet-end is cost effective. But to reproduce industry conditions, the basis weight of the sheet must be kept constant. To this aim, step tests were made to obtain a simplified model of the important variables affecting headbox consistency. First estimates of PI controller parameters were obtained and fine tuned on-line. The controller was tested with step changes and intentional disturbances. It was able to maintain the headbox consistency at its setpoint.

## 3.1 Experimental

### 3.1.1 Pilot paper machine

Paprican's pilot paper machine is a twin-wire type with three roll presses followed by a shoe press. The second press is necessary to transfer the sheet, all of the others are optional. Its operational speed is 1000 m/min (max: 2500 m/min). The sheet is 20 inches wide at the headbox and between 12 and 14 inches wide at the wet-sampler. With all chests full, the machine can continuously produce paper at 1000 m/min for 3h30. The normal basis weight is between 45-50 g/m<sup>2</sup>. The minimum and maximum produced on this machine is 18 and 86 g/m<sup>2</sup> respectively. Figure 3.1 shows a schematic diagram of the pilot machine approach system (level control is not shown). The consistency and the level are controlled for every stock tanks, pulpers, and couch pit. The machine chest level and consistency are not

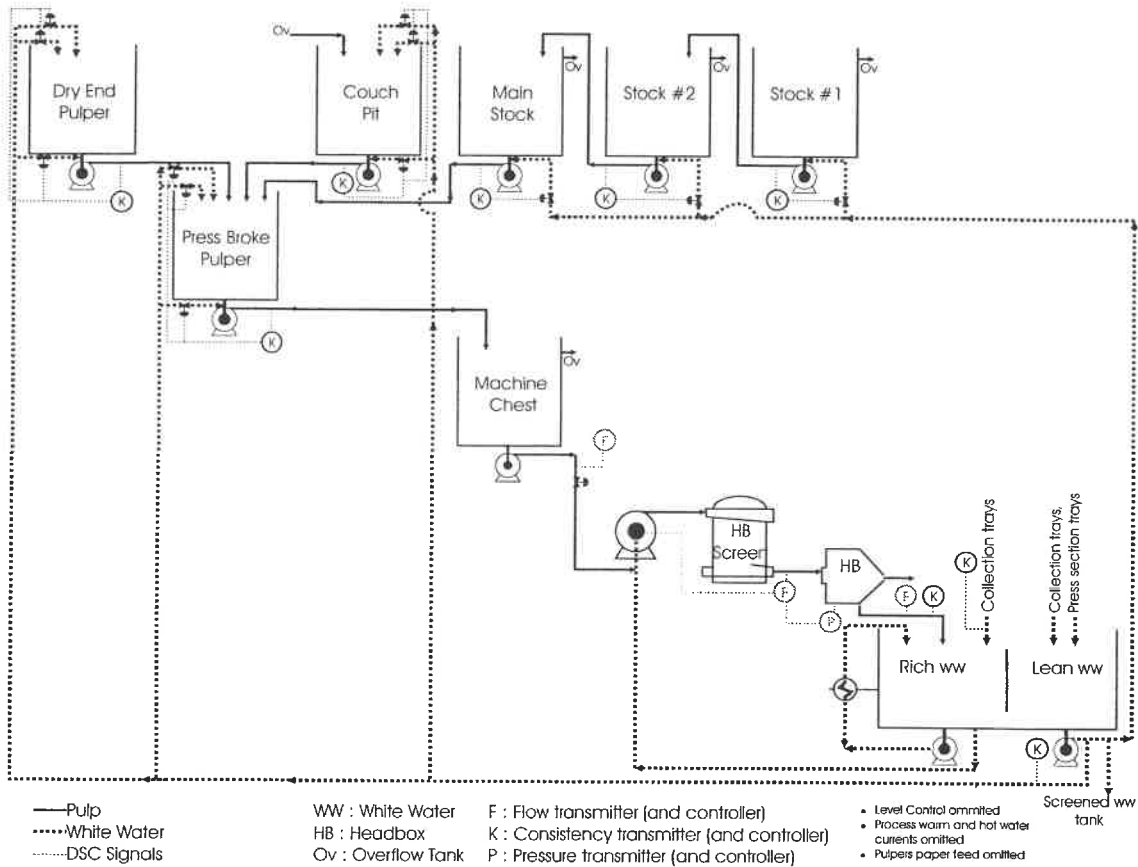


Figure 3.1: Schematic of the approach system of Paprican's pilot plant.

controlled. For every test run (except when sampling), the machine was running on full recycle. The machine is equipped with two KajaaniRMI sensors located on the headbox recirculation and on the first white water tray. Every sensor is connected to a Toshiba MCS-1200 distributed control system. Over 100 points are archived with PI version 3.2 of OSI Software. For this study, over 30 points of interest (consistency, flowrates, valve positions, etc.) were collected at an interval of 1 sec in PI software (see Table 3.1).

Table 3.1: Sensors values archived for the headbox consistency analysis

Sensor Number	Description	Unit
KV_761_576	Couch Pit Consistency CV #1	%
KW_761_577	Couch Pit Consistency CV #2	%
KV_761_578	Couch Pit Consistency CV #3	%
KTSP_761_575	Couch Pit Consistency SP	%
KT_761_575	Couch Pit Consistency Transmitter	%
KW_761_601	D.E. Pulper Consistency CV#1	%
KV_761_602	D.E. Pulper Consistency CV#2	%
KV_761_603	D.E. Pulper Consistency CV#3	%
KTSP_761_600	D.E. Pulper Consistency SP	%
KT_761_600	D.E. Pulper Consistency Transmitter	%
FT_761_110	Fan Pump #1 Feed FLOW	L/MIN
SY_761_055	Fan Pump #1 Speed Control	%
KV_761_055	HB Feed #1 Consistency CV	%
KTSP_761_055	HB Feed #1 Consistency SP	%
HB_TOT_CONSIS	HB Feed #1 Consistency Transmitter	%
FTSP_761_055	HB Feed #1 Flow SP	L/MIN
FT_761_055	HB Feed #1 Flow Transmitter	L/MIN
FT_770_011	HB to Rich WW SILO	L/MIN
PT_770_001	HB Pressure Transmitter	psi
KT_710_060	Lean WW Silo Consistency Transmitter	%
KV_761_255	Main Stock Chest Consistency CV	%
KTSP_761_255	Main Stock Chest Consistency SP	%
KT_761_255	Main Stock Chest Consistency Transmitter	%
KV_761_552	Pressbroke Pulper Consistency CV#1	%
KV_761_553	Pressbroke Pulper Consistency CV#2	%
KW_761_551	Pressbroke Pulper Consistency CV#3	%
KTSP_761_550	Pressbroke Pulper Consistency SP	%
KT_761_550	Pressbroke Pulper Consistency Transmitter	%
WW_TOT_CONSIS	Rich WW Silo Consistency Transmitter	%
KV_761_155	Stock Tank#1 Consistency CV	%
KTSP_761_155	Stock Tank#1 Consistency SP	%
KV_761_205	Stock Tank#2 Consistency CV	%
KTSP_761_205	Stock Tank#2 Consistency SP	%
KT_761_205	Stock Tank#2 Consistency Transmitter	%



### 3.1.2 Open loop tests

To better design control strategies, it is important to understand the interactions between the controlled variables and the manipulated variables. Papermaking, being a multivariable process, headbox consistency is bound to be dependent on many variables. The key is to isolate the most important variables and to assess their interactions. Evidently, the effect of the thick stock valve must be quantified.

For machine runnability, the machine total flow must be constant. This is controlled by maintaining a stable headbox pressure, which through Bernoulli's equation, mass balance, and geometry consideration (equations 3.1 to 3.4) calculated the required headbox flow.

$$\frac{P_1}{\rho} + \frac{1}{2}v_1^2 + gZ_1 = \frac{P_2}{\rho} + \frac{1}{2}v_2^2 + gZ_2 \quad (3.1)$$

$$v_1 = \frac{A_2 v_2}{A_1} \quad (3.2)$$

$$Z_2 - Z_1 = L_1 \sin \theta \quad (3.3)$$

$$v_2 = \left[ \frac{2}{1 - \frac{A_2^2}{A_1^2}} \left( \frac{P_1 - P_2}{\rho} - gL_1 \sin \theta \right) \right]^{1/2} \quad (3.4)$$

where

$P$  pressure

$\rho$  density of pulp furnish

$v$  speed

$Z$  elevation from reference point

$A$  cross-sectional area

$L$  width of headbox

$\theta$  headbox angle from horizontal plane

$_1$  location of the headbox pressure sensor

## 2 headbox lip opening

This calculated flow is sent as setpoint to a flow controller which compares it with the sensor value, installed before the headbox, and manipulates the fanpump velocity accordingly. Changing the fanpump velocity effectively changes the dilution rate of the thick stock, modifying the headbox consistency. Therefore, a second objective of the modelling task is to assess the importance of the fanpump velocity on the headbox consistency. Thirdly, an alternate strategy would be to include a machine chest flow controller. To do this, a model between the thick stock valve and the machine chest flow is needed. The matrix  $\mathbf{G}$  of models constructed is detailed in Table 3.2.

Table 3.2: Definition of models built for analyzing headbox consistency interactions

	Thick stock valve $u_1$	Fanpump velocity $u_2$	Machine chest flowrate $u_3$
Headbox consistency $y_1$	$g_{11}$	$g_{12}$	$g_{13}$
Headbox flowrate $y_2$	$g_{21}$	$g_{22}$	$g_{23}$
Machine chest flowrate $u_3$	$g_{31}$	—	—

The models are constructed according to the method described in section 2.1. With the headbox pressure/flow loops opened, the machine chest valve and fanpump velocity are varied. To simplify, the fanpump velocity is expressed in percentage of its scale ( 0 %: fanpump closed and 100 %: 1800 rpm ). The data was collected with the paper machine running a thermomechanical pulp with no filler and no additives (the ash content was smaller than 0.5%). The pulp pH was around 6 and it was not controlled on the paper machine. The RMi consistency sensors were calibrated prior to the runs with the same pulp. Some tests were conducted before the installation

of the consistency sensors. The data retrieved from these runs (relation between variables  $y_2, y_3, u_1, u_2, u_3$ ) were also used in the model building process. Appendix C presents the identification data with the detailed calculations of the model building procedure.

### 3.1.3 Models

Two types of models are kept from the identification procedure: the *best* one and the FOPDT model (or equivalently OE(1,1)). This enables one to design the PI controller with a simple model and to test it on more elaborate models. Table 3.3 presents the  $\mathbf{G}$  matrix with the OE(1,1) models and Table 3.4 presents the  $\mathbf{G}$  matrix of the more complicated models. These models also include disturbance transfer functions that are presented in Table 3.5. The models are presented in their discrete form. The sampling time was 1 second. The tables also show the percentage of fit (see (2.10)) of the model on the validation data. The models built are all linear models. With the data, it is possible to estimate the range where the linearity is respected. For each model, this range is also presented in Tables 3.3 and 3.4. Using only the identification and validation data in the linear range, the fit ( $R^2$ ) of the models is computed and presented in the tables. From the tables, we can see that using the machine chest flowrate ( $u_3$ ) as the manipulated variable gives a larger linear range. The non-linearities of the valve are restricted to the model between the valve and the flowrate.

With the models, the steady-state gain matrix is computed (3.5). Using the machine chest valve ( $u_1$ ) and the headbox flowrate ( $u_2$ ) as manipulated variables, a two by two system is obtained. The RGA (Relative Gain Array) of this system is given in (3.6). The RGA indicates that the two loops have little interactions. If the machine chest valve is replaced by the machine chest flowrate  $u_3$  as a manipulated

Table 3.3: Matrix of Output-Error(1,1) models

	Thick Stock Valve $u_1$ (%)	Fan pump velocity $u_2$ (%)	Machine Chest Flowrate $u_3$ (L/min)
Headbox Consistency $y_1$ (%)	$\frac{0.0007003q^{-45}}{1-0.9794q^{-1}}$	$\frac{-0.0004126q^{-35}}{1-0.9808q^{-1}}$	$\frac{1.891 \times 10^{-5}q^{-27}}{1-0.9709q^{-1}}$
fit % ( $R^2$ )	65.0	52.4	86.7
linear range	$60 \leq u_1 \leq 70$	$38.2 \leq u_2 \leq 42.2$	$416 \leq u_3 \leq 1316$
linear fit % ( $R^2$ )	$0.89 \leq y_1 \leq 0.93$ 80.4	$0.895 \leq y_1 \leq 0.905$ 68.1	$0.51 \leq y_1 \leq 1.11$ 87.9
Headbox Flowrate $y_2$ (L/min)	$\frac{-0.3553q^{-15}}{1-0.942q^{-1}}$	$\frac{23.37q^{-5}}{1-0.7948q^{-1}}$	$\frac{-0.2279q^{-10}}{1+0.7997q^{-1}}$
fit % ( $R^2$ )	57.8	83.0	53.7
linear range	$61 \leq u_1 \leq 69$	$37.1 \leq u_2 \leq 47.1$	$200 \leq u_3 \leq 1200$
linear fit % ( $R^2$ )	$3460 \leq y_2 \leq 3540$ 57.8	$2800 \leq y_2 \leq 4000$ 91.7	$3450 \leq y_2 \leq 3600$ 67.1
Machine Chest Flowrate $u_3$ (L/min)	$\frac{1.918q^{-6}}{1-0.9579q^{-1}}$	-	-
fit % ( $R^2$ )	85.0		
linear range	$60 \leq u_1 \leq 70$		
linear fit % ( $R^2$ )	$750 \leq u_3 \leq 1250$ 82.5		

variable, the RGA is given by (3.7). In this configuration, the system also has little interactions.

$$\widehat{\mathbf{K}} = \begin{matrix} & u_1 & u_2 & u_3 & & \\ \begin{matrix} y_1 \\ y_2 \end{matrix} & \begin{matrix} 0.0325 \\ -6.1125 \end{matrix} & \begin{matrix} -0.0213 \\ 111.9076 \end{matrix} & \begin{matrix} 0.0007 \\ -0.1272 \end{matrix} & \begin{matrix} y_1 \\ y_2 \end{matrix} & \end{matrix} \quad (3.5)$$

$$\Lambda^{12} = \begin{bmatrix} 1.0371 & -0.0371 \\ -0.0371 & 1.0371 \end{bmatrix} \quad (3.6)$$

$$\Lambda^{32} = \begin{bmatrix} 1.0376 & -0.0376 \\ -0.0376 & 1.0376 \end{bmatrix} \quad (3.7)$$

The RGA analysis tends to show that no problem should occur in controlling this system. The condition number of each system was also computed. Since this measure is sensitive to scaling (Skogestad & Postlethwaite 1996), the gain matrix was scaled using (3.8). The maximum values used are the sensor or actuator maximum values. For the valve and fanpump, it is 100. For the headbox consistency, it is 1.5 %. For the headbox flowrate, it is 9000 L/min. For the machine chest flowrate, it is 2100 L/min. After scaling, the input and output ranges are from 0 to 1. The condition number of each scaled matrices is presented in (3.10) and (3.11). Both control configurations show small condition numbers. Both configurations should be as easy to control.

$$\mathbf{K} = \mathbf{D}_y^{-1} \widehat{\mathbf{K}} \mathbf{D}_u \quad (3.8)$$

$$\text{where} \quad (3.9)$$

$\mathbf{K}$  scaled matrix

$\mathbf{D}_y$  output scaling =  $\hat{\mathbf{y}}_{max}$

$\mathbf{D}_u$  input scaling =  $\hat{\mathbf{u}}_{max}$

$\widehat{\mathbf{K}}$  unscaled matrix

$$\gamma(\mathbf{K}^{12}) = \gamma \left( \begin{bmatrix} 2.1691 & -1.4223 \\ -0.0679 & 1.2434 \end{bmatrix} \right) = 2.83 \quad (3.10)$$

$$\gamma(\mathbf{K}^{32}) = \gamma \left( \begin{bmatrix} 0.9369 & -1.4223 \\ -0.0297 & 1.2434 \end{bmatrix} \right) = 3.69 \quad (3.11)$$

Table 3.4: Matrix of elaborate models

	Thick Stock Valve $u_1$ (%)	Fan pump velocity $u_2$ (%)	Machine Chest Flowrate $u_3$ (L/min)
Headbox Consistency $y_1$ (%)	$g_{11}$	$\frac{-0.2806q^{-15}}{1-1.499q^{-1}+0.5446q^{-2}}$	$g_{13}$
fit % ( $R^2$ )	71.0	53.8	88.7
linear range	$60 \leq u_1 \leq 70$	$38.2 \leq u_2 \leq 42.2$	$416 \leq u_3 \leq 1316$
linear fit % ( $R^2$ )	$0.89 \leq y_1 \leq 0.93$ 79.7	$0.895 \leq y_1 \leq 0.905$ 69.1	$0.51 \leq y_1 \leq 1.11$ 88.7
Headbox Flowrate $y_2$ (L/min)	$g_{21}$	$\frac{15.78q^{-5}}{1-1.181q^{-1}+0.3225q^{-2}}$	$g_{23}$
fit % ( $R^2$ )	58.2	85.5	56.1
linear range	$61 \leq u_1 \leq 69$ $3460 \leq y_2 \leq 3540$	$37.1 \leq u_2 \leq 47.1$ $2800 \leq y_2 \leq 4000$	$200 \leq u_3 \leq 1200$ $3450 \leq y_2 \leq 3600$
linear fit % ( $R^2$ )	58.2	92.1	70.5
Machine Chest Flowrate $u_3$ (L/min)	$\frac{1.167q^{-7}}{1-0.9751q^{-1}}$	—	—
fit % ( $R^2$ )	82.4		
linear range	$60 \leq u_1 \leq 70$ $750 \leq u_3 \leq 1250$		
linear fit % ( $R^2$ )	82.6		

$$g_{11} = \frac{5.511 \times 10^{-5} q^{-37}}{1 - 0.9247q^{-1} - 0.9946q^{-2} + 0.9209q^{-3}}$$

$$g_{13} = \frac{1.352 \times 10^{-5} q^{-31}}{1 - 1.98q^{-1} + 1.571q^{-2} - 0.5714q^{-3}}$$

$$g_{21} = \frac{-0.1564q^{-16}}{1 - 1.899q^{-1} + 0.8368q^{-2} + 0.1949q^{-3} + 0.2531q^{-4} - 0.6451q^{-5} + 0.321q^{-6} - 0.1227q^{-7} + 0.0913q^{-8}}$$

$$g_{23} = \frac{-0.1449q^{-10} + 0.1369q^{-11}}{1 - 2.002q^{-1} + 1.465q^{-2} - 0.4001q^{-3}}$$

Table 3.5: Matrix of disturbance models

	$d_1$	$d_2$	$d_3$
Headbox Consistency $y_1$ (%)	$\frac{1-0.0376q^{-1}}{1-0.9978q^{-1}}$	$g_{12d}$	$g_{13d}$
Headbox Flowrate $y_2$ (L/min)	$g_{21d}$	$g_{22d}$	$g_{23d}$
Machine Chest Flowrate $u_3$ (L/min)	$\frac{1-0.6634q^{-1}}{(1-0.9796q^{-1})(1-0.9751q^{-1})}$	—	—

$$g_{12d} = \frac{1-0.9455q^{-1}}{1-1.912q^{-1}+0.9082q^{-2}-0.02705q^{-3}+0.03174q^{-4}}$$

$$g_{13d} = \frac{1-0.8916q^{-1}}{1+0.2054q^{-1}-0.3766q^{-2}-0.5045q^{-3}-0.2986q^{-4}} \frac{1}{1-1.98q^{-1}+1.571q^{-2}-0.5714q^{-3}}$$

$$g_{21d} = \frac{1-0.0542q^{-1}}{1-1.398q^{-1}+0.4226q^{-2}}$$

$$g_{22d} = \frac{1-0.9814q^{-1}}{(1-0.9991q^{-1})(1-1.181q^{-1}+0.3225q^{-2})}$$

$$g_{23d} = \frac{1-0.9603q^{-1}}{(1-0.2335q^{-1}-0.4518q^{-2}-0.3088q^{-3})(1-2.002q^{-1}+1.465q^{-2}-0.4001q^{-3})}$$

### 3.1.4 Controller synthesis

PID controllers are available with the DCS interface. Because of the noisy nature of the process, PI controllers are used. The tuning method chosen is the lambda tuning method for its convenient use and well-connected relation with the process. The discrete time domain transfer functions are transformed into the Laplace domain. The resulting controller values are used in discrete simulation. This practice is acceptable since the sampling time used is fast enough to show the process dynamics (Seborg, Edgar & Mellichamp 1989).

The principle of lambda tuning determines a closed loop reference trajectory and finds the controller parameters that yield this trajectory. For a FOPDT reference trajectory (3.12) with a truncated Taylor series replacing the delay  $e^{-\theta s} \approx 1 - \theta s$  and FOPDT model (3.13), the PI controller (3.14) parameters expressions are given by (3.15) and (3.16).

$$g_{ref} = \frac{e^{-\theta s}}{\lambda s + 1} \quad (3.12)$$

$$g_{model} = \frac{K_p e^{-\theta s}}{\tau_p s + 1} \quad (3.13)$$

$$g_c = K_c \left( 1 + \frac{1}{\tau_i} \right) \quad (3.14)$$

$$\tau_i = \tau_p \quad (3.15)$$

$$K_c = \frac{\tau_p}{K_p(\lambda + \theta)} \quad (3.16)$$

Unless stated otherwise, all PI controllers used in simulations and in trials are tuned with the lambda rule. However, some fine tuning is generally required. Figure 3.2(a) presents the basic feedback control strategy. Figure 3.2(b) presents a more complicated strategy where the flow is cascade controlled. A one way decoupled strategy was also tested (Figure 3.2(c)). A static decoupler was installed on the



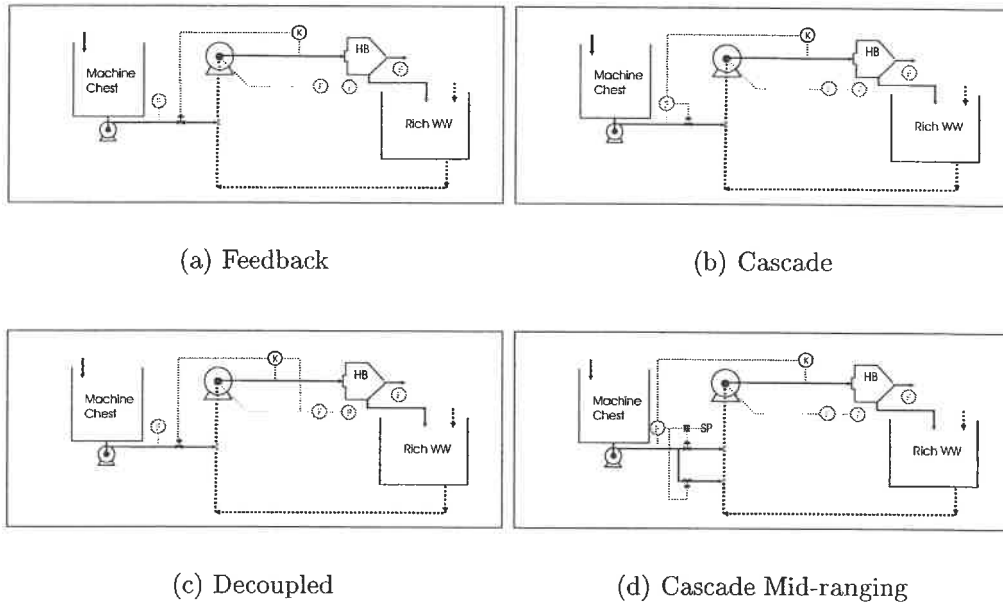
machine. It was tuned using the ratio of the estimated process gain ( $-\frac{K_{12}}{K_{11}}$ ). During the tests, it was noticed that the machine chest valve was not very precise and fast. To improve its performance, a cascade mid-ranging strategy was implemented 3.2(d). Table 3.6 presents the simple and more elaborated models between the machine chest flowrate ( $u_3$ ) and the smaller precision valve ( $u_4$ ). The small precision valve is tuned according to the above algorithm. The big valve is tuned to react very slowly since the main control is achieved using the small valve (Luyben 1990).

Table 3.6: Models between  $u_3$  and small valve  $u_4$ 

	OE(1,1) Model	Elaborate Model
$u_3$	$\frac{0.3843q^{-3}}{1-0.8483q^{-1}}u_4$	$\frac{0.06637q^{-2}}{1-2.671q^{-1}+2.908q^{-2}-1.528q^{-3}+0.3207q^{-4}}u_4$ $+ \frac{1-1.589q^{-1}+0.3489q^{-2}+0.07989q^{-3}+0.1608q^{-4}}{1-3.063q^{-1}+3.301q^{-2}-1.413q^{-3}+0.1747q^{-4}}d_4$
fit % ( $R^2$ )	79.3	83.2
linear range		$0 \leq u_4 \leq 100$ $900 \leq u_3 \leq 1100$
linear fit % ( $R^2$ )	77.2	77.5

### 3.1.5 Simulation

To simulate the different strategies, equations between the controlled variables and the reference trajectories are necessary. For convenience, matrix notation is used. The process is defined by (3.17) or (3.18). The superscripts <sup>12</sup> or <sup>32</sup> refer to the input used: <sup>1</sup> stands for machine chest valve, <sup>2</sup> stands for fanpump rpm, and <sup>3</sup> stands for machine chest flowrate. The transfer functions for each matrix entry are given in Table 3.4. To obtain the closed loop transfer function, the manipulated variables vector is replaced in (3.19) by the different controller expressions. All of the simulations are done using scaled process transfer functions. The scaling used



— Pulp	WW : White Water	F : Flow transmitter and /or controller
..... White Water	HB : Headbox	K : Consistency transmitter and /or controller
..... DSC Signals		P : Pressure transmitter and /or controller

Figure 3.2: Different control strategies implemented on the pilot paper machine

is described in (3.8).

$$\mathbf{G}^{12} = \begin{bmatrix} g_{11} & g_{12} \\ g_{21} & g_{22} \end{bmatrix} \quad (3.17)$$

$$\mathbf{G}^{32} = \begin{bmatrix} g_{13} & g_{12} \\ g_{23} & g_{22} \end{bmatrix} \quad (3.18)$$

$$\begin{bmatrix} y_1 \\ y_2 \end{bmatrix} = \begin{bmatrix} g_{11} & g_{12} \\ g_{21} & g_{22} \end{bmatrix} \begin{bmatrix} u_1 \\ u_2 \end{bmatrix} \quad (3.19)$$

$$\mathbf{y} = \mathbf{G} \mathbf{u}$$

### Feedback Control

For feedback control, the  $\mathbf{u}$  expression is given by (3.20). Substituting into (3.19) and solving for  $\mathbf{y}$  yields (3.21). The symbols  $g_{c1}$  and  $g_{c2}$  represent the controller transfer functions.  $g_{c1}$  controls the headbox consistency and  $g_{c2}$  controls the headbox flowrate.

$$\begin{bmatrix} u_1 \\ u_2 \end{bmatrix} = \begin{bmatrix} g_{c1} & 0 \\ 0 & g_{c2} \end{bmatrix} \begin{bmatrix} y_1^{sp} - y_1 \\ y_2^{sp} - y_2 \end{bmatrix} \quad (3.20)$$

$$\mathbf{u} = \mathbf{G}_c^{feedback} \mathbf{e}$$

$$\mathbf{y} = (\mathbf{I} - \mathbf{G}^{12} \mathbf{G}_c^{feedback})^{-1} \mathbf{G}^{12} \mathbf{G}_c^{feedback} \mathbf{y}^{sp} \quad (3.21)$$

### Cascade control

For cascade control, the  $\mathbf{u}$  expression is given by (3.22). Substituting into (3.19) and solving for  $\mathbf{y}$  yields (3.24). The  $\mathbf{G}_c^{cascade}$  matrix has an additional term  $g_{CL}^{u_1}$  (3.23). This term is the closed loop equation relating the master controller output

to the machine chest flowrate. The symbols  $g_{c1}$ ,  $g_{c2}$ , and  $g_{c3}$  represent the controller transfer functions.  $g_{c1}$  controls the headbox consistency,  $g_{c2}$  controls the headbox flowrate, and  $g_{c3}$  controls the machine chest flowrate.

$$\begin{bmatrix} u_3 \\ u_2 \end{bmatrix} = \begin{bmatrix} g_{CL}^{u_1} g_{c1} & 0 \\ 0 & g_{c2} \end{bmatrix} \begin{bmatrix} y_1^{sp} - y_1 \\ y_2^{sp} - y_2 \end{bmatrix} \quad (3.22)$$

$$\mathbf{u} = \mathbf{G}_c^{cascade} \mathbf{e}$$

$$g_{CL}^{u_1} = \frac{g_{c3} g_{31}}{1 + g_{c3} g_{31}} \quad (3.23)$$

$$\mathbf{y} = \left( \mathbf{I} - \mathbf{G}^{32} \mathbf{G}_c^{cascade} \right)^{-1} \mathbf{G}^{32} \mathbf{G}_c^{cascade} \mathbf{y}^{sp} \quad (3.24)$$

### One-way decoupled control

For decoupled control, the  $\mathbf{u}$  expression is given by (3.25). Substituting into (3.19) and solving for  $\mathbf{y}$  yields (3.26). The  $\mathbf{G}_c^{decoupled}$  matrix has an additional term  $D_{12}g_{c2}$ . The decoupler informs the headbox consistency loop of fanpump changes happening in the headbox flowrate loop. The symbols  $g_{c1}$  and  $g_{c2}$  represent the controller transfer functions.  $g_{c1}$  controls the headbox consistency and  $g_{c2}$  controls the headbox flowrate.

$$\begin{bmatrix} u_1 \\ u_2 \end{bmatrix} = \begin{bmatrix} g_{c1} & D_{12}g_{c2} \\ 0 & g_{c2} \end{bmatrix} \begin{bmatrix} y_1^{sp} - y_1 \\ y_2^{sp} - y_2 \end{bmatrix} \quad (3.25)$$

$$\mathbf{u} = \mathbf{G}_c^{decoupled} \mathbf{e}$$

$$\mathbf{y} = \left( \mathbf{I} - \mathbf{G}^{12} \mathbf{G}_c^{decoupled} \right)^{-1} \mathbf{G}^{12} \mathbf{G}_c^{decoupled} \mathbf{y}^{sp} \quad (3.26)$$

### Mid-ranging control

For mid-ranging control, the basic strategy is the cascade with additional small valve and controller. The additional valve is controlling the machine chest flowrate. The

machine chest valve has a new controller that ensures a predefined opening of the valve. This way, the bulk of the flow is passing through the machine chest valve but the control is done with the small valve. The  $\mathbf{u}$  expression is given by (3.27). Substituting into (3.19) and solving for  $\mathbf{y}$  yields (3.30). The  $\mathbf{G}_c^{mid}$  matrix has an additional term  $g_{CL}^{u4}$  (3.28). This is the closed loop trajectory between the machine chest flowrate and its setpoint. The definition of  $g_{34}$  is given in Table 3.6. The  $\mathbf{u}$  has a new term as compared with the previous expressions. The  $\mathbf{G}_c^{u1}$  matrix gives the transfer function between the machine chest valve setpoint and the machine chest flowrate (3.29). The symbols  $g_{ci}$  represents the controller transfer functions.  $g_{c1}$  controls the headbox consistency,  $g_{c2}$  controls the headbox flowrate,  $g_{c3}$  controls the valve, and  $g_{c4}$  controls the machine chest flowrate.

$$\begin{bmatrix} u_3 \\ u_2 \end{bmatrix} = \begin{bmatrix} g_{CL}^{u4} g_{c1} & 0 \\ 0 & g_{c2} \end{bmatrix} \begin{bmatrix} y_1^{sp} - y_1 \\ y_2^{sp} - y_2 \end{bmatrix} + \begin{bmatrix} g_{CL}^{u1} \\ 0 \end{bmatrix} u_1^{sp} \quad (3.27)$$

$$\mathbf{u} = \mathbf{G}_c^{mid} \mathbf{e} + \mathbf{G}_c^{u1} u_1^{sp}$$

$$g_{CL}^{u4} = \frac{(g_{34} - g_{31}g_{c3}) g_{c4}}{1 + (g_{34} - g_{31}g_{c3}) g_{c4}} \quad (3.28)$$

$$g_{CL}^{u1} = \frac{g_{31}g_{c3}}{1 + (g_{34} - g_{31}g_{c3}) g_{c4}} \quad (3.29)$$

$$\mathbf{y} = (\mathbf{I} - \mathbf{G}^{32} \mathbf{G}_c^{mid})^{-1} [\mathbf{G}^{32} \mathbf{G}_c^{mid} \mathbf{y}^{sp} + \mathbf{G}^{32} \mathbf{G}_c^{u1} u_1^{sp}] \quad (3.30)$$

Figures 3.3 and 3.4 present the response to setpoint changes in headbox consistency and flowrate. Since only a static decoupler is used and the system steady state interactions are small, there are no advantages to using this strategy. In simulation, the cascade strategy performs better in rejecting disturbances. The setpoint change is slower than with feedback or decoupled strategies but servo-behaviour of the system is less important than the regulatory. The mid-ranging strategy can outperform the cascade strategy if the master controller is tuned more aggressively.

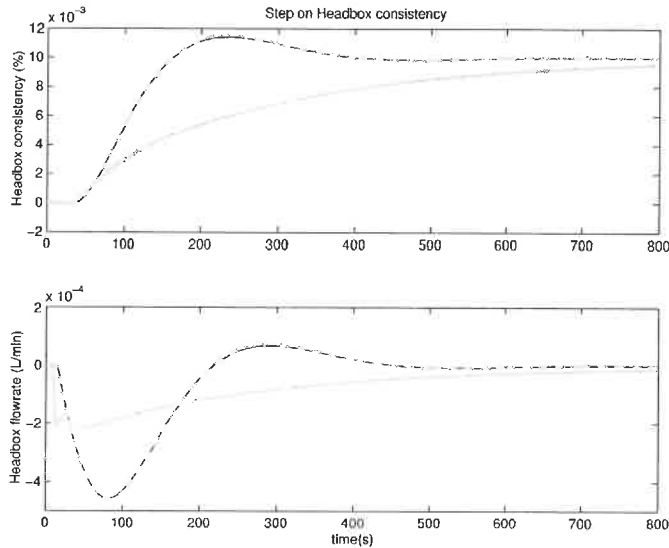


Figure 3.3: Comparison of the response to a setpoint change in headbox consistency of the different control strategies. Solid black line: feedback strategy, dotted black line: cascade strategy, dash grey line: decoupled strategy, solid grey line: mid-ranging strategy.

This is easily done in simulation but more risky on the real process. Since the lambda parameter was not allowed to be smaller than the dominant time constant, the performance of the mid-ranging strategy is equivalent to the cascade one.

## 3.2 Results

Figure 3.5 presents the headbox consistency with and without control. We can see that the controller ensures smaller variations. Furthermore, the average value of the headbox consistency is the setpoint. But, we do not achieve the industry standard of 1 % variation around the setpoint. Contrary to the simulation, but not surprisingly, all of the strategies tested yielded similar results. The noise prevented from detecting the small variations between the different strategies. Unless otherwise stated, all figures present the normal feedback strategy (Figure 3.2(a)).

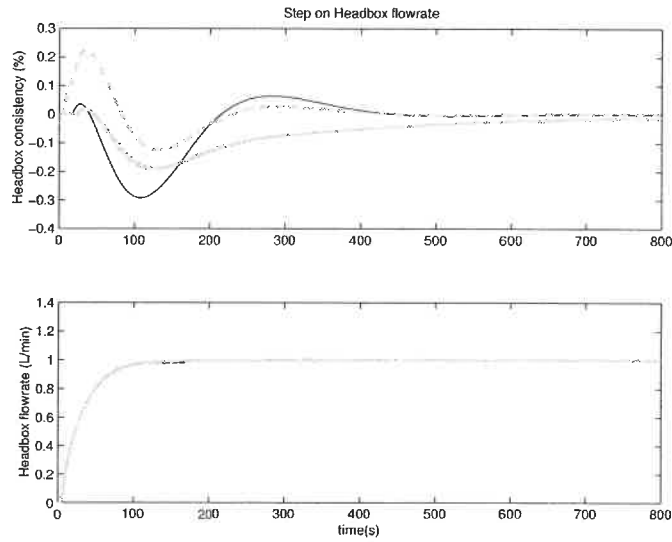


Figure 3.4: Comparison of the response to a setpoint change in headbox flowrate of the different control strategies. Solid black line: feedback strategy, dotted black line: cascade strategy, dash grey line: decoupled strategy, solid grey line: mid-ranging strategy.

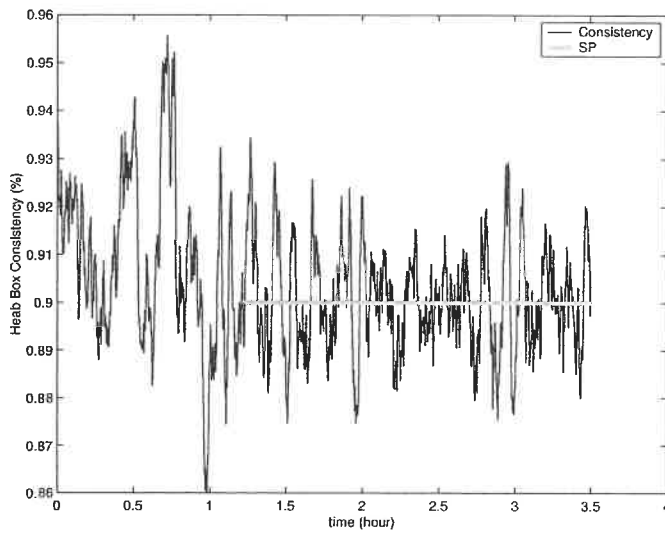


Figure 3.5: Headbox consistency without and with control

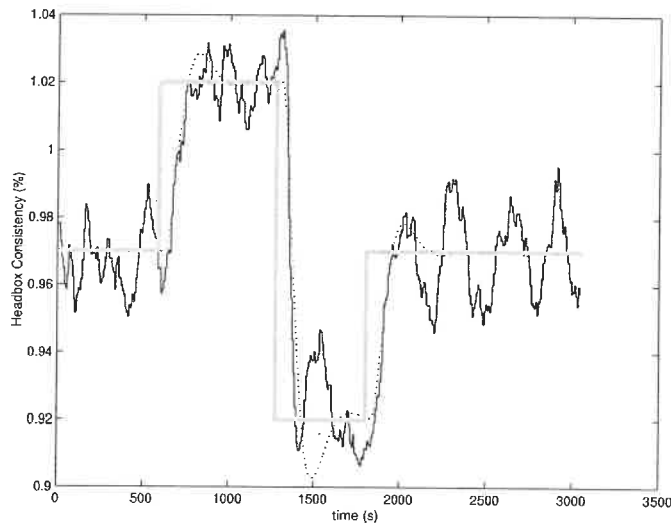


Figure 3.6: Headbox consistency setpoint changes. Black line: machine data, grey line: setpoint, dash line: simulation

### 3.2.1 Setpoint changes

To test the loop performance, various setpoint changes were applied. Figure 3.6 presents a typical response. As predicted with the model, the system needs approximately 4 minutes to reach the new setpoint. This response time is quite acceptable considering the small frequency of setpoint changes during papermaking. During normal operation, headbox consistency setpoint changes will occur only during grade changes.

### 3.2.2 Provoked disturbances

To test more realistically the control loop, disturbances were provoked by changing the headbox recirculation flowrate and by changing the machine speed. Figure 3.7 presents the results of the disturbances on the headbox consistency. At time 0.7 hour, the headbox recirculation flowrate was reduced from 270 to 0. No effect can be seen on the headbox consistency. At time 0.9 hour, the machine speed was



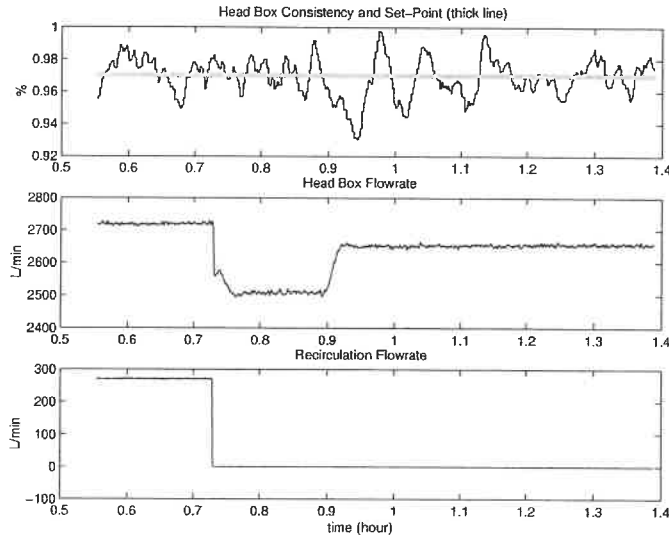


Figure 3.7: Effect of known disturbances on the headbox consistency control loop

increased from 950 m/min to 1000 m/min. This disturbance was seen on the headbox consistency. It took approximately thirty minutes to correct it. This performance needs improvement, but a speed variation of this amplitude during normal operation is rare. It is worth noting that the controller was able to handle such a variation and that smaller (and more realistic) speed variations will be corrected rapidly and in a similar manner.

### 3.2.3 Periodicity propagation

A closer look at Figures 3.5, 3.6, and 3.7 shows periodicity in the headbox consistency signal. It is important to know where the oscillations originated and what their influences on the resulting basis weight were. Three possible causes are:

#### 1. Press Broke Pulper Propagation

Looking at Figure 3.1, we can see that the machine chest level and consistency are not controlled. One can imagine that perturbations at the press

broke pulper will affect the machine chest. The actual press broke level control results in a varying flow of pulp toward the machine chest. The press broke level control diverts the necessary amount back into the pulper to maintain its setpoint. The remaining goes to the machine chest. The level in the press broke varies accordingly with the dilution flowrate added by the press broke consistency controller. This controller is tuned very aggressively in order to react rapidly to sheet breaks. But, during our trials, the paper machine was running on full recycle (i.e., no paper was produced), leading to a very oscillatory press broke pulper consistency. This, in turn, leads to an oscillatory machine chest level. The level affects the machine chest pump, which in turn affects the pressure in the line between the machine chest valve and the fanpump. The result is that for a same valve opening, different flowrates are obtained and, thus, different headbox consistency.

2. Headbox flowrate and consistency loops interactions. The headbox flowrate controller is badly tuned and creates oscillations in the machine flow. This propagates to the headbox consistency.

3. Headbox consistency controller tuning.

The chosen tuning leads to imaginary poles and to sustained oscillations in its controlled variable.

The purpose of this section is to discriminate between the above possibilities and identify the most probable one. Possibility 1 and 2 are going to be investigated using auto-covariance analysis. For the third hypothesis, the closed loop poles are going to be computed using the estimated models.

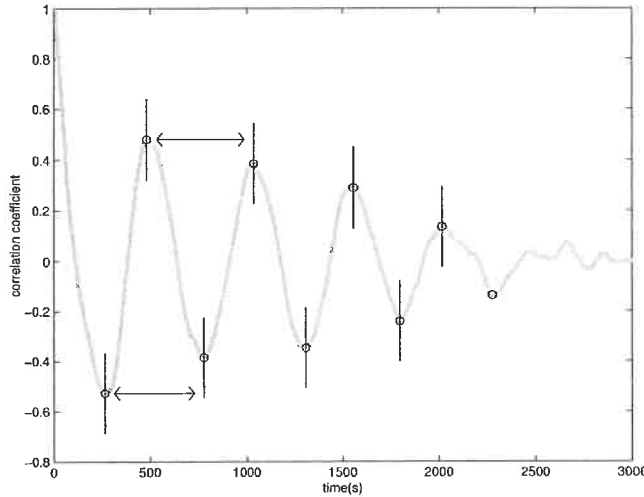


Figure 3.8: Autocorrelogram of the press broke pulper consistency. An example of the periodicity estimation.

### Press Broke Pulper Oscillations

To test this hypothesis, the auto-covariance of each signal in the propagation chain (press broke control valve and consistency; machine chest level, pressure, and control valve; headbox consistency) is computed. Then, the periodicity of the signal can be easily verified (Nobleza & Roche 1988). The period is estimated by taking the average time between two consecutive minimum or maximum peaks in the sine wave. Figure 3.8 gives an example with the points used to compute the period. Table 3.7 presents the estimated period of each signal for every different run where the headbox controller was tested. The first column indicates the chronological run number, and which controller was activated:  $PBP$  stands for Press Broke Pulper consistency controller, and  $HB$  stands for HeadBox consistency controller. The couch pit consistency controller was always on. The level control in both chests was also active. When – is marked, no period could be estimated.

From Table 3.7, a number of conclusions may be drawn. When there are con-

Table 3.7: Estimated period of different signals of the approach system

Runs	Couch Pit		Press Broke		Machine Chest			Headbox
	CV (s)	K (s)	CV (s)	K (s)	Level (s)	P (s)	CV (s)	K (s)
5	–	–	–	–	–	–	–	–
8	–	–	–	120	310	475	–	285
2 <i>HB</i>	–	–	–	–	–	–	–	340
4 <i>HB</i>	245	220	–	310	305	215	–	215
6 <i>HB</i>	160	130	–	280	–	315	–	280
3 <i>PBP</i>	–	–	430	520	500	–	–	–
11 <i>PBP</i>	310	230	310	310	320	N/A	–	730
1 <i>HB PBP</i>	–	–	–	280	N/A	600	–	520
7 <i>HB PBP</i>	–	–	405	410	420	685	415	430
9 <i>HB PBP</i>	–	–	450	540	520	–	–	610
10 <i>HB PBP</i>	300	355	460	460	490	N/A	–	475
12 <i>HB PBP</i>	–	250	310	310	–	N/A	–	400

sistency variations at the couch pit, they are propagated to the press broke pulper. For all except run 12, the couch pit consistency period is similar to its control valve period. This hints that the controller was overly aggressive. But, for more than half the runs, there is no period in both the couch pit consistency and control valve. Therefore, for most papermaking conditions, this loop is correctly tuned. When the press broke consistency controller is active, its controlled and manipulated variables exhibit a similar period (for all but run 1). This definitely suggest an aggressive controller. Runs 3 and 11 show that the periodicity propagates to the machine chest. When the period is slow enough, the machine chest is able to dampen the signal (run 3). When the Headbox and Press Broke controllers are active, the damping effect of the machine chest is greatly reduced (runs 1, 7, 9, 10, and 12). Headbox control seems to enhance to periodicity propagation but does not seem to be its cause. For all runs except run 7, the machine chest control valve does not exhibit a period. If the headbox controller is responsible, its manipulated variable should also

exhibit a period. There are four runs without the Press Broke controller and which exhibit periodic signals (run 8, 2, 4, and 6). Very likely, there is another cause for the periodicity signal, but this analysis was unable to identify it. However, the press broke consistency control is partly responsible for the generation of the periodicity propagation.

To verify the second hypothesis, the headbox flowrate autocorrelation signal was also computed for each different run. The signals were not periodic. Furthermore, during identification runs (see C.1.1), the headbox consistency signal was periodic. During these runs, the headbox flowrate controller was inactive. These observations infer that, the interactions between the two loops are not responsible for the headbox periodic signal.

Lastly, the poles of the headbox consistency closed-loop characteristic equation are computed. All the poles are inside the unit circle. However, some poles have imaginary parts. The resulting control loop can show some amplitude decreasing oscillating responses but not a sustained oscillating controlled signal. Of course, this conclusion is based on the identified model. But, as shown in Figure 3.6, the controlled model is able to reproduce the signal reasonably well. Of all the hypotheses analyzed, the most probable one is the press broke consistency controller propagation. However, this controller is not the only cause of periodicity generation, and more thorough tests are required.

### 3.2.4 Basis weight

The aim of this control loop is to maintain the basis weight at a fixed point. This is achieved through maintaining a desired setpoint for the headbox consistency. The preceding results show that the controller can guarantee the mean of the headbox consistency signal to be the setpoint. Even if to date, the headbox control is not

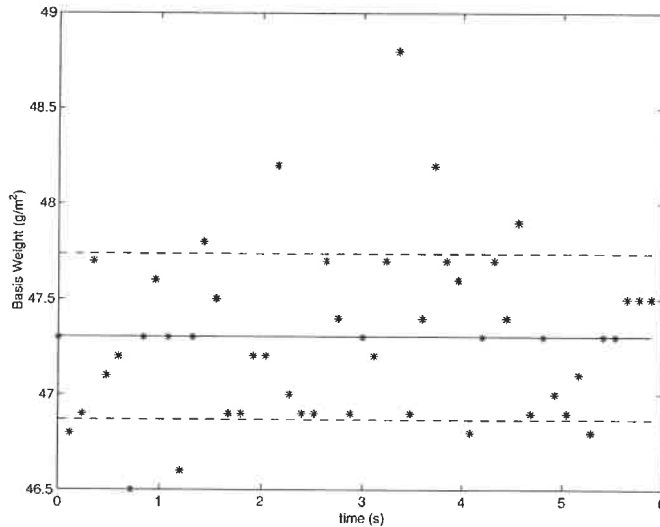


Figure 3.9: Basis weight of samples

perfect, it is important to verify that the final objective can be reached. Wet samples were collected at the wet-sampler, dried and weighted. The samples are measured at a 0.12 second interval. The control strategy used during that run is the mid-ranging one (see Figure 3.2(d)). Figure 3.9 shows the basis weight of the collected samples. The actual standard deviation is  $0.44 \text{ g/m}^2$  for an average basis weight of  $47.3 \text{ g/m}^2$ . Out of the 50 samples, 42 are in range of  $\pm 1\%$  of the sample mean value. This is slightly worst than industry performance. Improving the control should bring all samples in the  $\pm 1\%$  interval. To be able to cascade the headbox consistency loop with a basis weight loop, a basis weight predictor is required. The predictor would calculate the setpoint or a setpoint range of the inner loop.

### 3.3 Conclusion

This chapter showed the implementation of a headbox consistency control loop. From identification runs, models between headbox consistency and flowrate were

constructed. The resulting two by two multivariable system was slightly interacting. Different strategies were tested in simulation and on the paper machine. All of the strategies performed similarly. On the paper machine, the headbox consistency signal is periodic. With auto-correlation analysis, part of this periodicity is attributed to the press broke pulper consistency controller. Based on this analysis, this controller tuning must be revised. However, the basis weight of the samples collected were within industry standards. This headbox consistency control is able to maintain its setpoint, and consequently, to maintain a stable basis weight. Future work involves cascading this loop with the dry-end one, developing a basis weight predictor useful when the machine is running only the wet-end, and studying the periodicity propagation along the recycled loops in the machine flowsheet.

# Chapter 4

## Control Strategies

In the previous chapter, a control strategy only based in the wet-end was developed. The main advantage of such a strategy is its independence from the rest of the paper machine. This strategy will keep the headbox consistency (and the basis weight) constant even if no paper is produced by the machine. But, most of the time, the paper machine is producing paper. Therefore, the objective of this chapter is to develop an integrated control strategy for the wet-end and dry-end of a paper machine. Based on the experiments presented in the previous chapter and on the literature review, any combinations of input variables with output variables are possible. But, the question remains: which pairing is best and what are the potential benefit. Using input-output models built from the plant data, the first question is addressed. Then, using input-output models and the model presented in section 2.2, controllers are designed and tested. The results of simulations carried out using these controllers address the second question.

### 4.1 Models

The CSPP paper machine (see section 2.2.2 for more details) is used for data collection. Steps were applied to each manipulated variable. Variables were varied



one at a time. The initial paper machine conditions are: a machine chest flowrate of 80 L/min (basis weight control loop open), PCC concentration on pulp of 20 % (which correspond to a filler flowrate of 3.7 L/min), bentonite dosage of 1 kg/ton (which correspond to a flowrate of 0.6 L/min at a concentration of 3 g/L), and CPAM dosage of 0.35 kg/ton (which correspond to a flowrate of 0.4 L/min at a concentration of 1.5 g/L). Appendix D presents the data and a detailed procedure to obtain the models presented in Table 4.1. Many models also have a disturbance transfer functions. This part of the models is presented in Appendix D. The manipulated and controlled variables are chosen in function of the nonlinear model, which is used for control strategy validation. Six output variables are studied: headbox consistency ( $y_1$ ), headbox ash consistency ( $y_3$ ), white water consistency ( $y_4$ ), white water ash consistency ( $y_5$ ), sheet ash content ( $y_8$ ) and basis weight ( $y_9$ ). Five input variables are considered: thick stock flowrate ( $u_3$ ), bentonite flowrate ( $u_5$ ), CPAM flowrate ( $u_6$ ), ratio of bentonite to CPAM ( $u_7$ ), and fresh filler flowrate ( $u_8$ ).<sup>1</sup>

It is a well-known fact that the paper machine process is nonlinear. Every input-output data used in this chapter confirm this fact. Often, the nonlinearity is static and affects only the gain. And, in most of the models, the static offset is small enough to allow a linear model to approximate the whole data set. In two specific cases, approximate models were not enough. The first case, the gain and the dynamics of the filler flowrate acting on headbox ash and total consistency are a function of the direction of the step. Unfortunately, only one step up and one step down is available. The slower dynamics for the step down could be attributed to an unobserved change in the machine conditions or more generally to unknown disturbances. With no repetitions, it is impossible to distinguish between these possibilities. In Table 4.1, the two models are presented. For the control analysis,

---

<sup>1</sup>The variables are numbered sequentially. The subscript numbers meaning is kept from the previous chapter.

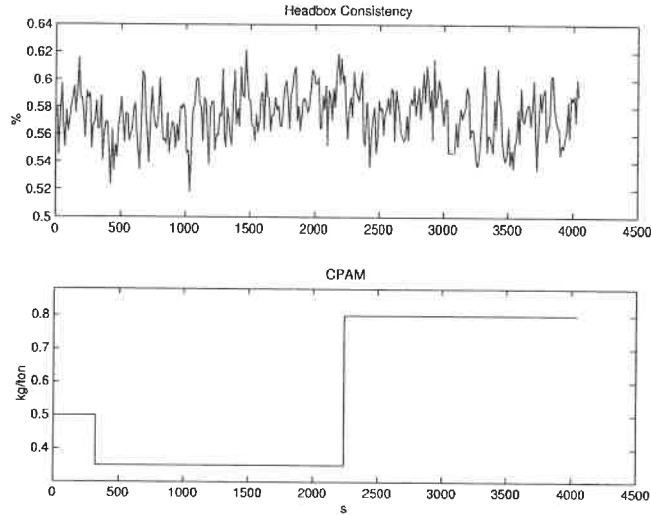


Figure 4.1: Identification data for the model between headbox consistency and CPAM

the worst-case model (smallest gain, slower dynamics) is used. The second case, the sign of the gain of the models having the ratio of bentonite to CPAM as a manipulated variable is a function of ratio range. In this case also, two models are computed. The two models will be kept for the control analysis as not all the variables are sensitive enough to see the second range effects. There are 8 cases where the noise prevents the effect of the manipulated variables from being observed. Figure 4.1 presents an example. The missing models are: headbox consistency ( $y_1$ ) and bentonite ( $u_5$ ), CPAM ( $u_6$ ), ratio ( $u_7$ ); headbox ash consistency ( $y_3$ ) and bentonite ( $u_5$ ), CPAM ( $u_6$ ), ratio ( $u_7$ ); sheet ash content ( $y_8$ ) and high ratio range ( $u_{7\text{High range}}$ ); and basis weight ( $y_9$ ) and the high ratio range ( $u_{7\text{High range}}$ ).

The accuracy of the input-output models is strongly dependant on the input data used. In this case, the data contained a high noise ratio and high scarcity. Furthermore, the sampling period was somewhat high to correctly estimate wet-end dynamics. A sampling period of 12 seconds is used in the wet-end. This is

the smallest possible period available from the data acquisition system. A sampling period of 10 seconds is used in the dry-end. Again, this is the smallest period allowed by the system.

Table 4.1: Models for the CSPP paper machine

	MC flowrate L/min $u_3$	Bentonite flowrate L/min $u_5$	CPAM flowrate L/min $u_6$	Ratio $u_7$	Filler flowrate L/min $u_8$
HB K					
$y_1$	$g_{13}$	—	—	—	$g_{18U}$
$R^2$ %	63.7				55.4
linear range	$70 \leq u_3 \leq 90$ $0.5 \leq y_1 \leq 0.7$				$4.55 \leq u_8 \leq 5.42$ $0.58 \leq y_1 \leq 0.7$
$R^2$ %					$g_{18D}$ 55.1
linear range					$5.42 \geq u_8 \geq 3.68$ $0.73 \geq y_1 \geq 0.53$
HB Ash K					
$y_3$	$g_{33}$	—	—	—	$g_{38U}$
$R^2$ %	63.7				55.4
linear range	$70 \leq u_3 \leq 90$ $17 \leq y_3 \leq 23$				$4.55 \leq u_8 \leq 5.42$ $18 \leq y_3 \leq 22$
$R^2$ %					$g_{38D}$ 55.2
linear range					$5.42 \geq u_8 \geq 3.68$ $22 \geq y_3 \geq 16$
WW K					
$y_4$	$g_{43}$	$g_{45}$	$g_{46}$	$g_{47L}$	$g_{48}$
$R^2$ %	67.9	71.1	61.3	66.9	65.9
linear range	$70 \leq u_3 \leq 90$ $0.02 \leq y_4 \leq 0.03$	$0 \leq u_5 \leq 2.9$ $0.015 \leq y_4 \leq 0.04$	$0.4 \leq u_6 \leq 0.92$ $0.01 \leq y_4 \leq 0.03$	$0 \leq u_{7L} \leq 3$ $0.01 \leq y_4 \leq 0.04$	$3.68 \leq u_8 \leq 5.42$ $0.025 \leq y_4 \leq 0.04$
$R^2$ %				$g_{47H}$ 63.7	
linear range				$3 \leq u_{7H} \leq 7$ $0.01 \leq y_4 \leq 0.03$	

Table 4.1: (continued)

	MC flowrate L/min $u_3$	Bentonite flowrate L/min $u_5$	CPAM flowrate L/min $u_6$	Ratio $u_7$	Filler flowrate L/min $u_8$
WW					
Ash K					
$y_5$	953	955	956	957L	958
$R^2$ %	63.7	79.9	61.6	67.3	69.7
linear	$70 \leq u_3 \leq 90$	$0 \leq u_5 \leq 2.9$	$0.4 \leq u_6 \leq 0.92$	$0 \leq u_{7L} \leq 3$	$3.68 \leq u_8 \leq 5.42$
range	$45 \leq y_5 \leq 65$	$30 \leq y_5 \leq 84$	$40 \leq y_5 \leq 60$	$28 \leq y_5 \leq 82$	$50 \leq y_5 \leq 90$
$R^2$ %				957H 52.2	
linear				$3 \leq u_{7H} \leq 7$	
range				$28 \leq y_5 \leq 60$	
Ash					
$y_8$	983	985	986	987L	988
$R^2$ %	24.4	39.1	18.1	52.3	81.8
linear	$70 \leq u_3 \leq 80$	$0 \leq u_5 \leq 2.9$	$0.23 \leq u_6 \leq 0.58$	$0 \leq u_{7L} \leq 3$	$3.68 \leq u_8 \leq 5.42$
range	$16.5 \leq y_8 \leq 17$	$14.5 \leq y_8 \leq 16.5$	$15 \leq y_8 \leq 17$	$14.5 \leq y_8 \leq 16.5$	$16 \leq y_8 \leq 22$
BW					
$y_9$	993	995	996	997L	998
$R^2$ %	80.9	29.5	17.1	46.7	62.8
linear	$70 \leq u_3 \leq 80$	$0 \leq u_5 \leq 2.9$	$0.23 \leq u_6 \leq 0.58$	$0 \leq u_{7L} \leq 3$	$3.68 \leq u_8 \leq 5.42$
range	$61 \leq y_9 \leq 67$	$58.5 \leq y_9 \leq 64$	$58 \leq y_9 \leq 63$	$56 \leq y_9 \leq 64$	$58 \leq y_9 \leq 68$

$$g_{13} = \frac{0.0004126}{1 - 0.9472q^{-1}} \quad (4.1)$$

$$g_{18U} = \frac{0.05074}{1 - 0.613q^{-1}} \quad (4.2)$$

$$g_{18D} = \frac{0.0006832q^{-2}}{1 - 0.9709q^{-1}} \quad (4.3)$$

$$g_{33} = \frac{0.01962q^{-3}}{1 - 0.08171q^{-1} - 0.8303q^{-2}} \quad (4.4)$$

$$g_{38U} = \frac{1.53}{1 - 0.6256q^{-1}} \quad (4.5)$$

$$g_{38D} = \frac{0.02139q^{-2}}{1 - 0.9709q^{-1}} \quad (4.6)$$

$$g_{43} = \frac{2.332 \times 10^{-5}q^{-8} - 2.345 \times 10^{-5}q^{-9}}{1 - 1.928q^{-1} + 0.9278q^{-2}} \quad (4.7)$$

$$g_{45} = \frac{-0.0005081q^{-5}}{1 - 1.6q^{-1} + 0.5466q^{-2} + 0.4146q^{-3} - 0.2722q^{-4}} \quad (4.8)$$

$$g_{46} = \frac{-0.003667q^{-6}}{1 - 0.8233q^{-1}} \quad (4.9)$$

$$g_{47L} = \frac{-0.001382q^{-6}}{1 - 0.742q^{-1}} \quad (4.10)$$

$$g_{47H} = \frac{0.0005875q^{-6} + 0.0001927q^{-7}}{1 - 0.07693q^{-1} - 0.6274q^{-2}} \quad (4.11)$$

$$g_{48} = \frac{0.001241q^{-10}}{1 - 0.84q^{-1}} \quad (4.12)$$

$$g_{53} = \frac{0.03159q^{-9} - 0.03172q^{-10}}{1 - 2.315q^{-1} + 1.674q^{-2} - 0.3594q^{-3}} \quad (4.13)$$

$$g_{55} = \frac{-4.89q^{-7} + 2.828q^{-8} + 1.934q^{-9}}{1 - 1.001q^{-1} - 0.3781q^{-2} + 0.39q^{-3}} \quad (4.14)$$

$$g_{56} = \frac{-7.646q^{-6}}{1 - 0.8292q^{-1}} \quad (4.15)$$

$$g_{57L} = \frac{-2.049q^{-6} - 3.235q^{-7}}{1 - 0.1273q^{-1} - 0.4106q^{-2}} \quad (4.16)$$

$$g_{57H} = \frac{0.8728q^{-4}}{1 + 0.03019q^{-1} - 1.233q^{-2} - 0.1282q^{-3} + 0.487q^{-4}} \quad (4.17)$$

$$g_{58} = \frac{1.736q^{-10}}{1 - 0.8989q^{-1}} \quad (4.18)$$

$$g_{83} = \frac{0.04882q^{-15}}{1 - 0.1336q^{-1}} \quad (4.19)$$

$$g_{85} = \frac{0.3953q^{-10} - 0.3794q^{-11}}{1 - 1.451q^{-1} + 0.4889q^{-2}} \quad (4.20)$$

$$g_{86} = \frac{1.241q^{-10}}{1 - 0.2243q^{-1}} \quad (4.21)$$

$$g_{87L} = \frac{0.04055q^{-16}}{1 - 0.9415q^{-1}} \quad (4.22)$$

$$g_{88} = \frac{0.2649q^{-15}}{1 - 0.9112q^{-1}} \quad (4.23)$$

$$g_{93} = \frac{0.06467q^{-17}}{1 - 0.8643q^{-1}} \quad (4.24)$$

$$g_{95} = \frac{0.6558q^{-10}}{1 - 0.3733q^{-1}} \quad (4.25)$$

$$g_{96} = \frac{3.125q^{-8} - 2.642q^{-9}}{1 - 0.9244q^{-1}} \quad (4.26)$$

$$g_{97L} = \frac{0.2415q^{-14}}{1 - 0.9898q^{-1}} \quad (4.27)$$

$$g_{98} = \frac{-1.32q^{-4} + 1.379q^{-5}}{1 - 0.9697q^{-1}} \quad (4.28)$$

## 4.2 Interactions Analysis

### 4.2.1 Scaling

As explained in a preceding section (section 3.1.3), various control indices are sensible to the scaling of the system. Furthermore, it is easier to understand the interaction between the different variables when they are on the same scale, namely varying from 0 to 1. To obtain such a system, the input variables and the output variable need to be scaled. The input variables are simply divided by their maximum allowed value. Equation (4.29) presents the scaling matrix used and its relation to the unscaled manipulated vector. The maximum values for the flowrate variable is the maximum allowed by the pump. The maximum value for the filler flowrate pump is 5 L/min. However during the experiment, part of the filler was feed directly in the machine chest. With that method, the added amount of filler is illimitable. During the experiments, the PCC concentration on pulp was varied from 20 to 30 %. Using a value of 40 % seems reasonable to do the scaling with respect to the type of paper produced (fine paper). The maximum value of flowrate can now be deduced. For the ratio, its maximum value is  $\infty$ , which is of little use in scaling. Papermachine normal ratio based on dosage is approximately 10. During

the experiments, the maximum dosage ratio used was 14. To allow for experimental variance, a maximum dosage ratio of 20 is used for scaling. Transformed to flowrate ratio, the maximum is then 10.

$$\begin{bmatrix} u_3 \\ u_5 \\ u_6 \\ u_7 \\ u_8 \end{bmatrix} = \begin{bmatrix} 140 & 0 & 0 & 0 & 0 \\ 0 & 3 & 0 & 0 & 0 \\ 0 & 0 & 2 & 0 & 0 \\ 0 & 0 & 0 & 10 & 0 \\ 0 & 0 & 0 & 0 & 7 \end{bmatrix}^{-1} \begin{bmatrix} \hat{u}_3 \\ \hat{u}_5 \\ \hat{u}_6 \\ \hat{u}_7 \\ \hat{u}_8 \end{bmatrix} \quad (4.29)$$

The output scaling requires more insight into the process. Two types of scaling are possible: based on the maximum expected change in reference value and based on the maximum expected control error (Skogestad & Postlethwaite 1996). The principal aim of this controller is to reject disturbances. Therefore, a scaling based on the maximum expected control error is used. An educated guess is made to find this maximum. The machine normal operating range is subtracted from the machine normal setpoint range. The biggest absolute value is used as the maximum expected control error. Equation (4.30) presents the scaling matrix used and the relation between the scaled and unscaled vectors.

$$\begin{bmatrix} y_1 \\ y_3 \\ y_4 \\ y_5 \\ y_8 \\ y_9 \end{bmatrix} = \begin{bmatrix} 1 & 0 & 0 & 0 & 0 & 0 \\ 0 & 25 & 0 & 0 & 0 & 0 \\ 0 & 0 & 0.5 & 0 & 0 & 0 \\ 0 & 0 & 0 & 60 & 0 & 0 \\ 0 & 0 & 0 & 0 & 25 & 0 \\ 0 & 0 & 0 & 0 & 0 & 100 \end{bmatrix}^{-1} \begin{bmatrix} \hat{y}_1 \\ \hat{y}_3 \\ \hat{y}_4 \\ \hat{y}_5 \\ \hat{y}_8 \\ \hat{y}_9 \end{bmatrix} \quad (4.30)$$

### 4.2.2 Variables selection

From the identification procedure, five input variables and six output variables are obtained. To implement a control strategy, controlled and manipulated variables need to be chosen. Without preselection, there is 30 possible combinations. The majority of them do not have any physical meaning. Of the five possible manipulated variables, only 3 are independent: the machine chest flowrate ( $u_3$ ), a retention aid flowrate ( $u_5$  or  $u_6$  or  $u_7$ ) and the filler flowrate ( $u_8$ ). Therefore, the feedback control system will be a 3 x 3 system. According to the goal of the strategy, wet-end and dry-end variables need to be included. Of the six possible controlled variables, two (ash content ( $y_8$ ) and basis weight ( $y_9$ )) are in the dry-end and need to be controlled. Physically, these two should be paired with the machine chest flowrate ( $u_3$ ) and the filler flowrate ( $u_8$ ). In the four remaining output variables, headbox total ( $y_1$ ) and ash ( $y_3$ ) consistencies are not affected by the retention aid flowrate ( $u_5$  or  $u_6$  or  $u_7$ ). Therefore, the choices left to be made are: white water total ( $y_4$ ) or ash ( $y_5$ ) consistencies as the remaining controlled variable; and bentonite flowrate ( $u_5$ ) or CPAM flowrate ( $u_6$ ) or Ratio of bentonite to CPAM ( $u_7$ ) as remaining manipulated variables.

To discriminate between the possibilities, the steady-state RGA is calculated. We are looking for a RGA with the least interactions (pairing element nearest to one). Another useful measure is the condition number of the steady-state gain matrix. This value should be minimum. This indicates an easier control problem as the multivariable plant directionality is smallest. This is seen in the maximum singular value ( $\bar{\sigma}$ ) and minimum singular value ( $\underline{\sigma}$ ) which represent the biggest and smallest gain of the plant respectively. For an easy control, it is desired to have the plant gain similar in all input directions. The following pages present the RGA ( $\Lambda$ ), the condition number ( $\gamma$ ), the maximum ( $\bar{\sigma}$ ) and the minimum ( $\underline{\sigma}$ ) singular values for the



possible control strategies. To easily identify the control strategy under study, the  $\Lambda$  and  $\mathbf{K}$  have preceding and proceeding superscripts. The preceding superscripts identify the controlled variables. The first superscript is the first row of the matrix, the second superscript is the second row and so on. The proceeding superscripts identify the manipulated variables. The first superscript is the first column of the matrix, the second superscript is the second column and so on. For example, if  ${}^{489}\mathbf{K}^{358}$  is the strategy under study, the controlled variables are  $y_4$  (white water consistency),  $y_8$  (ash content), and  $y_9$  (basis weight), and the manipulated variables are  $u_3$  (machine chest flowrate),  $u_5$  (bentonite flowrate), and  $u_8$  (filler flowrate). The matrix element on the second row, third column ( $k_{23}$ ) is the gain between  $y_8$  (ash content) and  $u_8$  (filler flowrate).

*$y_4, y_8, y_9$  controlled variables with  $u_3, u_5, u_8$  manipulated variables*

Matrix (4.31) presents the RGA for this possibility. (4.32) shows the condition number.

$${}^{489}\Lambda^{358} = \begin{bmatrix} 0.125 & \boxed{0.762} & 0.112 \\ -0.111 & 0.114 & \boxed{0.997} \\ \boxed{0.985} & 0.124 & -0.109 \end{bmatrix} \quad (4.31)$$

$$\gamma({}^{489}\mathbf{K}^{358}) = \gamma \left( \begin{bmatrix} 0.15 & -0.0342 & 0.109 \\ 0.316 & 0.0505 & 0.836 \\ 0.667 & 0.0314 & 0.137 \end{bmatrix} \right) = 23.2 \quad (4.32)$$

$$\underline{\sigma}({}^{489}\mathbf{K}^{358}) = 0.0439 \quad \bar{\sigma}({}^{489}\mathbf{K}^{358}) = 1.02$$

*$y_4, y_8, y_9$  controlled variables with  $u_3, u_6, u_8$  manipulated variables*

Matrix (4.33) presents the RGA for this possibility. (4.34) shows the condition

number.

$${}^{489}\Lambda^{368} = \begin{bmatrix} 0.219 & \boxed{0.701} & 0.0804 \\ -0.13 & 0.109 & \boxed{1.02} \\ \boxed{0.911} & 0.19 & -0.102 \end{bmatrix} \quad (4.33)$$

$$\gamma({}^{489}\mathbf{K}^{368}) = \gamma\left(\begin{bmatrix} 0.15 & -0.083 & 0.109 \\ 0.316 & 0.128 & 0.836 \\ 0.667 & 0.128 & 0.137 \end{bmatrix}\right) = 8.96 \quad (4.34)$$

$$\underline{\sigma}({}^{489}\mathbf{K}^{368}) = 0.114 \quad \bar{\sigma}({}^{489}\mathbf{K}^{368}) = 1.03$$

$y_4, y_8, y_9$  controlled variables with  $u_3, u_{7H}, u_8$  manipulated variables

Matrix (4.35) presents the RGA for this possibility. (4.36) shows the condition number.

$${}^{489}\Lambda^{378} = \begin{bmatrix} 0 & \boxed{1} & 0 \\ -0.0838 & 0 & \boxed{1.08} \\ \boxed{1.08} & 0 & -0.0838 \end{bmatrix} \quad (4.35)$$

$$\gamma({}^{489}\mathbf{K}^{378}) = \gamma\left(\begin{bmatrix} 0.15 & 0.0528 & 0.109 \\ 0.316 & 0 & 0.836 \\ 0.667 & 0 & 0.137 \end{bmatrix}\right) = 19.6 \quad (4.36)$$

$$\underline{\sigma}({}^{489}\mathbf{K}^{378}) = 0.0517 \quad \bar{\sigma}({}^{489}\mathbf{K}^{378}) = 1.01$$

$y_4, y_8, y_9$  controlled variables with  $u_3, u_{7L}, u_8$  manipulated variables

Matrix (4.37) presents the RGA for this possibility. (4.38) shows the condition number.

$${}^{489}\Lambda^{378} = \begin{bmatrix} \boxed{1.02} & 0.194 & -0.214 \\ -0.301 & 0.0507 & \boxed{1.25} \\ 0.281 & \boxed{0.756} & -0.0362 \end{bmatrix} \quad (4.37)$$

$$\gamma \left( {}^{489}\mathbf{K}^{378} \right) = \gamma \left( \begin{bmatrix} 0.15 & -0.107 & 0.109 \\ 0.316 & 0.277 & 0.836 \\ 0.667 & 2.37 & 0.137 \end{bmatrix} \right) = 18.7 \quad (4.38)$$

$$\underline{\sigma} \left( {}^{489}\mathbf{K}^{378} \right) = 0.134 \quad \bar{\sigma} \left( {}^{489}\mathbf{K}^{378} \right) = 2.5$$

$y_5, y_8, y_9$  controlled variables with  $u_3, u_5, u_8$  manipulated variables

Matrix (4.39) presents the RGA for this possibility. (4.40) shows the condition number.

$${}^{589}\Lambda^{358} = \begin{bmatrix} 0.192 & \boxed{0.7011} & 0.107 \\ -0.103 & 0.0834 & \boxed{1.02} \\ \boxed{0.912} & 0.215 & -0.127 \end{bmatrix} \quad (4.39)$$

$$\gamma \left( {}^{589}\mathbf{K}^{358} \right) = \gamma \left( \begin{bmatrix} 4.41 & -0.606 & 2 \\ 0.316 & 0.0505 & 0.836 \\ 0.667 & 0.0314 & 0.137 \end{bmatrix} \right) = 36.2 \quad (4.40)$$

$$\underline{\sigma} \left( {}^{589}\mathbf{K}^{358} \right) = 0.137 \quad \bar{\sigma} \left( {}^{589}\mathbf{K}^{358} \right) = 4.96$$

$y_5, y_8, y_9$  controlled variables with  $u_3, u_6, u_8$  manipulated variables

Matrix (4.41) presents the RGA for this possibility. (4.42) shows the condition number.

$${}^{589}\Lambda^{368} = \begin{bmatrix} 0.314 & \boxed{0.613} & 0.0722 \\ -0.116 & 0.0751 & \boxed{1.04} \\ \boxed{0.802} & 0.311 & -0.113 \end{bmatrix} \quad (4.41)$$

$$\gamma \left( {}^{589}\mathbf{K}^{368} \right) = \gamma \left( \begin{bmatrix} 4.41 & -1.49 & 2 \\ 0.316 & 0.128 & 0.836 \\ 0.667 & 0.128 & 0.137 \end{bmatrix} \right) = 14.7 \quad (4.42)$$

$$\underline{\sigma}({}^{589}\mathbf{K}^{368}) = 0.35 \quad \bar{\sigma}({}^{589}\mathbf{K}^{368}) = 5.13$$

$y_5, y_8, y_9$  controlled variables with  $u_3, u_{7H}, u_8$  manipulated variables

Matrix (4.43) presents the RGA for this possibility. (4.44) shows the condition number.

$${}^{589}\Lambda^{378} = \begin{bmatrix} 0 & \boxed{1} & 0 \\ -0.0838 & 0 & \boxed{1.08} \\ \boxed{1.08} & 0 & -0.0838 \end{bmatrix} \quad (4.43)$$

$$\gamma({}^{589}\mathbf{K}^{378}) = \gamma \left( \begin{bmatrix} 4.41 & 0.934 & 2 \\ 0.316 & 0 & 0.836 \\ 0.667 & 0 & 0.137 \end{bmatrix} \right) = 34.1 \quad (4.44)$$

$$\underline{\sigma}({}^{589}\mathbf{K}^{378}) = 0.147 \quad \bar{\sigma}({}^{589}\mathbf{K}^{378}) = 5.01$$

$y_5, y_8, y_9$  controlled variables with  $u_3, u_{7L}, u_8$  manipulated variables

Matrix (4.45) presents the RGA for this possibility. (4.46) shows the condition number.

$${}^{589}\Lambda^{378} = \begin{bmatrix} \boxed{1.02} & 0.117 & -0.134 \\ -0.188 & 0.0242 & \boxed{1.16} \\ 0.17 & \boxed{0.859} & -0.0296 \end{bmatrix} \quad (4.45)$$

$$\gamma({}^{589}\mathbf{K}^{378}) = \gamma \left( \begin{bmatrix} 4.41 & -1.91 & 2 \\ 0.316 & 0.277 & 0.836 \\ 0.667 & 2.37 & 0.137 \end{bmatrix} \right) = 8.12 \quad (4.46)$$

$$\underline{\sigma}({}^{589}\mathbf{K}^{378}) = 0.644 \quad \bar{\sigma}({}^{589}\mathbf{K}^{378}) = 5.23$$

The steady-state RGAs are similar with respect to the controlled variables. They give the same pairing for the same potential manipulated variables. The condition number is also similar. This is not surprising as the white water total consistency ( $y_4$ ) is mainly composed of fines and fillers. However, condition numbers are slightly better for white water ash consistency while the RGA are similar. But, as only fine papers contain fillers, the strategy will be more general if white water total consistency is used. For the manipulated variables, the result is clear if the ratio of the bentonite to CPAM is in the high range (3 to 7). Then, the pairing is: white water consistency with retention aid chemical flowrate, ash content with filler flowrate, and basis weight with machine chest flowrate. This pairing is what is physically expected. The retention aid that gives smallest condition number is flowrate of CPAM. This confirms a very popular strategy of Table 1.5. The normal operating ratio of paper machines is in the high range. During the trial, a lower range (0 to 3) was tested. The RGA in this case gives a different pairing: white water consistency with machine chest flowrate, ash content with filler flowrate, and basis weight with ratio of chemicals. From a physical standpoint, this pairing does not make much sense. Nonetheless, an interesting conclusion can be drawn. From the gain matrix, we see that the ratio has an important effect on basis weight. This is due to the effect of the chemical on the retention level of the machine. This suggests that the normal paper machine operations overdose retention chemicals thereby reducing their incremental effect. On the other hand, the high ratio range has more *forgiveness* for error. Since the low ratio range is not normally used in mills, the chosen control strategy is: white water total consistency with CPAM flowrate, ash content with filler flowrate, and basis weight with machine chest flowrate. Based on the RGA, the system is slightly interacting since the diagonal element are all near

one. This is based on the steady state gain of the model. To make sure, the RGA was computed over a range of frequencies.

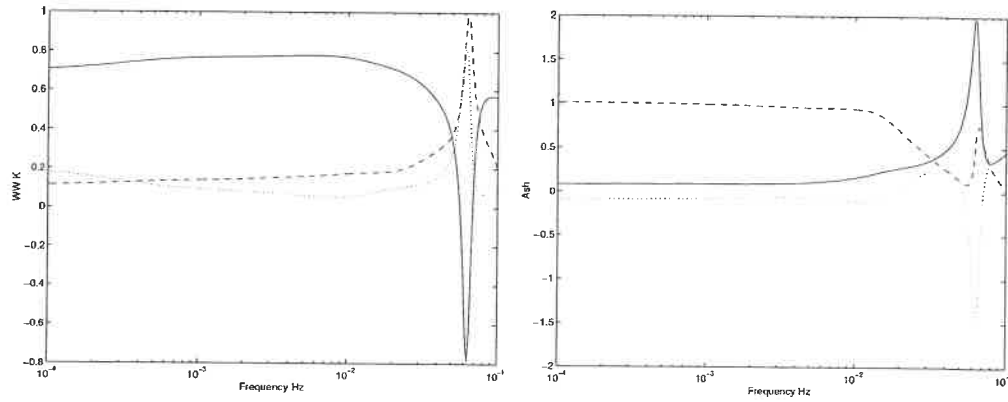
Figure 4.2 presents the RGA in the frequency range of  $10^{-4}$  to  $10^{-1}$  Hz. The steady state analysis is valid up to 30 seconds. At this point, the RGA values peaks in opposite direction. According to theory, a reverse pairing would be better for the dynamic responses. But, in this case, one can not conclude because the accuracy of the models is questionable. The sampling periods are 12 seconds for the wet-end measurement and 10 seconds for the dry-end measurement. This sampling allows us to draw conclusion for the steady state but not for higher frequencies. The same can be conclude from Figure 4.3. Figure 4.3 presents the largest and smallest singular values in the frequency range of  $10^{-4}$  to  $10^1$  Hz. As the frequency raises, the lower and singular values are closer to each other. This would suggest an easier control, but again, model accuracy is questionable.

## 4.3 Controller Types and Tuning

Once the models have been obtained, and the manipulated and controlled variables have been chosen, the controller can be designed. Two types of controllers have been tested on the nonlinear first principal paper machine model of Cho et al. (2001a). The following subsection explains each type of controller and its tuning.

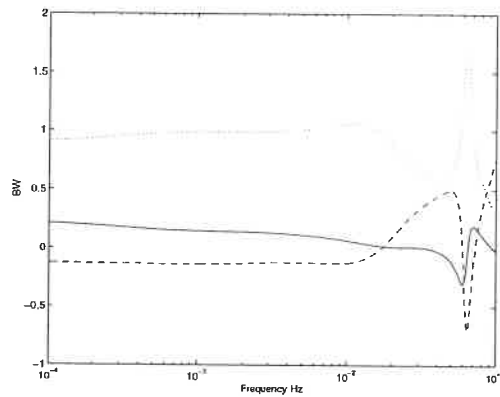
### 4.3.1 Standard controllers

To judge controller performance, one must compare them with the standard industry controllers: PI and PID. According to two (as in the PI case) or three (as in the PID case) tuning parameters and the difference between the setpoint and the controlled variable, the manipulated variable is calculated (4.47). To improve the performance of PID controllers, a filter (4.48) or a lead-lag element (4.49) can be added. This



(a) WW K

(b) Ash



(c) BW

Figure 4.2: RGA over the frequency range. The solid lines are associated with CPAM flowrate input, the dashed with the Filler flowrate input and the dotted with the MC flowrate input.

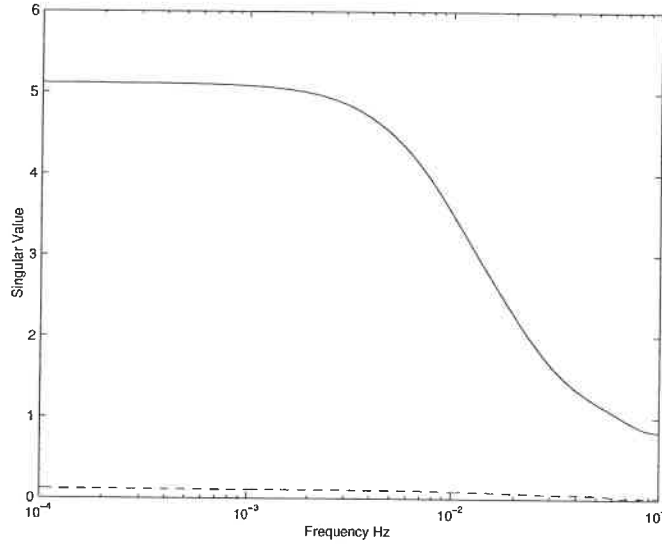


Figure 4.3: Singular values over the frequency range. The solid line is associated with the maximum singular value and the dashed line with the minimum.

give rise to extra tuning parameters. To ease the tuning of such controllers, direct synthesis or lambda tuning method is used (Ogunnaike & Ray 1994).

$$u = K_c \left( 1 + \frac{1}{\tau_{IS}} + \tau_{DS} \right) e \quad (4.47)$$

$$u = K_c \left( 1 + \frac{1}{\tau_{IS}} + \tau_{DS} \right) \left( \frac{1}{\tau_{FS} + 1} \right) e \quad (4.48)$$

$$u = K_c \left( 1 + \frac{1}{\tau_{IS}} + \tau_{DS} \right) \left( \frac{\tau_{LDS} + 1}{\tau_{LGS} + 1} \right) e \quad (4.49)$$

$$(4.50)$$

This type of controllers have been tuned by Kolko (2001). The nonlinear model is used to generate data around a steady state. Then, the data are best-fitted to linear transfer functions. Next, the models are used to obtain the controller's parameters. Table 4.2 presents the resulting controller type for each loop of the three by three system.

Kolko (2001) also studied the traditional control approach to multivariable sys-



Table 4.2: Traditional controller types obtained by direct synthesis method

Manipulated variable Controlled variable	Controller type
CPAM flowrate White water total consistency	PID + first-order filter
Filler flowrate Sheet ash content	PID + first-order filter + lead/lag element
Machine chest flowrate Basis weight	PID + first-order filter + lead/lag element

Source : Kolko (2001)

tems. Steady-state decouplers between the interacting loops were tested on the nonlinear model. The decouplers are tuned with the steady-state gain of the linear models. For example, if a decoupler is installed between loop 1 and loop 2, its value is calculated as in (4.51).

$$D = -\frac{k_{12}}{k_{11}} \quad (4.51)$$

where

$D$  Decoupler gain

$k_{12}$  gain of loop 2 on loop 1

$k_{11}$  gain of the model of loop 1

### 4.3.2 MPC controller

Model predictive control (MPC) has been used in the petroleum industry since the late 70's. The reported very good results have spread the application of MPC to all kinds of chemical process industries (Refining, Chemicals, Pulp and Paper, Gas, Air Separation, Food Processing, Furnaces, etc.) (Qin & Badgwell 1996). For the wet-end of paper machines, Lang et al. (1999) reported using a MPC to control basis weight, sheet ash content, and white water consistency. Due to the lack of

mathematical proof (although this an active research area) regarding the stability and robustness of MPC controllers, it is difficult to measure the benefits of these types of controllers over classical control. The most common alternative used is brute-force simulation. This section presents a short overview of the MPC algorithm and gives the simulation results. The next section compares the MPC results with those of the traditional control methods.

### MPC algorithm

A general consensus exists on the differences between model based control and classical control. A process model is a part of a MPC controller. The control objective function solves an open-loop optimisation problem over a fixed horizon. The horizon moves forward at each time step (receding horizon). The constraints are easily incorporated in the objective function. The primary and most important drawback of MPC technology is the need of a dynamic model. Obtaining a model is time consuming and expensive. The improvement of the MPC must be significant to justify the model building phase.

Figure 4.4 presents a typical MPC calculation. The starting model is obtained by calculating step response coefficients from the transfer function identified previously. At each MPC calculation, the process model update is the point at which the feedback enters the loop. The model prediction is compared with the measured value and the difference is added to the future model estimates (4.52 - 4.53).

$$b_k = y_k^m - y_k \quad (4.52)$$

$$y_{k+j} = \mathbf{M}u_{k+j} + b_k \quad (4.53)$$

where

$y_k^m$  measured value

$y_k$  model estimated value

**M** matrix of step coefficients

Once the model is updated, the sequence of future input moves is calculated from the objective function (4.54) subjected to the input and output constraints (4.55, 4.56 and 4.57).

$$\min_{\Delta u_k \dots \Delta u_{k+m-1}} \sum_{l=1}^p \left\| \Gamma_l^y (y_{k+l|k} - r_{k+l}) \right\|^2 + \sum_{l=1}^m \left\| \Gamma_l^u (\Delta u_{k+l-1}) \right\|^2 \quad (4.54)$$

$$u_{min} \leq u_k \leq u_{max} \quad (4.55)$$

$$|\Delta u_k| \leq \Delta u_{max} \quad (4.56)$$

$$y_{min} \leq y_{k+1|k} \leq y_{max} \quad (4.57)$$

where

$m$  control horizon

$p$  prediction horizon

$\Gamma^y$  output weighting matrix

$r$  reference values, possibly time-varying

$\Gamma^u$  input weighting matrix

The input and output weighting matrices are used to penalise certain outputs or inputs at certain time intervals. Those matrices can be used as tuning parameters. The constraints allow the specification of minimum and maximum values of the inputs and the outputs. Also, for the inputs, it is possible to specify the maximum rate of change. When constraints are used, the objective function must be solved

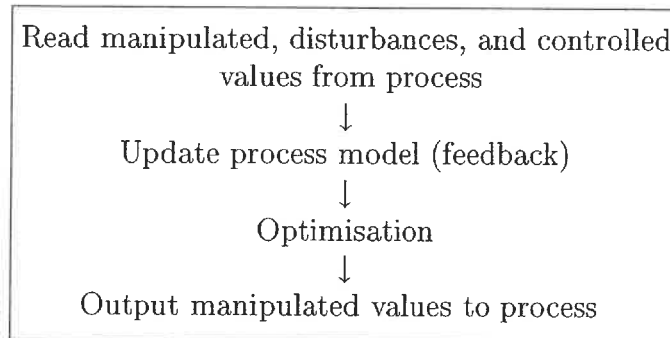


Figure 4.4: Calculation flowsheet of MPC algorithm  
*Source:* adapted from Qin & Badgwell (1996)

using quadratic programming and the resulting control law is nonlinear. This is why the stability and robustness of the closed loop system is difficult to analyze analytically. Although  $m$  input moves are calculated, only the first one is applied to the plant. At the next sampling interval, the optimisation is repeated with the horizon moved one step forward. This version of the MPC algorithm is known as Dynamic Matrix Control (DMC) (Garcia, Prett & Morari 1989).

To tune this controller, there are four available parameters:  $p$ , the prediction horizon;  $m$ , the number of control moves;  $\Gamma^u$ , the input weighting; and  $\Gamma^y$  the output weighting. The prediction horizon relates to the closed-loop time constant. Since the system can not react faster than the time delay, the prediction horizon must be at least equal and preferably greater than the time delay of the system. The number of control moves specifies to the controller how many input moves it can make to bring the system to the reference value. In general, increasing  $m$  leads to a more aggressive response. A rule of thumb used in tuning is to start the simulation with  $m = 1$ . The input weighting matrix is often used to detune the controller. Increasing it always has the effect of making the control action less aggressive (Morari & Ricker 1998). The output weighting matrix is used to raise the more importance of some of the controlled variables. It is especially useful if

the system is over-determined and it is unable to meet all of the controlled variable setpoints.

### MPC simulation results

The above MPC algorithm is implemented in Matlab through the function *cmpc* and *nlnmpc* of the MPC Toolbox. The combination of these functions with the Simulink nonlinear model of the paper machine simulates the response of controlled variables to various possible disturbances.

The MPC controller is tuned using simulations on the linear models. The guideline used through all the tuning simulations was to give away performance if robustness was improved. When the responses are acceptable, the same controller is tested on the nonlinear model. Fine tuning was done to improve the performance. At first, the constraints were the paper machine ones but they were modified in order to respect the validity region of the retention model. Table 4.3 presents the hard constraints on the manipulated variables. No constraint was imposed on the controlled variables. Table 4.4 presents the final controller parameters used in the simulations. Comparing the linear simulation tuning and the nonlinear ones, the number of control moves stayed the same. The prediction horizon was increased from 350 to 400 seconds. The major change occurs on the input weighting matrix. During the linear tuning, no weights were used. On the nonlinear model, using no weight lead to a very oscillatory behaviour. This can be explained by Figure 4.5. The nonlinear model does not reproduce well the pilot plant data. It is believed that the problem lies within the retention model and work is ongoing to solve it. However, when the MPC controller attempts to control this plant, its model gains are wrong. If there is no cost to move the manipulated variables, oscillation results.

The aim of the controller is to reject perturbations. Therefore, five different

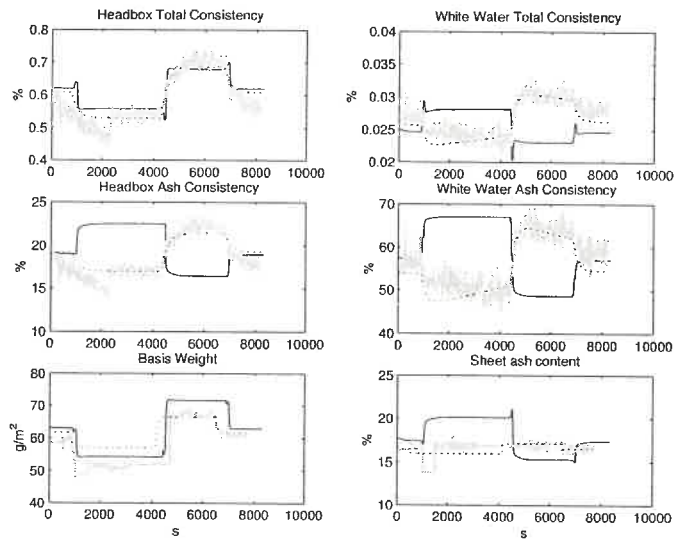


Figure 4.5: Responses of the different models to step changes in machine chest flowrate.

Step amplitude of -10 L/min at  $t=812$  s and step amplitude of 20 L/min at  $t=4304$  s.

Black line: nonlinear model. Dotted line: Input-Output model. Grey line: data.

Table 4.3: Hard constraints imposed on the manipulated variables

Variable	minimum	maximum	rate of change
CPAM flowrate	0	1	$\infty$
Filler flowrate	1	5	$\infty$
Machine chest flowrate	20	100	$\infty$

Table 4.4: MPC tuning parameter values

Parameter	Value
Control interval	10 s
Prediction horizon (P)	40
Control moves (M)	1
Manipulated variable weights	
CPAM flowrate	20
Filler flowrate	15
Machine chest flowrate	15
Controlled variable weights	
White water consistency	1
Ash Content	1
Basis weight	1

perturbations were tested. The perturbations were chosen as to represent possible situations on the paper machine. The first two perturbations were affecting the machine chest consistency. In the first case, a step change of 0.1 g/L was applied. In the second case, the consistency of the machine chest was a sine wave with an amplitude of 0.1 g/L and a period of 30 seconds. Then, changes in the strength of the retention chemical CPAM was tested. A step of 10 g/L was applied. Step change in filler flowrate was also tested. Lastly, a perturbation on the retention of the machine was tested. The fines fraction of the machine chest total consistency was step changed. Fines are difficult to retain and adding more fines ask for more chemicals, thereby modifying the retention on the machine. Figure 4.6 presents the response of the controlled and manipulated variables to a step change in filler concentration. The results of the other tests will be given in Table 4.6. For all

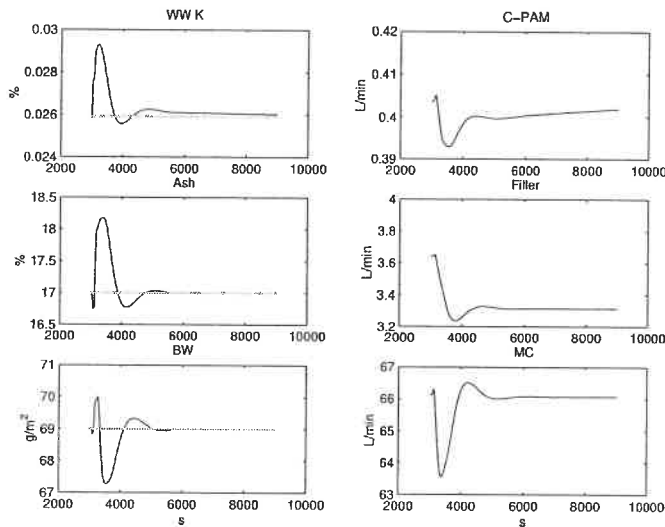


Figure 4.6: Response of controlled and manipulated variables to a step change in filler concentration. Step occurs at  $t=3000s$  from 100 g/L to 110 g/L. Black line: manipulated or controlled variables. Grey line: setpoint

the tests, the controller performs well for the basis weight controlled variable. The perturbations are rejected at a slower rate for the ash content. For all but filler flowrate perturbation, the controller is not able to bring the white water consistency back to its setpoint in less than 6000 s (1h40). The results correlates well with the linear models accuracies over the nonlinear model. These results stress the importance of good models for the MPC controller. Without them, the performance can be rather poor. The next section gives the results for different types of controllers applied on the nonlinear model.

## 4.4 Controller Comparison

To evaluate the performance of MPC controllers it is necessary to simulate them. Likewise, to compare the MPC controller against other type of controllers, simulations are useful. During this project, the nonlinear model was controlled with



different type of controllers: traditional controllers by Kolko (2001), MPC controller based on linearised models of the nonlinear model by El Ghali (2001), and MPC controller based on input/output data by this author. MPC tuning parameters used by El Ghali (2001) are shown in Table 4.5. Table 4.6 presents the comparison between the different controllers. The compared characteristics are: the settling times and the maximum amplitudes of each controlled variables. The settling time was recorded when 96 % of the perturbation was rejected. The maximum amplitude is based on the difference between the maximum value and the setpoint divide by the setpoint. The first column gives the results of traditional PID controllers (see Table 4.2). The second column gives the results for the same traditional controllers augmented with steady-state decouplers. The third column gives the first MPC implementation where the MPC models are linearised around a steady state of the nonlinear model. The last column gives the second MPC implementation where the MPC models are developed from input/output data from the pilot paper machine.

Table 4.5: MPC tuning parameter values for MPC 1 implementation

Parameter	Value
Control interval	2 s
Prediction horizon (P)	85
Control moves (M)	1
Manipulated variable weights	
CPAM flowrate	55
Filler flowrate	4.5
Machine chest flowrate	1.75
Controlled variable weights	
White water consistency	25
Ash Content	0.16
Basis weight	0.1

*Source* : El Ghali (2001)

Table 4.6: Performance of different type of controllers to different perturbations

	Conventional Controller (Kolko 2001)	Conventional Controller with decouplers (Kolko 2001)	MPC 1 (El Ghali 2001)	MPC 2
<b>Step on machine chest consistency (amplitude = +0.1 %)</b>				
WW K Settling time (s)	>2000	750	457	>6000
WW K maximum amplitude (%)	2.73	2.73	0.98	5.2
Ash Settling time (s)	>2000	1050	533	2150
Ash maximum amplitude (%)	7.60	8.40	4.82	2.9
BW Settling time (s)	1700	1000	564	1510
BW maximum amplitude (%)	8.47	8.47	3.37	3.1
<b>Sine on machine chest consistency (amplitude = 0.1 % period = 30 s)</b>				
WW K maximum amplitude (%)	0.7	1.4	1.3	2.6
Ash maximum amplitude (%)	3.6	4.0	3.7	0.6
BW maximum amplitude (%)	3.2	3.7	3.3	1.0
<b>Step on CPAM concentration (amplitude = +0.1 g/L)</b>				
WW K Settling time (s)	2250	750	176	>6000
WW K maximum amplitude (%)	4.9	4.9	4.8	4.9
Ash Settling time (s)	3000	750	311	6600
Ash maximum amplitude (%)	1.4	1.4	2.8	0.77
BW Settling time (s)	1750	900	633	2270
BW maximum amplitude (%)	0.29	0.29	0.55	0.27

Table 4.6: (continued)

	Conventional Controller (Kolko 2001)	Conventional Controller with decouplers (Kolko 2001)	MPC 1 (El Ghali 2001)	MPC 2
Step on filler concentration (amplitude = +10 g/L)				
WW K Settling time (s)	2700	750	222	5200
WW K maximum amplitude (%)	5.9	5.9	5.3	13.2
Ash Settling time (s)	2000	600	319	1620
Ash maximum amplitude (%)	9.2	9.2	9.8	7.0
BW Settling time (s)	2700	900	486	1900
BW maximum amplitude (%)	1.3	1.3	1.5	2.6
Step on machine chest fine fraction (amplitude = + 2 %)				
WW K Settling time (s)	2300	750	173	>6000
WW K maximum amplitude (%)	15.9	15.9	7.2	0.71
Ash Settling time (s)	3500	1000	993	>6000
Ash maximum amplitude (%)	1.4	1.2	1.3	0.03
BW Settling time (s)	3000	950	700	2010
BW maximum amplitude (%)	0.93	0.93	925	0.03

Table 4.6 shows the necessity and benefit of having a reliable linear model of the process. The third column shows better performance for all kind of perturbations. When the model and the plant are different, the MPC performance is comparable to conventional controllers. When conventional strategy is augmented with steady-state decouplers, it outperformed the MPC 2 implementation. However, the maximum amplitude achieved by the MPC 2 is almost always smaller than the decoupling strategy. MPC can be viewed as a dynamic decoupling algorithm. Dynamic decoupling performs better than steady-state decoupling. Traditional dynamic decoupling yields complicated equations, hence it is rarely used. MPC better performance are not really due to its dynamic decoupling feature but to the incorporation of our process knowledge (model, constraints) into the computation of manipulated moves. When our process realisation is partly false, the MPC controller performance suffers. To recommend an MPC installation, the gains of the MPC controller have to be weighted against the cost of developing and maintaining the models. Model maintenance is an important issue as processes change over time and MPC performance is directly related to the accuracy of its models.

In this chapter, an integrated control strategy for the CSPP pilot paper machine was developed. Based on paper machine data, input/output models were constructed. The output variables studied included: headbox total and ash consistencies, white water total and ash consistencies, sheet ash content, and basis weight. The input variables considered were: machine chest flowrate, bentonite flowrate, CPAM flowrate, ratio of bentonite to CPAM, and filler flowrate. From the models, different steady-state relative gain arrays corresponding to different potential control strategies were computed. Also, the condition number of the plant was examined. From these control indexes, the best strategy turned out to be the most widely used in mills: white water total consistency with CPAM flowrate, ash

content with filler flowrate, and basis weight with machine chest flowrate. This strategy was simulated on a nonlinear model developed by Byoung-Uk Cho as part of his PhD thesis. Different controllers were tested. Namely, PID controllers and MPC controllers. MPC outperformed PID controllers when its models are closed to the real process.

## Chapter 5

### Conclusions

One objective of this project is to quantify the interactions among the wet-end manipulated variables and the controlled variables. Doing this, it is postulated that the control gain of multivariate strategy could be estimated. Another project objective was to test an MPC integrated strategy and to assess its advantages over traditional PID control.

To satisfy the project objectives, models between the manipulated variables and the controlled variables were developed. Considerable efforts have been put into the model building phase. The models developed are of the input/output types. They have been obtained using a linear regression algorithm where the distance between the model predicted value and the data is minimised. The final model quality in term of accurately representing the process is dependant on the quality of the data it is based upon. Good data will contain enough dynamic information to show the underlying process. Concretely, this means a fast sampling rate (in the order of 10 times faster than the process time constant), many moves on the manipulated variables (sufficient input excitation), and a high signal-to-noise ratio.

Once the models have been obtained, it was possible to analyze the interaction between the different variables. The tool used to study the interactions is the rela-

tive gain array (RGA) and simulations. The variables under study were: headbox total and ash consistencies, white water total and ash consistency, sheet ash content, and basis weight for the controlled variables; and machine chest flowrate, bentonite flowrate, CPAM flowrate, ratio of bentonite to CPAM flowrate, and filler flowrate. Data have been collected using the pilot paper machine of Cégep de Trois-Rivières. Based on the RGA analysis, the less interacting combination of variables is white water consistency, sheet ash content, and basis weight combined with CPAM flowrate, filler flowrate, and machine chest flowrate. Of these three controlled variables, the one most affected by all manipulating variables is white water consistency. Therefore, this variable would gain from a multivariable type of controller where all the input moves are taken into account. This contradicts the literature results. Possible explanations could be related to the quality of the models on which this conclusion is based. Another cause could be the different layout of the paper machine used giving rise to different interactions between the manipulated variables. Some other concern is the quality of the model used in the literature MPC application.

During the course of this project, many simulations were performed to test the MPC. In one scenario, the MPC models were obtained from the input/output data. The resulting controller was then tested on a nonlinear model. The nonlinear model was based on mass balances around the headbox, wire, and wire pit. To model the unknown retention mechanism, a fitted function based on machine chest mass flowrate, filler mass flowrate, CPAM dosage and bentonite dosage was added to the model. In this case, the input/output models did not reproduce well the nonlinear model behaviour. The resulting controller performances were similar or poorer than a traditional PID strategy. The most difficult controlled variable to keep at its setpoint in spite of perturbations was the white water consistency, the variable most affected by the interactions of the manipulated variables. In the second

scenario, the MPC models were obtained by linearising the nonlinear model around a steady state. In this case, the MPC models did reproduce well the nonlinear model behaviour. This controller responses outperformed the traditional PID strategy and even outperformed the traditional approach to multivariable system: PID controller augmented with steady-state decouplers. Based on simulations, MPC controllers can give good control performance but their performance is tied to the accuracy of the model used.

Until now, the control strategy developed in this project did not address a very common paper machine problem: sheet break. In an integrated strategy, this problem becomes even more serious as the loss of the controlled variable can adversely affect the controller performance. To counteract this, the wet-end equivalent variables to the dry-end variables should be included in the MPC controller. The dry-end sheet ash content is a function of headbox ash consistency. Similarly, the dry-end basis weight is a function of headbox total consistency. To add these two wet-end variable into the MPC controller, a predictor need to be develop. This predictor would output a range for each wet-end variable. In normal operation, if the wet-end variables were within the predictor specified range, the controller would optimise basis weight, ash content, and white water consistency as normal. In normal operation, if the wet-end variables were outside the specified range, the controller would first move them into their range and then, move the other variables. In sheet break operation, the controller would use only the wet-end variables and associated predictors to keep the machine under control. Naturally, simulations are needed to confirm all this. This would be an interesting follow-up project to this one. But, before one can address this problem, it is necessary to test if the headbox total consistency can effectively control the basis weight of a paper machine.

Headbox consistency control loop of the Paprican pilot paper machine was closed.



The controller used was a conventional PI implemented on a Toshiba DCS. Open-loop runs were performed to collect data, and build input/output models. The headbox system was multivariable and had two interacting variables: headbox consistency and headbox flowrate. From the models, a relative gain array analysis was performed. The system showed slight interactions, mainly on the headbox consistency variable. There is a dynamic decoupling already built in the system. Since the headbox flowrate time constant is approximately ten times faster than the headbox consistency time constant, the headbox flowrate is, in effect, decoupled from the headbox consistency. Various control strategies were tested: feedback, feedback augmented with steady-state decoupler, cascade, and cascade with a fast and a slow control valve. All the strategies were tested on the paper machine. No differences were observed since for all strategies the noise masked the performance gain predicted by simulations. Still, the controller was able to keep the headbox consistency at its setpoint. Wet samples taken from the machine and successively dried showed that the controller was able to keep the basis weight constant. The next step is to develop a predictor.

Analysis of the consistency signals with auto-correlation revealed a periodic component in the signal. Part of this component was traced back to the press broke pulper controller. This controller was tuned very aggressively to react fast when a sheet break occurs. However, during our trial, the system was running in full recycle, i.e. producing no paper. Therefore the controller injected a periodic component in the system. This emphasises the importance of seeing the paper machine processes (approach system, wet-end, dry-end, recycle system) as a whole. It is also demonstrating that the overall paper machine performance is dependant on all the sub-processes. Since incorporating a whole process into one controller is a feature of model predictive control, adding more paper machine variables into a MPC

controller is an interesting future research avenue.

## References

- Artama, M. & Nokelainen, J. (1997), 'Control of retention and ash', *Paper Technology* (October), 34–44.
- Berger, R. (2000), Wet end management through charge analysis – establishing an on-line concept with laboratory instruments, *in* 'Scientific and Technical Advances in Wet End Chemistry', Pira, Barcelona, p. Paper 13.
- Bernier, J.-F. & Begin, B. (1994), 'Experience of a microparticle retention aid system', *Tappi Journal* **77**(11), 217–224.
- Boardman, D. E. (1993), 'Some practical observations on the use of cationic agents in the control of interfering substances', *Tappi Journal* **76**(12), 148–152.
- Brouwer, P. H. (1991), 'The relationship between zeta potential and ionic demand and how it affects wet-end retention', *Tappi Journal* (January), 170–179.
- Cho, B.-U., Garnier, G., Paradis, J. & Perrier, M. (2001*a*), Dynamics of filler retention with a PAM/bentonite system, *in* 'Proceedings of the 87th PAPTAC Annual Meeting', Montreal, Quebec, pp. B127–B134.
- Cho, B.-U., Garnier, G., Paradis, J. & Perrier, M. (2001*b*), 'Filler retention with a PAM/bentonite system – effect of collision efficiency', *submitted to Nordic pulp and paper research journal*. pp. 1–18.

- Chung, D., Cantrell, J. & Lefevre, G. (1993), 'Control of detrimental substances', *Pulp and Paper Canada* **94**(12), T403–T408.
- CPPA (2000), 'Cppla – 1998 annual review'.  
[www.cppa.org/english/cppa/rev98/page4\\_5.htm](http://www.cppa.org/english/cppa/rev98/page4_5.htm).
- El Ghali, S. (2001), Commande prédictive de la partie humide d'une machine à papier, Projet M.Ing, École Polytechnique de Montréal.
- Garcia, C. E., Prett, D. M. & Morari, M. (1989), 'Model predictive control: Theory and practice - a survey', *Automatica* **25**(3), 335–348.
- Gauss, K. (1809), *Theoria Motus Corporum Celestium, English Translation: Theory of the Motion of Heavenly Bodies*, Dover(1963), New York. Quoted by Ljung (1999), p. 545.
- Honig, D. S., Turnbull, R. J. & Wheeler, C. (1999), Retention systems for highly filled paper, in 'TAPPI 99 Proceedings', TAPPI Press, pp. 1335–1343.
- Kessler, B., Magee, K. & VanPembrook, K. (2000), Optimizing papermachine retention through tray consistency closed loop control and trend analysis, in 'TAPPI Papermakers Conference and Trade Fair', TAPPI Press, pp. 539–543.
- Kolko, B. (2001), Process control strategies for the wet-end of papermaking, Bachelor of engineering final year project, École Polytechnique de Montréal.
- Kortelainen, H. (1991), 'A monitoring system for the wet-end', *Paper Technology* (January), 12–16.
- Lang, D., Nokelainen, J., Rantala, T., Huhtelin, T., Tian, L. & Kuusisto, R. (1999), Multivariable controller integrating traditional scanner feedback controls with

- wet end measurements, *in* 'TAPPI 99 Proceedings', Vol. 2, Atlanta, USA, pp. 859–865.
- Laurikkala, M., Vuoti, M., Huhtelin, T. & Koivo, H. (1998), 'Paper quality controls by utilizing new measurement capabilities', *Pulp and Paper Canada* **99**(7), T224–T227.
- Ljung, L. (1999), *System Identification, Theory for the User*, PTR Prentice Hall Information and System Sciences Series, 2nd edn, Prentice-Hall, New Jersey.
- Luyben, W. L. (1990), *Process Modeling, Simulation and Control for Chemical Engineers*, Chemical Engineering Series, 2nd edn, McGraw-Hill International, Singapore.
- Miyanishi, T., Imamura, K. & Hata, K. (1990), 'A new wet-end control system with on-line sensors', *Tappi Journal* **73**(7), 128–132.
- Morari, M. & Ricker, N. (1998), 'Model predictive control toolbox for use with matlab , user guide, version 1'.
- Nazir, B. & Carnegie-Jones, J. (1991), 'Optimising wet-end chemistry - the practicalities', *Paper Technology* (December), 37–41.
- Nobleza, G. & Roche, A. (1988), The use of spectral analysis in process variability studies, Miscellaneous Reports MR 153, Pulp and Paper Institute of Canada.
- Nokelainen, J. & Piirainen, R. (1995), Wet end control-results and new possibilities, *in* 'An international conference on Papermaking and Paper machine Technology', pp. 21–30.

- Nokelainen, J., Piirainen, R. & Ramsey, B. (1993), Practical experiences with white water consistency control of a paper machine wet end, *in* '1993 Process Control Conference', Tappi Proceedings, pp. 3–13.
- Nokkelainen, J. (2000), On-line charge and retention controls for effective wet end management, *in* 'Scientific and Technical Advances in Wet End Chemistry', Pira, Barcelona, p. Paper 17.
- Ogunnaike, B. A. & Ray, W. H. (1994), *Process Dynamics, Modeling, and Control*, Topics in chemical engineering, Oxford University Press.
- Olsson, B. & Renaud, S. (2000), Wet-end control improvements in boardmaking applications, *in* 'TAPPI Papermakers Conference and Trade Fair', TAPPI Press, pp. 757–765.
- Patton, P. A. & Lee, D. T. (1993), 'Charge analysis: powerful tools in wet-end optimization', *Tappi Journal* **76**(8), 107–115.
- Piirto, M. & Koivo, H. (1991a), Advanced control of a paper machine wet end, *in* 'IFAC Symposium on Advanced Control of Chemical Processes', Toulouse, France, pp. 47–52.
- Piirto, M. & Koivo, H. (1991b), Hierarchical computer system for retention control in the wet end of a paper machine, *in* 'Proceedings IECON '91', Vol. 2, pp. 1413–1417.
- Proulx, R., Morissette, L. & Ruel, M. (1999), 'Perspectives et tendances des stratégies de contrôle au bout humide', *Les Papetières du Québec* **10**(6), 12–15.
- Proulx, R. & Renaud, S. (2000), Implementation and results of white water consis-

- tency control at the wet end, *in* 'TAPPI PCE and I Conference and ISA-PUPID 39th Annual symposium', TAPPI Press, pp. 85–95.
- Qin, S. J. & Badgwell, T. A. (1996), An overview of industrial model predictive control technology, *in* 'Proceedings of the Fifth International Conference on Chemical Process Control', Vol. 93 of *AIChE Symposium Series*, Cache and Aiche, Tahoe City, California, pp. 232–256.
- Rantala, T., Nokelainen, J. & Artama, M. (1999), Wet end management by controlling consistencies and charge, *in* 'TAPPI 99 Proceedings', pp. 1189–1211.
- Rantala, T., Tarhonen, P. & Koivo, H. (1993), Retention modeling and control in the paper machine wet end, *in* '12th World Congress International Federation of Automatic Control - Preprints', Vol. 6, Sydney, Australia, pp. 61–66.
- Rantala, T., Tarhonen, P. & Koivo, H. (1994a), 'Adaptive retention control in a paper machine', *Pulp and Paper Canada* **95**(8), T299–T303.
- Rantala, T., Tarhonen, P. & Koivo, H. (1994b), 'Control of paper machine wire retention', *Tappi Journal* **77**(12), 125–132.
- Renaud, S., Svensson, S. & Tomicic, M. (1998), Wet-end chemistry – case history: Paper machine improvements through polymer control, *in* 'Process Control, Electrical and Information Conference', Vol. 1, Tappi Press, Vancouver, BC , Canada, pp. 461–471.
- Scott, W. E. (1986), 'Fines management and control in wet-end chemistry', *Tappi Journal* **69**(11), 30–34.
- Scott, W. E. (1991), Papermaking chemistry, *in* B. A. Thorp, ed., 'Paper Machine

Operations', 3 edn, Vol. 7 of *Pulp and Paper Manufacture*, The joint textbook committee of the paper industry, Atlanta, pp. 140–187.

Scott, W. E. (1992), Surface colloid chemistry interactions important in stock preparation, in R. W. Hagemeyer & D. W. Manson, eds, 'Stock Preparation', 3 edn, Vol. 6 of *Pulp and Paper Manufacture*, The joint textbook committee of the paper industry, Atlanta, pp. 3–18.

Seborg, D. E., Edgar, T. F. & Mellichamp, D. A. (1989), *Process Dynamics and Control*, Wiley Series in Chemical Engineering, John Wiley & Sons, New York.

Skogestad, S. & Postlethwaite, I. (1996), *Multivariable Feedback Control, Analysis and Design*, John Wiley & Sons, Chichester.

Sopenlehto, T. (1995), On-line monitoring and control in the wet-end, in C. O. Au & I. Thorn, eds, 'Application of Wet End Paper Chemistry', Blackie Academic and Professional, pp. 173–182.

Stitt, J. B. (1998), 'Charge control helps tissue producers achieve quality, productivity benefits', *Pulp and Paper* **72**(May), 109–114.

Swerin, A. & Odberg, L. (1997), Some aspects of retention aids, in 'Fundamentals of papermaking materials -11th fundamental research symposium', Vol. 1, Pira International, Cambridge, UK, pp. 265–350.

Tomney, T., Pruszynski, P., Armstrong, J. & Hurley, R. (1998), 'Controlling filler retention in mechanical grades', *Pulp and Paper Canada* **99**(8), T274–T277.

Yeager, R. L. (1997), 'Retention analysis gives Avenor a window into the wet end', *Pulp and Paper* (4), 73–78.



## Appendix A

### Schematics of different wet-end control strategies reported in the literature

The following figures represent the different control strategies reported in the literature and explained in section 1.2.2, Table 1.5.

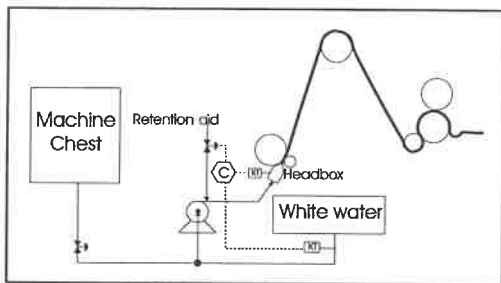


Figure A.1: Retention control

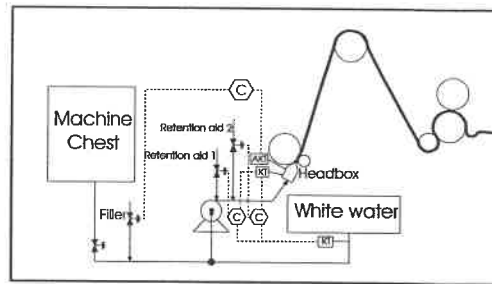


Figure A.2: Retention and headbox ash control

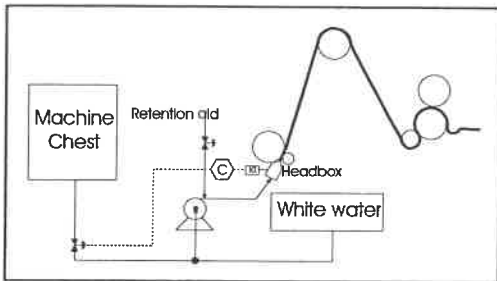


Figure A.3: Headbox consistency control

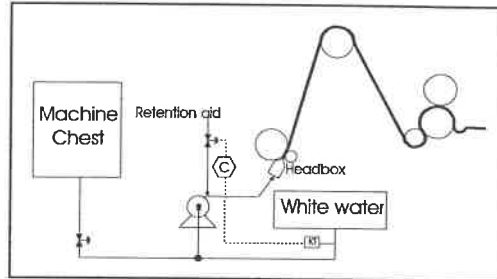


Figure A.4: White water consistency control

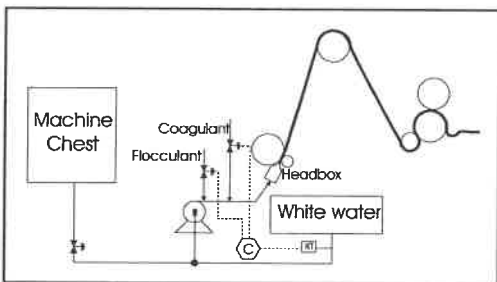


Figure A.5: White water consistency ratio control

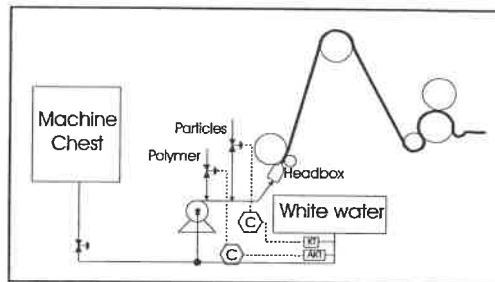


Figure A.6: White water ash and total consistencies control

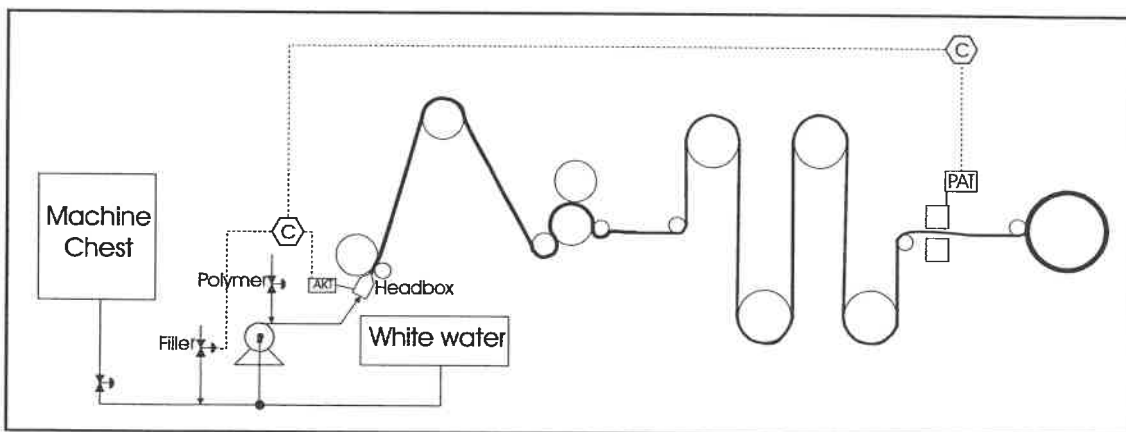


Figure A.7: Ash cascade control: outer loop: paper ash, inner loop: headbox ash consistency

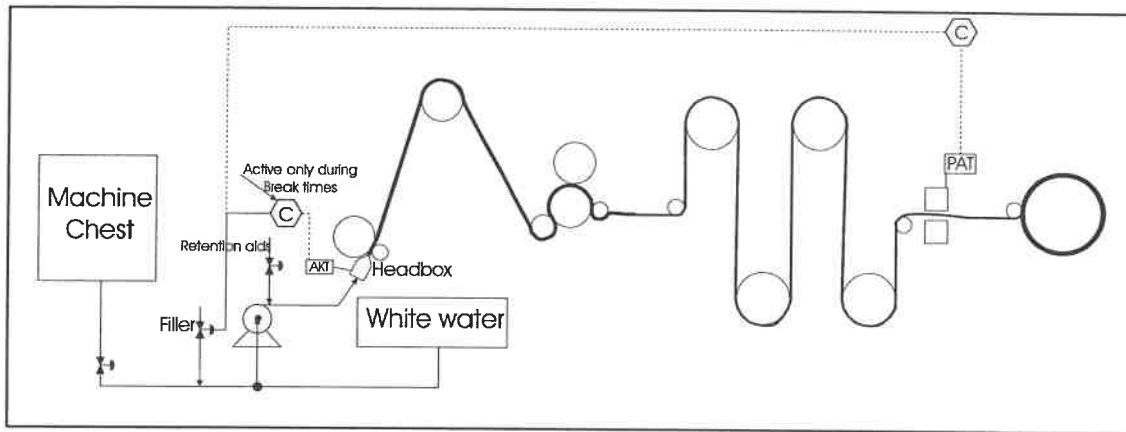


Figure A.8: Breaktime ash control

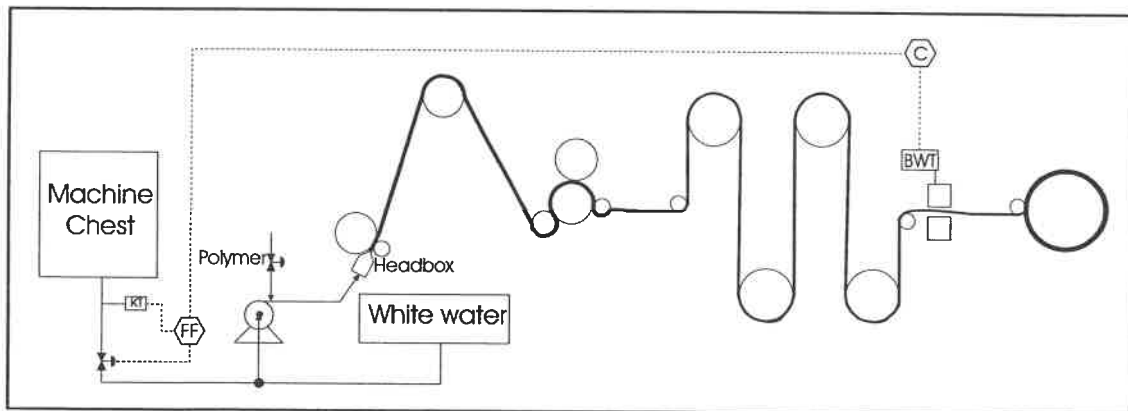


Figure A.9: Feedforward control of thick stock consistency

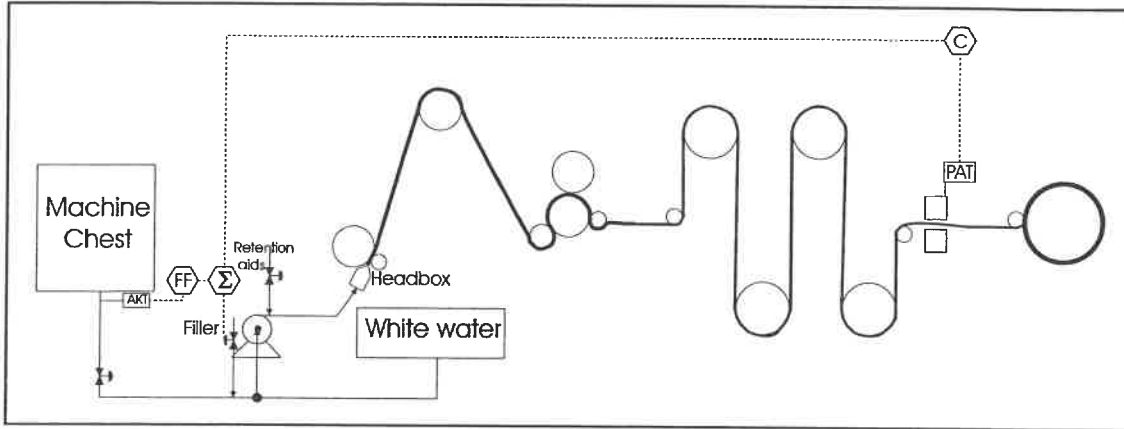


Figure A.10: Feedforward control of thick stock ash consistency

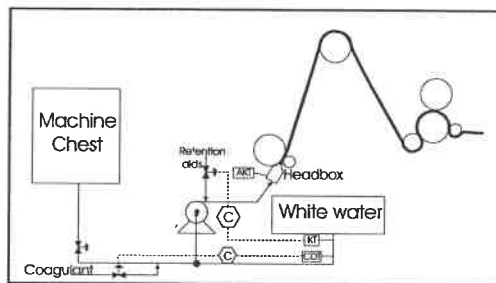


Figure A.11: Cationic demand and white water control

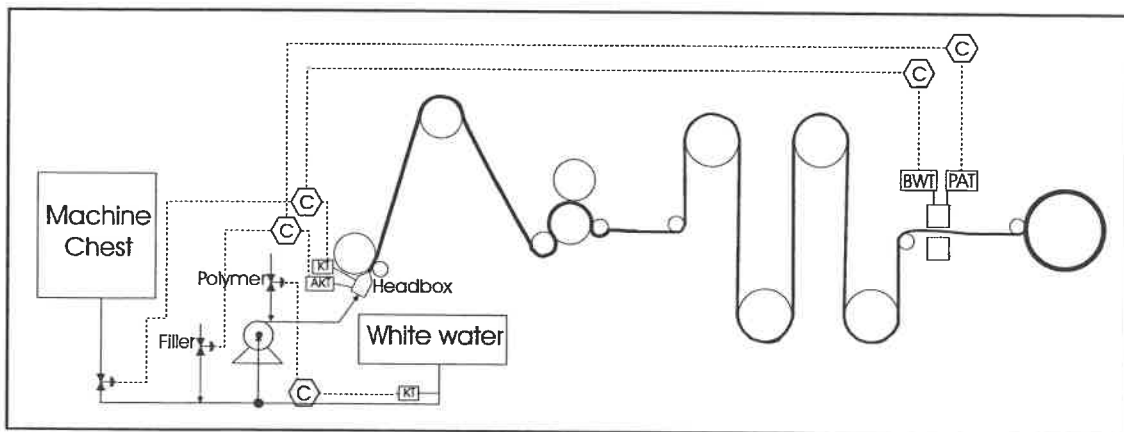


Figure A.12: Integrated strategy: cascade control for ash and basis weight, and white water consistency control

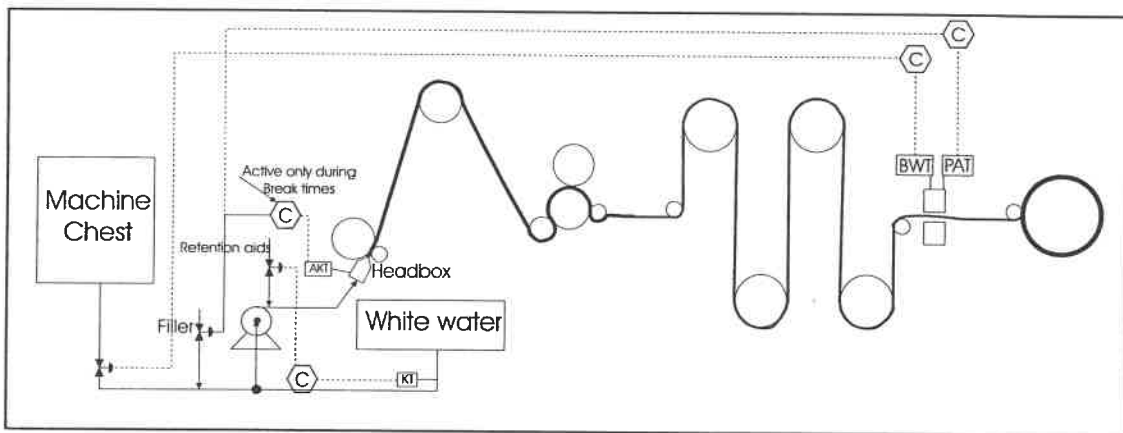


Figure A.13: Integrated strategy: white water consistency, basis weight and ash control

# Appendix B

## Linear Regression Algorithm

The one-step ahead prediction for the model described in (2.1) can be computed using B.1.

$$\hat{y}_{k|k-1} = H^{-1}(q^{-1})G(q^{-1})u_k + [1 - H^{-1}(q^{-1})] y_k \quad (\text{B.1})$$

For parametric models, we can stress the fact that there are unknown parameters by rewriting (2.1) as (B.2) where  $\theta$  is the vector of unknown parameters.

$$y_k = G(q^{-1}, \theta)u_k + H(q^{-1}, \theta)e_k \quad (\text{B.2})$$

The one step ahead prediction becomes:

$$\hat{y}_{k|\theta} = H^{-1}(q^{-1}, \theta)G(q^{-1}, \theta)u_k + [1 - H^{-1}(q^{-1}, \theta)] y_k \quad (\text{B.3})$$

For the general parametric model used (2.2), the one step ahead prediction is then: (with  $G(q^{-1}, \theta) = \frac{B(q^{-1})}{A(q^{-1})F(q^{-1})}$  and  $H(q^{-1}, \theta) = \frac{C(q^{-1})}{A(q^{-1})D(q^{-1})}$  )

$$\hat{y}_{k|\theta} = \frac{D(q^{-1})B(q^{-1})}{C(q^{-1})F(q^{-1})}u_k + \left[1 - \frac{A(q^{-1})D(q^{-1})}{C(q^{-1})}\right] y_k \quad (\text{B.4})$$

We can now find the prediction error by substituting B.4 into B.5:

$$\varepsilon_{k,\theta} = y_k - \hat{y}_{k,\theta} \quad (\text{B.5})$$

$$\varepsilon_{k,\theta} = \frac{D(q^{-1})}{C(q^{-1})} \left[ A(q^{-1})y_k - \frac{B(q^{-1})}{F(q^{-1})}u_k \right] \quad (\text{B.6})$$

Defining temporary variables ( $w_{k,\theta}$  and  $v_{k,\theta}$ ) we can build a regressor  $\psi$  (B.9) for the estimate  $\theta$  (B.10). Formally, B.9 is a pseudo-regressor because it is partly constructed using the current model.

$$w_{k,\theta} = \frac{B(q^{-1})}{F(q^{-1})}u_k \quad (\text{B.7})$$

$$v_{k,\theta} = A(q^{-1})y_k - w_{k,\theta} \quad (\text{B.8})$$

$$\psi_{k,\theta} = [-y_{k-1}, -y_{k-2}, \dots, -y_{k-na}, \quad (\text{B.9})$$

$$u_{k-1}, u_{k-2}, \dots, u_{k-nb},$$

$$-w_{k-1,\theta}, -w_{k-2,\theta}, \dots, -w_{k-nf,\theta},$$

$$\varepsilon_{k-1,\theta}, \varepsilon_{k-2,\theta}, \dots, \varepsilon_{k-nc,\theta},$$

$$-v_{k-1,\theta}, -v_{k-2,\theta}, \dots, -v_{k-nd,\theta}]^T$$

$$\theta = [a_1 a_2 \dots a_{na} b_1 b_2 \dots b_{nb} f_1 f_2 \dots f_{nf} c_1 c_2 \dots c_{nc} d_1 d_2 \dots d_{nd}]^T \quad (\text{B.10})$$

By multiplying  $\psi_{k,\theta}$  with  $\theta$  we obtain:

$$\begin{aligned} \psi_{k,\theta}^T \theta &= -a_1 y_{k-1} - a_2 y_{k-2} - \dots - a_{na} y_{k-na} \\ &\quad + b_1 u_{k-1} + b_2 u_{k-2} + \dots + b_{nb} u_{k-nb} \\ &\quad - f_1 w_{k-1,\theta} - f_2 w_{k-2,\theta} - \dots - f_{nf} w_{k-nf,\theta} \\ &\quad + c_1 \varepsilon_{k-1,\theta} + c_2 \varepsilon_{k-2,\theta} + \dots + c_{nc} \varepsilon_{k-nc,\theta} \\ &\quad - d_1 v_{k-1,\theta} - d_2 v_{k-2,\theta} - \dots - d_{nd} v_{k-nd,\theta} \end{aligned}$$

$$\begin{aligned}
&= -(a_1q^{-1} + a_2q^{-2} + \dots + a_{na}q^{-na})y_k \\
&\quad + (b_1q^{-1} + b_2q^{-2} + \dots + b_{nb}q^{-nb})u_k \\
&\quad - (f_1q^{-1} + f_2q^{-2} + \dots + f_{nf}q^{-nf})w_k \\
&\quad + (c_1q^{-1} + c_2q^{-2} + \dots + c_{nc}q^{-nc})\varepsilon_k \\
&\quad - (d_1q^{-1} + d_2q^{-2} + \dots + d_{nd}q^{-nd})v_k
\end{aligned}$$

Using the definition of  $A(q^{-1})$ ,  $B(q^{-1})$ ,  $F(q^{-1})$ ,  $C(q^{-1})$ ,  $D(q^{-1})$  given in equations 2.3 through 2.7, the above expression reduces to:

$$\begin{aligned}
\psi_{k,\theta}^T \theta &= (1 - A(q^{-1}))y_k + B(q^{-1})u_k + (1 - F(q^{-1}))w_k \\
&\quad + (C(q^{-1}) - 1)\varepsilon_k + (1 - D(q^{-1}))v_k
\end{aligned}$$

Substituting for  $\varepsilon_k$ (B.6), we obtain:

$$\begin{aligned}
\psi_{k,\theta}^T \theta &= (1 - A(q^{-1}))y_k + B(q^{-1})u_k \\
&\quad + (1 - F(q^{-1}))w_k + \left(1 - \frac{D(q^{-1})}{C(q^{-1})}\right)v_k
\end{aligned}$$

Substituting for  $v_k$ (B.8), we obtain:

$$\begin{aligned}
\psi_{k,\theta}^T \theta &= \left(1 - \frac{A(q^{-1})D(q^{-1})}{C(q^{-1})}\right)y_k + B(q^{-1})u_k \\
&\quad + \left(\frac{D(q^{-1})}{C(q^{-1})} - F(q^{-1})\right)w_k
\end{aligned}$$

Finally, replacing  $w_k$ (B.7), we obtain:

$$\begin{aligned}
\psi_{k,\theta}^T \theta &= \left(1 - \frac{A(q^{-1})D(q^{-1})}{C(q^{-1})}\right)y_k + \frac{D(q^{-1})B(q^{-1})}{C(q^{-1})F(q^{-1})}u_k \\
&= \hat{y}_{k|\theta}
\end{aligned} \tag{B.11}$$



With (B.11), a series of equations can be formed (N being the total number of data in the sample) :

$$\begin{aligned} y_1 &= \psi_{1,\theta}^T \theta + \varepsilon_1 \\ y_2 &= \psi_{2,\theta}^T \theta + \varepsilon_2 \\ &\vdots \\ y_N &= \psi_{N,\theta}^T \theta + \varepsilon_N \end{aligned}$$

or equivalently:

$$\mathbf{Y}_N = \mathbf{\Psi}_{N,\theta} \theta + \mathbf{E}_N \quad (\text{B.12})$$

where  $\mathbf{Y}$ ,  $\mathbf{E}$  are  $[N \times 1]$  vectors and  $\mathbf{\Psi}$ , a  $[N \times (na + nb + nf + nc + nd)]$  matrix, is defined in (B.13).

$$\mathbf{\Psi}_{N,\theta} = \begin{bmatrix} \psi_{1,\theta}^T \\ \psi_{2,\theta}^T \\ \vdots \\ \psi_{N,\theta}^T \end{bmatrix} \quad (\text{B.13})$$

The next step is to find  $\theta$  that minimise the error vector. Formally, we can write:

$$\theta = \arg \min_{\theta} \mathbf{E}_N^T \mathbf{E}_N \quad (\text{B.14})$$

Replacing the error expression in B.14 by (B.12), we obtained B.16. This expression is known as a pseudo-linear regression. To solve this, we need to estimate the gradient. In Matlab, this is done using a Gauss-Newton iterative method (Ljung 1999, p327-328). Because of the iterative nature of the method, the solution found is dependent on the initial condition. The minimisation routine can certainly

find a local minimum. In the model building context, a local minimum can be acceptable if the validation procedure is satisfied. The representation sought is the *best* one and not the *true* one (Although it would be better to have the *real* model but this leads to the theological question: Is there such a thing as a *true* model?).

$$\mathbf{E}_N^T \mathbf{E}_N = (\mathbf{Y}_N - \Psi_{N,\theta} \theta)^T (\mathbf{Y}_N - \Psi_{N,\theta} \theta) \quad (\text{B.15})$$

$$\frac{\partial \mathbf{E}_N^T \mathbf{E}_N}{\partial \theta} = 2(\mathbf{Y}_N - \Psi_{N,\theta} \theta)^T \frac{\partial (\mathbf{Y}_N - \Psi_{N,\theta} \theta)}{\partial \theta} \quad (\text{B.16})$$

$$(\text{B.17})$$

The special case of (B.16) is the linear regression where the regressor does not depend on  $\theta$  (for example, in the case of ARX model). The estimate  $\theta$  becomes a quadratic function and a minimum can be guaranteed as in (B.18) and B.19.

$$\frac{\partial \mathbf{E}_N^T \mathbf{E}_N}{\partial \theta} = -2(\mathbf{Y}_N - \Psi_N \theta)^T \Psi_N = 0 \quad (\text{B.18})$$

$$\theta = (\Psi_N^T \Psi_N)^{-1} (\Psi_N^T \mathbf{Y}_N) \quad (\text{B.19})$$

This algorithm is implemented in Matlab through the *pem* function of the *System Identification Toolbox*. It was used to compute all of the models used in this project.

## Appendix C

# Identification Data and Models of Paprican Pilot Paper Machine

Before controlling the headbox consistency, models are necessary to test the control strategies. This appendix gives the detailed procedure and the design decisions made to obtain the models used in chapter 3. The model building procedure is explained in chapter 2.

Every model is presented in the same way. First, a figure presents the identification data. The identification figure consists of two parts. The first part, drawn with a solid line, represents the estimation data. The second part, drawn with a dash line, represents the validation data. Parametric models with a total number of parameters ranging from 2 to 15 are calculated and compared. Fourteen models are selected and presented on another figure. After a detailed analysis, the selected model is plotted against the validation data.

### C.1 Headbox consistency models ( $y_1$ )

From a simple mass balance around the headbox, one can readily identify two potential manipulated variables: the thick stock flowrate and the white water dilution rate. Physically, the manipulated variables could be : the thick stock valve position

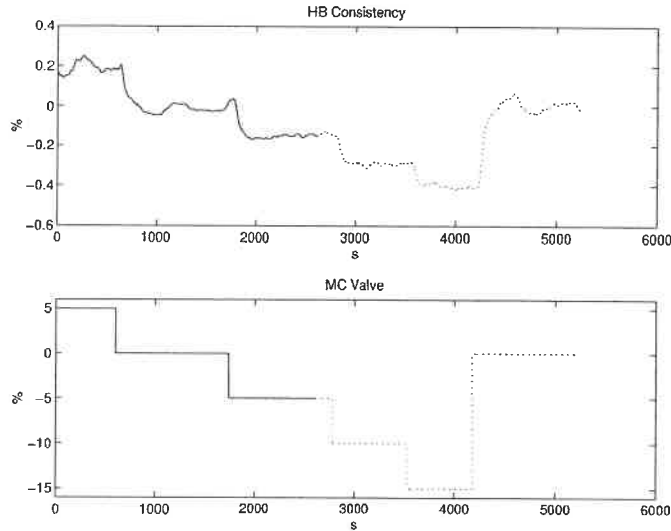


Figure C.1: Identification data for the model between  $y_1$  and  $u_1$

and the fanpump rpm. Another potential variable is the thick stock flowrate. In the latter case, a cascade strategy is necessary. The next few pages explain the model building procedure between these manipulated variables and the headbox consistency.

### C.1.1 Machine chest valve ( $u_1$ )

Figure C.1 presents the identification data. Figure C.2 presents the FPE (bar plot) and the fit (line plot) of the selected models. Inside the bar, from top to bottom are the respective values of  $na$ ,  $nb$ ,  $nc$ ,  $nd$ ,  $nf$ , and  $nk$ .

From the preliminary analysis, models 6, 9 and 11 are chosen to undergo a deeper analysis. Those models were selected because, respectively: a good FPE /fit combination for the number of parameter, the best FPE / fit combination and, the best fit. The models are presented in Table C.1. A pole/zero analysis reveals that models BJ(3,2,1,3) and BJ(4,3,1,3) do have a cancelation. It is interesting to note, that the two models have poles very close to the unit circle. The residuals

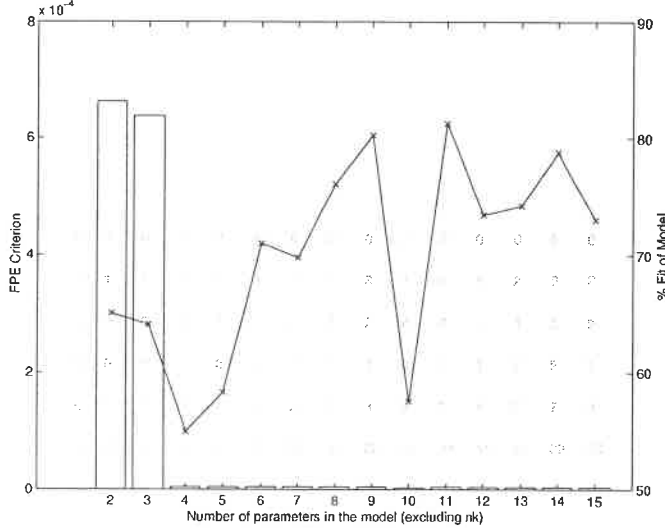


Figure C.2: Candidate models between  $y_1$  and  $u_1$

analysis shows a periodic auto-correlation of the error signal for all models. No cross-correlation between the error and input signals is detected. The BJ(1,1,1,3) is kept since the added parameters in the other models only try to model the valve non-linearity. The linearity range of this model is  $\pm 5\%$  in valve opening and  $\pm 0.2\%$  consistency. The nominal values are 65% for the valve and 0.91% for the consistency. The OE(1,1) model was also computed to serve for PI tuning. This model has an important auto-correlation between its residuals. There is significant cross-correlation between the residuals and the input. The important features of both models (equations C.1 and C.2) are described in Table C.2 and are graphed with the validation data in Figure C.3.

$$y_1 = \frac{0.0007003q^{-45}}{1 - 0.9794q^{-1}}u_1 + e \quad (\text{C.1})$$

$$y_1 = \frac{5.511 \times 10^{-5}q^{-37}}{1 - 0.9247q^{-1} - 0.9946q^{-2} + 0.9209q^{-3}}u_1 + \frac{1 - 0.0376q^{-1}}{1 - 0.9978q^{-1}}e \quad (\text{C.2})$$

Table C.1: Preliminary models between  $y_1$  and  $u_1$ 

Model Name	Model
BJ(1,1,1,3)	$y = \frac{5.511 \times 10^{-5} q^{-37}}{1 - 0.9247q^{-1} - 0.9946q^{-2} + 0.9209q^{-3}} u + \frac{1 - 0.0376q^{-1}}{1 - 0.9978q^{-1}} e$
BJ(3,2,1,3)	$y = \frac{-0.0001283q^{-35} + 0.0003547q^{-36} - 0.0002229q^{-37}}{1 - 2.524q^{-1} + 2.06q^{-2} - 0.5364q^{-3}} u + \frac{1 - 0.04277q^{-1} - 0.05077q^{-2}}{1 - 0.9972q^{-1}} e$
BJ(4,3,1,3)	$y = \frac{-2.227 \times 10^{-5} q^{-34} - 5.102 \times 10^{-5} q^{-35} + 0.0002512q^{-36} - 0.0001749q^{-37}}{1 - 2.57q^{-1} + 2.153q^{-2} - 0.5827q^{-3}} u + \frac{1 - 0.03976q^{-1} - 0.04641q^{-2} - 0.04475q^{-3}}{1 - 0.9979q^{-1}} e$

Table C.2: Characteristics of the chosen models between  $y_1$  and  $u_1$ 

Model Name	Equation Number	FPE	Fit (%)	Model Error Model Fit (%)	Linear Fit (%)
OE(1,1)	(C.1)	$6.62 \times 10^{-4}$	65.0	4.06	80.4
BJ(1,1,1,3)	(C.2)	$4.22 \times 10^{-6}$	71.0	-25.8	79.7

### C.1.2 Fanpump rpm ( $u_2$ )

The identification data is presented in Figure C.4. The fanpump rpm is expressed as a percentage of its scale. Figure C.5 presents the FPE (bar plot) and the fit (line plot) of the selected models. Inside the bar, from top to bottom are the respective values of  $na$ ,  $nb$ ,  $nc$ ,  $nd$ ,  $nf$ ,  $nk$ .

From the preliminary analysis, model 7 and 13 are chosen to undergo a deeper analysis. Those models were selected because, respectively: the best FPE / fit combination and, the best fit. Those models are presented in Table C.3. A pole/zero analysis shows no cancellation for the models under study. It is interesting to note, that the two models have poles very close to the unit circle. The residuals analysis shows some auto-correlation of the error signal and no cross-correlation between the error and input signals for both models. The impulse model of the error model is

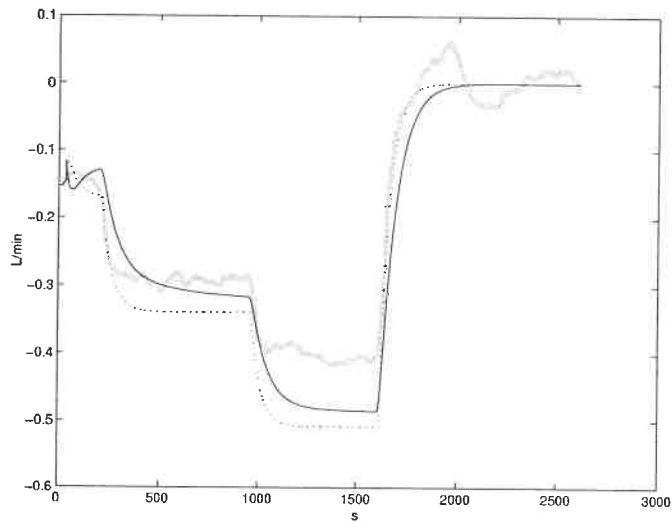


Figure C.3: Simulation of chosen models between  $y_1$  and  $u_1$  against validation data. OE(1,1) model : dotted line, *best* model : black line, validation data : grey line

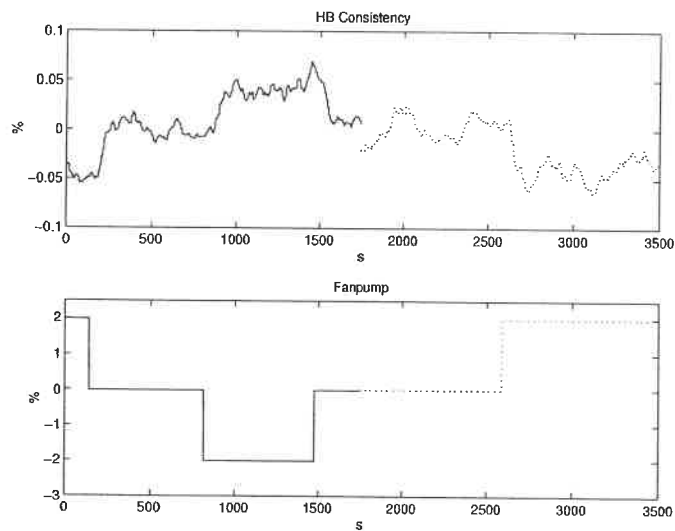


Figure C.4: Identification data for the model between  $y_1$  and  $u_2$

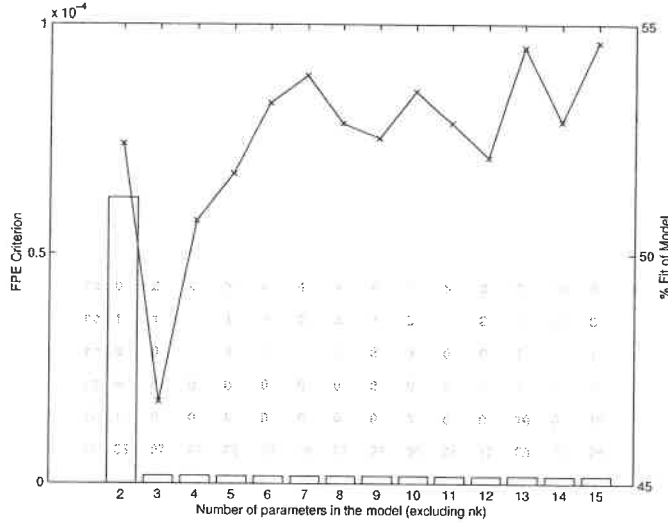


Figure C.5: Candidate models between  $y_1$  and  $u_2$

similar for the two models. There is no significant advantages to chose the more complicated model. Therefore, the ARMAX(4,2,1) is kept. The model can be considered linear over the whole data set. The linearity range of this model is  $\pm 2$  % in fanpump and  $\pm 0.05$  % consistency. The nominal values are 40.2 % for the fanpump and 0.90 % for the consistency. The OE(1,1) model was also computed to serve for PI tuning. This model has an important auto-correlation between its residuals. The model error fit is small. The important features of both models (equations C.3 and C.4) are described in Table C.4 and graphed with the validation data in Figure C.6.

$$y_1 = \frac{-0.0004126q^{-35}}{1 - 0.9808q^{-1}} u_2 + e \quad (\text{C.3})$$

$$\begin{aligned} (1 - 1.912q^{-1} + 0.9082q^{-2} - 0.02705q^{-3} + 0.03174q^{-4})y_1 &= (0.0003028q^{-1} - 0.0003251q^{-20})u_2 \\ &+ (1 - 0.9455q^{-1})e \end{aligned} \quad (\text{C.4})$$



Table C.3: Preliminary models between  $y_1$  and  $u_2$ 

Model Name	Model
ARMAX(4,2,1)	$(1 - 1.912q^{-1} + 0.9082q^{-2} - 0.02705q^{-3} + 0.03174q^{-4})y =$ $(0.0003028q^{-19} - 0.0003251q^{-20})u$ $+(1 - 0.9455q^{-1})e$
BJ(1,1,1,10)	$y = \frac{-5.564 \times 10^{-5} q^{-28}}{1 - 2.213q^{-1} + 1.547q^{-2} + 0.129q^{-3} - 0.312q^{-4}}$ $\frac{-0.3528q^{-5} - 0.1433q^{-6} + 0.1776q^{-7} + 1.155q^{-8} - 1.825q^{-9} + 0.8409q^{-10}}{1 - 0.9885q^{-1}}u$

Table C.4: Characteristics of the chosen models between  $y_1$  and  $u_2$ 

Model Name	Equation Number	FPE	Fit (%)	Model Error Model Fit (%)	Linear Fit (%)
OE(1,1)	(C.3)	$6.21 \times 10^{-5}$	52.4	-1.6	68.1
ARMAX(4,2,1)	(C.4)	$1.64 \times 10^{-6}$	53.8	-565	69.1

### C.1.3 Machine chest flowrate ( $u_3$ )

Figure C.7 presents the identification data. Figure C.8 presents the FPE (bar plot) and the fit (line plot) of the selected models. Inside the bar, from top to bottom are the respective values of  $na$ ,  $nb$ ,  $nc$ ,  $nd$ ,  $nf$ , and  $nk$ .

From the preliminary analysis, models 6, 9 and 15 are chosen to undergo a deeper analysis. Those models were selected because, respectively: a good, a better and the best FPE /fit combination. The models are presented in Table C.5. A pole/zero analysis reveals that model ARMAX(2,3,1) does have a cancelation. The analysis of the residuals shows a periodic auto-correlation of the error signal for all models. No cross-correlation between the error and input signals is detected. The ARAR-MAX(3,1,1,4) is kept since adding more parameters yields a very small improvement. The whole data set can be considered linear. Then, the linearity range is -600 to 300 L/min for the flowrate and -0.4 to 0.2% for the consistency. The nominal values are

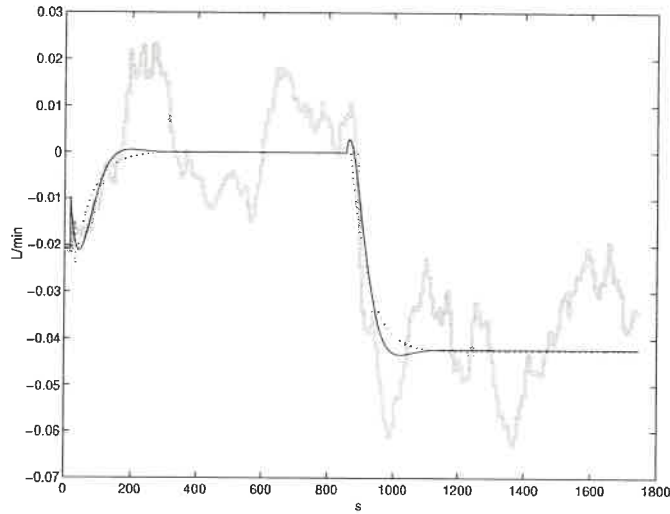


Figure C.6: Simulation of chosen models between  $y_1$  and  $u_2$  against validation data. OE(1,1) model : dotted line, *best* model : black line, validation data : grey line

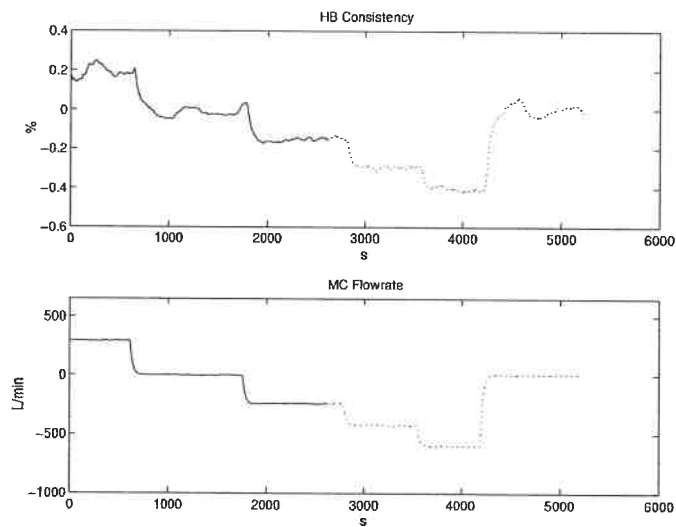


Figure C.7: Identification data for the model between  $y_1$  and  $u_3$

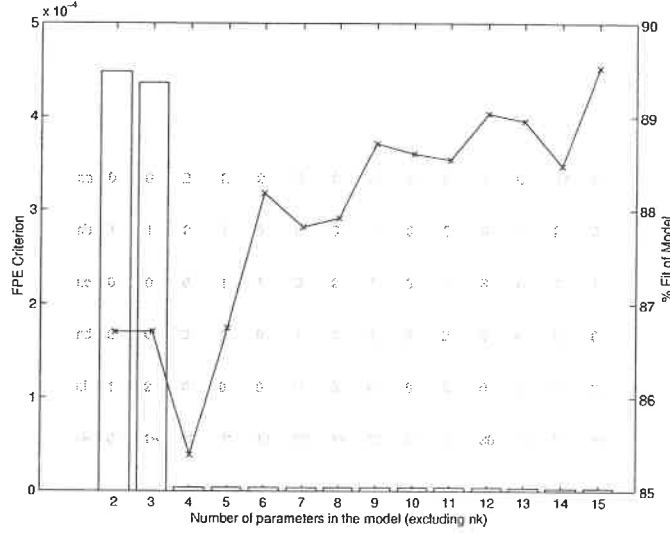


Figure C.8: Candidate models between  $y_1$  and  $u_3$

1016 L/min for the flowrate and 0.91 % for the consistency. The OE(1,1) model was also computed to serve for PI tuning. This model has an important auto-correlation between its residuals. There is significant cross-correlation between the residuals and the input. The important features of both models (C.5 and C.6) are described in Table C.6 and are graphed with the validation data in Figure C.9.

$$y_1 = \frac{1.891 \times 10^{-5} q^{-27}}{1 - 0.9709 q^{-1}} u_3 + e \quad (\text{C.5})$$

$$y_1 = \frac{1.352 \times 10^{-5} q^{-31}}{1 - 1.98 q^{-1} + 1.571 q^{-2} - 0.5714 q^{-3}} u_3 \quad (\text{C.6})$$

$$+ \frac{1 - 0.8916 q^{-1}}{1 + 0.2054 q^{-1} - 0.3766 q^{-2} - 0.5045 q^{-3} - 0.2986 q^{-4}}$$

$$\frac{1}{1 - 1.98 q^{-1} + 1.571 q^{-2} - 0.5714 q^{-3}} e$$

Table C.5: Preliminary models between  $y_1$  and  $u_3$ 

Model Name	Model
ARMAX(2,3,1)	$(1 - 1.953q^{-1} + 0.9532q^{-2})y =$ $(-0.000191q^{-19} + 0.0004084q^{-20} - 0.0002172q^{-21})u$ $+(1 - 0.952q^{-1})e$
ARARMAX(3,1,1,4)	$(1 - 1.98q^{-1} + 1.571q^{-2} - 0.5714q^{-3})y =$ $(1.352 \times 10^{-5}q^{-31})u$ $+\frac{1-0.8916q^{-1}}{1+0.2054q^{-1}-0.3766q^{-2}-0.5045q^{-3}-0.2986q^{-4}}e$
BJ(3,1,9,2)	$y = \frac{-9.679 \times 10^{-5}q^{-19} + 9.701 \times 10^{-5}q^{-20} + 3.257e-005q^{-21}}{1-0.04788q^{-1}-0.9044q^{-2}}u$ $+\frac{1-0.2838q^{-1}}{1-1.121q^{-1}+0.1547q^{-2}-0.01565q^{-3}+0.01124q^{-4}}$ $\frac{-0.01121q^{-5}+0.01528q^{-6}-0.08721q^{-7}-0.477q^{-8}+0.5344q^{-9}}{e}$

Table C.6: Characteristics of the chosen models between  $y_1$  and  $u_3$ 

Model Name	Equation Number	FPE	Fit (%)	Model Error Model Fit (%)	Linear Fit (%)
OE(1,1)	(C.5)	$4.48 \times 10^{-4}$	86.7	-599	87.9
BJ(1,1,1,3)	(C.6)	$3.88 \times 10^{-6}$	88.7	-8293	88.7

## C.2 Headbox flowrate models ( $y_2$ )

The headbox consistency is the primary output variable of interest. From a simple mass balance around the headbox, it is evident that the consistency will be influenced by the headbox flowrate. For machine stability, this variable is already controlled. Then, building models between headbox flowrate and the manipulated variables will defined a multivariable 2 by 2 system.

### C.2.1 Machine chest valve ( $u_1$ )

The identification data is presented in Figure C.10. Figure C.11 presents the FPE (bar plot) and the fit (line plot) of the selected models. Inside the bar, from top to

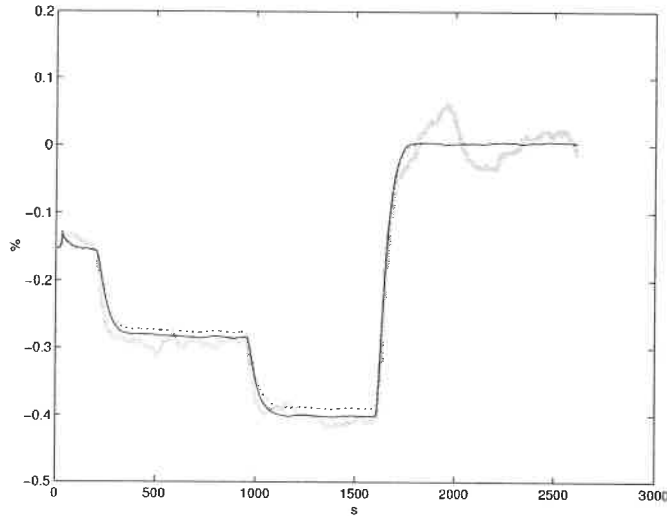


Figure C.9: Simulation of chosen models between  $y_1$  and  $u_3$  against validation data. OE(1,1) model : dotted line, *best* model : black line, validation data : grey line

bottom are the respective values of  $na$ ,  $nb$ ,  $nc$ ,  $nd$ ,  $nf$ ,  $nk$ .

From the preliminary analysis, model 6 and 14 are chosen to undergo a deeper analysis. These models were selected because, respectively: a good FPE / fit combination for the number of parameters and, the best fit. The models are presented in Table C.7. Both models do not have a zero. The residuals analysis shows some auto-correlation of the error signal for both models. Model BJ(1,1,2,2) shows cross-correlation between the error and input signals. However its impulse error model fit is negative. Therefore, it is chosen. The linearity range of this model is  $\pm 4\%$  in valve opening and  $\pm 40$  L/min flowrate (this is equivalent to the validation set). The nominal values are 65 % for the valve and 3500 L/min for the flowrate. The OE(1,1) model was also computed to serve for PI tuning. This model has an important auto-correlation between its residuals and cross-correlation with the input sequence. The important features of both models (C.7 and C.8) are described in Table C.8 and are graphed with the validation data in Figure C.12. The difference

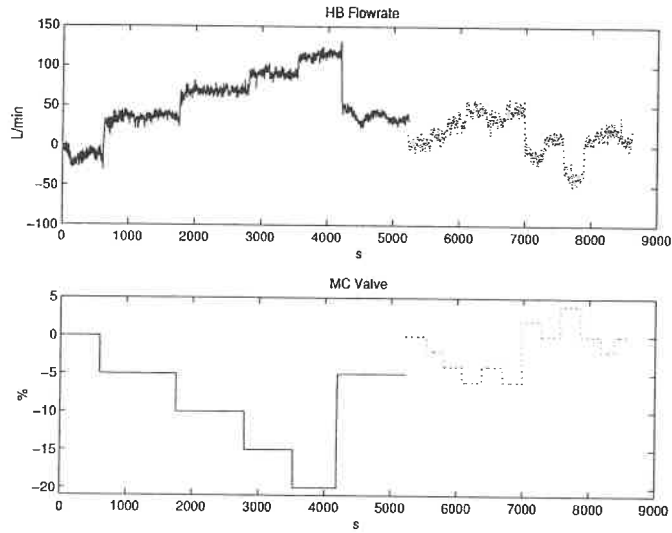


Figure C.10: Identification Data for the Model between  $y_2$  and  $u_1$

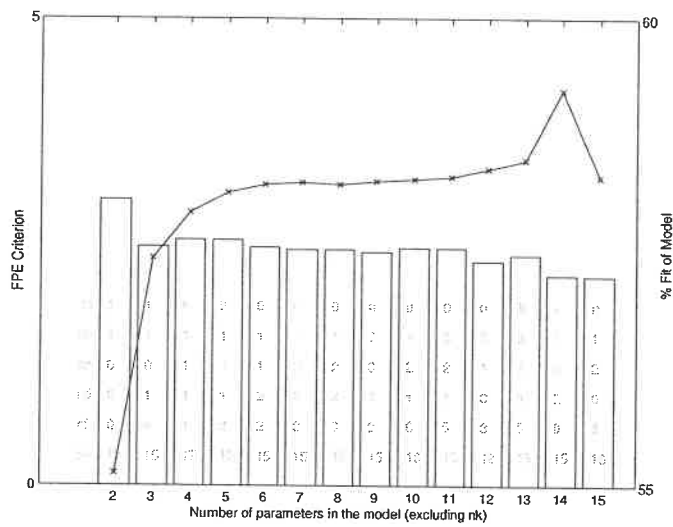


Figure C.11: Candidate Models between  $y_2$  and  $u_1$

for both models is very small and the simplest model represents the data as well as the complicated model. The elaborate model is only kept to be consistent with the other models.

Table C.7: Preliminary models between  $y_2$  and  $u_1$ 

Model Name	Model
BJ(1,1,2,2)	$y = \frac{-0.2806q^{-15}}{1-1.499q^{-1}+0.5446q^{-2}}u + \frac{1-0.0542q^{-1}}{1-1.398q^{-1}+0.4226q^{-2}}e$
ARARMAX(7,1,4,2)	$(1 - 2.236q^{-1} + 1.385q^{-2} + 0.3668q^{-3} - 0.395q^{-4} - 0.3696q^{-5} + 0.4235q^{-6} - 0.1538q^{-7})y = (-0.119q^{-15})u + \frac{1-2.205q^{-1}+1.356q^{-2}+0.2581q^{-3}-0.4052q^{-4}}{1-1.239q^{-1}+0.2394q^{-2}}e$

$$y_2 = \frac{-0.3553q^{-15}}{1 - 0.942q^{-1}}u_1 + e \quad (C.7)$$

$$y_2 = \frac{-0.2806q^{-15}}{1 - 1.499q^{-1} + 0.5446q^{-2}}u_1 + \frac{1 - 0.0542q^{-1}}{1 - 1.398q^{-1} + 0.4226q^{-2}}e \quad (C.8)$$

Table C.8: Characteristics of the chosen models between  $y_2$  and  $u_1$ 

Model Name	Equation Number	FPE	Fit (%)	Model Error Model Fit (%)	Linear Fit (%)
OE(1,1)	(C.7)	78.9	57.8	1.4	57.8
BJ(1,1,2,2)	(C.8)	2.56	58.2	-10.5	58.2

### C.2.2 Fanpump rpm ( $u_2$ )

The identification data is presented in Figure C.13. The fanpump rpm is expressed as a percentage of its scale. Figure C.14 presents the FPE (bar plot) and the fit (line plot) of the selected models. Inside the bar, from top to bottom are the respective values of  $na$ ,  $nb$ ,  $nc$ ,  $nd$ ,  $nf$ , and  $nk$ .

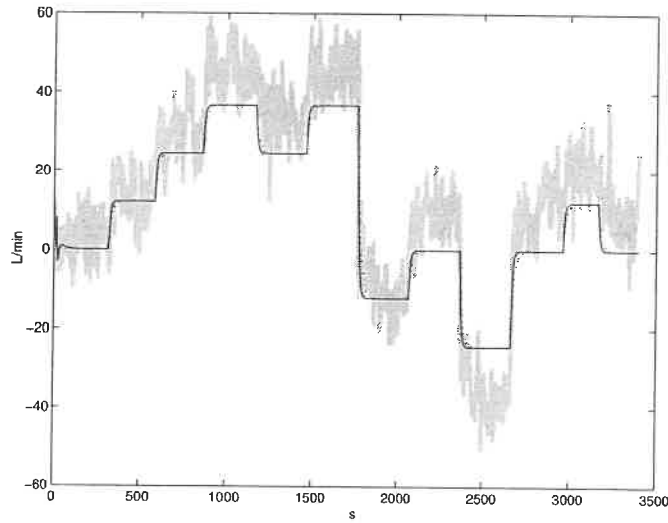


Figure C.12: Simulation of chosen models between  $y_2$  and  $u_1$  against validation data. OE(1,1) model : dash line, *best* model : black line, validation data : grey line

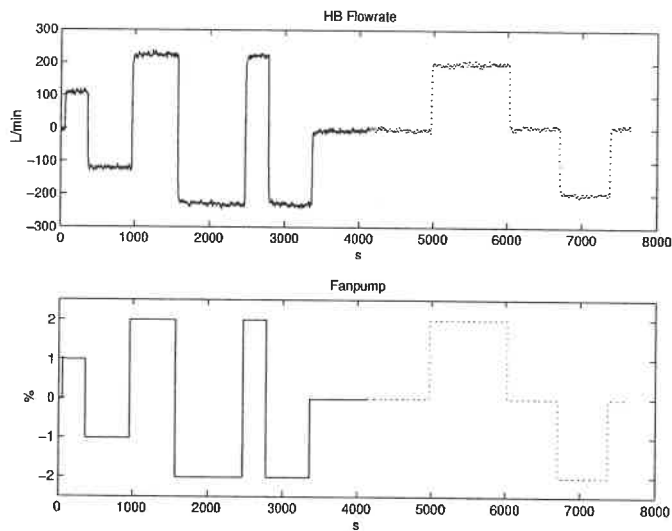


Figure C.13: Identification Data for the Model between  $y_2$  and  $u_2$



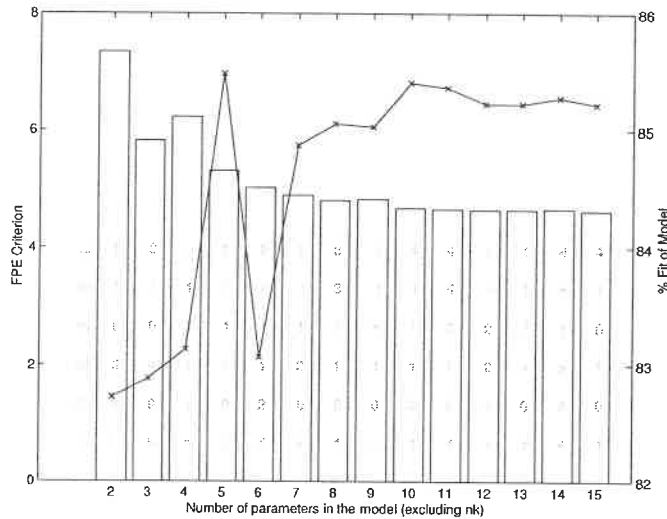


Figure C.14: Candidate Models between  $y_2$  and  $u_2$

From the preliminary analysis, model 5 and 10 are chosen to undergo a deeper analysis. These models were selected because, respectively: the best fit, and the best FPE / fit combination. Those models are presented in Table C.9. The first model, ARARMAX(2,1,1,1), do not have a zero. The second model, ARARMAX(4,4,1,1), has 5 distinct poles and 3 distinct zeros. The residuals analysis shows auto-correlation of the error signal and cross-correlation between the error and input signals for both models. The impulse model of the error model presents a similar fit for both models. (8.5 % against 6.9 %). There is no striking advantages to choosing the more complicated model. Therefore, the ARARMAX(2,1,1,1) is kept. Two extra data sets are available to estimate the linearity range. The linearity range of this model is  $\pm 5\%$  in fanpump rpm and  $\pm 700$  of L/min flowrate. The nominal values are 42.1 % for the fanpump and 700 L/min for the flowrate. The OE(1,1) model was also computed to serve for PI tuning. This model has an important auto-correlation between its residuals and cross-correlation with the input sequence. Furthermore, the model error fit is 70 %. The important features of both models (C.9 and C.10)

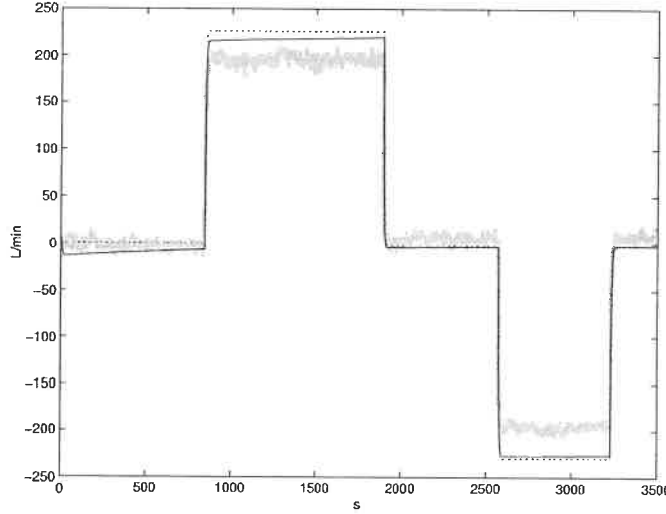


Figure C.15: Simulation of chosen models between  $y_2$  and  $u_2$  against validation data. OE(1,1) model : dotted line, *best* model : black line, validation data : grey line

are described in Table C.10 and are graphed with the validation data in Figure C.15.

Table C.9: Preliminary models between  $y_2$  and  $u_2$

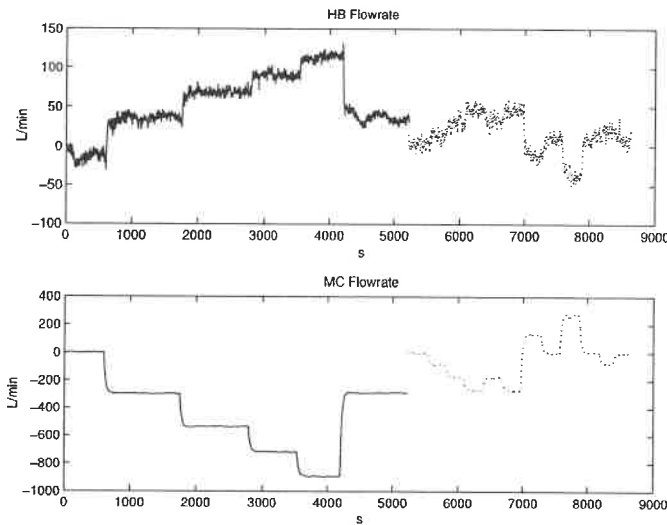
Model Name	Model
ARARMAX(2,1,1,1)	$(1 - 1.181q^{-1} + 0.3225q^{-2})y = (15.78q^{-5})u + \frac{1-0.9814q^{-1}}{1-0.9991q^{-1}}e$
ARARMAX(4,4,1,1)	$(1 - 1.054q^{-1} + 0.2273q^{-2} - 0.1395q^{-3} + 0.113q^{-4})y = (5.318q^{-4} + 11.36q^{-5} + 1.439q^{-6} - 1.671q^{-7})u + \frac{1-0.9781q^{-1}}{1-0.9986q^{-1}}e$

$$y_2 = \frac{23.37q^{-5}}{1 - 0.7948q^{-1}}u_2 + e \quad (\text{C.9})$$

$$(1 - 1.181q^{-1} + 0.3225q^{-2})y_2 = (15.78q^{-5})u_2 + \frac{1 - 0.9814q^{-1}}{1 - 0.9991q^{-1}}e \quad (\text{C.10})$$

Table C.10: Characteristics of the chosen models between  $y_2$  and  $u_2$ 

Model Name	Equation Number	FPE	Fit (%)	Model Error Model Fit (%)	Linear Fit (%)
OE(1,1)	(C.9)	46.21	83.0	70.0	91.7
ARARMAX(2,1,1,1)	(C.10)	5.31	85.5	8.5	92.1

Figure C.16: Identification data for the model between  $y_2$  and  $u_3$ 

### C.2.3 Machine chest flowrate ( $u_3$ )

The identification data is presented in Figure C.16. Figure C.17 presents the FPE (bar plot) and the fit (line plot) of the selected models. Inside the bar, from top to bottom are the respective values of  $na$ ,  $nb$ ,  $nc$ ,  $nd$ ,  $nf$ , and  $nk$ .

From the preliminary analysis, model 9, 12, and 15 are chosen to undergo a deeper analysis. These models were selected because, respectively: a good FPE/fit combination, the best FPE/fit combination, and the best fit. The models are presented in Table C.11. None of the models have a pole/zero cancellation. The residuals analysis shows some auto-correlation of the error signal and no cross-correlation between the error and input signals for all models. The impulse model of the error

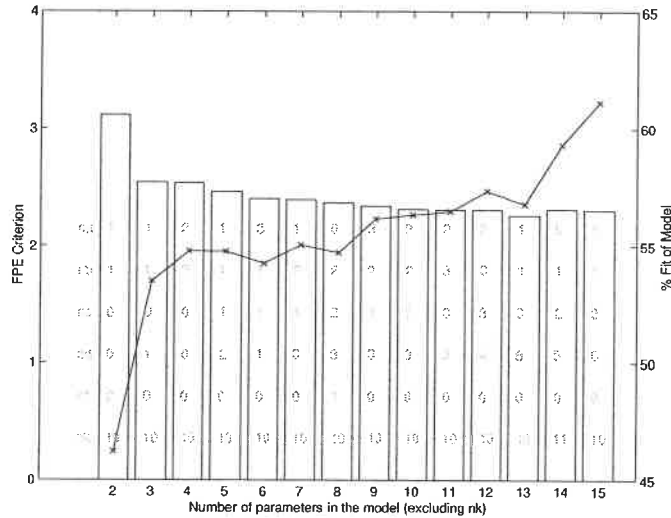


Figure C.17: Candidate models between  $y_2$  and  $u_3$

model presents a similar fit. The ARARMAX(5,1,3,6) model has the best fit on the validation data but not on the identification data. There is no major advantages to chose the more complicated model. Therefore, the ARARMAX(3,2,1,3) is kept. The linearity range of this model is the whole data set. The nominal values are 1000 L/min for the machine chest flowrate and 3500 L/min for the headbox flowrate. The OE(1,1) model was also computed to serve for PI tuning. This model has an important auto-correlation between its residuals and has cross-correlation with the input sequence. The important features of both models (C.11 and C.12) are described in Table C.12 and are graphed with the validation data in Figure C.18. As can be seen from the graph, the extra parameters of model ARARMAX(3,2,1,3) do not greatly improve the fit. The complicated model is retained only to test control strategies on a different model.

$$y_2 = \frac{-0.2279q^{-10}}{1 + 0.7997q^{-1}}u_3 + e \quad (\text{C.11})$$

Table C.11: Preliminary models between  $y_2$  and  $u_3$ 

Model Name	Model
ARARMAX(3,2,1,3)	$(1 - 2.002q^{-1} + 1.465q^{-2} - 0.4001q^{-3})y =$ $(-0.1449q^{-10} + 0.1369q^{-11})u$ $+ \frac{1 - 0.9603q^{-1}}{1 - 0.2335q^{-1} - 0.4518q^{-2} - 0.3088q^{-3}} e$
ARARMAX(2,3,3,4)	$(1 - 1.406q^{-1} + 0.5511q^{-2})y =$ $(-0.141q^{-10} + 0.01173q^{-11} + 0.1102q^{-12})u$ $+ \frac{1 + 0.1989q^{-1} - 0.5496q^{-2} - 0.5038q^{-3}}{1 + 0.3023q^{-1} - 0.6331q^{-2} - 0.6898q^{-3} + 0.02942q^{-4}} e$
ARARMAX(5,1,3,6)	$(1 - 0.3549q^{-1} - 0.5595q^{-2} + 0.08452q^{-3} + 0.4561q^{-4}$ $+ 0.005741q^{-5})y = (-0.09551q^{-10})u$ $+ \frac{1 - 2.104q^{-1} + 1.746q^{-2} - 0.632q^{-3}}{1 - 3.044q^{-1} + 4.244q^{-2} - 3.709q^{-3} + 2.169q^{-4} - 0.9018q^{-5} + 0.2417q^{-6}} e$

$$(1 - 2.002q^{-1} + 1.465q^{-2} - 0.4001q^{-3})y_2 = -0.1449q^{-10} + 0.1369q^{-11}u_3 \quad (\text{C.12})$$

$$+ \frac{1 - 0.9603q^{-1}}{1 - 0.2335q^{-1} - 0.4518q^{-2} - 0.3088q^{-3}} e$$

Table C.12: Characteristics of the chosen models between  $y_2$  and  $u_3$ 

Model Name	Equation Number	FPE	Fit (%)	Model Error Model Fit (%)	Linear Fit (%)
OE(1,1)	(C.11)	52.6	53.7	-83	67.1
ARARMAX(3,2,1,3)	(C.12)	2.34	56.1	-631	70.5

### C.3 Machine chest flowrate models ( $u_3$ )

When a cascade strategy is used, the manipulated variable for headbox consistency and flowrate changes from machine chest valve to machine chest flowrate. It is necessary to have a model between the machine chest flowrate and valve. This model is built in the following section. After some tests, the low precision of the

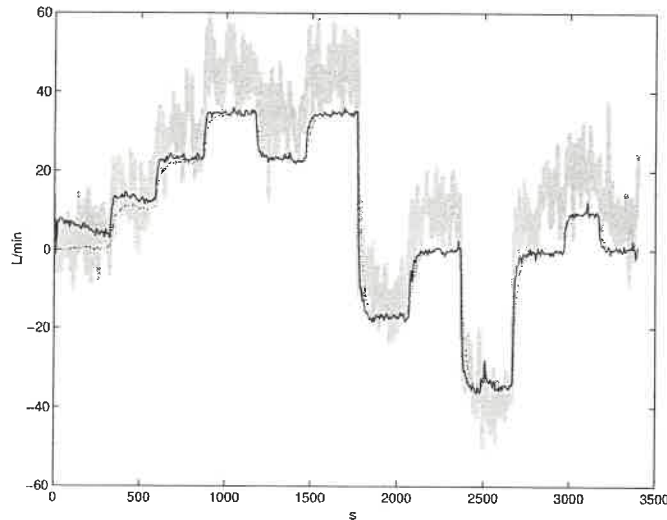


Figure C.18: Simulation of chosen models between  $y_2$  and  $u_3$  against validation data. OE(1,1) model : dotted line, *best* model : black line, validation data : grey line

control valve demands an improvement. Hence, a mid-ranging strategy was put in place where the bulk of the flow passes through the machine valve and the small adjustments are made with the small machine chest valve ( $u_4$ ).

### C.3.1 Machine chest valve ( $u_1$ )

The identification data is presented in Figure C.19. Figure C.20 presents the FPE (bar plot) and the fit (line plot) of the selected models. Inside the bar, from top to bottom are the respective values of  $na$ ,  $nb$ ,  $nc$ ,  $nd$ ,  $nf$ , and  $nk$ .

From the preliminary analysis, models 4, 7 and 9 are chosen to undergo a deeper analysis. These models were selected because, respectively: a very good FPE / fit combination, the best fit, and the best FPE / fit combination. The models are presented in Table C.13. A pole zero analysis shows that model ARMAX(4,2,1) zero cancels one of its poles. It is therefore eliminated. The residuals analysis shows some cross-correlation between the error and input signals for both remaining

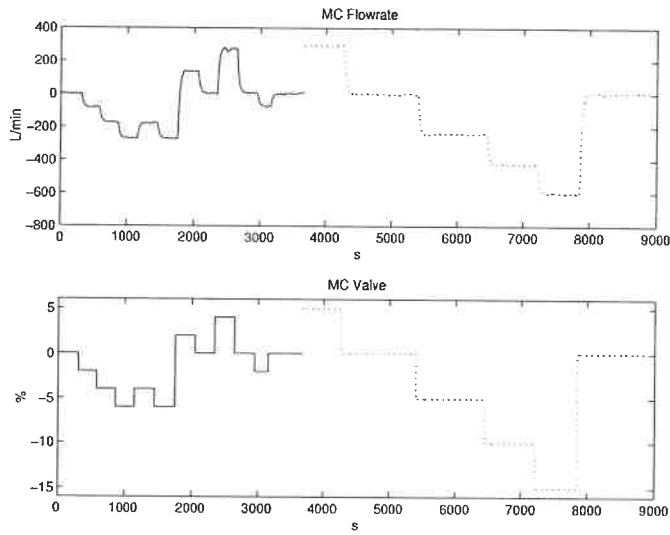


Figure C.19: Identification data for the model between  $u_3$  and  $u_1$

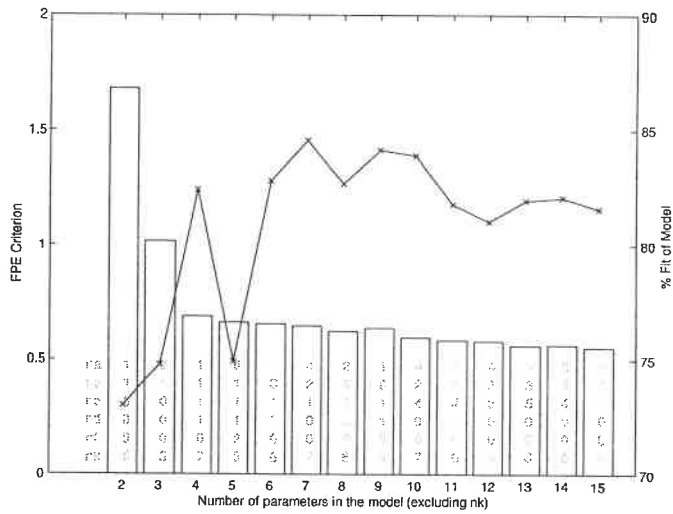


Figure C.20: Candidate models between  $u_3$  and  $u_1$

models. The impulse model of the error model is similar for the two models. There is no significant advantages to choosing the more complicated model. Therefore, the ARARMAX(1,1,1,1) is kept. The linearity range of this model is  $\pm 5\%$  in valve opening and  $\pm 250$  L/min of flowrate. The nominal values are 65 % for the valve and 1000 L/min for the flowrate. The OE(1,1) model was also computed to serve for PI tuning. This model has an important auto-correlation between its residuals. The model error fit is small. The important features of both models (C.13 and C.14) are described in Table C.14 and are graphed with the validation data in Figure C.21.

Table C.13: Preliminary models between  $u_3$  and  $u_1$ 

Model Name	Model
ARARMAX(1,1,1,1)	$(1 - 0.9751q^{-1})y = (1.167q^{-7})u$ $+ \frac{1-0.6634q^{-1}}{1-0.9796q^{-1}}e$
ARMAX(4,2,1)	$(1 - 2.062q^{-1} + 1.007q^{-2} + 0.1991q^{-3} - 0.1443q^{-4})y =$ $(1.309q^{-7} - 1.303q^{-8})u$ $+(1 - 0.9204q^{-1})e$
ARARMAX(1,6,1,1)	$(1 - 0.9569q^{-1})y =$ $(0.7863q^{-6} - 0.05256q^{-7} + 0.4809q^{-8}$ $+ 0.4287q^{-9} - 0.03254q^{-10} + 0.3995q^{-11})u$ $+ \frac{1-0.6957q^{-1}}{1-0.9932q^{-1}}e$

Note:  $u_3$  is denoted  $y$  in this table.

$$u_3 = \frac{1.918q^{-6}}{1 - 0.9579q^{-1}}u_1 + e \quad (\text{C.13})$$

$$(1 - 0.9751q^{-1})u_3 = (1.167q^{-7})u_1 + \frac{1 - 0.6634q^{-1}}{1 - 0.9796q^{-1}}e \quad (\text{C.14})$$



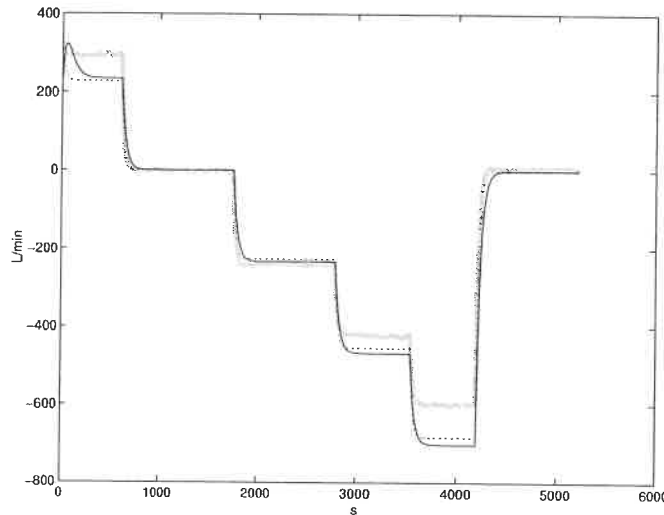


Figure C.21: Simulation of chosen models between  $u_3$  and  $u_1$  against validation data. OE(1,1) model : dotted line, *best* model : black line, validation data : grey line

Table C.14: Characteristics of the chosen models between  $u_3$  and  $u_1$

Model Name	Equation Number	FPE	Fit (%)	Model Error Model Fit (%)	Linear Fit (%)
OE(1,1)	C.13	803	85.0	1.9	82.5
ARARMAX(1,1,1,1)	C.14	0.69	82.4	-4.0	82.6

### C.3.2 Small machine chest valve ( $u_4$ )

The identification data is presented in Figure C.22. Figure C.23 presents the FPE (bar plot) and the fit (line plot) of the selected models. Inside the bar, from top to bottom are the respective values of  $na$ ,  $nb$ ,  $nc$ ,  $nd$ ,  $nf$ , and  $nk$ .

From the preliminary analysis, model 4, 8, and 13 are chosen to undergo a deeper analysis. These models were selected because, respectively: a fit equivalent to model 8, the lowest FPE, and the best FPE / fit combination. Those models are presented in Table C.15. A pole-zero cancelation analysis eliminates the ARMAX(3,4,1) model. For the two remaining models, the residuals analysis yields sim-

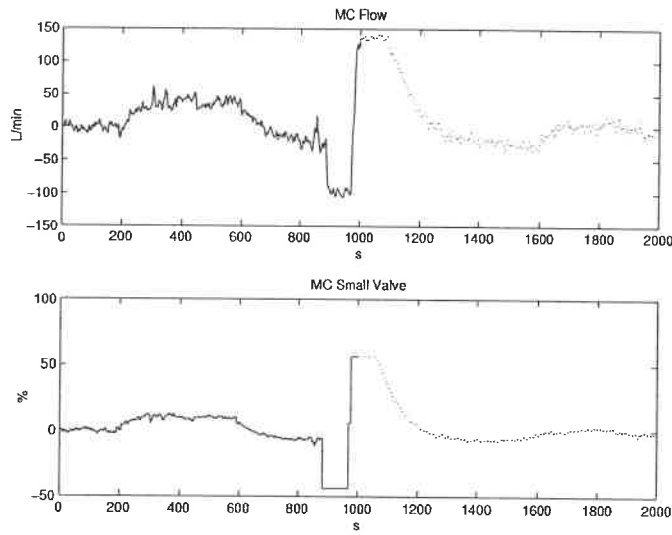


Figure C.22: Identification Data for the Model between  $u_3$  and  $u_4$

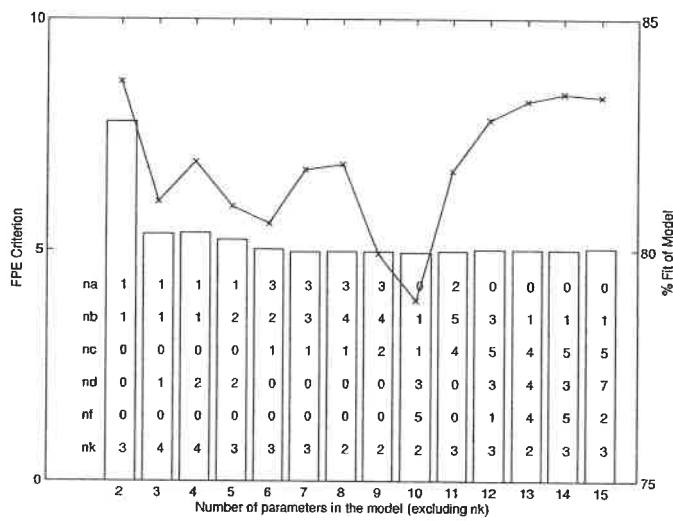


Figure C.23: Candidate Models between  $u_3$  and  $u_4$

ilar results but the BJ(1,4,4,4) has residuals with less cross-correlation. The impulse model of the residual (model error model) gives a fit of 24.5 % for the ARARX(1,1,2) model. The BJ(1,4,4,4) error model fit is 7 %. Therefore, the BJ(1,4,4,4) model is chosen as the *best* model. The linearity range of this model is taken as the whole range of the valve since only one step in each direction is available. The OE(1,1) model was also computed to serve for PI tuning. This model has an important cross-correlation between its residuals. Furthermore, the model error fit is 18 %. The important features of both models (C.15 and C.16) are described in Table C.16 and are graphed with the validation data in Figure C.24.

Table C.15: Preliminary models between  $u_3$  and  $u_4$ 

Model Name	Model
ARARX(1,1,2)	$(1 - 0.8982q^{-1})y =$ $(0.2594q^{-4})u$ $+ \frac{1}{1 - 0.6333q^{-1} + 0.1033q^{-2}}e$
ARMAX(3,4,1)	$(1 - 2.372q^{-1} + 1.863q^{-2} - 0.4897q^{-3})y =$ $(0.03052q^{-2} + 0.08241q^{-3} - 0.01005q^{-4} - 0.1006q^{-5})u$ $+ (1 - 0.9517q^{-1})e$
BJ(1,4,4,4)	$y = \frac{0.06637q^{-2}}{1 - 2.671q^{-1} + 2.908q^{-2} - 1.528q^{-3} + 0.3207q^{-4}}u$ $+ \frac{1 - 1.589q^{-1} + 0.3489q^{-2} + 0.07989q^{-3} + 0.1608q^{-4}}{1 - 3.063q^{-1} + 3.301q^{-2} - 1.413q^{-3} + 0.1747q^{-4}}e$

Note:  $u_3$  is denoted  $y$  in this table.

$$u_3 = \frac{0.3843q^{-3}}{1 - 0.8483q^{-1}}u_4 + e \quad (\text{C.15})$$

$$u_3 = \frac{0.06637q^{-2}}{1 - 2.671q^{-1} + 2.908q^{-2} - 1.528q^{-3} + 0.3207q^{-4}}u_4$$

$$+ \frac{1 - 1.589q^{-1} + 0.3489q^{-2} + 0.07989q^{-3} + 0.1608q^{-4}}{1 - 3.063q^{-1} + 3.301q^{-2} - 1.413q^{-3} + 0.1747q^{-4}}e \quad (\text{C.16})$$

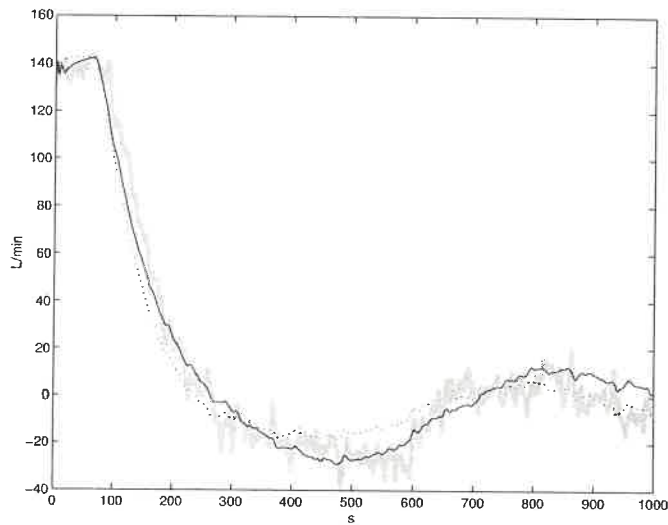


Figure C.24: Simulation of chosen models between  $u_3$  and  $u_4$  against validation data. OE(1,1) model : dotted line, *best* model : black line, validation data : grey line

Table C.16: Characteristics of the chosen models between  $u_3$  and  $u_4$

Model Name	Equation Number	FPE	Fit (%)	Model Error Model Fit (%)	Linear Fit (%)
OE(1,1)	(C.15)	109.04	79.3	18.7	77.2
BJ(1,4,4,4)	(C.16)	5.00	83.2	7.3	77.5

## Appendix D

# Identification Data and Models of CSPP Pilot Paper Machine

To devise and test different control strategies, models between potential output variables and potential input variables are necessary. This appendix presents in detail the procedure and the design decisions made to obtain the models used in chapter 4. The model building procedure is explained in chapter 2. The sampling period for the wet-end variables is 12 seconds and for the dry-end variables is 10 seconds.

Every model is presented in the same manner. First, a figure presents the identification data. The identification figure has two set of data . The first set, drawn with a solid line, represents the estimation data. The second set, drawn with a dotted line, represents the validation data. Second, parametric models with a total number of parameters ranging from 2 to 15 are calculated and compared. Fourteen *best* models are selected and presented on a following figure. Lastly, after a detailed analysis, the selected model is plotted against the validation data. This last graph is made with Matlab System Identification Toolbox function *compare*. The *compare* function handles the initialisation of the model in such a way as to yield the best fit value. As a side effect, the first few points on the graph do not behave as expected

from a linear model. Since this does not affect the resulting model, this feature of the *compare* function was not disabled.

## D.1 Headbox consistency models ( $y_1$ )

As seen from the models of chapter 3, headbox consistency is influenced by the machine chest flowrate. On this machine, the headbox is open and the total flow is not controlled. Therefore, the effects of the fanpump velocity on headbox consistency are not of concern. The pulp used in this trial contains filler. Therefore, filler is added to keep the sheet ash content to its setpoint. The headbox consistency will be affected by the fresh filler flowrate. The effect of retention additives (C-PAM and Bentonite) are negligible because the quantity added is small. Consistency is a measure of solid material in water. At the headbox, this quantity does not vary much with varying additive flowrate. The noisy data did confirm this. The effect of retention additive on headbox consistencies (total and ash) is assumed to be zero. The next few pages explain the model building procedure between machine chest and filler and headbox consistency.

### D.1.1 Machine chest flowrate ( $u_3$ )

The identification data is presented in Figure D.1. Figure D.2 presents the FPE (bar plot) and the fit (line plot) of the selected models. Inside the bar, from top to bottom are the respective values of  $na$ ,  $nb$ ,  $nc$ ,  $nd$ ,  $nf$ , and  $nk$ .

From the preliminary analysis, models 5, 7 and 10 are chosen to undergo a deeper analysis. These models were selected because, respectively: a good FPE /fit combination for the number of parameter, a better FPE /fit combination, and the best FPE / fit combination. However a pole/zero analysis reveals a cancellation for every model. Therefore, models 2,3,and 4 are going to be analyzed. Those

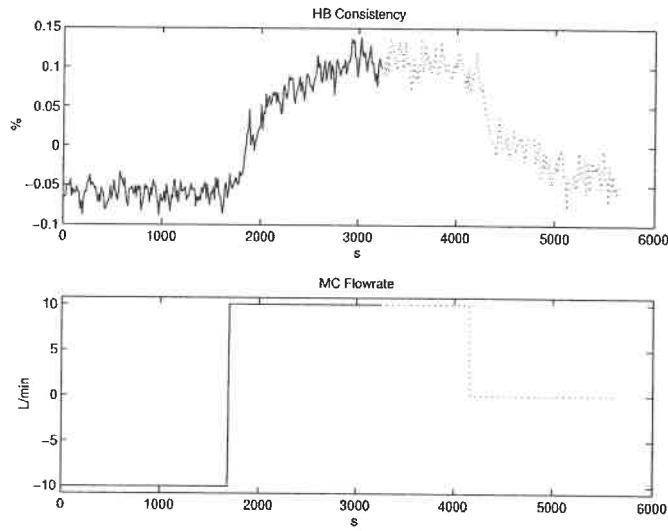


Figure D.1: Identification data for the model between  $y_1$  and  $u_3$

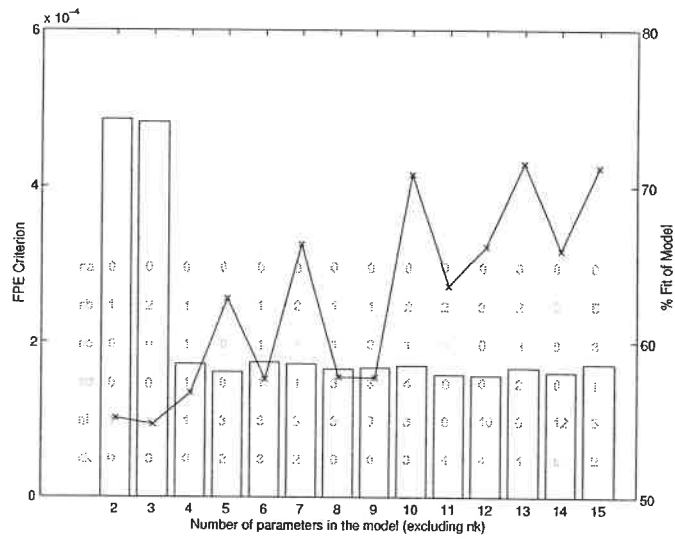


Figure D.2: Candidate models between  $y_1$  and  $u_3$

models are presented in Table D.1. They do not have pole/zero cancellation. The residuals analysis shows auto-correlation of the error signal for every models except BJ(1,1,1,1). No cross-correlation between the error and input signals is detected for every models. The model error model fit is highest (28 %) for the BJ(1,1,1,1). The two OE models are equivalent and the simplest one is kept (D.1). The linearity range of this model is  $\pm 10$  % in machine flowrate and  $\pm 0.1$  % consistency (the whole data set). The nominal values are 80 L/min for the flowrate and 0.60 % for the consistency.

Table D.1: Preliminary models between  $y_1$  and  $u_3$ 

Model Name	Model
OE(1,1)	$y = \frac{0.0004126}{1-0.9472q^{-1}}u + e$
OE(2,1)	$y = \frac{0.001058-0.0006856q^{-1}}{1-0.952q^{-1}}u + e$
BJ(1,1,1,1)	$y = \frac{0.0003598}{1-0.9544q^{-1}}u + \frac{1-0.3096q^{-1}}{1-0.9032q^{-1}}e$

$$y_1 = \frac{0.0004126}{1 - 0.9472q^{-1}}u_3 + e \quad (\text{D.1})$$

Table D.2: Characteristics of the chosen model between  $y_1$  and  $u_3$ 

Model Name	Equation Number	FPE	Fit (%)	Model Error Model Fit (%)	Linear Fit (%)
OE(1,1)	(D.1)	$4.85 \times 10^{-4}$	55.1	15.3	63.7

### D.1.2 Fresh filler flowrate ( $u_8$ )

The identification data is presented in Figure D.4. For this model, only two steps are available. A quick glance at the data shows a static non-linearity. For the same step



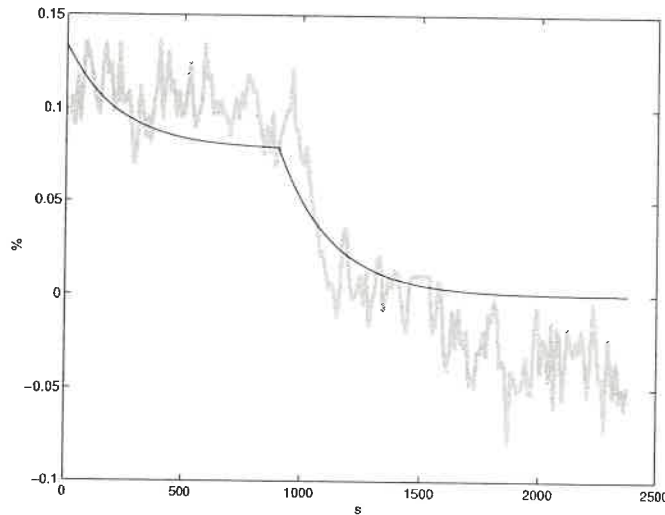


Figure D.3: Simulation of chosen model between  $y_1$  and  $u_3$  against validation data.  
*best model* : black line, *validation data* : grey line

size, the gain in one direction is twice the gain in the other direction. Furthermore, the dynamics are slower for the step down. To get somewhat representative models, two models are identified. Figure D.4(a) presents the data for a step up. Figure D.4(b) presents the data for a step down. Figure D.5(a) presents the FPE (bar plot) and the fit (line plot) of the selected models for the step up and Figure D.5(b) for the step down. Inside the bar, from top to bottom are the respective values of  $na$ ,  $nb$ ,  $nc$ ,  $nd$ ,  $nf$ , and  $nk$ .

From the preliminary analysis of Figure D.5(a), model 2 and 11 are chosen to undergo a deeper analysis. These models were selected because, respectively: a good FPE /fit combination for the number of parameter, and the best fit. The models are presented in Table D.3. A pole zero analysis reveals that model ARMAX(2,3,6) has a cancellation. The residuals analysis shows auto-correlation of the error signal for model OE(1,1). No cross-correlation between the error and input signals is detected. The simpler model, OE(1,1) is kept (D.2). The linear range is 4.55 to 5.42 L/min

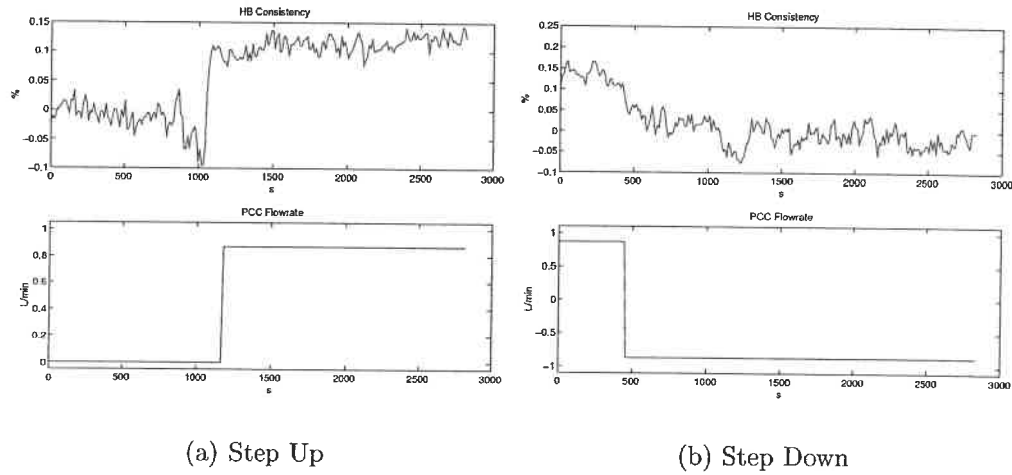


Figure D.4: Identification data for the model between  $y_1$  and  $u_8$

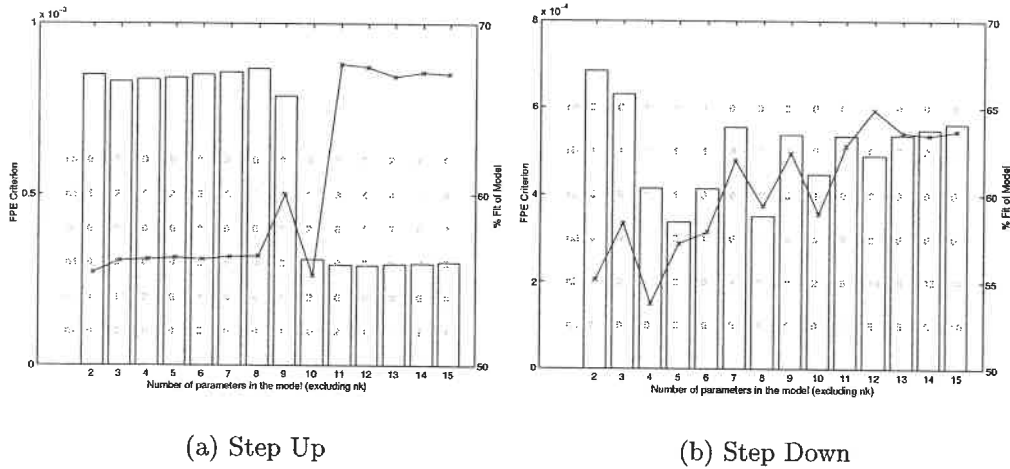


Figure D.5: Candidate models between  $y_1$  and  $u_8$

in filler flowrate and 0.58 to 0.70 % in headbox consistency.

From the preliminary analysis of Figure D.5(b), model 2 and 7 are chosen to undergo a deeper analysis. These models were selected because, respectively: a good FPE /fit combination for the number of parameter, and a better FPE / fit combination. The models are presented in Table D.4. A pole zero analysis reveals that model OE(3,4) has a cancellation. The residuals analysis shows auto-correlation of the error signal for model OE(1,1). No cross-correlation between the error and input signals is detected. The simpler model, OE(1,1) is kept (D.3). The linear range is 5.42 to 3.68 L/min in filler flowrate and 0.73 to 0.53 % in headbox consistency. Table D.5 summarises some of the models characteristics. Figure D.6 compares the model response with the validation data.

Table D.3: Preliminary models between  $y_1$  and  $u_8$  for the step up

Model Name	Model
OE(1,1)	$y = \frac{0.05074}{1-0.613q^{-1}}u + e$
ARMAX(2,3,6)	$(1 - 2.029q^{-1} + 1.08q^{-2})y = (0.05102q^{-2} - 0.08261q^{-3} + 0.03809q^{-4})u + (1 - 1.297q^{-1} + 0.2537q^{-2} - 0.06951q^{-3} + 0.1724q^{-4} - 0.1385q^{-5} + 0.2351q^{-6})e$

Table D.4: Preliminary models between  $y_1$  and  $u_8$  for the step down

Model Name	Model
OE(1,1)	$y = \frac{0.0006832q^{-2}}{1-0.9709q^{-1}}u + e$
OE(3,4)	$y = \frac{-0.001499q^{-9}+0.00303q^{-10}-0.001531q^{-11}}{1-3.582q^{-1}+4.758q^{-2}-2.768q^{-3}+0.5923q^{-4}}u + e$

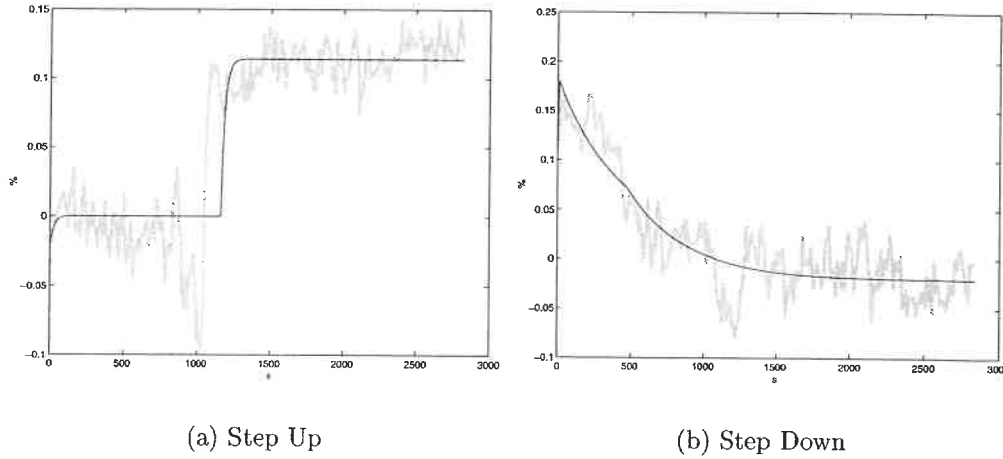


Figure D.6: Simulation of chosen models between  $y_1$  and  $u_8$  against validation data.

*best model* : black line, validation data : grey line

$$y_1 = \frac{0.05074}{1 - 0.613q^{-1}} u_8(\text{Step Up}) + e \quad (\text{D.2})$$

$$y_1 = \frac{0.0006832q^{-2}}{1 - 0.9709q^{-1}} u_8(\text{Step Down}) + e \quad (\text{D.3})$$

Table D.5: Characteristics of the chosen models between  $y_1$  and  $u_8$

Model Name	Equation Number	FPE	Fit (%)	Model Error Model Fit (%)	Linear Fit (%)
OE(1,1) Step Up	(D.2)	$8.50 \times 10^{-4}$	55.4	no fit	55.4
OE(1,1) Step Down	(D.3)	$6.84 \times 10^{-4}$	55.1	no fit	55.1

## D.2 Headbox ash consistency models ( $y_3$ )

This output variable should be more sensitive to filler flowrate. This section builds models to study the interaction of this output variable with the input variables.

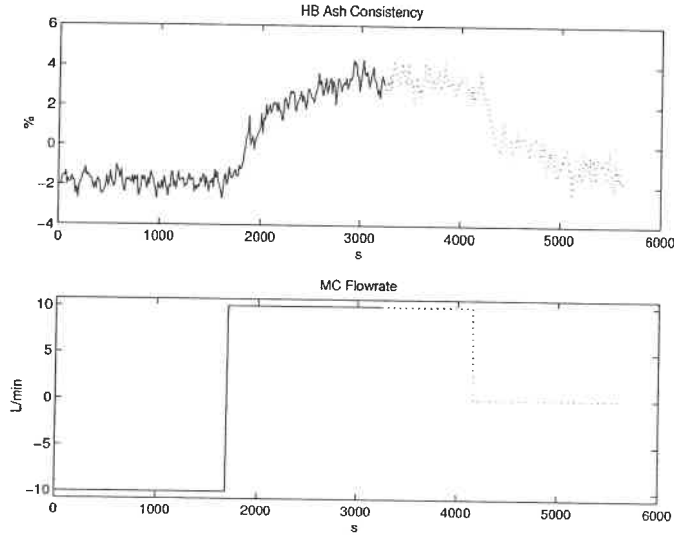
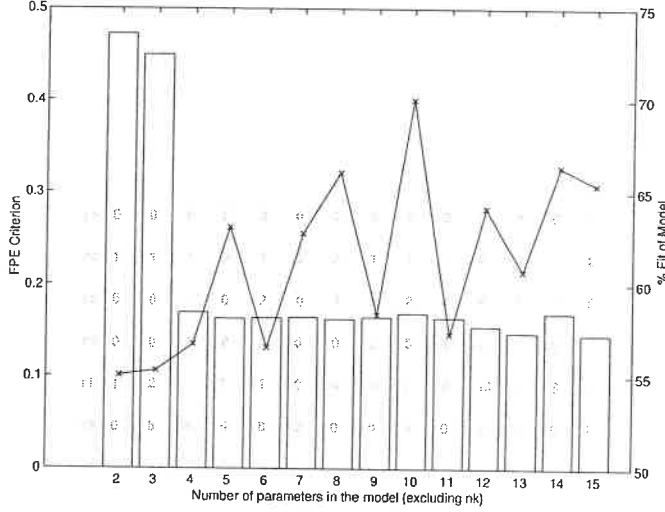


Figure D.7: Identification data for the model between  $y_3$  and  $u_3$

### D.2.1 Machine chest flowrate ( $u_3$ )

The identification data is presented in Figure D.7. Figure D.8 presents the FPE (bar plot) and the fit (line plot) of the selected models. Inside the bar, from top to bottom are the respective values of  $na$ ,  $nb$ ,  $nc$ ,  $nd$ ,  $nf$ , and  $nk$ .

From the preliminary analysis, model 5, 8 and 10 are chosen to undergo a deeper analysis. These models were selected because, respectively: a good FPE /fit combination for the number of parameter, the best FPE / fit combination, and the best fit. The models are presented in Table D.6. Models OE(3,2) and ARMAX(2,2,4) have a zero that is cancelled by a pole. The remaining model shows no auto-correlation of its error signal and no cross-correlation between the error and input signals. It is therefore chosen (D.4). The whole data set is assumed to be linear. Then, the range is  $\pm 10\%$  in machine flowrate and  $-2$  to  $4\%$  in ash consistency. The nominal values are  $80$  L/min for the flowrate and  $18.9\%$  for the ash consistency. Table D.7 summarises some of the model characteristics. Figure D.9 compares the model

Figure D.8: Candidate models between  $y_3$  and  $u_3$ 

response with the validation data.

Table D.6: Preliminary models between  $y_3$  and  $u_3$ 

Model Name	Model
OE(3,2)	$y = \frac{0.01332q^{-4} - 0.01743q^{-5} + 0.004048q^{-6}}{1 - 1.966q^{-1} + 0.9654q^{-2}}u + e$
ARMAX(2,2,4)	$(1 - 1.97q^{-1} + 0.97q^{-2})y = (0.008115 - 0.008123q^{-1})u + (1 - 1.492q^{-1} + 0.3718q^{-2} - 0.03438q^{-3} + 0.1521q^{-4})e$
BJ(1,2,5,2)	$y = \frac{0.01962q^{-3}}{1 - 0.08171q^{-1} - 0.8303q^{-2}}u + \frac{1 - 1.85q^{-1} + 0.8483q^{-2}}{1 - 2.357q^{-1} + 1.663q^{-2} - 0.1455q^{-3} - 0.2517q^{-4} + 0.09064q^{-5}}e$

$$y_3 = \frac{0.01962q^{-3}}{1 - 0.08171q^{-1} - 0.8303q^{-2}}u_3 \quad (D.4)$$

$$+ \frac{1 - 1.85q^{-1} + 0.8483q^{-2}}{1 - 2.357q^{-1} + 1.663q^{-2} - 0.1455q^{-3} - 0.2517q^{-4} + 0.09064q^{-5}}e$$

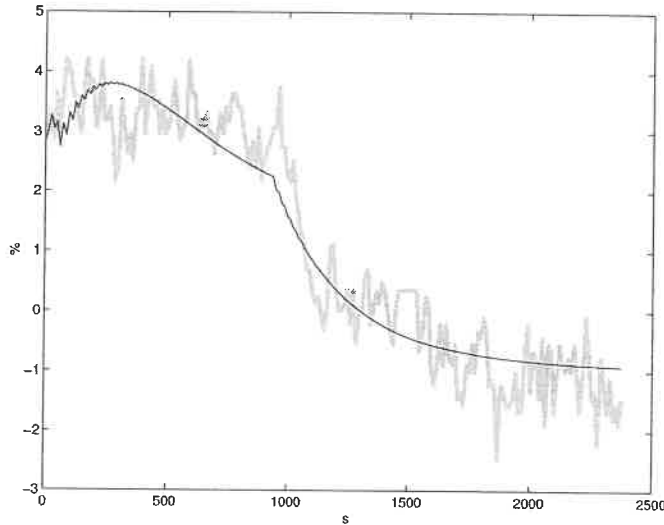


Figure D.9: Simulation of chosen model between  $y_3$  and  $u_3$  against validation data.  
*best model* : black line, validation data : grey line

Table D.7: Characteristics of the chosen model between  $y_3$  and  $u_3$

Model Name	Equation Number	FPE	Fit (%)	Model Error Model Fit (%)	Linear Fit (%)
BJ(1,2,5,2)	(D.4)	0.16	70.0	3.68	62.4

### D.2.2 Fresh filler flowrate ( $u_8$ )

The identification data is presented in Figure D.10. For this model, only two steps are available. A quick glance at the data shows non-linearity. For the same step size, the gain in one direction is twice the gain in the other direction. Furthermore, the dynamics are slower for the step down. To get somewhat representative models, two models are identified. Figure D.10(a) presents the data for the step up. Figure D.10(b) presents the data for the step down. Figure D.11(a) presents the FPE (bar plot) and the fit (line plot) of the selected models for the step up and Figure D.11(b) for the step down. Inside the bar, from top to bottom are the respective values of  $na$ ,  $nb$ ,  $nc$ ,  $nd$ ,  $nf$ , and  $nk$ .

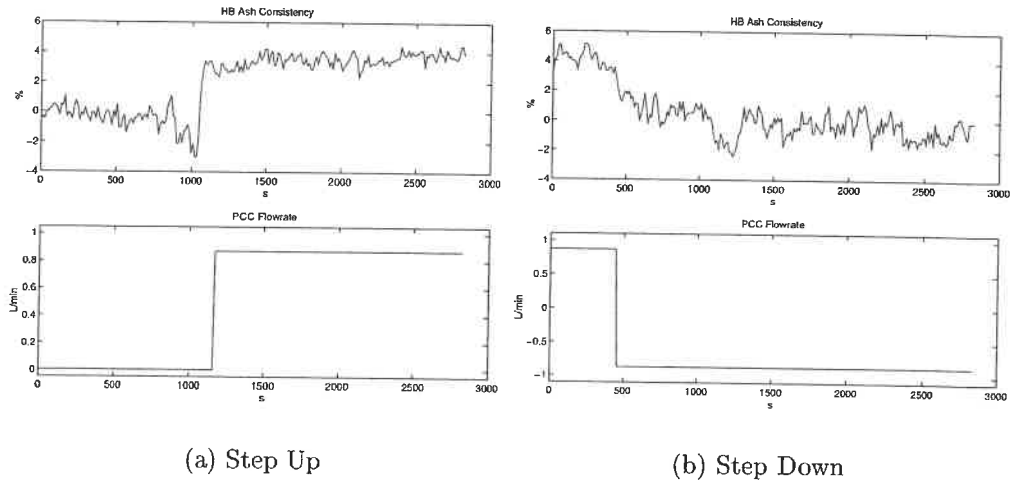


Figure D.10: Identification data for the model between  $y_3$  and  $u_8$

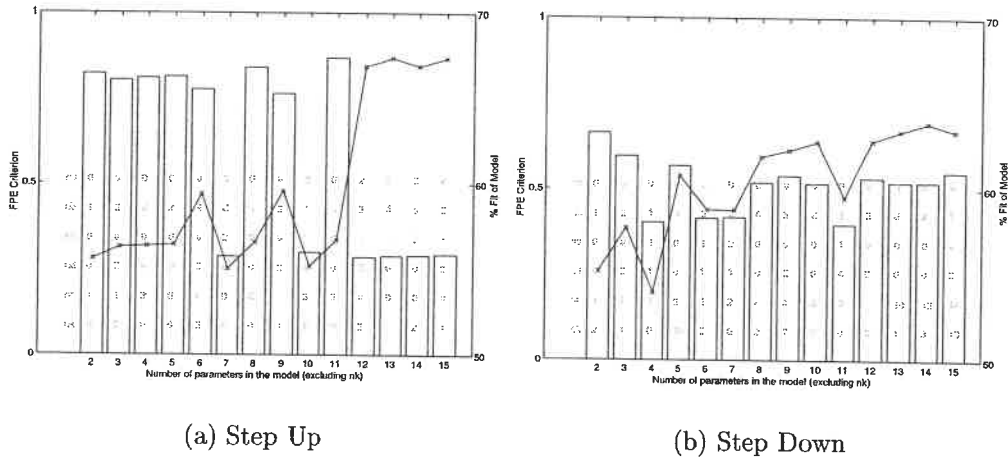


Figure D.11: Candidate models between  $y_3$  and  $u_8$



From the preliminary analysis of Figure D.11(a), model 2 and 6 are chosen to undergo a deeper analysis. These models were selected because of good FPE /fit combination. The models are presented in Table D.8. A pole zero analysis reveals that model OE(4,2) has a cancellation. The residuals analysis shows auto-correlation of the error signal for model OE(1,1). No cross-correlation between the error and input signals is detected. The simpler model, OE(1,1) is kept (D.5). The linear range is 4.55 to 5.42 L/min in filler flowrate and 18 to 22 % in headbox consistency.

From the preliminary analysis of Figure D.11(b), model 2 and 5 are chosen to undergo a deeper analysis. These models were selected because of good FPE /fit combination for the number of parameters. The models are presented in Table D.9. Both models do not have pole / zero cancellation. The residuals analysis shows auto-correlation of the error signal for both models. No cross-correlation between the error and input signals is detected. The small improvement gained by adding more parameters is not justified. Therefore, the simpler model, OE(1,1), is kept (D.6). The linear range is 5.42 to 3.68 % in filler flowrate and 22 to 16 % in headbox consistency. Table D.10 summarises some of the models characteristics. Figure D.12 compares the model response with the validation data.

Table D.8: Preliminary models between  $y_3$  and  $u_8$  for the step up

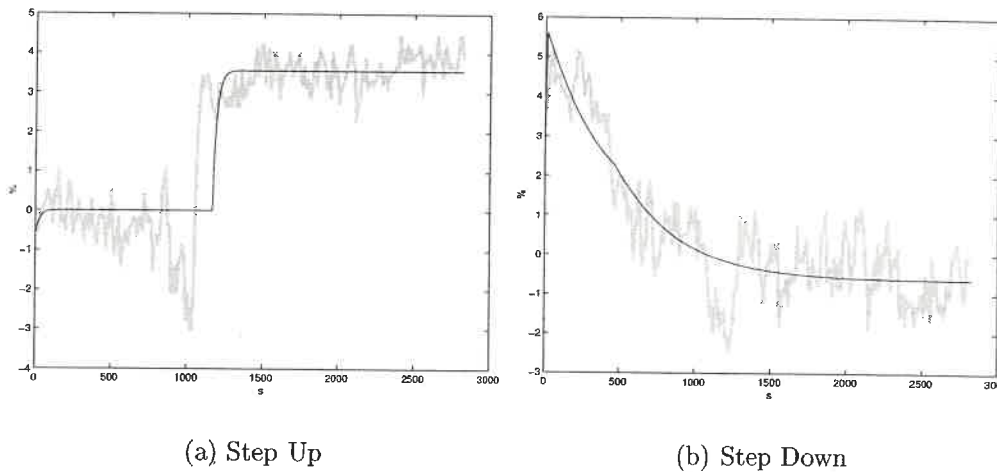
Model Name	Model
OE(1,1)	$y = \frac{1.53}{1-0.6256q^{-1}}u + e$
OE(4,2)	$y = \frac{2.643q^{-3}-5.122q^{-4}+2.221q^{-5}+0.2699q^{-6}}{1-2.017q^{-1}+1.02q^{-2}}u + e$

$$y_3 = \frac{1.53}{1 - 0.6256q^{-1}}u_{8(\text{Step Up})} + e \quad (\text{D.5})$$

$$y_3 = \frac{0.02139q^{-2}}{1 - 0.9709q^{-1}}u_{8(\text{Step Down})} + e \quad (\text{D.6})$$

Table D.9: Preliminary models between  $y_3$  and  $u_8$  for the step down

Model Name	Model
OE(1,1)	$y = \frac{0.02139q^{-2}}{1-0.9709q^{-1}}u + e$
OE(3,2)	$y = \frac{-0.03088q^{-10}-0.07556q^{-11}+0.1081q^{-12}}{1-1.975q^{-1}+0.9786q^{-2}}u + e$

Figure D.12: Simulation of chosen models between  $y_3$  and  $u_8$  against validation data. *best* model : black line, validation data : grey line

## D.3 White water consistency models ( $y_4$ )

Today, retention control on a machine uses white water consistency as controlled variable. This section builds models to study the effect of the input variables on the white water consistency.

### D.3.1 Machine chest flowrate ( $u_3$ )

The identification data is presented in Figure D.13. Figure D.14 presents the FPE (bar plot) and the fit (line plot) of the selected models. Inside the bar, from top to bottom are the respective values of  $na$ ,  $nb$ ,  $nc$ ,  $nd$ ,  $nf$ , and  $nk$ .

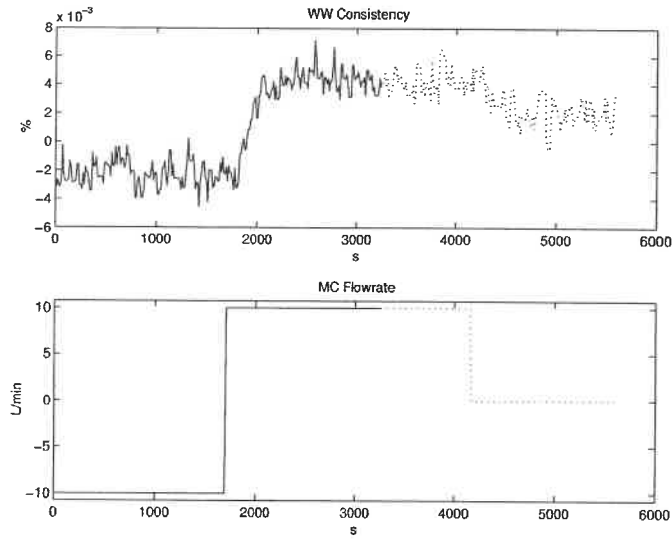


Figure D.13: Identification data for the model between  $y_4$  and  $u_3$

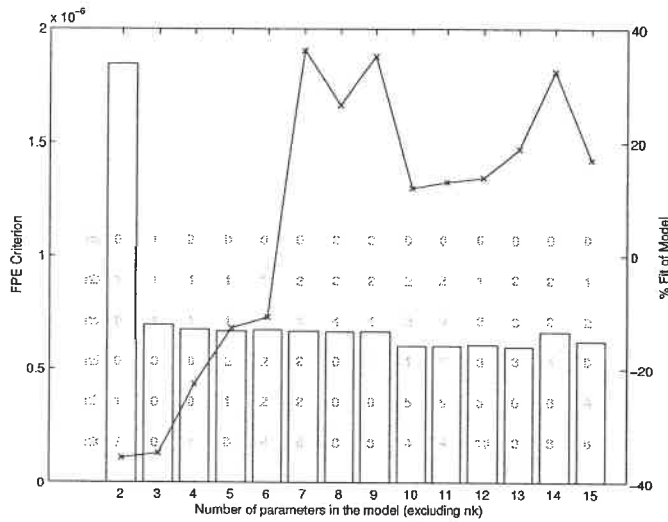


Figure D.14: Candidate models between  $y_4$  and  $u_3$

Table D.10: Characteristics of the chosen models between  $y_3$  and  $u_8$ 

Model Name	Equation Number	FPE	Fit (%)	Model Error Model Fit (%)	Linear Fit (%)
OE(1,1) <sub>Step Up</sub>	(D.5)	0.82	55.6	-28.9	55.6
OE(1,1) <sub>Step Down</sub>	(D.6)	0.66	55.2	no fit	55.2

From the preliminary analysis, model 7 and 9 are chosen to undergo a deeper analysis. These models were selected because, respectively: the best fit and a good fit. These models are presented in Table D.11. Both models almost have a pole/zero cancellation. Both models show no auto-correlation of their error signal and no cross-correlation between the error and input signals. The simplest one is chosen (D.7). The whole data set is assumed to be linear. Then, the range is  $\pm 10\%$  in machine flowrate and  $-0.002$  to  $0.005\%$  in white water consistency. The nominal values are 80 L/min for the flowrate and 0.026 % for the consistency. Table D.12 summarises some of the model characteristics. Figure D.15 compares the model response with the validation data.

Table D.11: Preliminary models between  $y_4$  and  $u_3$ 

Model Name	Model
BJ(2,1,2,2)	$y = \frac{2.332e-005q^{-8} - 2.345e-005q^{-9}}{1 - 1.928q^{-1} + 0.9278q^{-2}}u + \frac{1 - 0.8486q^{-1}}{1 - 1.358q^{-1} + 0.3902q^{-2}}e$
ARARMAX(2,2,4,1)	$(1 - 1.929q^{-1} + 0.9286q^{-2})y = (2.319e - 005q^{-8} - 2.335e - 005q^{-9})u + \frac{1 - 0.3847q^{-1} - 1.265q^{-2} + 0.3911q^{-3} + 0.2517q^{-4}}{1 + 1.003q^{-1}}e$

$$y_4 = \frac{2.332 \times 10^{-5}q^{-8} - 2.345 \times 10^{-5}q^{-9}}{1 - 1.928q^{-1} + 0.9278q^{-2}}u_3 + \frac{1 - 0.8486q^{-1}}{1 - 1.358q^{-1} + 0.3902q^{-2}}e \quad (\text{D.7})$$

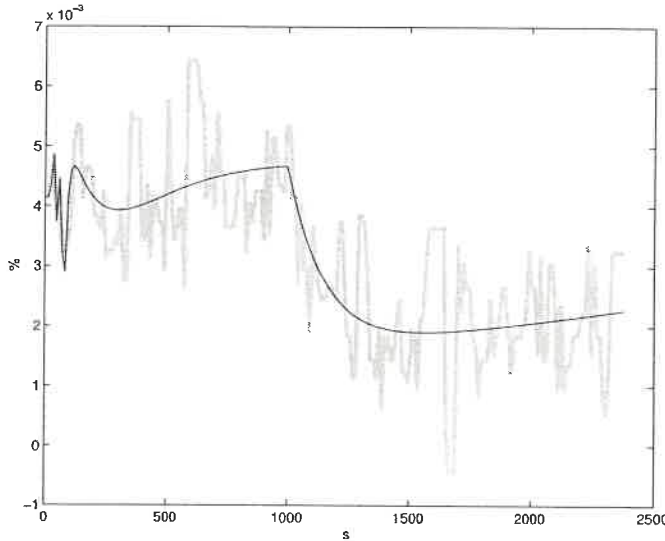


Figure D.15: Simulation of chosen model between  $y_4$  and  $u_3$  against validation data.

*best model* : black line, validation data : grey line

Table D.12: Characteristics of the chosen model between  $y_4$  and  $u_3$

Model Name	Equation Number	FPE	Fit (%)	Model Error Model Fit (%)	Linear Fit (%)
BJ(2,1,2,2)	(D.7)	$6.67 \times 10^{-7}$	36.2	12.41	67.9

### D.3.2 Bentonite flowrate ( $u_5$ )

The identification data is presented in Figure D.16. Figure D.17 presents the FPE (bar plot) and the fit (line plot) of the selected models. Inside the bar, from top to bottom are the respective values of  $na$ ,  $nb$ ,  $nc$ ,  $nd$ ,  $nf$ , and  $nk$ .

From the preliminary analysis, only model 10 represents somewhat the data (D.8). This is due to the gain non-linearity of the data (there is a factor of 3). But because the dynamics are similar, a linear model with an average gain is able to represent the data set. The chosen model does not have a pole/zero cancellation. The model shows some auto-correlation of its residuals and no cross-correlation

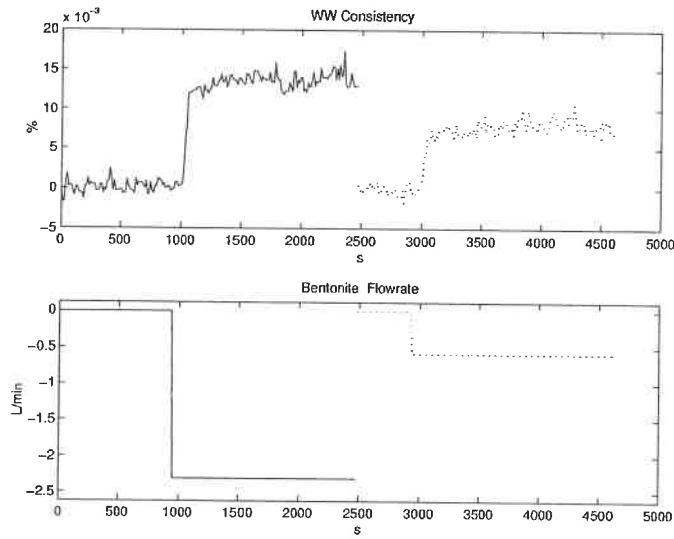


Figure D.16: Identification data for the model between  $y_4$  and  $u_5$

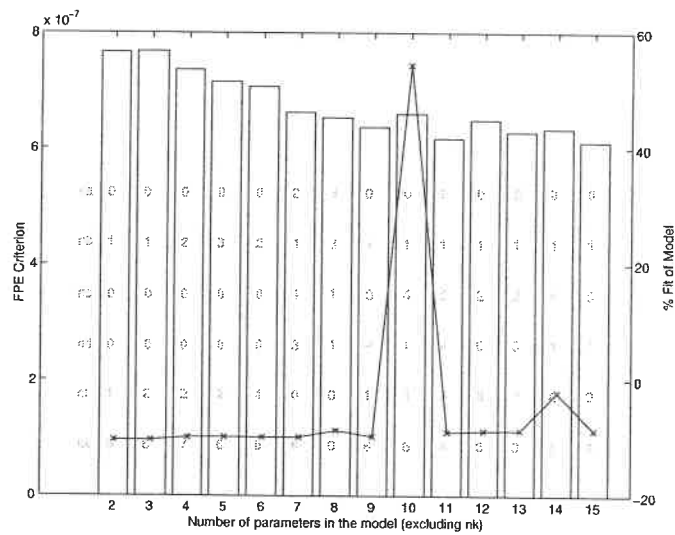


Figure D.17: Candidate models between  $y_4$  and  $u_5$

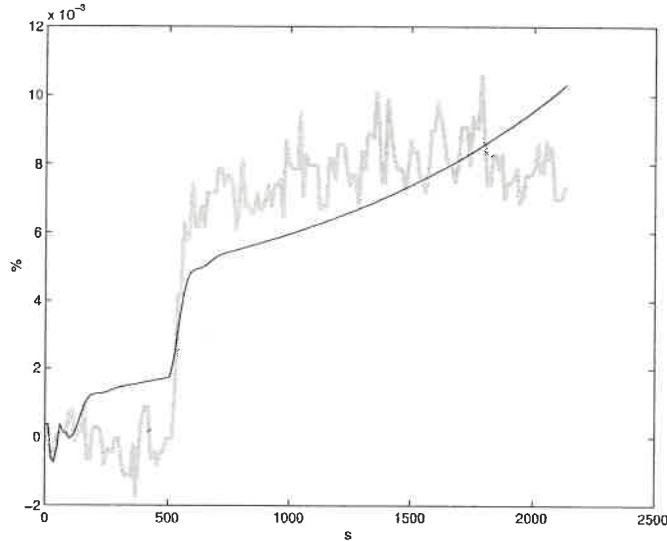


Figure D.18: Simulation of chosen model between  $y_4$  and  $u_5$  against validation data.

*best model* : black line, *validation data* : grey line

between the residuals and the input signal. The whole data set is assumed to be linear. Then, the range are 0 to 2.9 L/min for the bentonite flow and 0.015 to 0.04 % for the white water consistency. Table D.13 summarises some of the model characteristics. Figure D.18 compares the model response with the validation data.

$$y_4 = \frac{-0.0005081q^{-5}}{1 - 1.6q^{-1} + 0.5466q^{-2} + 0.4146q^{-3} - 0.2722q^{-4}}u_5 + \frac{1 - 0.5677q^{-1} - 0.2048q^{-2} - 0.05867q^{-3} - 0.1873q^{-4}}{1 - 1.01q^{-1}}e \quad (\text{D.8})$$

Table D.13: Characteristics of the chosen model between  $y_4$  and  $u_5$

Model Name	Equation Number	FPE	Fit (%)	Model Error Model Fit (%)	Linear Fit (%)
BJ(1,4,1,4)	(D.8)	$6.6 \times 10^{-7}$	54.4	-	71.1

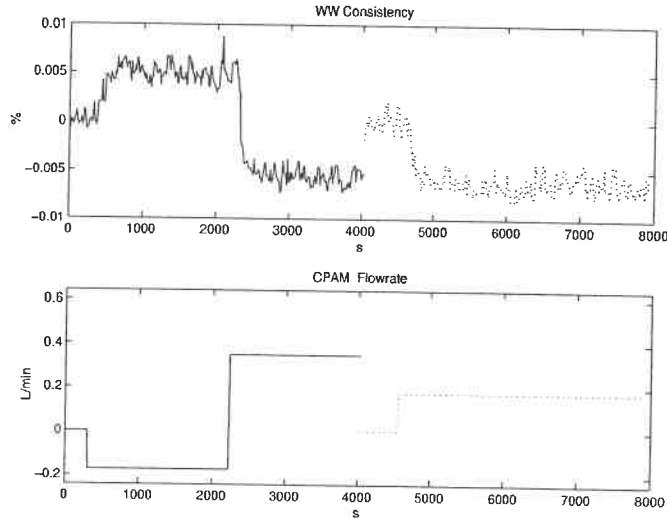


Figure D.19: Identification data for the model between  $y_4$  and  $u_6$

### D.3.3 C-PAM flowrate ( $u_6$ )

The identification data is presented in Figure D.19. Figure D.20 presents the FPE (bar plot) and the fit (line plot) of the selected models. Inside the bar, from top to bottom are the respective values of  $na$ ,  $nb$ ,  $nc$ ,  $nd$ ,  $nf$ , and  $nk$ .

From the preliminary analysis, models 5, 8 and 10 are chosen to undergo a deeper analysis. These models were selected because they present good FPE / fit combinations. The models are presented in Table D.14. Model ARARMAX(2,5,2,1) has a pole/zero cancellation. The remaining models show no auto-correlation of their residuals and no cross-correlation between the residuals and the input signal. The simplest one, BJ(1,1,2,1), is chosen (D.9). The whole data set is assumed to be linear. Then, the range is 0.404 – 0.924 L/min in CPAM and 0.01-0.03 % in white water consistency. Table D.15 summarises some of the model characteristics. Figure D.21 compares the model response with the validation data.



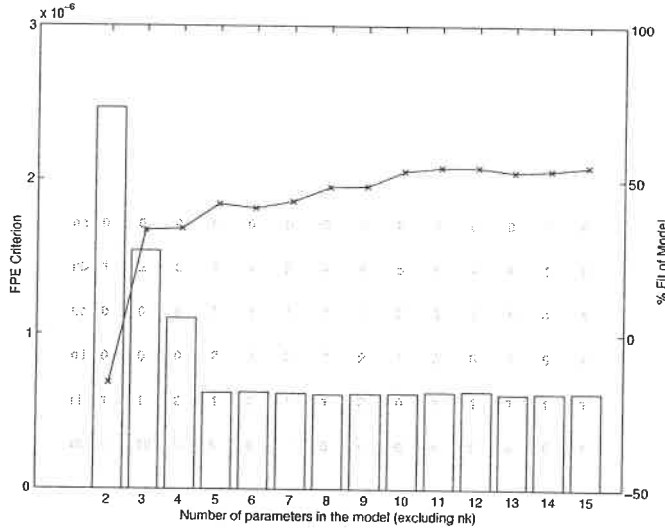


Figure D.20: Candidate models between  $y_4$  and  $u_6$

$$y_4 = \frac{-0.003667q^{-6}}{1 - 0.8233q^{-1}}u_6 + \frac{1 - 0.9526q^{-1}}{1 - 1.57q^{-1} + 0.5704q^{-2}}e \quad (\text{D.9})$$

### D.3.4 Ratio of bentonite to C-PAM ( $u_7$ )

The identification data is presented in Figure D.22. A quick glance at the data shows a gain sign reversal. In the range of a ratio of 0 to 3, the gain is negative. In the range of a ratio of 3 to 7, the gain is positive. Two models are identified, one for each range. Figure D.22(a) presents the data for the low range (ratio of 0 to 3). Figure D.22(b) presents the data for the high range (ratio of 3 to 7). Figure D.23(a) presents the FPE (bar plot) and the fit (line plot) of the selected models for the low range and Figure D.23(b) for the high range. Inside the bar, from top to bottom are the respective values of  $na$ ,  $nb$ ,  $nc$ ,  $nd$ ,  $nf$ , and  $nk$ .

From the preliminary analysis of Figure D.23(a), model 5 and 10 are chosen to undergo a deeper analysis. These models were selected because, respectively: a

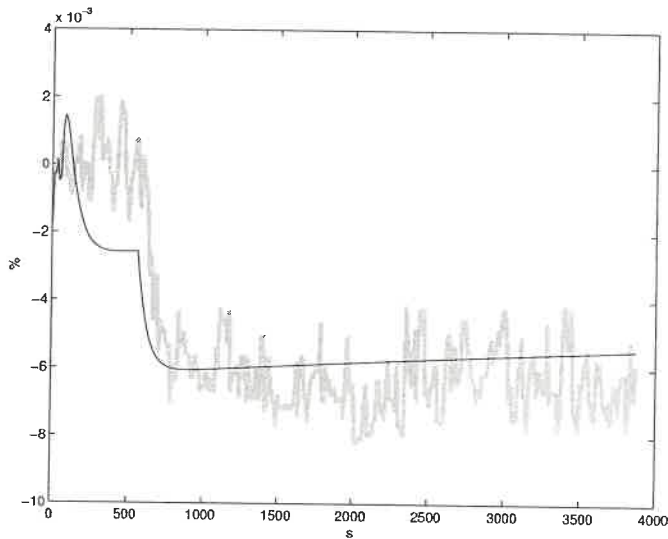
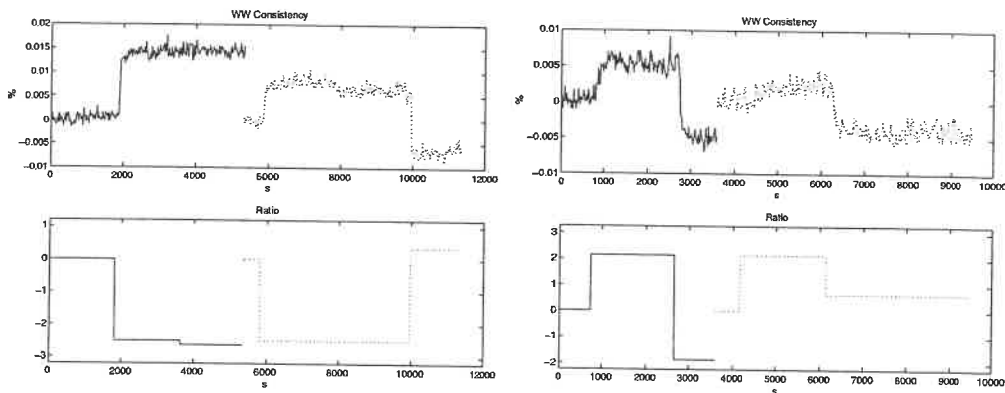


Figure D.21: Simulation of chosen model between  $y_4$  and  $u_6$  against validation data.  
*best model* : black line, validation data : grey line



(a) Low range

(b) High range

Figure D.22: Identification data for the models between  $y_4$  and  $u_7$

Table D.14: Preliminary models between  $y_4$  and  $u_6$ 

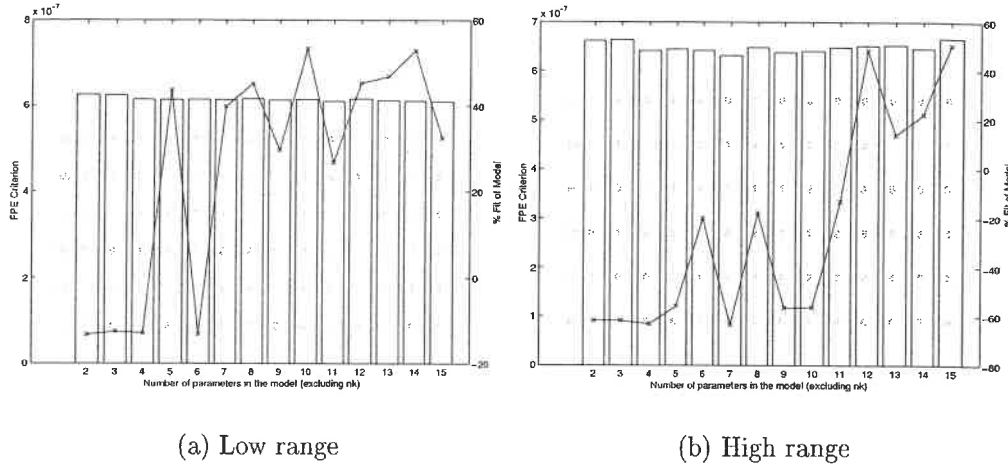
Model Name	Model
BJ(1,1,2,1)	$y = \frac{-0.003667q^{-6}}{1-0.8233q^{-1}}u + \frac{1-0.9526q^{-1}}{1-1.57q^{-1}+0.5704q^{-2}}e$
BJ(4,1,2,1)	$y = \frac{-0.003505q^{-6}+0.002294q^{-7}-0.007566q^{-8}+0.00613q^{-9}}{1-0.876q^{-1}}u + \frac{1-0.9537q^{-1}}{1-1.571q^{-1}+0.5713q^{-2}}e$
ARARMAX(2,5,2,1)	$(1-1.871q^{-1}+0.8711q^{-2})y = (-0.00363q^{-6}+0.005872q^{-7}-0.009665q^{-8}+0.01346q^{-9}-0.006034q^{-10})u + \frac{1-1.808q^{-1}+0.8138q^{-2}}{1-0.4962q^{-1}}e$

Table D.15: Characteristics of the chosen model between  $y_4$  and  $u_6$ 

Model Name	Equation Number	FPE	Fit (%)	Model Error Model Fit (%)	Linear Fit (%)
BJ(1,1,2,1)	(D.9)	$6.25 \times 10^{-7}$	42.2	6.6	61.3

good FPE /fit combination for the number of parameter, and the best fit. The models are presented in Table D.16. A pole / zero analysis reveals no cancellation. The residuals analysis shows auto-correlation of the error signal for both model. No cross-correlation between the error and input signals is detected. Graphing both models with the validation data shows that model BJ(3,1,2,4) oscillates. This model does noise fitting. Therefore, BJ(1,1,2,1) is chosen (D.10). The linear range is a ratio of bentonite to CPAM from 0 to 3 and 0.013 to 0.04 % in white water consistency.

From the preliminary analysis of Figure D.23(b), model 12 and 15 are chosen to undergo a deeper analysis. These models were selected because, respectively: a good FPE /fit combination for the number of parameter, and the best fit. The models are presented in Table D.17. A pole / zero analysis reveals no cancellation. The residuals analysis shows auto-correlation of the error signal for both models. No cross-correlation between the error and input signals is detected. The simpler

Figure D.23: Candidate models between  $y_4$  and  $u_7$ 

model is kept (D.11). The linear range is a ratio of bentonite to CPAM from 3 to 7 and 0.014 to 0.03 % in white water consistency. Table D.18 summarises some of the models characteristics. Figure D.24 compares the model response with the validation data.

Table D.16: Preliminary models between  $y_4$  and  $u_7$  for the low range

Model Name	Model
BJ(1,1,2,1)	$y = \frac{-0.001382q^{-6}}{1-0.742q^{-1}}u + \frac{1-0.9849q^{-1}}{1-1.513q^{-1}+0.5141q^{-2}}e$
BJ(3,1,2,4)	$y = \frac{-0.0008444q^{-6}-0.002543q^{-7}-0.001739q^{-8}}{1+0.9236q^{-1}-0.6782q^{-2}-0.4541q^{-3}+0.1745q^{-4}}u + \frac{1-0.9802q^{-1}}{1-1.484q^{-1}+0.484q^{-2}}e$

$$y_4 = \frac{-0.001382q^{-6}}{1-0.742q^{-1}}u_{7(\text{Low range})} + \frac{1-0.9849q^{-1}}{1-1.513q^{-1}+0.5141q^{-2}}e \quad (\text{D.10})$$

$$y_4 = \frac{0.0005875q^{-6} + 0.0001927q^{-7}}{1-0.07693q^{-1}-0.6274q^{-2}}u_{7(\text{High range})} \quad (\text{D.11})$$

Table D.17: Preliminary models between  $y_4$  and  $u_7$  for the high range

Model Name	Model
BJ(2,3,5,2)	$y = \frac{0.0005875q^{-6} + 0.0001927q^{-7}}{1 - 0.07693q^{-1} - 0.6274q^{-2}} u$ $+ \frac{1 - 1.63q^{-1} + 1.512q^{-2} - 0.8941q^{-3}}{1 - 2.105q^{-1} + 2.306q^{-2} - 1.677q^{-3} + 0.4446q^{-4} + 0.03049q^{-5}} e$
BJ(1,3,4,7)	$y = \frac{0.0004644q^{-6}}{1 - 0.3976q^{-1} - 1.085q^{-2} + 0.3925q^{-3} + 0.5542q^{-4} - 0.1548q^{-5} - 0.0474q^{-6} - 0.08557q^{-7}} u$ $+ \frac{1 - 2.719q^{-1} + 2.725q^{-2} - 1.009q^{-3}}{1 - 3.194q^{-1} + 4.007q^{-2} - 2.29q^{-3} + 0.4761q^{-4}} e$

$$+ \frac{1 - 1.63q^{-1} + 1.512q^{-2} - 0.8941q^{-3}}{1 - 2.105q^{-1} + 2.306q^{-2} - 1.677q^{-3} + 0.4446q^{-4} + 0.03049q^{-5}} e$$

Table D.18: Characteristics of the chosen models between  $y_4$  and  $u_7$ 

Model Name	Equation Number	FPE	Fit (%)	Model Error Model Fit (%)	Linear Fit (%)
BJ(1,1,2,1) <sub>Low range</sub>	(D.10)	$6.14 \times 10^{-7}$	47.26	43.7	66.9
BJ(2,3,5,2) <sub>High range</sub>	(D.11)	$6.51 \times 10^{-7}$	48.2	-106	63.7

### D.3.5 Fresh filler flowrate ( $u_8$ ).

The identification data is presented in Figure D.25. Figure D.26 presents the FPE (bar plot) and the fit (line plot) of the selected models. Inside the bar, from top to bottom are the respective values of  $na$ ,  $nb$ ,  $nc$ ,  $nd$ ,  $nf$ , and  $nk$ .

From the preliminary analysis, models 2, 6 and 8 are chosen to undergo a deeper analysis. These models were selected because they present good FPE / fit combinations. The models are presented in Table D.19. Models BJ(2,1,1,2) and BJ(2,2,2,2) have pole/zero cancellations. The remaining model ARX(1,1) shows some auto-correlation of its residuals and no cross-correlation between the residuals and the input signal. It is therefore chosen (D.12). The whole data set is assumed to be linear. Then, the range is  $\pm 0.87$  L/min in filler flowrate and  $\pm 0.007$  % in white

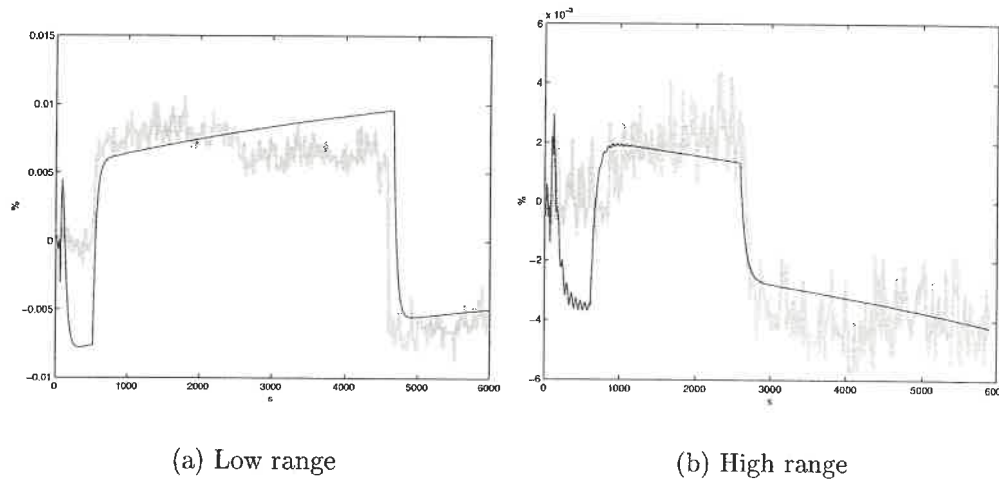


Figure D.24: Simulation of chosen models between  $y_4$  and  $u_7$  against validation data.

*best model* : black line, validation data : grey line

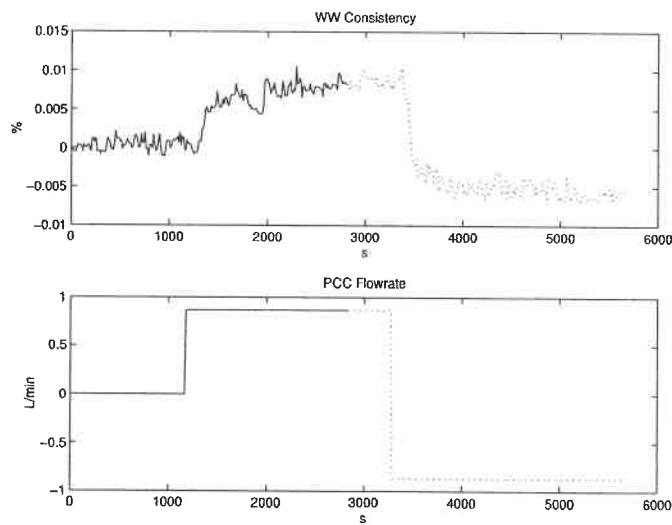
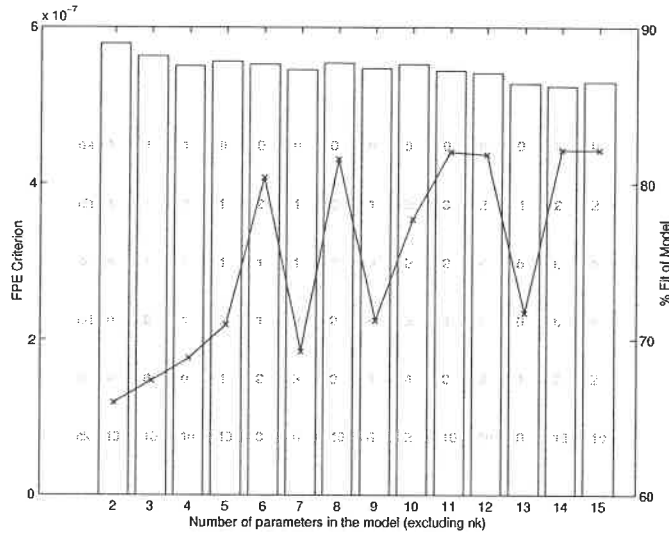


Figure D.25: Identification data for the model between  $y_4$  and  $u_8$

Figure D.26: Candidate models between  $y_4$  and  $u_8$ 

water consistency. The nominal values are 4.55 L/min for the filler flowrate and 0.033 % for the white water consistency. Table D.20 summarises some of the model characteristics. Figure D.27 compares the model response with the validation data.

Table D.19: Preliminary models between  $y_4$  and  $u_8$ 

Model Name	Model
ARX(1,1)	$y = \frac{0.001241q^{-10}}{1-0.84q^{-1}}u + \frac{1}{1-0.84q^{-1}}e$
BJ(2,1,1,2)	$y = \frac{0.0006879q^{-8}-0.0006924q^{-9}}{1-1.907q^{-1}+0.9064q^{-2}}u + \frac{1-0.08274q^{-1}}{1-0.7048q^{-1}}e$
BJ(2,2,2,2)	$y = \frac{0.0009738q^{-10}-0.0009783q^{-11}}{1-1.858q^{-1}+0.8573q^{-2}}u + \frac{1-0.4806q^{-1}-0.05399q^{-2}}{1-1.078q^{-1}+0.2161q^{-2}}e$

$$y_4 = \frac{0.001241q^{-10}}{1-0.84q^{-1}}u_8 + \frac{1}{1-0.84q^{-1}}e \quad (\text{D.12})$$

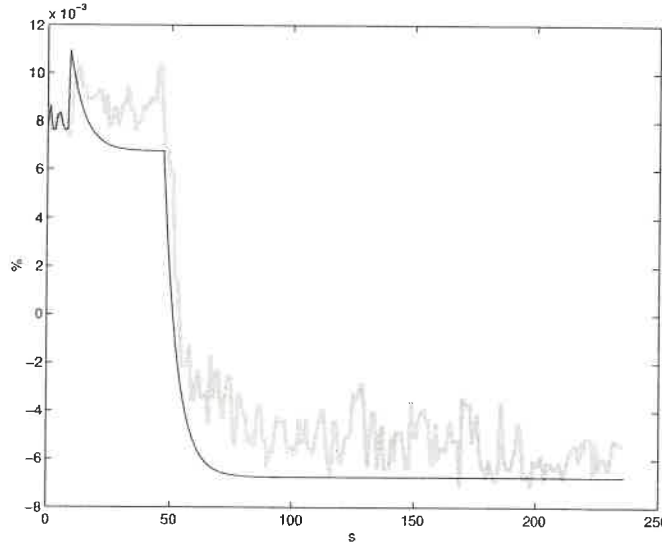


Figure D.27: Simulation of chosen model between  $y_4$  and  $u_8$  against validation data.

*best model* : black line, validation data : grey line

Table D.20: Characteristics of the chosen model between  $y_4$  and  $u_8$

Model Name	Equation Number	FPE	Fit (%)	Model Error Model Fit (%)	Linear Fit (%)
ARX(1,1)	(D.12)	$5.79 \times 10^{-7}$	65.9	–	70.8

## D.4 White water ash consistency models ( $y_5$ )

An alternative controlled variable for a retention control strategy is white water ash consistency. This section builds models to study the effect of the input variables on the white water ash consistency.

### D.4.1 Machine chest flowrate ( $u_3$ )

The identification data is presented in Figure D.28. Figure D.29 presents the FPE (bar plot) and the fit (line plot) of the selected models. Inside the bar, from top to bottom are the respective values of  $na$ ,  $nb$ ,  $nc$ ,  $nd$ ,  $nf$ , and  $nk$ .



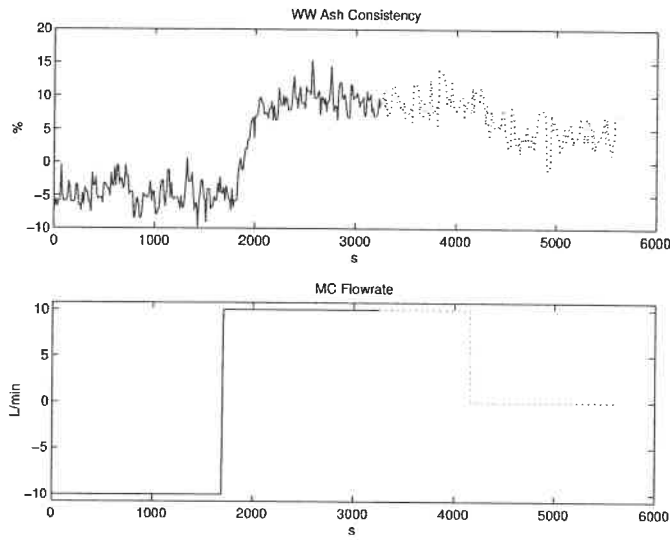


Figure D.28: Identification data for the model between  $y_5$  and  $u_3$

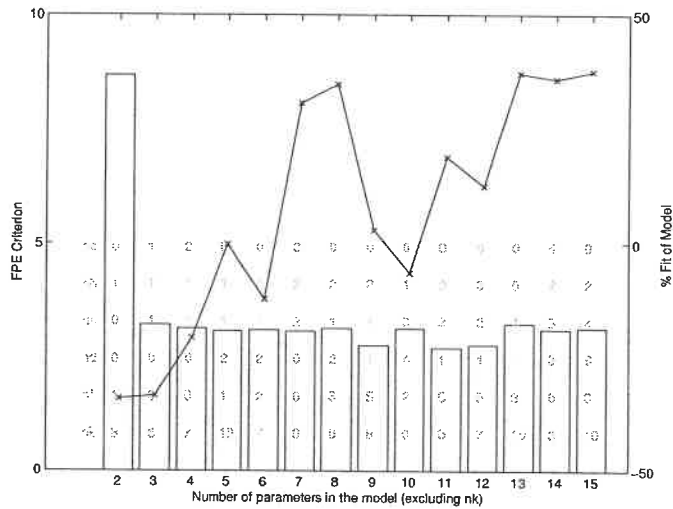


Figure D.29: Candidate models between  $y_5$  and  $u_3$

From the preliminary analysis, models 7 and 8 are chosen to undergo a deeper analysis. These models were selected because, respectively: a good fit and the best fit. The models are presented in Table D.21. Both models have almost a pole/zero cancellation. Both models show no auto-correlation of their error signal and no cross-correlation between the error and input signals. Even if there is almost a pole/zero cancellation, model ARMAX(3,2,2) is chosen because using a model with lesser parameters gives a much smaller fit. The whole data set is assumed to be linear. Then, the range is  $\pm 10\%$  in machine flowrate and  $\pm 10\%$  in ash consistency. The nominal values are 80 L/min for the flowrate and 54.6 % for the ash consistency. Table D.22 summarises some of the model characteristics. Figure D.30 compares the model response with the validation data.

Table D.21: Preliminary models between  $y_5$  and  $u_3$ 

Model Name	Model
ARMAX(3,2,2)	$(1 - 2.315q^{-1} + 1.674q^{-2} - 0.3594q^{-3})y =$ $(0.03159q^{-9} - 0.03172q^{-10})u$ $+(1 - 1.814q^{-1} + 0.8122q^{-2})e$
BJ(2,1,2,3)	$y = \frac{0.06313q^{-6} - 0.06342q^{-7}}{1 - 1.366q^{-1} - 0.1789q^{-2} + 0.5451q^{-3}}u$ $+ \frac{1 - 0.8124q^{-1}}{1 - 1.344q^{-1} + 0.3825q^{-2}}e$

$$y_5 = \frac{0.03159q^{-9} - 0.03172q^{-10}}{1 - 2.315q^{-1} + 1.674q^{-2} - 0.3594q^{-3}}u_3 + \frac{1 - 1.814q^{-1} + 0.8122q^{-2}}{1 - 2.315q^{-1} + 1.674q^{-2} - 0.3594q^{-3}}e \quad (\text{D.13})$$

#### D.4.2 Bentonite flowrate ( $u_5$ )

The identification data is presented in Figure D.31. Figure D.32 presents the FPE (bar plot) and the fit (line plot) of the selected models. Inside the bar, from top to

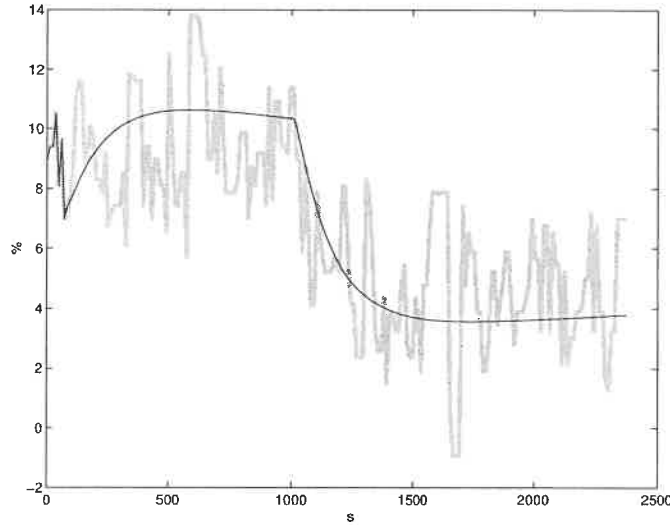


Figure D.30: Simulation of chosen model between  $y_5$  and  $u_3$  against validation data.

*best model* : black line, validation data : grey line

Table D.22: Characteristics of the chosen model between  $y_5$  and  $u_3$

Model Name	Equation Number	FPE	Fit (%)	Model Error Model Fit (%)	Linear Fit (%)
ARMAX(3,2,2)	(D.13)	3.07	30.7	20.1	63.7

bottom are the respective values of  $na$ ,  $nb$ ,  $nc$ ,  $nd$ ,  $nf$ , and  $nk$ .

From the preliminary analysis, model 6 and 10 are chosen to undergo a deeper analysis. These models were selected because, respectively: a good FPE/fit and the best fit. These models are presented in Table D.23. Model OE(3,3) has a pole/zero cancellation and auto-correlation of its error signal. Both models do not have cross-correlation between the error and input signals. Model BJ(3,2,2,3) almost have a pole/zero cancellation and no auto-correlation of its error signal. It is therefore chosen. From the first step, the process gain is evaluated at 13 %/(L/min). From the second step, the process gain is evaluated at 34 %/(L/min). Since the model precision is not very high, the whole data set is assumed linear. Then, the range is 0

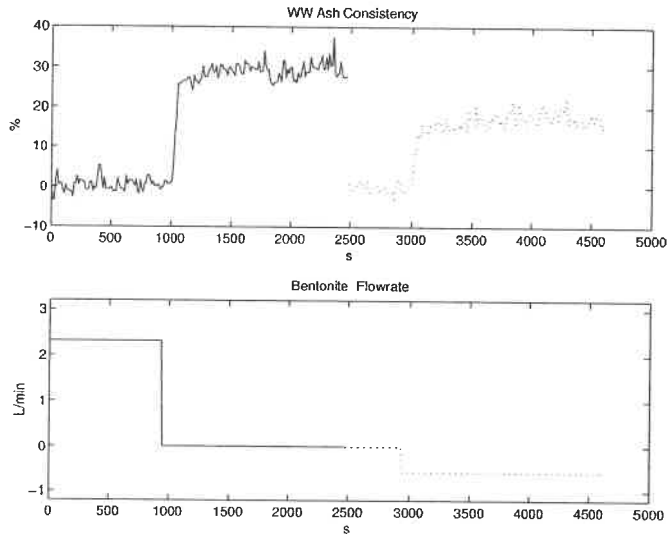


Figure D.31: Identification data for the model between  $y_5$  and  $u_5$

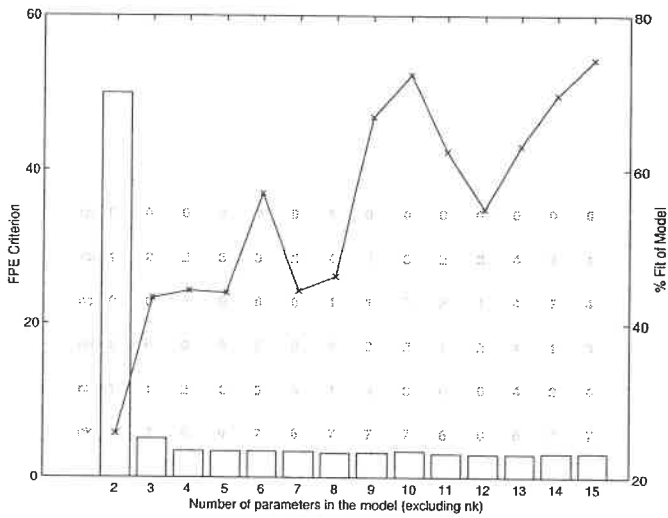


Figure D.32: Candidate models between  $y_5$  and  $u_5$

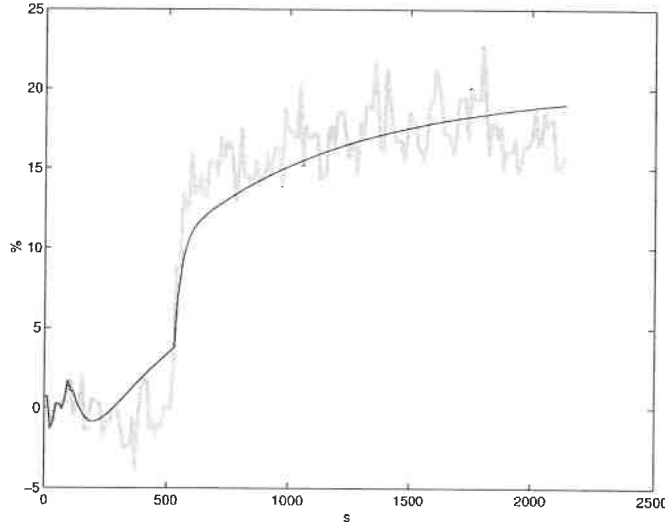


Figure D.33: Simulation of chosen model between  $y_5$  and  $u_5$  against validation data.

*best* model : black line, validation data : grey line

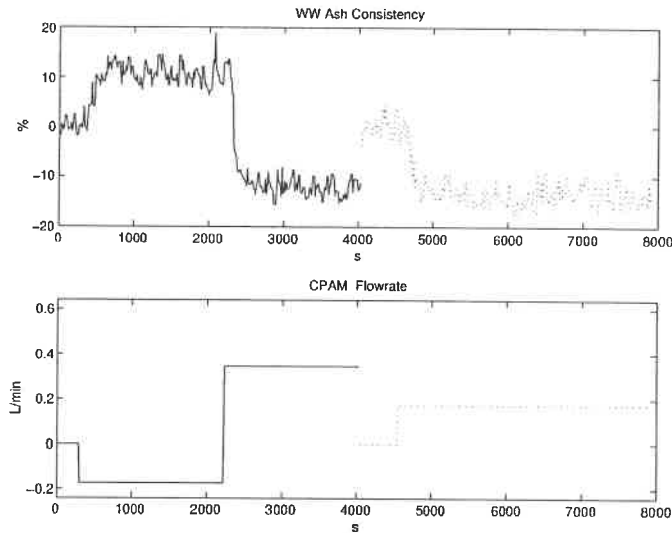
to 2.9 L/min of bentonite and 30 to 84 % in ash consistency. Table D.24 summarises some of the model characteristics. Figure D.33 compares the model response with the validation data.

Model Name	Model
OE(3,3)	$y = \frac{-5.546q^{-7} + 10.57q^{-8} - 5.026q^{-9}}{1 - 2.386q^{-1} + 1.815q^{-2} - 0.4288q^{-3}} u + e$
BJ(3,2,2,3)	$y = \frac{-4.89q^{-7} + 2.828q^{-8} + 1.934q^{-9}}{1 - 1.001q^{-1} - 0.3781q^{-2} + 0.39q^{-3}} u + \frac{1 - 1.266q^{-1} + 0.2583q^{-2}}{1 - 1.733q^{-1} + 0.733q^{-2}} e$

$$y_5 = \frac{-4.89q^{-7} + 2.828q^{-8} + 1.934q^{-9}}{1 - 1.001q^{-1} - 0.3781q^{-2} + 0.39q^{-3}} u_5 + \frac{1 - 1.266q^{-1} + 0.2583q^{-2}}{1 - 1.733q^{-1} + 0.733q^{-2}} e \quad (\text{D.14})$$

Table D.24: Characteristics of the chosen model between  $y_5$  and  $u_5$ 

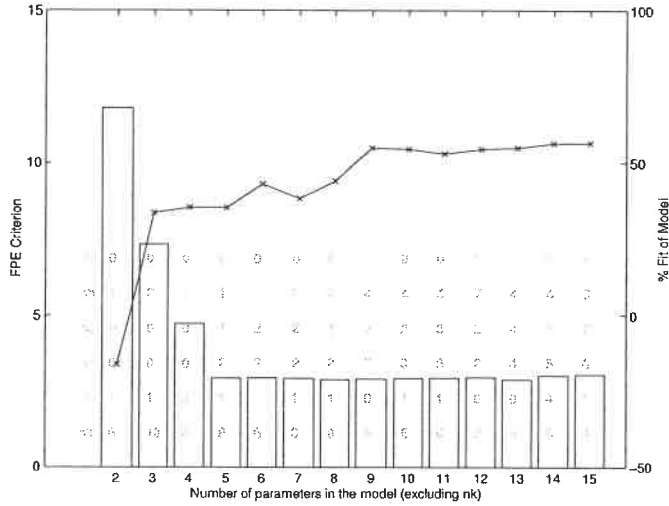
Model Name	Equation Number	FPE	Fit (%)	Model Error Model Fit (%)	Linear Fit (%)
BJ(3,2,2,3)	(D.14)	3.36	72.3	no fit	79.9

Figure D.34: Identification data for the model between  $y_5$  and  $u_6$ 

### D.4.3 C-PAM flowrate ( $u_6$ )

The identification data is presented in Figure D.34. Figure D.35 presents the FPE (bar plot) and the fit (line plot) of the selected models. Inside the bar, from top to bottom are the respective values of  $na$ ,  $nb$ ,  $nc$ ,  $nd$ ,  $nf$ , and  $nk$ .

From the preliminary analysis, models 5, 6 and 9 are chosen to undergo a deeper analysis. These models were selected because they present good FPE / fit combinations. The models are presented in Table D.25. Model ARARMAX(1,4,2,2) has a pole/zero cancellation. The remaining models show no auto-correlation of their residuals and no cross-correlation between the residuals and the input signal. The model error model fit is smaller for model BJ(1,2,2,1). Therefore, it is chosen (D.15). The whole data set is assumed to be linear. Then, the range is 0.404 – 0.924 L/min

Figure D.35: Candidate models between  $y_5$  and  $u_6$ 

in CPAM and 40 – 60 % in white water ash consistency. Table D.26 summarises some of the model characteristics. Figure D.36 compares the model response with the validation data.

Table D.25: Preliminary models between  $y_5$  and  $u_6$ 

Model Name	Model
BJ(1,1,2,1)	$y = \frac{-7.636q^{-6}}{1-0.8287q^{-1}}u + \frac{1-0.9501q^{-1}}{1-1.593q^{-1}+0.594q^{-2}}e$
BJ(1,2,2,1)	$y = \frac{-7.646q^{-6}}{1-0.8292q^{-1}}u + \frac{1-0.9676q^{-1}+0.01126q^{-2}}{1-1.601q^{-1}+0.6012q^{-2}}e$
ARARMAX(1,4,2,2)	$(1 - 0.8948q^{-1})y = (-7.799q^{-6} + 5.182q^{-7} - 16.45q^{-8} + 14.08q^{-9})u + \frac{1-1.811q^{-1}+0.8134q^{-2}}{1-1.55q^{-1}+0.5488q^{-2}}e$

$$y_5 = \frac{-7.646q^{-6}}{1 - 0.8292q^{-1}}u_6 + \frac{1 - 0.9676q^{-1} + 0.01126q^{-2}}{1 - 1.601q^{-1} + 0.6012q^{-2}}e \quad (\text{D.15})$$

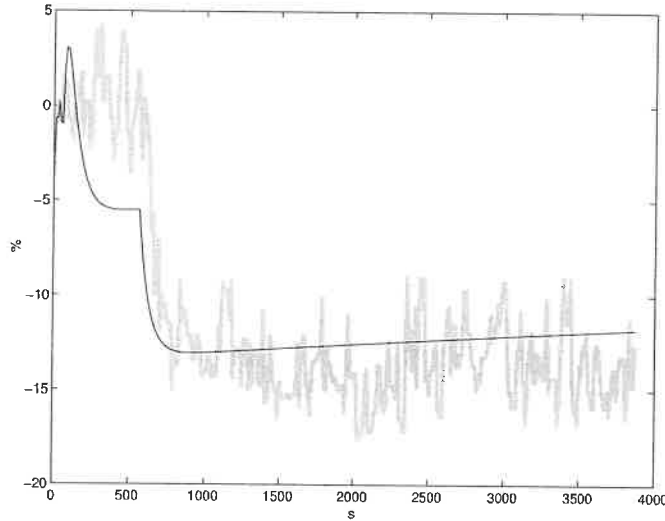


Figure D.36: Simulation of chosen model between  $y_5$  and  $u_6$  against validation data.

*best model* : black line, validation data : grey line

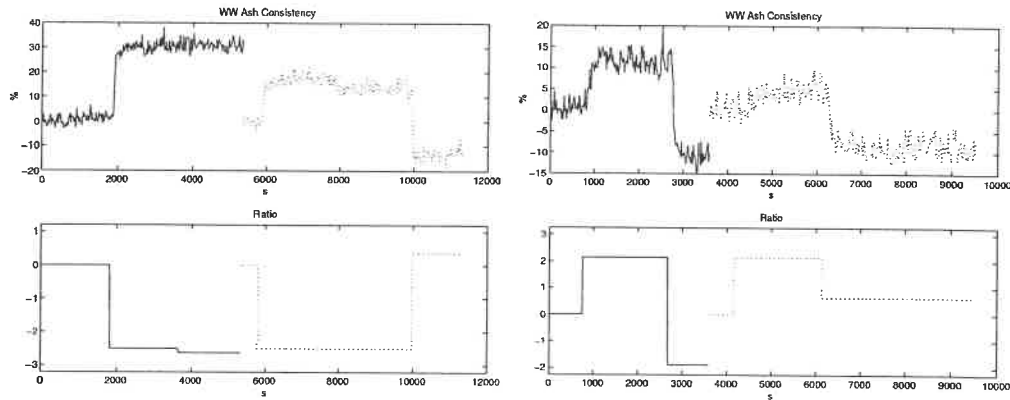
Table D.26: Characteristics of the chosen model between  $y_5$  and  $u_6$

Model Name	Equation Number	FPE	Fit (%)	Model Error Model Fit (%)	Linear Fit (%)
BJ(1,2,2,1)	(D.15)	2.92	42.9	8.1	61.6

#### D.4.4 Ratio of bentonite to C-PAM ( $u_7$ )

The identification data is presented in Figure D.37. A quick glance at the data shows a gain sign reversal. In the range of a ratio of 0 to 3, the gain is negative. In the range of a ratio of 3 to 7, the gain is positive. Two models are identified, one for each range. Figure D.37(a) presents the data for the low range (ratio of 0 to 3). Figure D.37(b) presents the data for the high range (ratio of 3 to 7). Figure D.38(a) presents the FPE (bar plot) and the fit (line plot) of the selected models for the low range and Figure D.38(b) for the high range. Inside the bar, from top to bottom are the respective values of  $na$ ,  $nb$ ,  $nc$ ,  $nd$ ,  $nf$ , and  $nk$ .

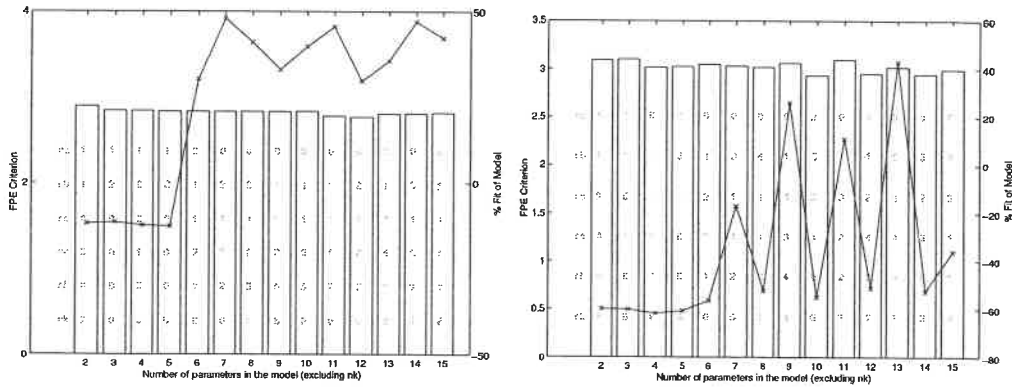




(a) Low range

(b) High range

Figure D.37: Identification data for the models between  $y_5$  and  $u_7$



(a) Low range

(b) High range

Figure D.38: Candidate models between  $y_5$  and  $u_7$

From the preliminary analysis of Figure D.38(a), model 7 and 11 are chosen to undergo a deeper analysis. These models were selected because of good FPE / fit combination for the number of parameters. The models are presented in Table D.27. A pole / zero analysis reveals no cancellation. The residuals analysis shows auto-correlation of the error signal for both models. There is also cross-correlation between the error and input signals. Graphing both model against the validation data, model BJ(1,1,2,7) shows overfitting of noise. Therefore, BJ(2,1,2,2) is chosen (D.16). The linear range is a ratio of bentonite to CPAM from 0 to 3 and 28 to 82 % in white water ash consistency.

From the preliminary analysis of Figure D.38(b), model 9 and 11 are chosen to undergo a deeper analysis. These models were selected because good FPE / fit combination for the number of parameters. The models are presented in Table D.28. A pole / zero analysis reveals a cancellation for model BJ(4,3,2,2). The residuals analysis shows auto-correlation of the error signal for both models. No cross-correlation between the error and input signals is detected. The simpler model is kept (D.17). The linear range is a ratio of bentonite to CPAM from 3 to 7 and 28 to 60 % in white water ash consistency. Table D.29 summarises some of the models characteristics. Figure D.39 compares the model response with the validation data.

Table D.27: Preliminary models between  $y_5$  and  $u_7$  for the low range

Model Name	Model
BJ(2,1,2,2)	$y = \frac{-2.049q^{-6} - 3.235q^{-7}}{1 - 0.1273q^{-1} - 0.4106q^{-2}}u$ $+ \frac{1 - 0.9856q^{-1}}{1 - 1.526q^{-1} + 0.5266q^{-2}}e$
BJ(1,1,2,7)	$y = \frac{-2.012q^{-6}}{1 - 1.459q^{-1} + 0.8991q^{-2} - 0.5837q^{-3} + 1.051q^{-4} - 1.388q^{-5} + 0.9414q^{-6} - 0.2856q^{-7}}u$ $+ \frac{1 - 0.9802q^{-1}}{1 - 1.488q^{-1} + 0.4893q^{-2}}e$

$$y_5 = \frac{-2.049q^{-6} - 3.235q^{-7}}{1 - 0.1273q^{-1} - 0.4106q^{-2}}u_{7(\text{Low range})} + \frac{1 - 0.9856q^{-1}}{1 - 1.526q^{-1} + 0.5266q^{-2}}e \quad (\text{D.16})$$

Table D.28: Preliminary models between  $y_5$  and  $u_7$  for the high range

Model Name	Model
BJ(1,1,3,4)	$y = \frac{0.8728q^{-4}}{1+0.03019q^{-1}-1.233q^{-2}-0.1282q^{-3}+0.487q^{-4}}u + \frac{1-1.01q^{-1}}{1-1.525q^{-1}+0.5177q^{-2}+0.007515q^{-3}}e$
BJ(4,3,2,2)	$y = \frac{0.7896q^{-7}+2.33q^{-8}-0.03758q^{-9}-1.439q^{-10}}{1+0.0885q^{-1}-0.7936q^{-2}}u + \frac{1-1.006q^{-1}+0.002574q^{-2}-0.005936q^{-3}}{1-1.539q^{-1}+0.54q^{-2}}e$

$$y_5 = \frac{0.8728q^{-4}}{1 + 0.03019q^{-1} - 1.233q^{-2} - 0.1282q^{-3} + 0.487q^{-4}}u_{7(\text{High range})} + \frac{1 - 1.01q^{-1}}{1 - 1.525q^{-1} + 0.5177q^{-2} + 0.007515q^{-3}}e \quad (\text{D.17})$$

Table D.29: Characteristics of the chosen models between  $y_5$  and  $u_7$ 

Model Name	Equation Number	FPE	Fit (%)	Model Error Model Fit (%)	Linear Fit (%)
BJ(1,1,2,1) <sub>Low range</sub>	(D.16)	2.83	47.9	48.1	67.3
BJ(1,1,3,4) <sub>High range</sub>	(D.17)	3.06	26.0	-49	52.2

#### D.4.5 Fresh filler flowrate ( $u_8$ )

The identification data is presented in Figure D.40. Figure D.41 presents the FPE (bar plot) and the fit (line plot) of the selected models. Inside the bar, from top to bottom are the respective values of  $na$ ,  $nb$ ,  $nc$ ,  $nd$ ,  $nf$ , and  $nk$ .

From the preliminary analysis, model 6 and 11 are chosen to undergo a deeper analysis. These models were selected because, respectively: the best fit and the best FPE / fit combination. But, both models have a pole/zero cancellation. As a second choice, models 2,3, and 4 are analyzed. The models are presented in Table D.30. All models show some auto-correlation of their error signal and no cross-correlation

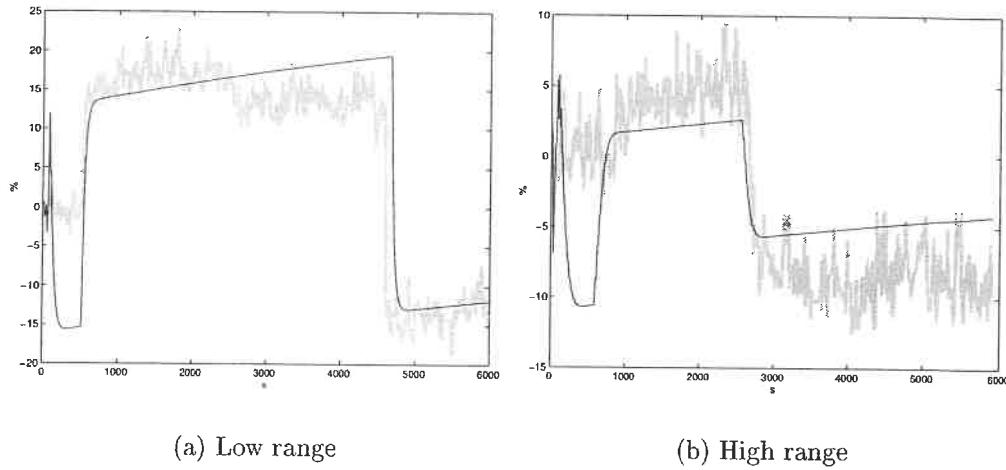


Figure D.39: Simulation of chosen models between  $y_5$  and  $u_7$  against validation data.

*best model* : black line, *validation data* : grey line

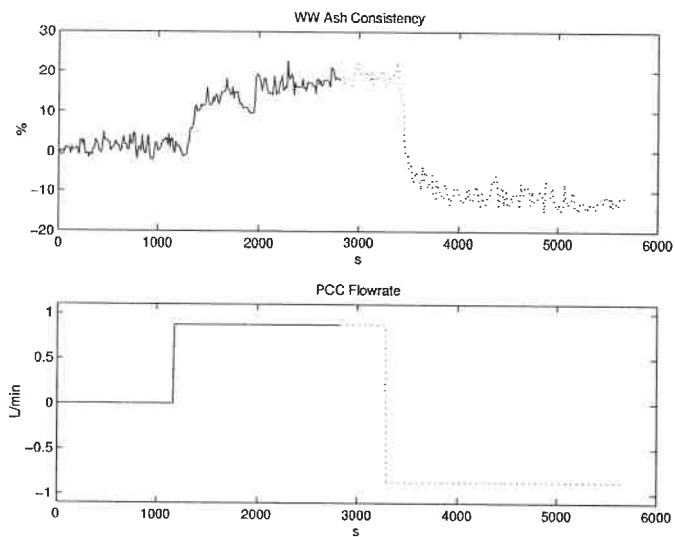


Figure D.40: Identification data for the model between  $y_5$  and  $u_8$

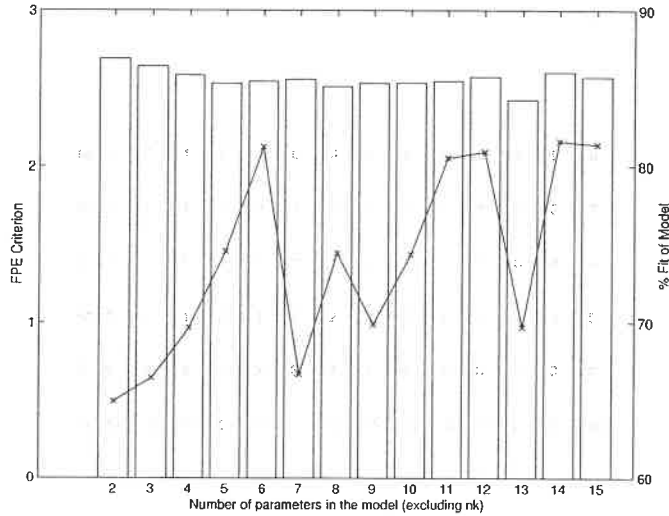


Figure D.41: Candidate models between  $y_5$  and  $u_8$

between the error and input signals. The simplest one is chosen. The whole data set is assumed to be linear. Then, the range is  $\pm 0.87$  L/min in filler flowrate and  $\pm 20$  % in ash consistency. The nominal values are 4.55 L/min for the filler and 69.5 % for the ash consistency. Table D.31 summarises some of the model characteristics. Figure D.42 compares the model response with the validation data.

Table D.30: Preliminary models between  $y_5$  and  $u_8$

Model Name	Model
ARX(1,1)	$(1 - 0.8266q^{-1})y = (2.915q^{-10})u + e$
ARMAX(1,1,1)	$(1 - 0.8653q^{-1})y = (2.308q^{-10})u + (1 - 0.2382q^{-1})e$
ARMAX(1,1,1)	$y = \frac{1.736q^{-10}}{1-0.8989q^{-1}}u + \frac{1-0.6869q^{-1}}{(1-0.4125q^{-1})(1-0.8989q^{-1})}e$

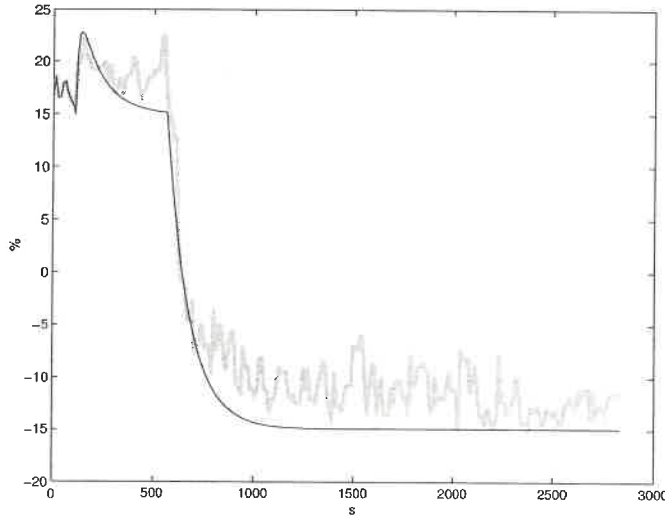


Figure D.42: Simulation of chosen model between  $y_5$  and  $u_8$  against validation data.

*best model* : black line, validation data : grey line

$$y_5 = \frac{1.736q^{-10}}{1 - 0.8989q^{-1}}u_8 + \frac{1 - 0.6869q^{-1}}{(1 - 0.4125q^{-1})(1 - 0.8989q^{-1})}e \quad (\text{D.18})$$

Table D.31: Characteristics of the chosen models between  $y_5$  and  $u_3$

Model Name	Equation Number	FPE	Fit (%)	Model Error Model Fit (%)	Linear Fit (%)
ARARMAX(1,1,1,1)	(D.18)	2.59	69.7	no fit	72.8

## D.5 Ash Content models ( $y_8$ )

To integrate wet-end and dry-end strategies, some dry-end variables are needed. Ash content was chosen because of its importance on paper quality. Models between ash content and wet-end input variables are built in this section.

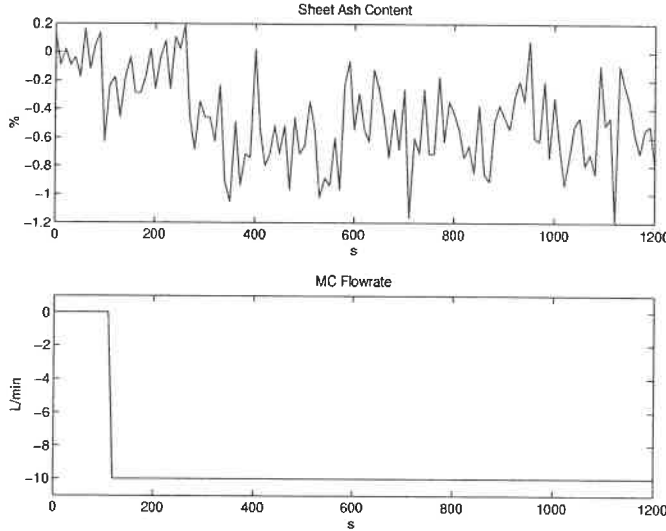
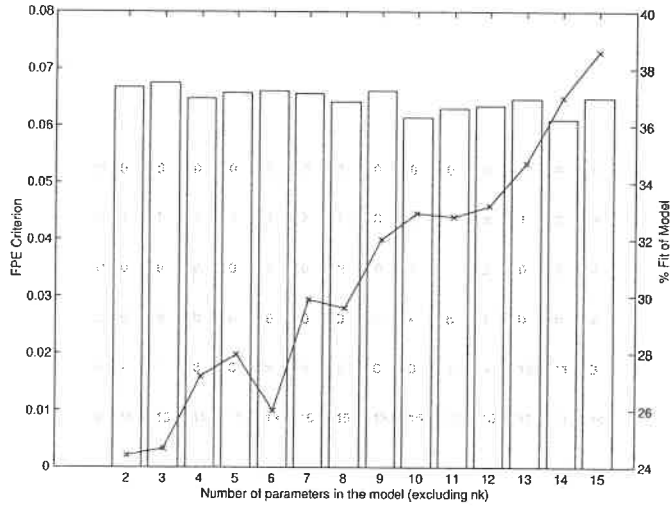


Figure D.43: Identification data for the model between  $y_8$  and  $u_3$

### D.5.1 Machine chest flowrate ( $u_3$ )

The identification data is presented in Figure D.43. Due to sheet breaks, only one step is available to compute the model. The same data is used for the identification and validation set. Figure D.44 presents the FPE (bar plot) and the fit (line plot) of the selected models. Inside the bar, from top to bottom are the respective values of  $na$ ,  $nb$ ,  $nc$ ,  $nd$ ,  $nf$ , and  $nk$ . We can see that all models poorly reproduce the data. Since the signal to noise ratio is high, this result is not surprising.

From the preliminary analysis, models 2 and 7 are chosen to undergo a deeper analysis. Even if models with a higher number of parameters have a better FPE and fit, they only model the noise behaviour by adding poles on the unit circle. The selected models are presented in Table D.32. The models show no auto-correlation of their residuals and no cross-correlation between the residuals and the input. Model OE(2,5) has poles on the unit circle and is therefore trying to model noise behaviour. Therefore, the simpler model is kept (D.19). The whole data set is assumed to be

Figure D.44: Candidate models between  $y_8$  and  $u_3$ 

linear. Then, the range is 0 to -10 L/min in machine flowrate and 0 to -0.5 % in ash content. The nominal values are 80 L/min for the flowrate and 17 % for the ash content. Table D.33 summarises some of the model characteristics. Figure D.45 compares the model response with the validation data.

Table D.32: Preliminary models between  $y_8$  and  $u_3$ 

Model Name	Model
OE(1,1)	$y = \frac{0.04882q^{-15}}{1-0.1336q^{-1}}u + e$
OE(2,5)	$y = \frac{0.05814q^{-15}+0.07083q^{-16}}{1+1.357q^{-1}+0.8886q^{-2}+0.2375q^{-3}-0.5137q^{-4}-0.6836q^{-5}}u + e$

$$y_8 = \frac{0.04882q^{-15}}{1 - 0.1336q^{-1}}u_3 + e \quad (\text{D.19})$$



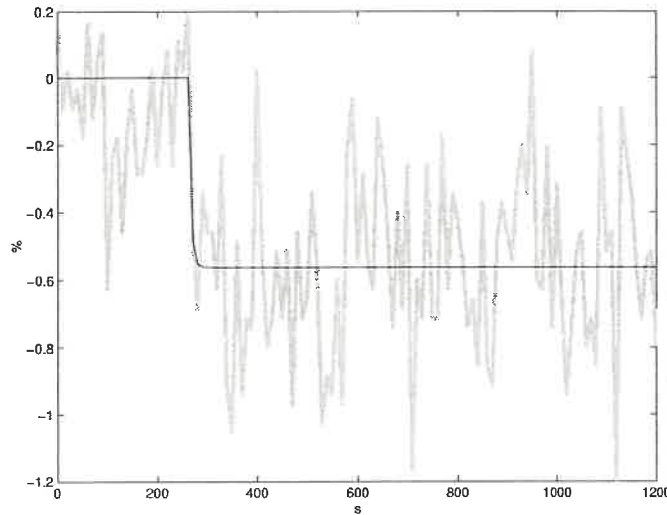


Figure D.45: Simulation of chosen model between  $y_8$  and  $u_3$  against validation data.

*best* model : black line, validation data : grey line

Table D.33: Characteristics of the chosen model between  $y_8$  and  $u_3$

Model Name	Equation Number	FPE	Fit (%)	Model Error Model Fit (%)	Linear Fit (%)
OE(1,1)	(D.19)	0.067	24.4	no fit	24.4

## D.5.2 Bentonite flowrate ( $u_5$ )

The identification data is presented in Figure D.46. Figure D.47 presents the FPE (bar plot) and the fit (line plot) of the selected models. Inside the bar, from top to bottom are the respective values of  $na$ ,  $nb$ ,  $nc$ ,  $nd$ ,  $nf$ , and  $nk$ .

From the preliminary analysis, models 8 and 10 are chosen to undergo a deeper analysis. These models were selected because they present good FPE / fit combinations. The selected models are presented in Table D.34. Both models show auto-correlation of the residuals and no cross-correlation between the residuals and the input. They have no pole / zero cancellation. Their model error model fit are similar. Therefore, the simpler model is kept (D.20). The whole data set is assumed

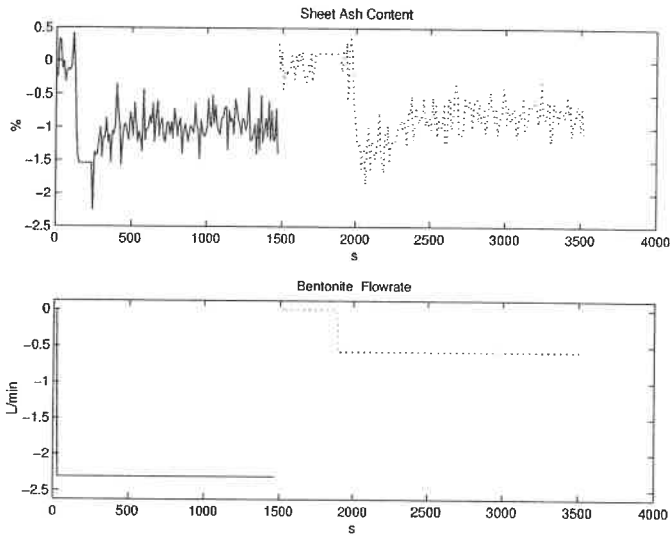


Figure D.46: Identification data for the model between  $y_8$  and  $u_5$

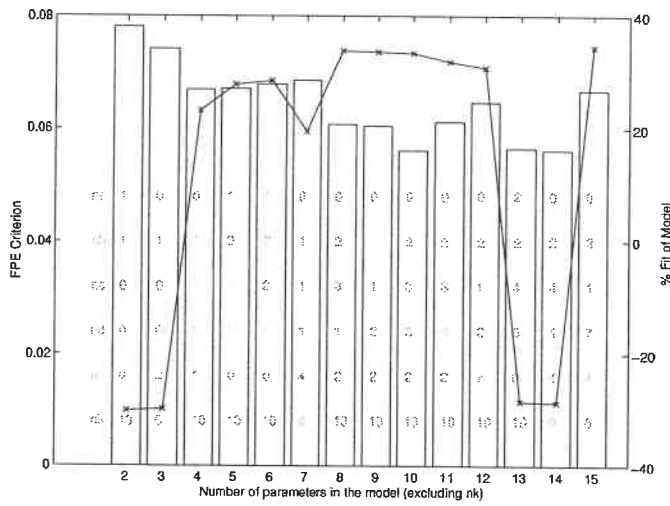


Figure D.47: Candidate models between  $y_8$  and  $u_5$

to be linear. Then, the range is 0 to 2.9 L/min of bentonite and 14.5 to 16.5 % of sheet ash content. Table D.35 summarises some of the model characteristics. Figure D.48 compares the model response with the validation data.

$$y_8 = \frac{0.3953q^{-10} - 0.3794q^{-11}}{1 - 1.451q^{-1} + 0.4889q^{-2}}u_5 + \frac{1 - 1.127q^{-1} + 0.1474q^{-2} - 0.02953q^{-3}}{1 - 1.001q^{-1}}e \quad (\text{D.20})$$

Table D.34: Preliminary models between  $y_8$  and  $u_5$

Model Name	Model
BJ(2,3,1,2)	$y = \frac{0.3953q^{-10} - 0.3794q^{-11}}{1 - 1.451q^{-1} + 0.4889q^{-2}}u + \frac{1 - 1.127q^{-1} + 0.1474q^{-2} - 0.02953q^{-3}}{1 - 1.001q^{-1}}e$
BJ(2,3,3,2)	$y = \frac{0.4316q^{-10} - 0.4147q^{-11}}{1 - 1.408q^{-1} + 0.4483q^{-2}}u + \frac{1 - 0.187q^{-1} + 0.1756q^{-2} - 1.016q^{-3}}{1 - 0.1285q^{-1} + 0.0483q^{-2} - 0.9164q^{-3}}e$

Table D.35: Characteristics of the chosen model between  $y_8$  and  $u_5$

Model Name	Equation Number	FPE	Fit (%)	Model Error Model Fit (%)	Linear Fit (%)
BJ(2,3,1,2)	(D.20)	0.061	33.8	–	39.1

### D.5.3 C-PAM flowrate ( $u_6$ )

The identification data is presented in Figure D.49. Figure D.50 presents the FPE (bar plot) and the fit (line plot) of the selected models. Inside the bar, from top to bottom are the respective values of  $na$ ,  $nb$ ,  $nc$ ,  $nd$ ,  $nf$ , and  $nk$ . The ash content signal is noisy. The resulting models have poor fit values.

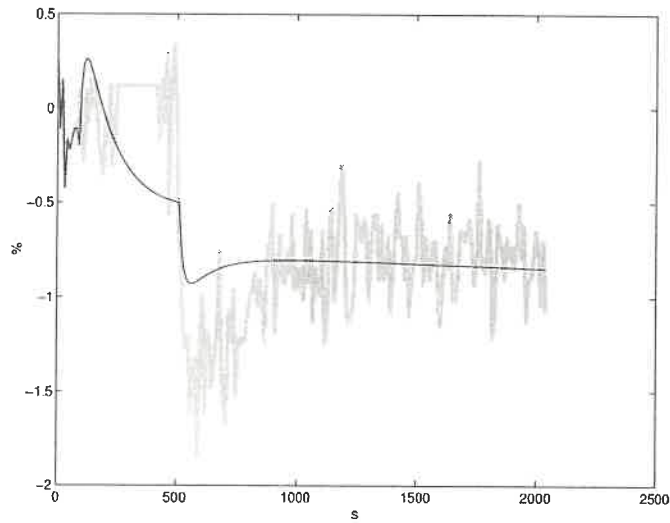


Figure D.48: Simulation of chosen model between  $y_8$  and  $u_5$  against validation data.

*best model* : black line, *validation data* : grey line

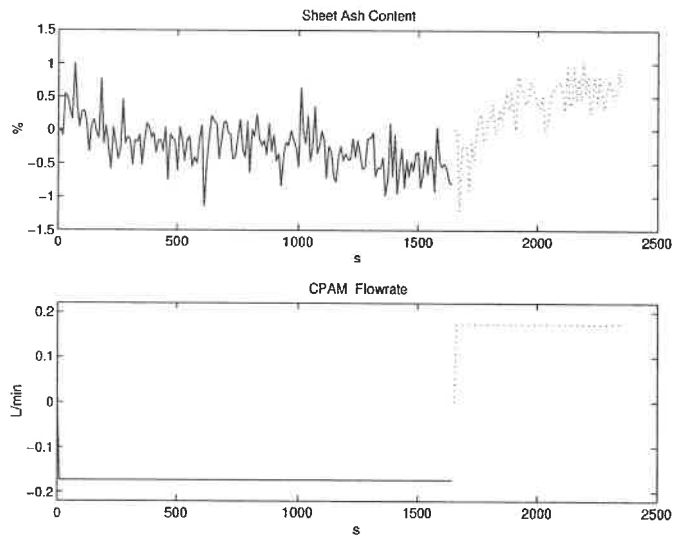


Figure D.49: Identification data for the model between  $y_8$  and  $u_6$

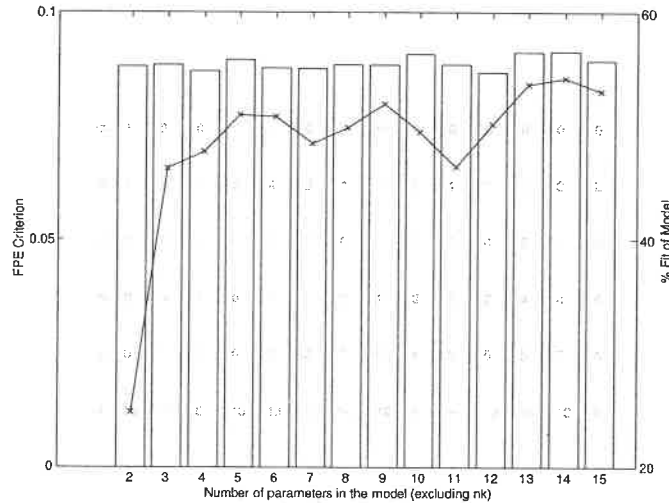


Figure D.50: Candidate models between  $y_8$  and  $u_6$

From the preliminary analysis, models 2, 5 and 6 are chosen to undergo a deeper analysis. These models were selected because they present good FPE / fit combinations. Furthermore, higher order models try to model the noise with poles on the unit circle. The selected models are presented in Table D.36. Models ARMAX(1,3,1) and ARMAX(1,4,1) have a pole/zero cancellation. The remaining model shows some auto-correlation of its residuals and no cross-correlation between the residuals and the input. Therefore, this model is kept (D.21). The whole data set is assumed to be linear. Then, the range is 0.231 to 0.578 L/min of C-PAM and 15 to 17 % of sheet ash content. Table D.37 summarises some of the model characteristics. Figure D.51 compares the model response with the validation data.

$$y_8 = \frac{1.241q^{-10}}{1 - 0.2243q^{-1}}u_6 + \frac{1}{1 - 0.2243q^{-1}}e \quad (\text{D.21})$$

Table D.36: Preliminary models between  $y_8$  and  $u_6$ 

Model Name	Model
ARX(1,1)	$y = \frac{1.241q^{-10}}{1-0.2243q^{-1}}u + \frac{1}{1-0.2243q^{-1}}e$
ARMAX(1,3,1)	$(1 - 1.017q^{-1})y = (0.2911q^{-15} + 0.4191q^{-16} - 0.7201q^{-17})u + (1 - 1.01q^{-1})e$
ARMAX(1,4,1)	$(1 - 1.025q^{-1})y = (-1.202q^{-16} + 0.2433q^{-17} + 4.619q^{-18} - 3.684q^{-19})u + (1 - 1.01q^{-1})e$

Table D.37: Characteristics of the chosen model between  $y_8$  and  $u_6$ 

Model Name	Equation Number	FPE	Fit (%)	Model Error Model Fit (%)	Linear Fit (%)
ARX(1,1)	(D.21)	0.10	24.9	-	18.1

#### D.5.4 Ratio of bentonite to C-PAM ( $u_7$ )

The identification data is presented in Figure D.52. Figure D.53 presents the FPE (bar plot) and the fit (line plot) of the selected models. Inside the bar, from top to bottom are the respective values of  $na$ ,  $nb$ ,  $nc$ ,  $nd$ ,  $nf$ , and  $nk$ .

From the preliminary analysis, model 2 is chosen (D.22). From Figure D.53, we can see that adding parameters improves the model for the estimation data (the FPE decreases as the number of parameters increases), but worsens the fit on the validation data. The chosen model shows no auto-correlation of its residuals and no cross-correlation between the residuals and the input. The whole data set is assumed to be linear. The linear ranges are a ratio of bentonite to CPAM from 0 to 3 and 14.5 to 16.5 % in sheet ash content. Table D.38 summarises some of the model characteristics. Figure D.54 compares the model response with the validation data.

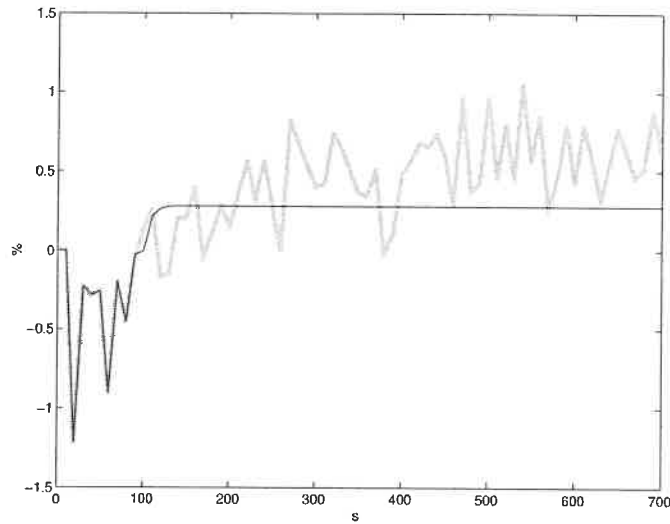


Figure D.51: Simulation of chosen model between  $y_8$  and  $u_6$  against validation data.

*best model* : black line, *validation data* : grey line

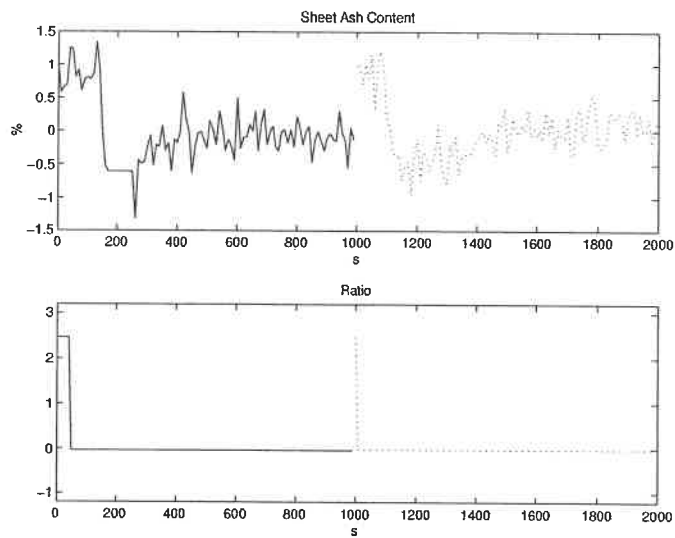
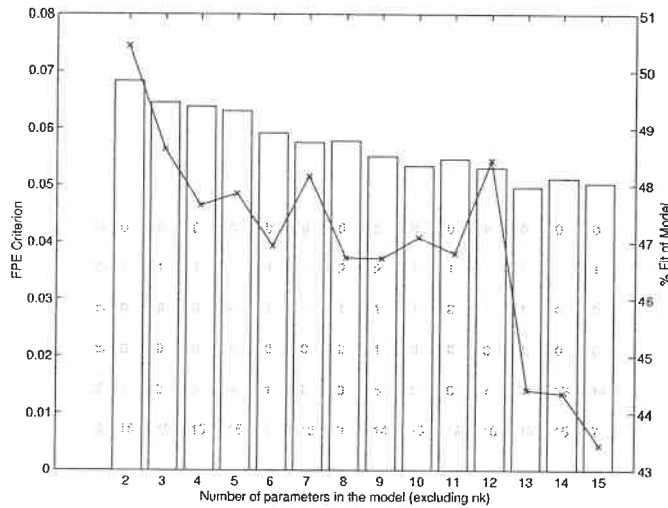


Figure D.52: Identification data for the model between  $y_8$  and  $u_7$

Figure D.53: Candidate models between  $y_8$  and  $u_7$ 

$$y_8 = \frac{0.04055q^{-16}}{1 - 0.9415q^{-1}}u_7 + e \quad (\text{D.22})$$

Table D.38: Characteristics of the chosen model between  $y_8$  and  $u_7$ 

Model Name	Equation Number	FPE	Fit (%)	Model Error Model Fit (%)	Linear Fit (%)
OE(1,1)	(D.22)	0.068	48.6	12.7	52.3

### D.5.5 Fresh filler flowrate ( $u_8$ )

The identification data is presented in Figure D.55. Figure D.56 presents the FPE (bar plot) and the fit (line plot) of the selected models. Inside the bar, from top to bottom are the respective values of  $na$ ,  $nb$ ,  $nc$ ,  $nd$ ,  $nf$ , and  $nk$ .

From the preliminary analysis, model 2 is chosen. Since all models give a similar fit on both the estimation and validation data, the simpler model is kept. Nonetheless, the standard procedure was performed. Models OE(1,1) shows auto-correlation



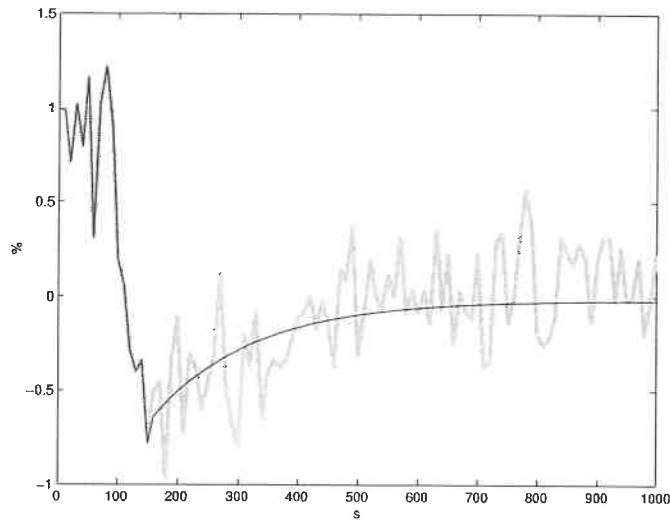


Figure D.54: Simulation of chosen model between  $y_8$  and  $u_7$  against validation data.  
*best model* : black line, validation data : grey line

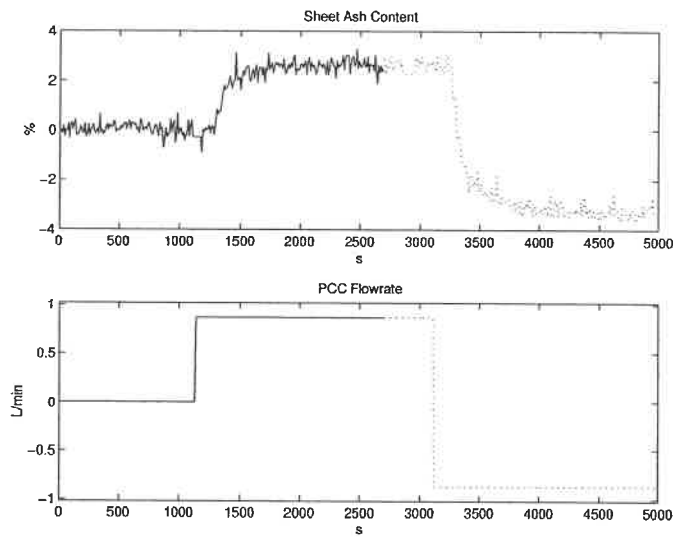


Figure D.55: Identification data for the model between  $y_8$  and  $u_8$

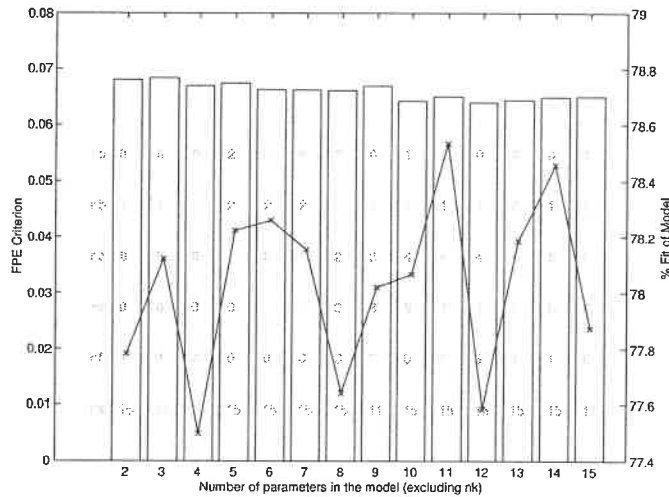


Figure D.56: Candidate models between  $y_8$  and  $u_8$

of the residuals and no cross-correlation between the residuals and the input. More complicated models (for example model with 11 parameters) did also show auto-correlation. With this data, there is no justification for a more complicated model. The whole data set is assumed to be linear. Then, the range is  $\pm 0.87$  L/min in filler flowrate and  $\pm 3$  % in ash content. The nominal values are 4.55 L/min for the filler flowrate and 18.9 % for the ash content. Table D.39 summarises some of the model characteristics. Figure D.57 compares the model response with the validation data.

$$y_8 = \frac{0.2649q^{-15}}{1 - 0.9112q^{-1}}u_8 + e \quad (\text{D.23})$$

Table D.39: Characteristics of the chosen model between  $y_8$  and  $u_8$

Model Name	Equation Number	FPE	Fit (%)	Model Error Model Fit (%)	Linear Fit (%)
OE(1,1)	(D.23)	0.068	77.8	–	81.8

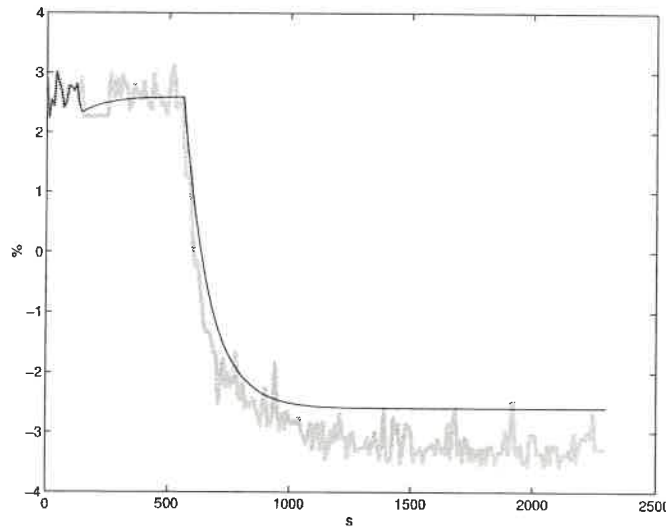


Figure D.57: Simulation of chosen model between  $y_8$  and  $u_8$  against validation data.

*best model* : black line, validation data : grey line

## D.6 Basis weight models ( $y_9$ )

Basis weight is a very important controlled variable in the paper production. It is also a very important selling and cost property of paper. Those models goals are to study the effect of wet-end variables on the basis weight.

### D.6.1 Machine chest flowrate ( $u_3$ )

The identification data is presented in Figure D.58. Due to sheet breaks, only one step is available to compute the model. The same data is used for the identification and validation set. Figure D.59 presents the FPE (bar plot) and the fit (line plot) of the selected models. Inside the bar, from top to bottom are the respective values of  $na$ ,  $nb$ ,  $nc$ ,  $nd$ ,  $nf$ , and  $nk$ .

From the preliminary analysis, models 2, 4 and 7 are chosen to undergo a deeper analysis. Even if models with a higher number of parameters have better FPE and

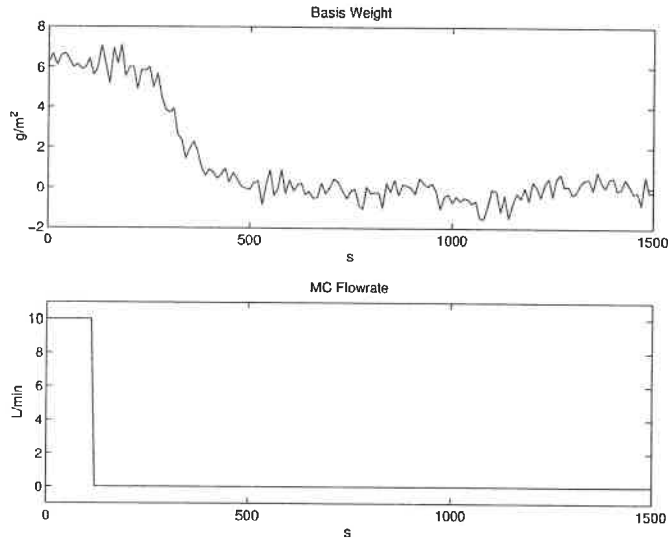


Figure D.58: Identification data for the model between  $y_9$  and  $u_3$

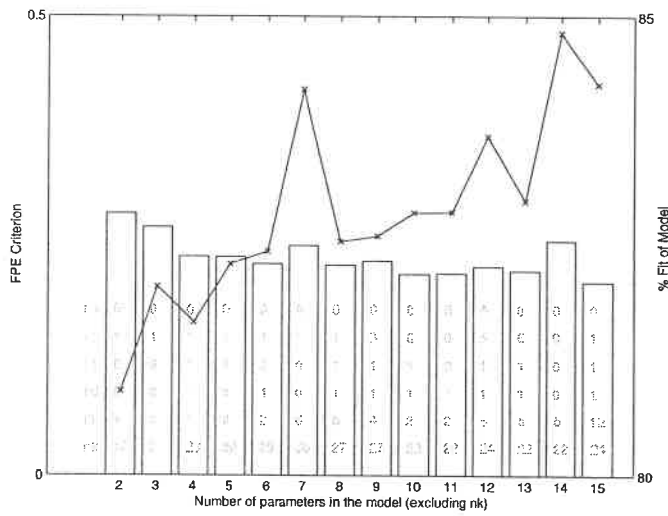


Figure D.59: Candidate models between  $y_9$  and  $u_3$

fit, they only model the noise behaviour by adding poles on the unit circle. The selected models are presented in Table D.40. The models shows no auto-correlation of the residuals and no cross-correlation between the residuals and the input. The model error model fit is similar for the three models. Therefore, the simpler one is kept (D.24). The whole data set is assumed to be linear. Then, the range is 0 to 10 L/min in machine flowrate and 0 to 6 g/m<sup>2</sup> in basis weight. The nominal values are 80 L/min for the flowrate and 61.2 g/m<sup>2</sup> for the basis weight. Table D.41 summarises some of the model characteristics. Figure D.60 compares the model response with the validation data.

Table D.40: Preliminary models between  $y_9$  and  $u_3$ 

Model Name	Model
OE(1,1)	$y = \frac{0.06467q^{-17}}{1-0.8643q^{-1}}u + e$
ARARMAX(1,1,1,1)	$y = \frac{-0.0173q^{-23}}{1-0.7243q^{-1}}u + \frac{1-0.6833q^{-1}}{1-0.8631q^{-1}}e$
OE(1,6)	$y = \frac{0.003853q^{-30}}{1-1.493q^{-1}+0.3343q^{-2}-0.513q^{-3}+0.3625q^{-4}+0.9552q^{-5}-0.6436q^{-6}}u + e$

$$y_9 = \frac{0.06467q^{-17}}{1 - 0.8643q^{-1}}u_3 + e \quad (\text{D.24})$$

Table D.41: Characteristics of the chosen model between  $y_9$  and  $u_3$ 

Model Name	Equation Number	FPE	Fit (%)	Model Error Model Fit (%)	Linear Fit (%)
OE(1,1)	(D.24)	0.29	80.9	6.96	80.9

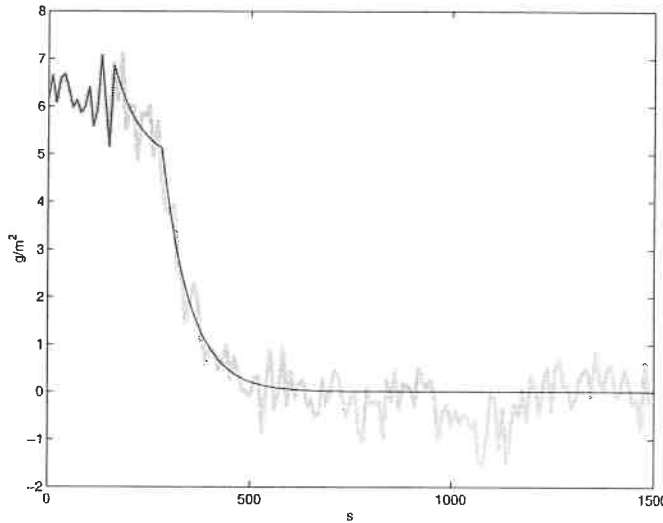


Figure D.60: Simulation of chosen model between  $y_9$  and  $u_3$  against validation data.

*best model* : black line, validation data : grey line

## D.6.2 Bentonite flowrate ( $u_5$ )

The identification data is presented in Figure D.61. Figure D.62 presents the FPE (bar plot) and the fit (line plot) of the selected models. Inside the bar, from top to bottom are the respective values of  $na$ ,  $nb$ ,  $nc$ ,  $nd$ ,  $nf$ ,  $nk$ .

From the preliminary analysis, models 2, 9 and 12 are chosen to undergo a deeper analysis. These models were selected because they present good FPE / fit combinations. Model 2 is selected for its simplicity. The selected models are presented in Table D.42. All the models show auto-correlation of the residuals and no cross-correlation between the residuals and the input. Models ARMAX(1,4,4) and OE(6,4,1,1) have a pole/zero cancellation. Therefore, the simpler model is kept (D.25) even if the fit value is very low. There are two reasons for this: a steady-state offset and the noise of the basis weight signal. The whole data set is assumed to be linear. Then, the range is 0 to 2.9 L/min of bentonite and 58.5 to 64 g/m<sup>2</sup> of

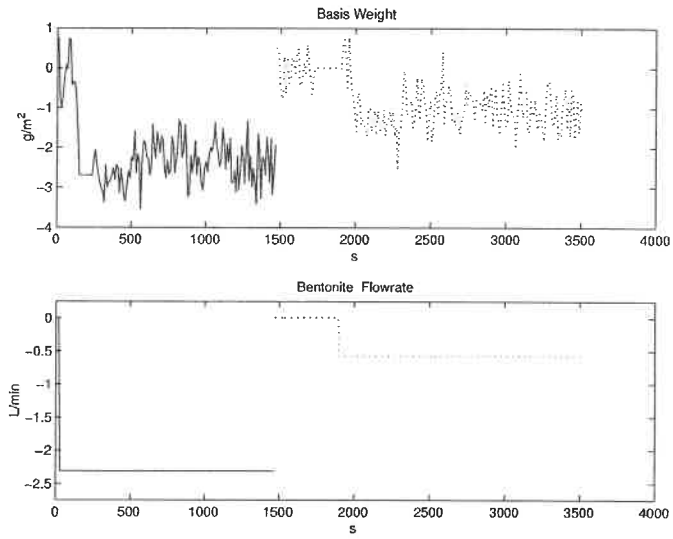


Figure D.61: Identification data for the model between  $y_9$  and  $u_5$

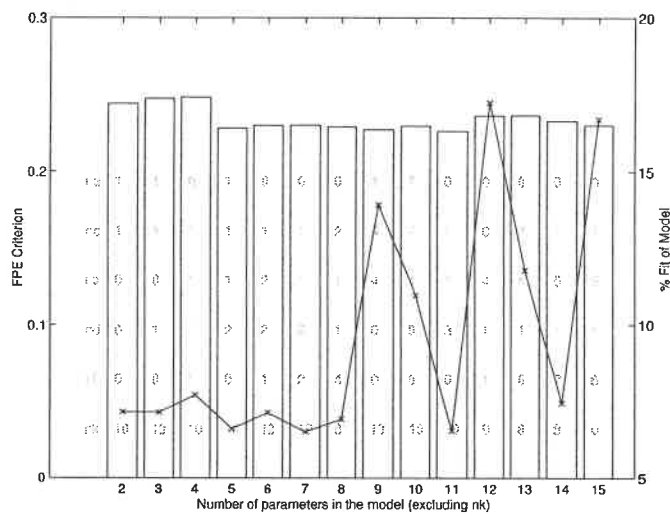


Figure D.62: Candidate models between  $y_9$  and  $u_5$

basis weight. Table D.43 summarises some of the model characteristics. Figure D.63 compares the model response with the validation data.

Table D.42: Preliminary models between  $y_9$  and  $u_5$ 

Model Name	Model
ARX(1,1)	$y = \frac{0.6558q^{-10}}{1-0.3733q^{-1}}u + \frac{1}{1-0.3733q^{-1}}e$
ARMAX(1,4,4)	$(1 - 0.9878q^{-1})y = (0.2387q^{-10} + 0.2482q^{-11} + 0.003178q^{-12} - 0.4792q^{-13})u + (1 - 0.6935q^{-1} - 0.3591q^{-2} + 0.3843q^{-3} - 0.3478q^{-4})e$
BJ(6,4,1,1)	$y = \frac{-0.4394q^{-9} + 0.4362q^{-10} + 0.7383q^{-11} - 0.3252q^{-12} - 0.4614q^{-13} + 0.09064q^{-14}}{1 - 0.9747q^{-1}}u + \frac{1 - 0.5922q^{-1} - 0.3064q^{-2} + 0.3886q^{-3} - 0.2995q^{-4}}{1 - q^{-1}}e$

$$y_9 = \frac{0.6558q^{-10}}{1 - 0.3733q^{-1}}u_5 + \frac{1}{1 - 0.3733q^{-1}}e \quad (\text{D.25})$$

Table D.43: Characteristics of the chosen model between  $y_9$  and  $u_5$ 

Model Name	Equation Number	FPE	Fit (%)	Model Error Model Fit (%)	Linear Fit (%)
ARX(1,1)	(D.25)	0.24	7.2	-	24.8

### D.6.3 C-PAM flowrate ( $u_6$ )

The identification data is presented in Figure D.64. Figure D.65 presents the FPE (bar plot) and the fit (line plot) of the selected models. Inside the bar, from top to bottom are the respective values of  $na$ ,  $nb$ ,  $nc$ ,  $nd$ ,  $nf$ , and  $nk$ . The basis weight signal is noisy. The resulting models have poor fit values.

From the preliminary analysis, models 8 and 10 are chosen to undergo a deeper analysis. These models were selected because they present good FPE / fit combinations. Furthermore, higher order models only try to model the noise with poles



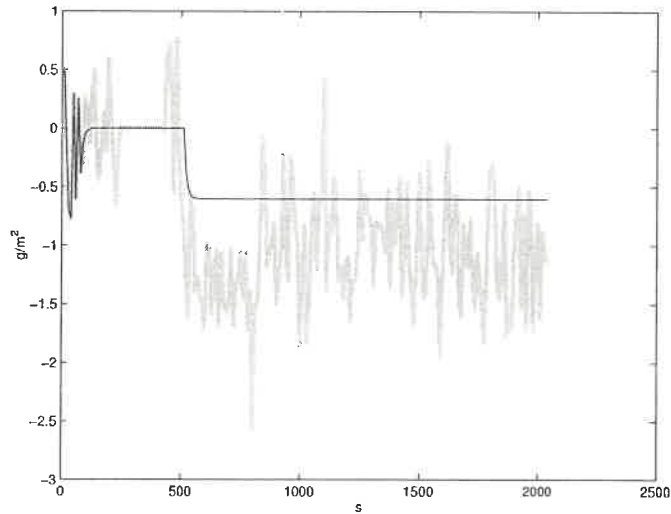


Figure D.63: Simulation of chosen model between  $y_9$  and  $u_5$  against validation data.

*best* model : black line, validation data : grey line

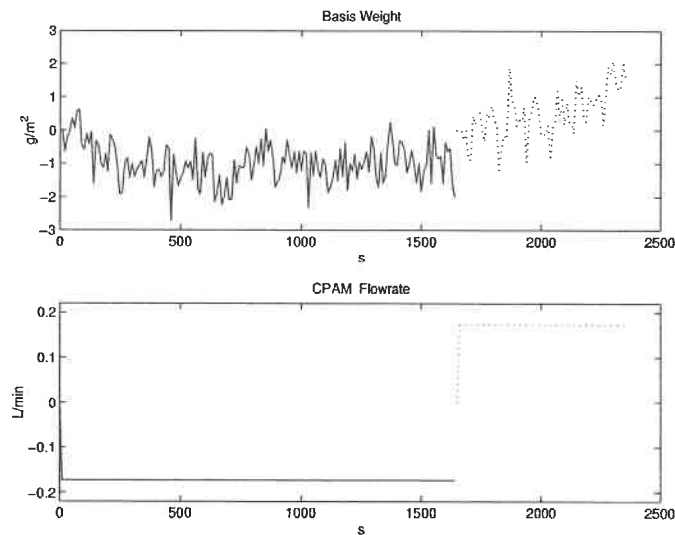
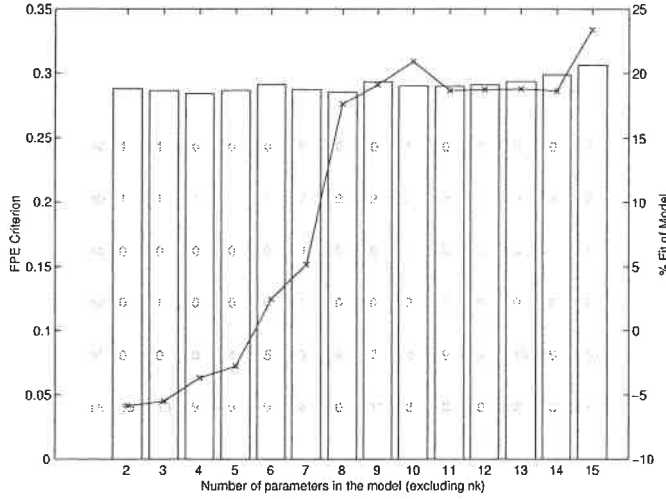


Figure D.64: Identification data for the model between  $y_9$  and  $u_6$

Figure D.65: Candidate models between  $y_9$  and  $u_6$ 

on the unit circle. The selected models are presented in Table D.44. Model OE(2,6) has a pole/zero cancellation. The remaining model shows no auto-correlation of its residuals and no cross-correlation between the residuals and the input. Therefore, this model is kept (D.26). The whole data set is assumed to be linear. Then, the range is 0.231 to 0.578 L/min of C-PAM and 58 to 63  $g/m^2$  of basis weight. Table D.45 summarises some of the model characteristics. Figure D.66 compares the model response with the validation data.

Table D.44: Preliminary models between  $y_9$  and  $u_6$ 

Model Name	Model
OE(2,6)	$y = \frac{3.57q^{-9} - 3.501q^{-10}}{1 - 0.09272q^{-1} - 0.77q^{-2} - 0.007593q^{-3} - 0.9328q^{-4} - 0.03187q^{-5} + 0.8477q^{-6}} u + e$
ARARMAX(1,2,4,3)	$y = \frac{3.125q^{-8} - 2.642q^{-9}}{1 - 0.9244q^{-1}} u + \frac{1 - 0.1755q^{-1} - 1.121q^{-2} - 0.5279q^{-3} + 0.8168q^{-4}}{(1 - 0.9244q^{-1})(1 + 0.606q^{-1} - 0.6031q^{-2} - 0.885q^{-3})} e$

$$y_9 = \frac{3.125q^{-8} - 2.642q^{-9}}{1 - 0.9244q^{-1}} u_6 \quad (D.26)$$

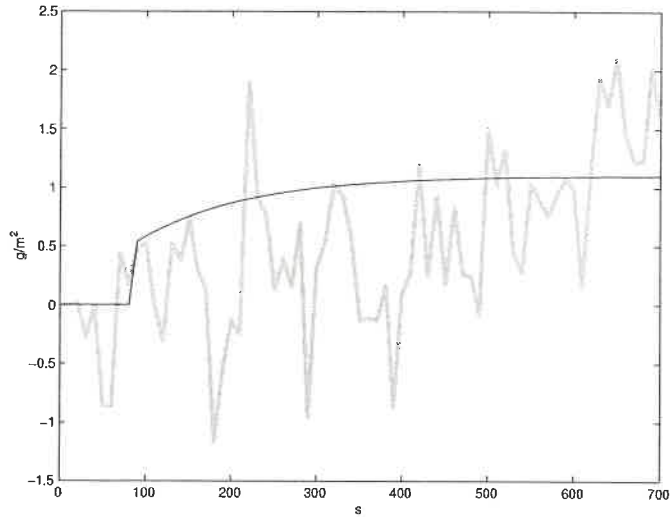


Figure D.66: Simulation of chosen model between  $y_9$  and  $u_6$  against validation data.

*best model* : black line, validation data : grey line

$$+ \frac{1 - 0.1755q^{-1} - 1.121q^{-2} - 0.5279q^{-3} + 0.8168q^{-4}}{(1 - 0.9244q^{-1})(1 + 0.606q^{-1} - 0.6031q^{-2} - 0.885q^{-3})}e$$

Table D.45: Characteristics of the chosen model between  $y_9$  and  $u_6$

Model Name	Equation Number	FPE	Fit (%)	Model Error Model Fit (%)	Linear Fit (%)
ARARMAX(1,2,4,3)	(D.26)	0.29	20.9	–	17.1

#### D.6.4 Ratio of bentonite to C-PAM ( $u_7$ )

The identification data is presented in Figure D.67. Figure D.68 presents the FPE (bar plot) and the fit (line plot) of the selected models. Inside the bar, from top to bottom are the respective values of  $na$ ,  $nb$ ,  $nc$ ,  $nd$ ,  $nf$ , and  $nk$ .

From the preliminary analysis, models 2, 5 and 9 are chosen to undergo a deeper analysis. These models were selected because they present good FPE / fit combinations. Model 2 is selected for its simplicity. The selected models are presented

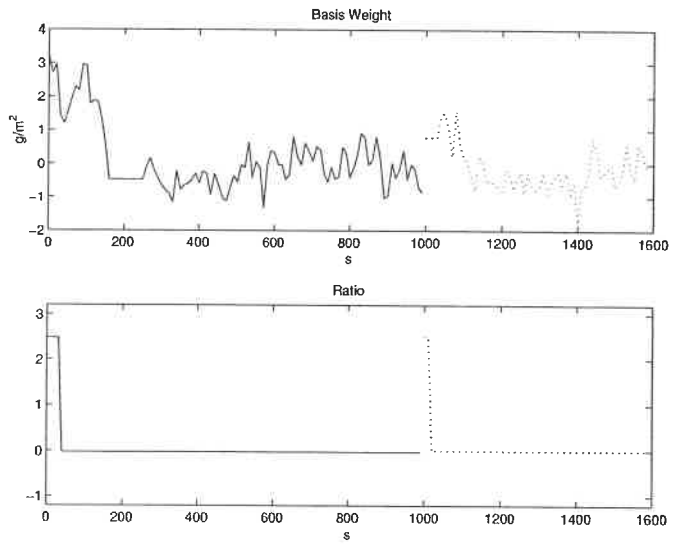


Figure D.67: Identification data for the model between  $y_9$  and  $u_7$

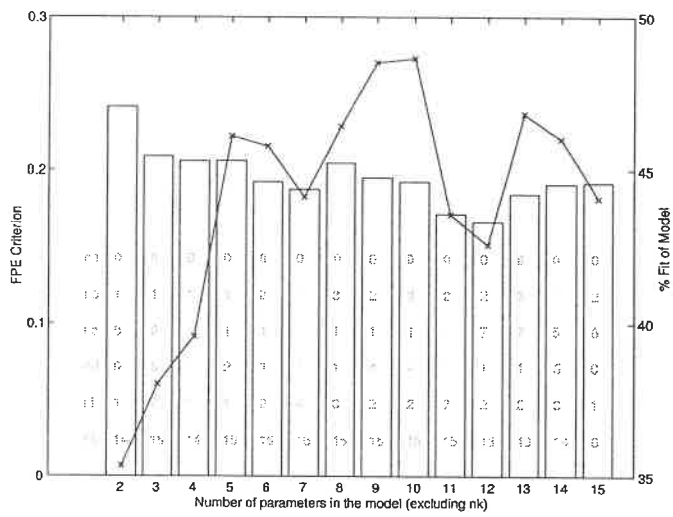


Figure D.68: Candidate models between  $y_9$  and  $u_7$

in Table D.46. Model BJ(2,1,4,2) has poles on the unit circle that simulate noise. Model BJ(1,1,2,1) has poles outside the unit circle. Since this process is known to be stable, this model is rejected. Model OE(1,1) shows no auto-correlation of the residuals and no cross-correlation between the residuals and the input. Therefore, it is kept (D.27). The linear ranges are a ratio of bentonite to CPAM from 0 to 3 and 56 to 64  $g/m^2$  in basis weight. Table D.47 summarises some of the model characteristics. Figure D.69 compares the model response with the validation data.

Table D.46: Preliminary models between  $y_9$  and  $u_7$

Model Name	Model
OE(1,1)	$y = \frac{0.2415q^{-14}}{1-0.9898q^{-1}}u + e$
BJ(1,1,2,1)	$y = \frac{0.01097q^{-16}}{1-0.9701q^{-1}}u + \frac{1+1.01q^{-1}}{1+0.5109q^{-1}-0.2188q^{-2}}e$
BJ(2,1,4,2)	$y = \frac{0.09091q^{-15}-0.03415q^{-16}}{1-1.981q^{-1}+0.9881q^{-2}}u + \frac{1-1.001q^{-1}}{1-1.221q^{-1}+0.5219q^{-2}-0.3355q^{-3}+0.2701q^{-4}}e$

$$y_9 = \frac{0.2415q^{-14}}{1-0.9898q^{-1}}u_7 + e \quad (D.27)$$

Table D.47: Characteristics of the chosen model between  $y_9$  and  $u_7$

Model Name	Equation Number	FPE	Fit (%)	Model Error Model Fit (%)	Linear Fit (%)
OE(1,1)	(D.27)	0.24	34.3	-0.08	46.7

### D.6.5 Fresh filler flowrate ( $u_8$ )

The identification data is presented in Figure D.70. Figure D.71 presents the FPE (bar plot) and the fit (line plot) of the selected models. Inside the bar, from top to

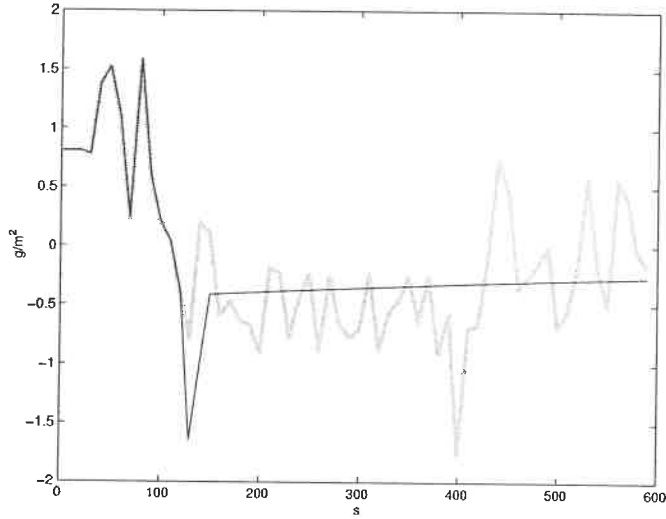


Figure D.69: Simulation of chosen model between  $y_9$  and  $u_7$  against validation data.

*best model* : black line, *validation data* : grey line

bottom are the respective values of  $na$ ,  $nb$ ,  $nc$ ,  $nd$ ,  $nf$ , and  $nk$ .

From the preliminary analysis, model 6 and 9 are chosen to undergo a deeper analysis. These models were selected because, respectively: a good fit / FPE for the number of parameters and the best fit. These models are presented in Table D.48. Both models do not have a pole/zero cancellation. Both models show some auto-correlation of their error signal and no cross-correlation between the error and input signals. The simplest one is chosen (D.28). The whole data set is assumed to be linear. Then, the range is  $\pm 0.87$  L/min in filler flowrate and  $\pm 5$  g/m<sup>2</sup> in basis weight. The nominal values are 4.55 L/min for the filler and 62.9 g/m<sup>2</sup> for the basis weight. Table D.49 summarises some of the model characteristics. Figure D.72 compares the model response with the validation data.

$$y_9 = \frac{-1.32q^{-4} + 1.379q^{-5}}{1 - 0.9697q^{-1}}u_8 + \frac{1 - 0.8902q^{-1}}{1 - 1.132q^{-1} + 0.1363q^{-2}}e \quad (\text{D.28})$$

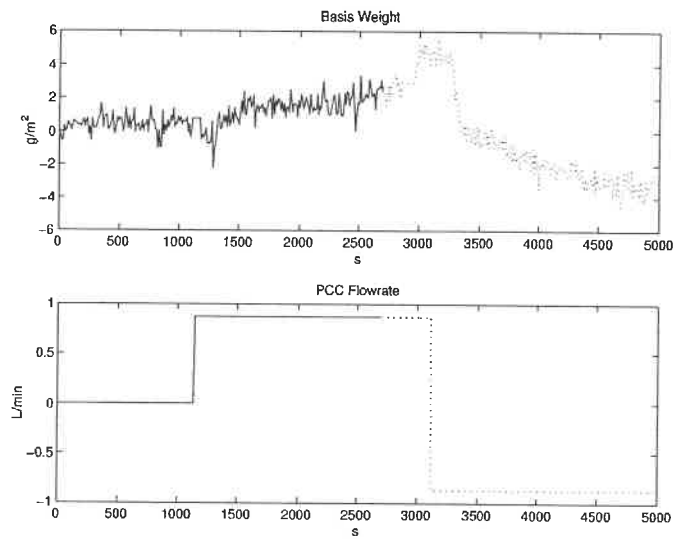


Figure D.70: Identification data for the model between  $y_9$  and  $u_8$

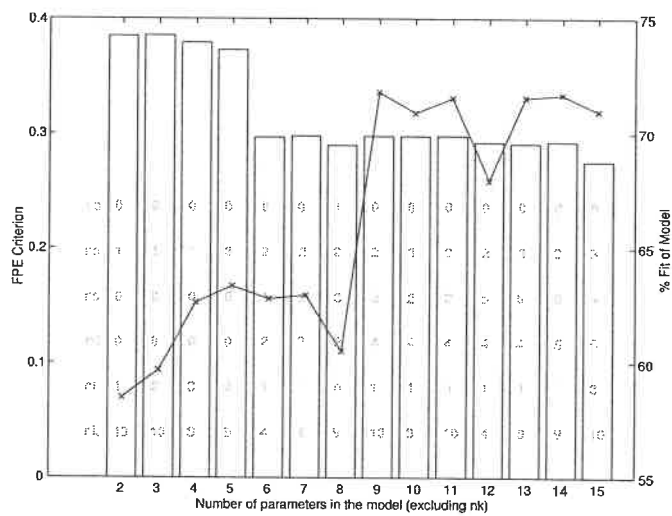


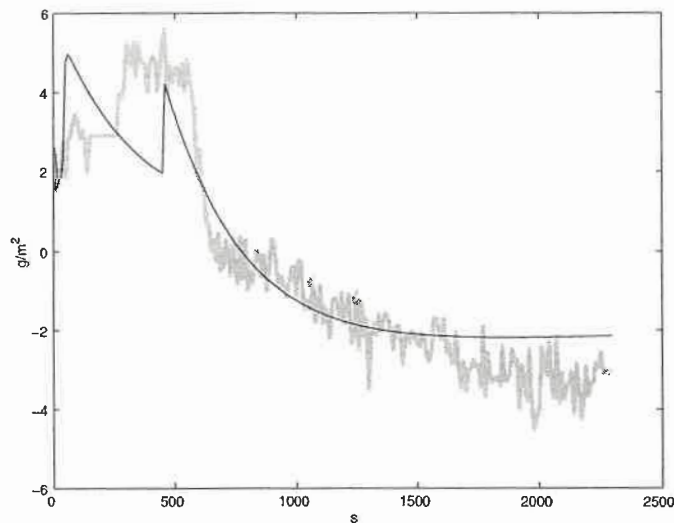
Figure D.71: Candidate models between  $y_9$  and  $u_8$

Table D.48: Preliminary models between  $y_9$  and  $u_8$ 

Model Name	Model
BJ(2,1,2,1)	$y = \frac{-1.32q^{-4}+1.379q^{-5}}{1-0.9697q^{-1}}u$ $+ \frac{1-0.8902q^{-1}}{1-1.132q^{-1}+0.1363q^{-2}}e$
BJ(2,2,4,1)	$y = \frac{-0.8511q^{-10}+0.9704q^{-11}}{1-0.9695q^{-1}}u$ $+ \frac{1-1.989q^{-1}+0.9897q^{-2}}{1-2.171q^{-1}+1.25q^{-2}+0.003706q^{-3}-0.08157q^{-4}}e$

Table D.49: Characteristics of the chosen model between  $y_9$  and  $u_8$ 

Model Name	Equation Number	FPE	Fit (%)	Model Error Model Fit (%)	Linear Fit (%)
BJ(2,1,2,1)	(D.28)	0.297	62.8	no fit	54.7

Figure D.72: Simulation of chosen model between  $y_9$  and  $u_8$  against validation data.

*best model* : black line, *validation data* : grey line



ÉCOLE POLYTECHNIQUE DE MONTRÉAL



3 9334 00269351 1